A Study of the Deformation Environment of the Outer Hebrides Fault Zone

Submitted for the degrees of PhD and DIC

Jill Walker
Imperial College

ERRATA

Page

2 Last line, 3rd para., 'pseudotachylyte' for 'pseudotachylte'.

47 2nd para., insert 'may have' between 'extensional displacement' and 'exceeded'.

238 Plate 5.4 inserted upside down.

244 2nd para., 'impregnated' for 'impreganated'

296 3rd para., 'Al_2O_3' for 'Al_{2o3}'.

419 Wenk, H.R., insert 'of' between 'products' and 'fracture'.

'accommodate' for 'accomodate' throughout.

Abstract

The Outer Hebrides Fault Zone is characterised by a complex assemblage of fault rocks, mostly developed from acid gneiss (Gray Gneiss). Large volumes of microbreccia are developed, and smaller amounts of cataclasite, ultracataclasite, pseudotachylyte, r-type mylonite, altered equivalents of all the above, and c-type mylonites.

Field mapping and thin section study have distinguished at least three phases of deformation during the evolution of the fault zone.

Initially, crystal plastic deformation produced r-type mylonites, forming contemporaneously with the Gray Gneiss during Laxfordian lower amphibolite facies shearing, at around 15 km deep and 540 degrees C. Microstructures suggest that the regime was at least locally compressional. Higher strain rates generated pseudotachylte.

Another compressional phase occurred during the Caledonian orogeny at 3-5 km, and around 100 degrees C, resulting in brittle deformation and giving rise to microbreccias by formation of pervasive sub-horizontal sets of microfractures. Ultracataclasite and a second

phase of pseudotachylyte were also generated.

Late Caledonian extensional, high level, brittle deformation followed, forming discrete, eastward-dipping fault planes within the microbreccias, and more ultracataclasite. During the Tertiary, a warm (c. 300 C), Fe-Mg bearing aqueous phase invaded the fault planes, causing widespread alteration to lower greenschist facies. Continuing extension formed c-type mylonites along the fault planes by leaching silica and depositing mafic phases. The fluid precipitated the silica into adjacent microbreccias.

Whole rock analyses revealed little geochemical difference between r-type mylonites and the parent Gray Gneiss, and mass balance supports this as an isochemical, isovolumetric reaction. Microbrecciation involves a volume increase, but little chemical change. Gray Gneiss and microbreccia alteration is isovolumetric, but involves chemical changes. Alteration of microbreccia mainly involves addition of SiO_2. The c-type mylonites show the greatest bulk chemical variation, and a volume decrease.

List of Contents

Acknowledgements

List of Figures
List of Plates
List of Tables

Chapter 1 - Introduction
1.1 Introduction to Field Area and Brief Geological Setting
1.2 Aims of Project and Structure of Thesis
1.3 Logistics of Fieldwork
1.4 Techniques Used
1.5 Fault Rock Classification
1.6 Fault Rock Terminology
1.7 Sense of Shear Indicators

Chapter 2 - Previous Work
2.1 Introduction
2.2 Nomenclature
2.3 Land-based Studies
2.4 Sub-Surface Studies

Chapter 3 - General Geology
3.1 Introduction
3.2 Lithostratigraphy
3.3 The Outer Hebrides Fault Zone
3.4 Other Faults and Lineaments
3.5 Tectonic Setting

Chapter 4 - Field Studies
4.1 Introduction
4.2 Malasgair and Shiltenish
4.3 Scalpay
4.4 Crogary na Hoe and North Lee
4.5 Usinish
4.6 The Sampling Traverses
4.7 Summary

Chapter 5 - Microstructures
5.1 Introduction
5.2 Country Rocks
5.3 The Microbreccias
5.4 Cataclasites
5.5 Gouges
5.6 Pseudotachylyte
5.7 C-type Mylonites
5.8 R-type Mylonites
5.9 Phyllonites
5.10 Conditions of Deformation

Chapter 6 - Geochemical Studies
6.1 Introduction
6.2 Description of the Bulk Chemistry of the Major Rock Types
6.3 Bulk Chemical Changes
6.4 Fe^{2+} Determinations
6.5 Mass Balance Calculations
6.6 Temperature, Quantity and Composition of the Fluid Phase
6.7 Amphibole Compositions

Chapter 7 - Synthesis
7.1 Introduction
7.2 Pre-Laxfordian Deformation
7.3 Laxfordian Compression
7.4 Caledonian Compression
7.5 Post-Caledonian Extension
7.6 Discussion - Aspects of the Model
7.7 Discussion - Defficencies of the Model
7.8 Discussion - Comparison with Other Models
7.9 Summary

Chapter 8 - Conclusions and Further Work

References

Appendix I - Mineral Analyses
Appendix II - Whole Rock Analyses
Appendix III - Fe^{2+} Determinations
Appendix IV - Density Determinations

Acknowledgements

I would like to thank the many people without whose help this thesis would have taken even longer to complete.

Several generations of inmates of the structural cubicles - Pete Bretan, Howard Obee, Yi Wang, Mohammed, Tony Page and Saranne Cessford, whose comments, constructive or otherwise, helped to formulate the ideas expressed here.

Honorary cubicle inmates Bob Maddock and Mark Enfield, for discussion and helpful advice.

Nick,Grace and Adolfo for teaching me the rudiments of photography and for printing the plates.

Alan Jones for help in sawing up my samples and for preparing a seemingly endless number of thin sections.

Dick Gittins for his tuition in the use of the SEM and SPECTA.

Peter Watkins, for his time and patience in teaching me the analytical techniques used in this project.

John Hume for lamb bones, and together with Mary Pugh, the opportunity to go down in history as collator of GEOlogic.

Rona Morrison and her family, for their unfailing kindliness and friendliness during my fieldwork, and especially the late Angus Morrison, who sadly passed away just before the completion of this thesis.

The policeman who stopped me near the Humber Bridge for having a car overloaded with specimens, but let me go without

jetisoning the cargo.

Kate Brodie for patiently reading, discussing and re-reading chapter after chapter.

Stan White for accepting me for this project, and signing all the necessary paperwork over the years.

John Craven, who took even longer than me to write up.

Mum, Dad, and all at Lowestoft Library, who never stopped nagging me to get on with it.

Bodie, Sheba and now Catriona, who have slowed down progress in writing up.

Most of all, to Andy, who tried to stop me in the first place.

List of Figures

1.1 Location of field area.

1.2 Simplified geological map of the Outer Hebrides.

1.3 Locations of mapped areas and sample traverses.

1.4 Classification of fault rock types.

1.5 Criteria to establish senses of displacement.

2.1 Locations of deep seismic and crustal refraction profiles.

2.2 An interpretation of the MOIST seismic profile.

3.1 Map showing areas of supracrustals on the Outer Hebrides.

3.2 Simplified map of the geology of South Harris.

3.3 Location of the Stornoway Formation and its bounding faults.

3.4 Formation of the Madadh Mor.

3.5 Map showing relationships between faults and basins.

3.6 Lineament map of the Outer Hebrides.

4.1 Field map of Malasgair and Shiltenish, Isle of Lewis.

4.2 Field map of the island of Scalpay, off Harris.

4.3 Field map of the Crogary na Hoe area, North Uist.

4.4 Field map of the North Lee area, North Uist.

4.5 Field map of the Usinish area, South Uist.

4.6 Cross-sections drawn along the sampling traverses.

5.1 Quartz c-axis fabric from an r-type mylonite.

6.1 Ranges of composition for selected rock types.
6.2 Variation of LOI with SiO_2).
6.3 Variation of LOI with Fe_2O_3 T.
6.4 Variation of LOI with MgO.
6.5 Variation of LOI with Al_2O_3.
6.6 Variation of Ba with SiO_2.
6.7 Variation of Sr with SiO_2.
6.8 Variation of Cr with SiO_2.
6.9 Variation of elements with microbrecciation.
6.10 Ranges of values for $FeO/(FeO + Fe_2O_3)$.
6.11 Composition-volume diagram for altered Gray Gneiss.
6.12 Composition-volume diagram for Gray Gneiss microbreccia.
6.13 Composition-volume diagram for r-type mylonite.
6.14 Composition-volume diagram for c-type mylonite.
6.15 Composition-volume diagram for c-type mylonite.
6.16 Mg/(Mg + Fe) v. Si for amphiboles from Corodale Gneiss.
6.17 Mg/(Mg + Fe) v. Si for amphiboles from Gray Gneiss.

7.1 Sequence of development of fault rocks.
7.2 Orientation of fractures with respect to principal stresses. 7.3 Orientation of foliation and degree of brecciation.

7.4 Fluid flow in the Outer Hebrides Fault Zone.

7.5 Mechanisms for outcrop of granulites above amphibolites.

7.6 Major stages in evolution of the Outer Hebrides Fault Zone.

List of Plates

4.1 Field photographs from Malasgair and Shildenish, Lewis.
4.2 Field photographs of Malasgair, Lewis, and Scalpay, Harris.
4.3 Field photographs from Scalpay, Harris.
4.4 Field photographs of Crogary na Hoe and North Lee, North Uist.
4.5 Field photographs from North Uist and Usinish, South Uist.

5.1 Textures and microstructures exhibited by the country rocks.
5.2 Textures and microstructures exhibited by the country rocks.
5.3 Textures and microstructures of altered Gray Gneiss and microbreccias.
5.4 Textures of altered Gray Gneiss microbreccias.
5.5 Microstructures of altered Gray Gneiss microbreccias.
5.6 Textures and microstructures of ultracataclasites and gouges.
5.7 Textures and microstructures of the pseudotachylytes.
5.8 Development of c-type mylonite textures.
5.9 Textures of c-type mylonites.
5.10 Microstructures of c-type mylonites.
5.11 Textures and microstructures of r-type mylonites.

5.12 Textures and microstructures of r-type mylonites

List of Tables

2.1 Geophysical surveys of the Outer Hebrides and NW Scotland.

3.1 Tectonothermal, intrusive and depositional events.

4.1 North/south and east/west variation in style of deformation.

6.1 Average analyses for major rock types.

7.1 Summary of the deformation history of the Fault Zone.

Chapter 1

Introduction

1.1 Introduction to Field Area and Brief Geological Setting

Geographical and Geomorphological Setting The Outer Hebrides are a gently curving archipelago approximately 200 km in length. They lie roughly 60 km west of mainland Scotland and are separated from it by The Minch (figure 1.1). Most of the landforms are attributable to glaciation, with very little in the way of drainage-influenced landscape. The islands were marginal to the major ice-sheets of Europe in the Pleistocene. Unlike the rest of Britain, the rise in sea-level resulting from the melting of the ice-sheets was not offset by a dramatic eustatic rebound, so that much of the Hebridean coastline has been drowned, with sea-level rising at around one metre per century prior to 6000 BC (Whittow, 1977). The glaciation has resulted in a low-lying topography which has since accumulated an extensive peat cover, giving poor exposure except in the mountains of South Harris and the low to moderate hills running down the eastern seaboard of the Uists.

Geological Setting The islands are composed of high-grade polycyclic Precambrian gneisses of the Lewisian complex (Dearnley, 1962). For the most part, these gneisses are of amphibolite facies and are acid in composition (termed Gray Gneisses), although a substantial area of more basic,

granulite facies rocks (the Corodale Gneisses (Coward, 1972)) outcrops on South Uist (see figure 1.2). A metaigneous complex, with associated metasediments, outcrops in South Harris (Dearnley, 1963) while other small isolated patches of metasediments (Coward et al., 1969) occur scattered across the Hebridean region. Precambrian Scourie dykes are reworked to varying degrees within the Gray Gneisses (Dearnley and Dunning, 1968; Watson, 1969; Coward et al., 1970; Fettes et al., in press), and Tertiary, and scarcer Permo-Triassic, basic dykes cut across earlier fabrics (Fettes and Mendum, 1987).

Along the eastern edge of the island chain is a wide zone of strongly deformed material - see figure 1.2 for location of the area affected. This is the Outer Hebrides Fault Zone and it comprises an assemblage of subparallel faults and shear zones (Sibson, 1977b) containing various fault rocks of differing ages and movement directions.

1.2 Aims of Project and Structure of Thesis

Aims of Project The aims of this thesis are, firstly, to attempt to piece together a regional deformation history for the Outer Hebrides Fault Zone and secondly, to determine the interaction of deformation, metamorphism and

fluid migration within the fault rocks by investigation of their bulk compositions.

Structure of Thesis The remainder of this chapter gives an introduction to the field area, discusses the techniques used in the study, the criteria used in the classification of fault rocks and ways of determining movement directions within the fault zone.

Chapter 2 gives a brief review of previous work in the area whilst Chapter 3 looks at the general geology of the area. Chapters 4, 5 and 6 discuss respectively field, microstructural and geochemical findings of the project, whilst Chapter 7 investigates the distribution of the fault rock types and attempts to tie all these observations together with a regional synthesis. General conclusions and suggestions for further work are presented in Chapter 8.

1.3 Logistics of Fieldwork

Fieldwork seasons and areas to be studied were determined by the problems of transport to, and accessibility of, areas of interest and the times of year likely to be conducive to outdoor activity.

Transport Transport in the major field seasons was by motorcycle, post-bus and hitch-hiking. For the shorter field seasons, a car was available, which greatly eased sample transportation problems. A limited road network makes access to many areas difficult. Extensive use was made of ferries to get between the islands, and a small boat was used on occasion to have a closer look at otherwise inaccessible coastal outcrops.

Terrain The ground in general is rough grazing or heather- covered, with areas of peat bog, and the coastline is heavily indented with sea-lochs running for many kilometres inland. The strong structural grain of the islands is exploited by numerous freshwater lochs which consequently tend to run for considerable distances in a particular direction.

Climate The Outer Hebrides are fairly mild in temperature, but get more than their fair share of precipitation, and strong winds. The field seasons were planned as far as possible for the period April to July, to catch the best weather and avoid the midges.

Selection of Areas for Study Areas were selected for study using the Ordnance Survey (OS) 1:50 000 series maps to assess probable degree of exposure and ease of access. Sibson's (1977b) geological maps of the Outer Hebrides

Fault Zone were also used to help pinpoint areas likely to be of geological interest. The following areas were selected for mapping and sampling in detail: Malasgair and Shiltenish, Scalpay, Crogary na Hoe, North Lee and Usinish (see figure 1.3 for their locations). To study systematically any changes in microstructure and bulk composition along and across the fault zone, nine traverses trending perpendicular to the strike of the fault zone were chosen. The positions of these traverses are also shown on figure 1.3: their selection was based on a combination of accessibility and the likelihood of containing a variety of fault rock types.

Taken together, the traverses and the mapping/sampling areas should give an indication of both east-west and north-south variations along the fault zone. In addition, a number of undeformed rock samples were collected for comparison. These came from the west coasts of North and South Uist, quarries on Grimsay, road cuts on North Uist, outcrops on Harris and Lewis (all well away from the fault zone) and also from the western end of each sample traverse, as far as exposure permitted.

1.4 Techniques Used

Field Mapping and Sampling Within the selected areas of

interest (figure 1.3), mapping was undertaken on either the 1:25 000 scale or the 1:10 000 scale (where exposure warranted) to gain structural data, large-scale movement indicators and information on the outcrop patterns of the different rock types. Reconnaissance mapping of some other areas was also carried out, using OS 1:50 000 maps. This scale was also used for the sampling traverses unless a 1:25 000 map was already available. Further details of the sampling procedure are given in section 4.6.

All samples, from both the mapping and the traverses, were orientated, and those for analysis were large enough to ensure that they were reasonably fresh, representative of the outcrop and overcame any problems of outcrop-scale inhomogeneities.

Optical Microscopy For each specimen an orientated thin section was prepared and a petrographic description made, detailing the fault rock type, the precursor, the mineralogy and the dominant style(s) of deformation, where these can be inferred. Other information was also recorded, such as sense-of-shear indicators, fractures and deformation history. Some of the samples (those with a reasonable number of suitably-sized quartz grains) were used for petrofabric analysis. Many of the rocks, particularly the c-type mylonitic and ultracataclastic specimens, proved to be too fine grained for optical

microscopy to reveal any detail. However, the optical microscope provided a useful tool for assessing which of these sections would be most suitable for electron microscopy.

Scanning Electron Microscopy A Jeol 733 SEM Superprobe with back-scattered electron (BSE) imaging was used to study the microstructures of those rocks with a grain size too small to be resolved optically. It also allowed accurate measurement of these and larger grain sizes. Resolution was still a problem with some of the ultracataclastic samples and the matrices of many of the c-type mylonites, owing to the ultrafine grain sizes involved.

The back-scattered technique makes use of standard carbon-coated, polished sections, and allows representation of the mean atomic weight of a mineral by means of its brightness on an imaging screen - the brighter the grain appears the higher its mean atomic weight. For a full account of the BSE method see Hall and Lloyd (1981), White et al. (1984) or Lloyd (1985).

The maximum practicable magnification was around 3000X, somewhat lower than the figure of X5000 given by White et al., 1984. A further problem with BSE imaging is that monomineralic polygranular aggregates will show no

contrast, unless another mineral phase is present along grain boundaries.

Electron Microprobe Analysis The SEM Superprobe includes an energy dispersive spectrometer and a Link Systems software package employing a ZAF correction routine, allowing both qualitative and quantitative mineral analysis. The quantitative program was utilised most extensively in this project to obtain mineral compositions for all rock types and to determine the mineralogy of the fine-grained materials. The fine grained nature of the fault rocks, combined with BSE imaging, makes the high resolution available on the SEM the most suitable technique for this purpose. Results of these analyses are presented in Appendix I.

Microchemical analyses undertaken in this way allowed chemical characterisation of individual phases, identification of zoning within grains and the study of retrogressive metamorphic reactions. The major limitation of this technique was the small grain size of many of the phases, with the possibility of spurious analyses across grain boundaries. Problems were encountered due to poor machine calibration (found to be caused by internal interference in the machine) for over a year of this project. Further complications arose as many phases were found to be non-stochiometric and to have low totals.

Whole Rock Analysis All samples from the traverses and some from the mapped areas were analysed, together with country rock specimens to act as 'controls'. This was done using standard techniques of Inductively Coupled Plasma (ICP) analysis (see Appendix II).

Fe2+ Determinations Selected samples were analysed for their Fe2+ content using a wet chemical technique. See Appendix III for details.

Density Determinations These are necessary for mass balance calculations. Selected samples were used, as the procedure is tedious, time-consuming and the precision is poor. For an account of the method and results, see Appendix IV.

1.5 Fault Rock Classification

Much confusion surrounds the classification of fault rocks, and there is as yet no agreed nomenclature. A review of the problems surrounding fault rock terminology is presented in Mawer (1985), whilst White (1982) reviews historical usage in the literature. Fundamental problems arise when authors use the same term to describe different features or processes, or disagree as to whether or not a

particular term carries a genetic implication. It is not proposed to discuss these matters here. The subject has been well aired, although not resolved, in the literature, e.g. Zeck (1974), Sibson (1977a), White (1982), Wise et al. (1984).

Most current classifications are textural, in that they initially subdivide fault rocks into foliated and random fabric textures. Sibson (1977a and b) (after Higgins, 1971) tried to do this by devising the mylonite and cataclasite series, with the aim of making purely textural distinctions. However, it is very difficult to avoid genetic implications in any such classification. For example, the use of the textural term 'cataclasite' implies fracture as a mechanism of grain size reduction.

In a similar scheme distinguishing foliated from non-foliated fault rocks, White (1982) attempted to accommodate the genetic connotations and introduced the terms c-type and r-type mylonites, where grain size reduction was predominantly by cataclastic or recrystallisation processes respectively. This classification experiences the opposite problem to that above, in that the genetic term 'mylonite' carries textural implications as to the presence of a foliation. This leads to the conclusion that textural and genetic characteristics are not independent of each other.

Thus it seems that the distinction between textural and genetic characteristics is somewhat artificial, and it is impossible to produce a workable classification purely on the basis of one of them. The classification used here (figure 1.4) is basically that of Higgins (1971) and Sibson (1977a and b), with a slight adaption to take in the c- and r- type divisions of White (1982).

It is becoming increasingly reported in the literature, and will be shown later in this thesis, that many rocks of cataclastic origin, especially gouges, possess a foliation, and this classification allows gouge to extend into the foliated field (figure 1.4). The processes shown on figure 1.4 that influence fault rock type (frictional melting, cataclasis and recrystallisation) are all represented in the fault rocks of the Outer Hebrides, together with a fourth, that of fluid/rock interaction. Fluid/rock interaction is an important process in fault zones and many faults show evidence for large-scale fluid movements (Beach and Fyfe (1972); Beach (1976, 1980); Sibson (1975 b, 1977 c); Etheridge et al. (1983); Kerrich et al. (1984); McCaig (1984); Brodie and Rutter (1985); Rutter and Brodie (1985); Kerrich and Hyndman (1986); Kerrich (1986); McCaig (1987)).

Limitations of the Classification It is not always possible to classify a rock in hand specimen, as the

predominant deformation process may not be recognisable. This is especially true for fine-grained, foliated rocks and, in the case of the Outer Hebridean rocks, those where there has been a high degree of fluid/rock interaction. Unfortunately, all classifications must resort to thin section examination to resolve this problem. This means that it is occasionally necessary to use field descriptions (such as 'flinty crush rock' - see section 2.3), which are subsequently modified on inspection of the thin section.

1.6 Fault Rock Terminology

The following section defines the terms as used in this thesis.

Fault Breccias and Fault Gouges Following Sibson (1977a), these are characterised by their incohesive nature, and texture of angular fragments set in a fine-grained matrix. A distinction between the two is made by a figure of 30% visible fragments (figure 1.4), above which the rock is a breccia, below which it is a gouge. Gouges are the finer grained of the two, and are more likely to exhibit a preferred alignment of minerals or a foliation due to formation of platey minerals by chemical alteration.

Of these rocks, only fault gouge has been found on the Outer Hebrides, and its outcrop is restricted to one locality. Hence it is not proposed to go into detail here. For further information, see Hall (1983) or Rutter et al. (1986). Typical features of the gouge are its incohesive nature, the presence of visible fragments set in a finer matrix, its greenish coloration and the presence of a weak foliation defined by alignment of platey minerals. Shear planes (Y,P and R) are common.

Pseudotachylyte This term is reserved for an ultra-fine grained, cohesive fault rock formed by melting due to rapid brittle failure and resultant frictional sliding along a discrete plane. A typical texture usually shows spalled-off clasts of quartzo-feldspathic material in a dark, isotropic matrix. Distinguishing characteristics are the presence of glass, flow banding, chill features and devitrification structures. Maddock (1986) presents a full account of pseudotachylyte generation and suggests that they can form to a depth of around 16 km. This just bridges the brittle/crystal-plastic transition established by Sibson (1977a) for quartz-dominant rocks (such as the Lewisian Gneiss of the Outer Hebrides) at constant strain.

Microbreccia This is volumetrically the most abundant fault rock on the Outer Hebrides, together with its altered counterparts. They are predominantly crush

microbreccias in the nomenclature of figure 1.4, with smaller amounts of crush breccia and fine crush breccia. They occur in zones, up to several kilometres in width, which split the host rock into a series of blocks, varying in scale from centimetres to hundreds of metres. The blocks themselves generally show signs of slight crushing internally and have frequently been rotated, although the bulk of the deformation has been taken up on the network of fractures that traverse the rocks. This takes the form of further crushing along the fractures, resulting in crush microbreccia formation (see figure 1.4).

Terminology becomes rather difficult here depending on the scale. The material along the fractures is generally fine crush breccia, whilst the fractures and their intervening blocks would more correctly be referred to as crush breccia. However, the characteristics of both are similar, although on different scales, and the boundaries between them are gradational. It is therefore proposed to use the term 'microbreccia' here to cover the assemblage of fractures and blocks.

The dominant texture of the microbreccias is one of angular (to subrounded) clasts of variable sizes set in a non-foliated, cohesive matrix which comprises up to 10% of the rock, with the whole traversed by numerous small fractures. Usually there has been very little displacement

across the fractures, although crushing may be extensive. Where movement has occurred along individual fractures, it is generally impossible to determine its extent. Slickensides or wear grooves may be present, indicating direction of motion.

Cataclasite Series These are cohesive, random-fabric fault rocks formed through brittle deformation by micro-cracking, crushing, frictional sliding and rigid body rotation. They differ from microbreccia and crush breccia in that the proportion of matrix to clasts is higher (see figure 1.4). The texture is one of angular fragments set in a finer grained matrix, and they are unfoliated. Depending on how far the process of grain size reduction has gone, the prefixes proto (>10 - 50% matrix) and ultra (> 90% matrix) can be applied (see figure 1.4). Heavily altered equivalents of the cataclasite series are common on the Outer Hebrides, but the grain size of the alteration products is generally so small that it is impossible to tell if they altered syn- or post-deformationally.

Mylonite Series The term mylonite was first used by Lapworth (1885) to describe cohesive, foliated fault rocks of the Moine Thrust Zone. Two distinct types of foliated fault rocks, in addition to the fault gouges, occur in the Outer Hebrides; a high temperature, plastically deformed

type and a lower temperature, brittle type. These will be described under the headings c-type and r-type mylonites (White, 1982) (figure 1.4). In a manner similar to that for the cataclasite series, both mylonite series can be divided into protomylonites (>10 to 50% matrix), mylonites (>50 to 90% matrix) and ultramylonites (>90% matrix).

C-type Mylonite This term was coined by White (1982) to cover mylonites which have deformed predominantly by brittle processes (micro-cracking, crushing, frictional sliding, rigid body rotation) and in which neomineralisation may be important. The foliation is defined by the preferred alignment of clasts or neominerals (usually by cataclastic flow), and should be visible in thin section.

The c-type mylonites of the Outer Hebrides are equivalent to the rocks that Sibson (1977b) termed 'phyllonites', but which, on investigation, can be seen to have deformed by cataclasis. They have generally undergone severe alteration or retrogression syn-deformationally. Fluid/rock interaction is an important process, and has resulted in the generation of a cohesive, poorly foliated, green coloured fault rock, with extensive neomineralisation. Because these rocks hydrated and actively retrogressed during deformation, they can take on a stronger foliation than their 'dry' counterparts under

similar pressures and temperatures. Important processes include formation of a weaker mineral assemblage, especially micaceous or clay minerals with a preferred orientation, strain softening and fluid enhanced sub-critical cracking.

R-type Mylonite This term was defined by White (1982) to describe mylonites in which the important processes were dynamic recrystallisation, sub-grain rotation and grain boundary diffusion. Quartz grains are characteristically drawn out into ribbons. The foliation of many ultramylonites is only detectable using electron microscopy. The r-type mylonites of the Outer Hebrides show a well-developed foliation, with mineralogical banding and elongation of quartz grains evident in hand specimen.

Phyllonite An equivalent of the r-type mylonite series (figure 1.4), but dynamically or statically retrogresed, this rock type was first described by Knopf (1931). Those of the Outer Hebrides usually retain some features indicating crystal plastic deformation (ribbon grains or a lenticular structure), although they generally bear a lower grade mineral assemblage than might be expected for plastically deformed rocks. It is thought for this reason that they retrogressed post-deformationally. In hand specimen, they appear well-foliated and possess a greenish

coloration

1.7 Sense of Shear Indicators

In a basement terrain such as the Outer Hebrides, there is often a lack of stratigraphy or marker horizons to determine displacement across faults, although Francis (1969) and Francis and Sibson (1973) have attempted to match rock types and structures across the fault zone on Barra. To overcome the problem, it is necessary to rely on less direct methods such as shear band orientation or asymmetry of folds. The sense of shear indicators used in this study are shown in figure 1.5. It is important to emphasize that none of them is particularly accurate on its own and that it is essential to look at indicators of several types and in conjunction with other field evidence before arriving at firm conclusions. A further problem is that of reactivation of existing indicators (particularly displaced markers and rotation of any pre-existing foliation) in an opposite sense. For an evaluation of sense of shear criteria see Simpson and Schmid (1983).

Figure 1.1

Location of field area.

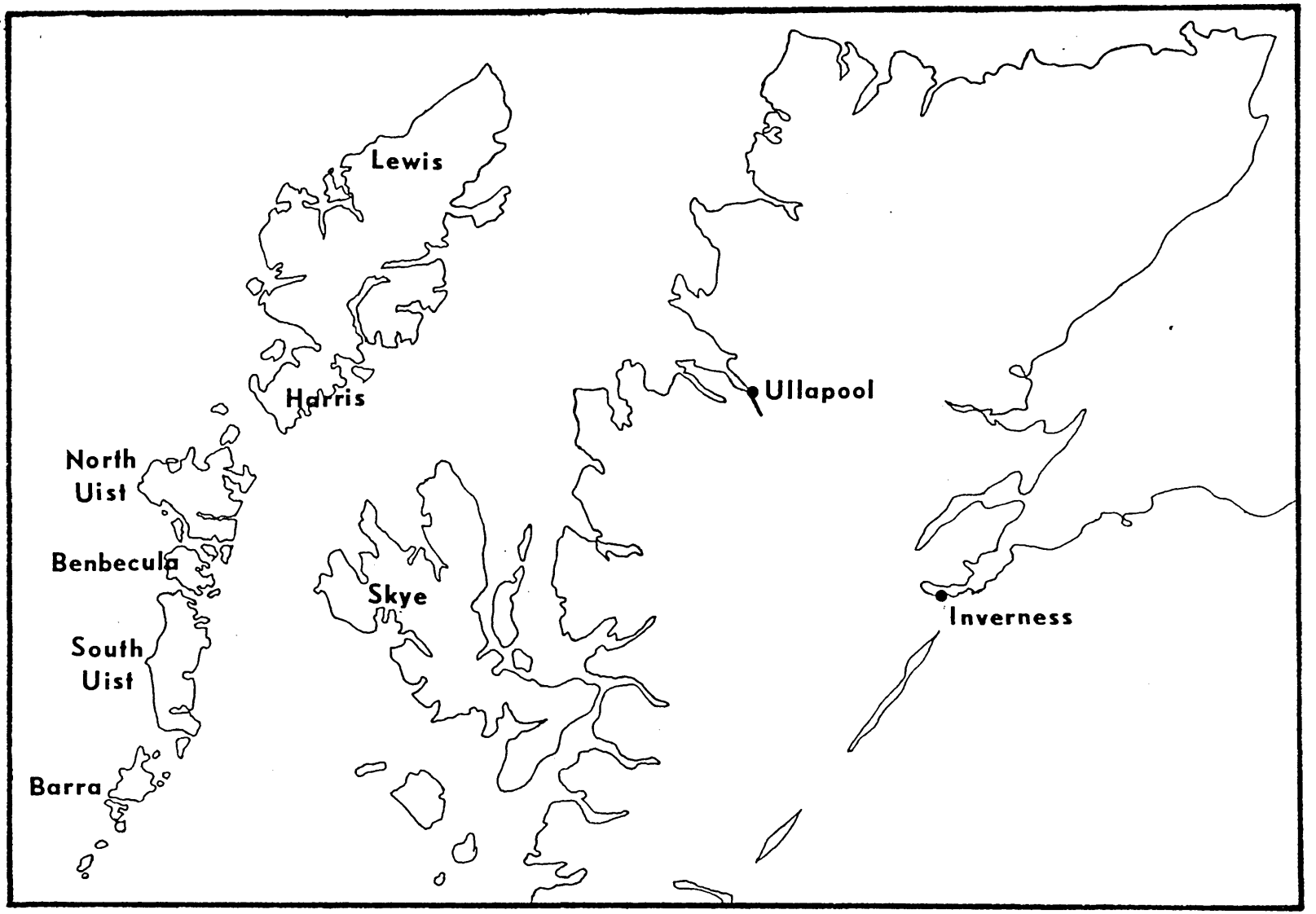

Lewis
Harris
North Uist
Benbecula
South Uist
Barra
Skye
Ullapool
Inverness

Figure 1.2

Simplified geological map of the Outer Hebrides, showing principal rock types and the area of deformed material associated with the Outer Hebrides Fault Zone. Note that there is no one discrete fault plane and the solid line (dashed where inferred) indicates the westernmost limit of fault related deformation.

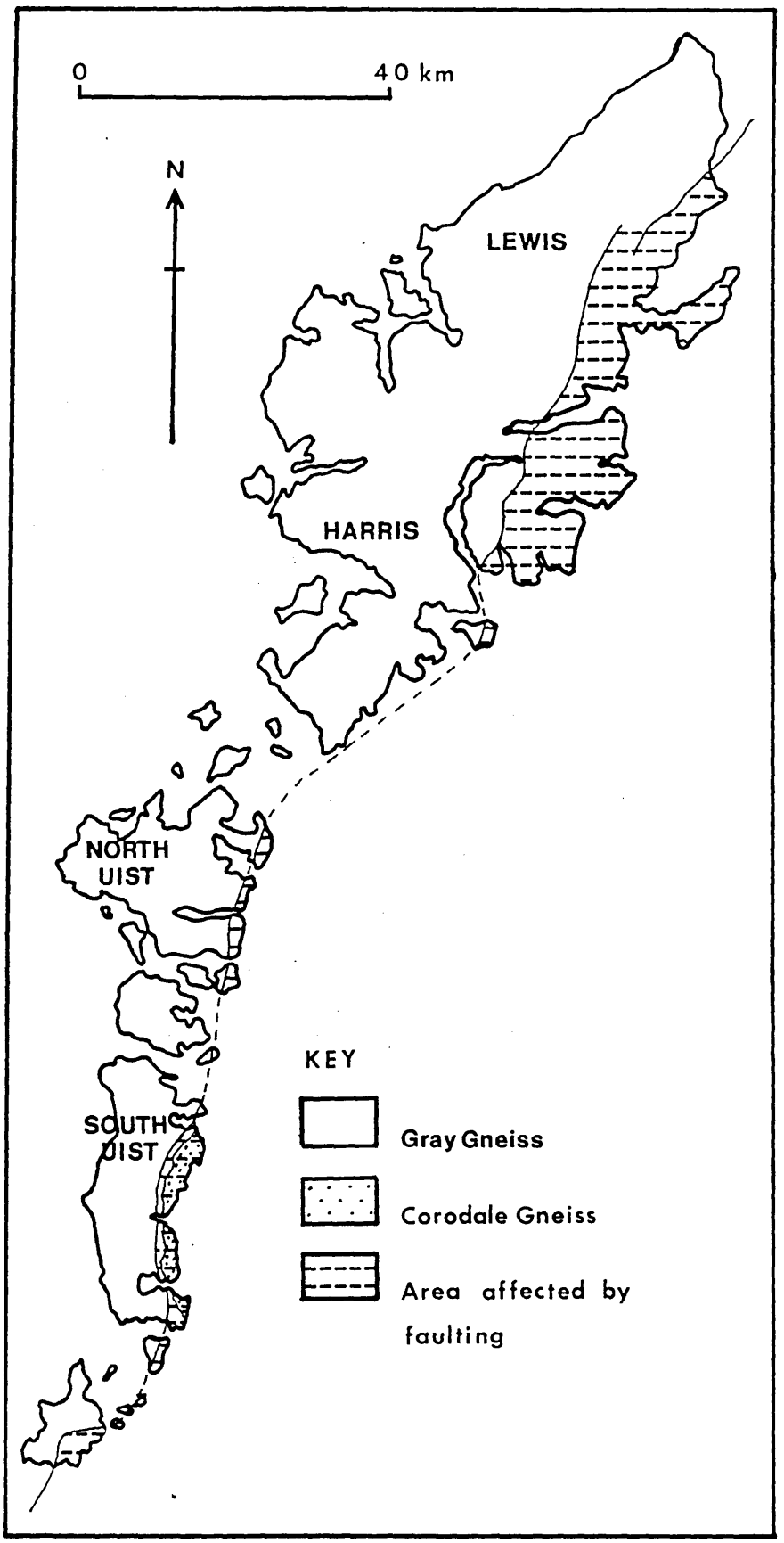

0
40 km
N
LEWIS
HARRIS
NORTH UIST
SOUTH UIST
KEY
Gray Gneiss
Corodale Gneiss
Area affected by faulting

Figure 1.3

Locations of mapped areas and sample traverses. Solid circles indicate areas where field mapping was concentrated. Heavy lines mark the positions of sampling traverses (M: Malasgair and Shiltenish; S: Scalpay; CnH: Crogary na Hoe; BG: Beinn Grotta;
NL: North Lee; B: Burrival; E: Eaval; EG: East Gerinish; LS: Loch Skipport/ Usinish; BnH: Ben na Hoe; NG: North Glendale - cross sections are presented in figure 4.6). The light line indicates the westernmost limit of fault related deformation and stipple represents outcrop of the Corodale Gneiss.

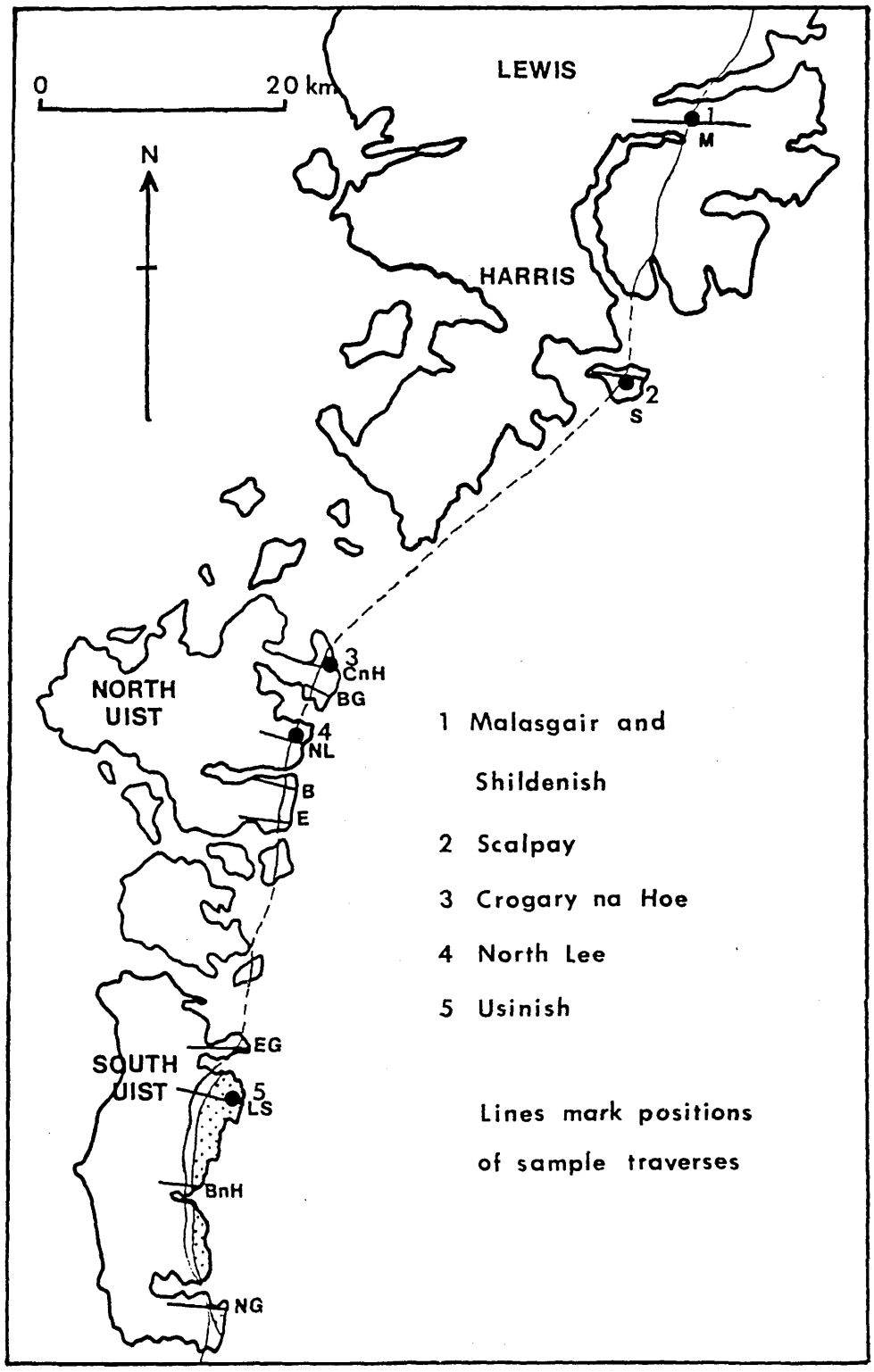

0
20 km
N
LEWIS
HARRIS
NORTH UIST
SOUTH UIST
1
M
2
S
3
CnH
BG
4
NL
B
E
EG
5
LS
BnH
NG
1 Malasgair and Shildenish
2 Scalpay
3 Crogary na Hoe
4 North Lee
5 Usinish
Lines mark positions of sample traverses

Figure 1.4

Classification of fault rock types.

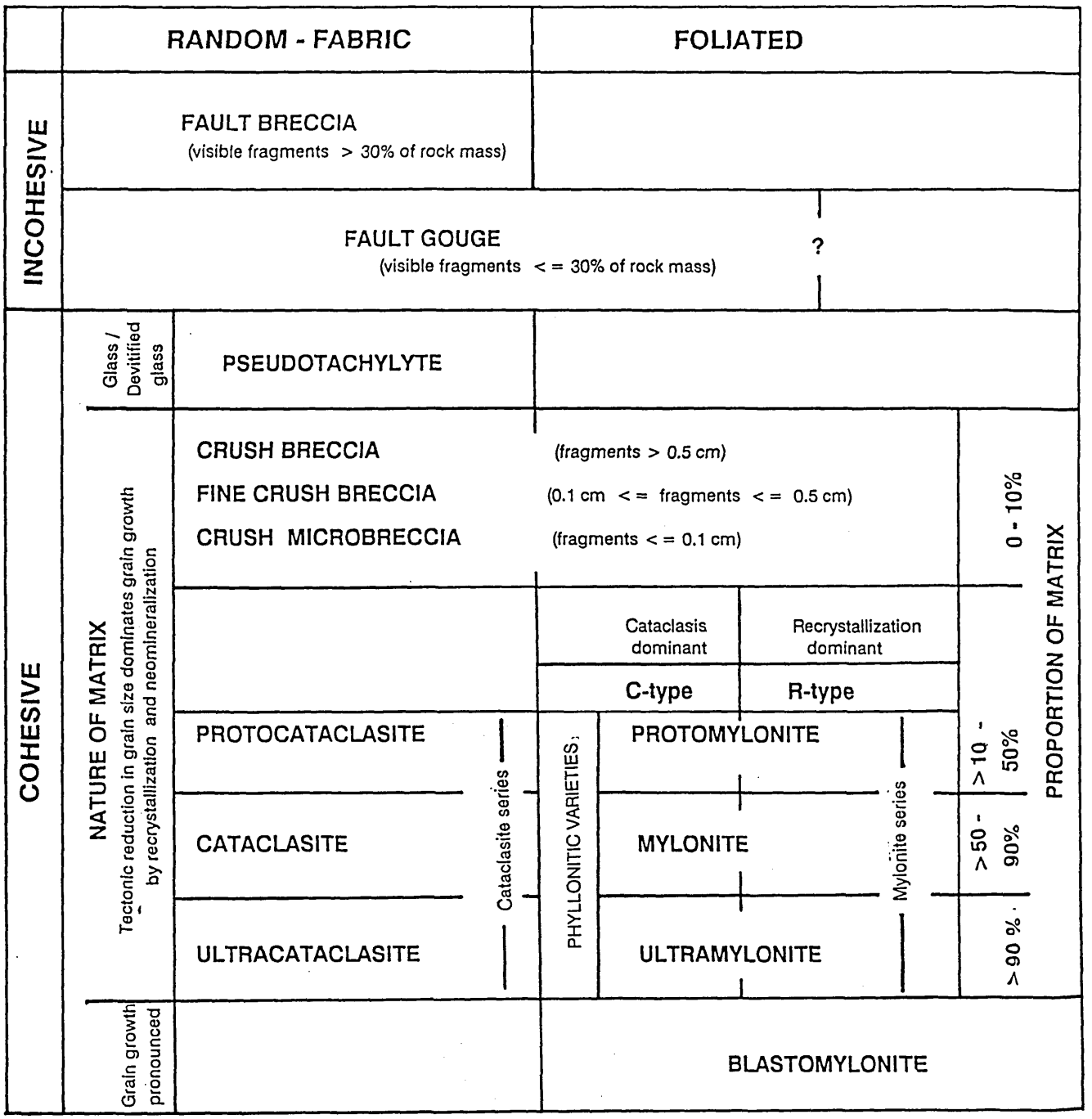

RANDOM - FABRIC
FOLIATED
INCOHESIVE
FAULT BRECCIA
(visible fragments > 30% of rock mass)
FAULT GOUGE
(visible fragments < = 30% of rock mass)
?
COHESIVE
NATURE OF MATRIX
Tectonic reduction in grain size dominates grain growth by recrystallization and neomineralization
Glass / Devitified glass
PSEUDOTACHYLYTE
CRUSH BRECCIA
(fragments > 0.5 cm)
FINE CRUSH BRECCIA
(0.1 cm < = fragments < = 0.5 cm)
CRUSH MICROBRECCIA
(fragments < = 0.1 cm)
0 - 10%
Cataclasis dominant
Recrystallization dominant
C-type
R-type
PROTOCATACLASITE
CATACLASITE
ULTRACATACLASITE
Cataclasite series
PHYLLONITIC VARIETIES:
PROTOMYLONITE
MYLONITE
ULTRAMYLONITE
Mylonite series
> 10 - 50%
> 50 - 90%
> 90 %
PROPORTION OF MATRIX
Grain growth pronounced
BLASTOMYLONITE

Figure 1.5

Criteria observed in the rocks of the Outer Hebrides Fault Zone which allow establishment of senses of displacement, drawn to represent a sinistral sense of shear.

1 Asymmetry of intrafolial folds.

2 and 3 Displaced markers, e.g. mineralogical banding, veining.

4 Rotation of pre-existing or generated foliation.

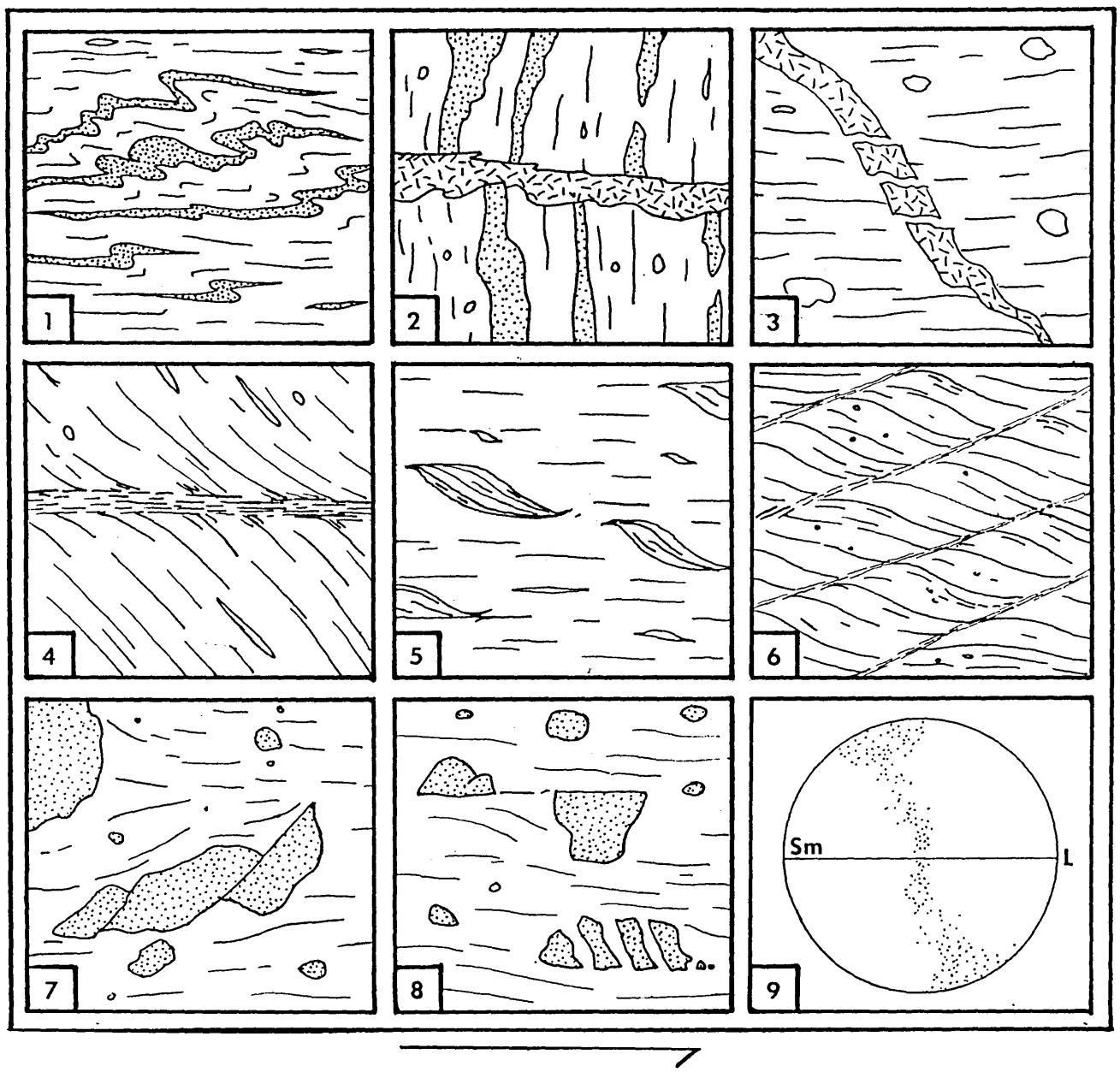
5 Asymmetry of pinched out tails of porphyroclasts, e.g. mica fish.

6 Shear band foliation oblique to mylonitic foliation. Best developed in phyllosilicate-rich rocks.

7 Shear fractures within relatively hard porphyroclasts, e.g. garnets.

8 Rotation of mineral fragments formed by tensile fracturing, and displaced fragments on micro-shears parallel to the main foliation.

9 Asymmetric quartz c-axis girdles with respect to the foliation.


1
2
3
4
5
6
7
8
9
Sm
L

Chapter 2

Previous Work

2.1 Introduction

Prior to the 1920's, no detailed geological map of the Outer Hebrides had been produced, although some descriptions of the lithologies present had been undertaken. These early descriptions are notable for the consistency with which their authors recorded the presence of fault rock products. For example, MacCulloch (1819) recorded ultracataclasite and pseudotachylyte on South Uist and Barra (describing them variously as "trap" and "basaltic paste") and the transition of crushed gneiss to "argillaceous schist" on the east coasts of North Uist and Lewis. His map (op. cit., volume III) shows the Hebrides as being composed of undifferentiated Lewisian gneiss with a narrow band of "argillaceous schist" running down the eastern coastline, approximating to the position of the Outer Hebrides Fault Zone. Heddle (1888) and Dougal (1928) recorded the presence of extensively crushed gneiss at various localities.

The fault was first recognised as such by Jehu and Craig, who produced a series of reports (1923, 1925, 1926, 1927, 1934) detailing many aspects of Hebridean geology. It was not until the work of Coward (1969) and Sibson (1977b) that much interest was shown in the fault, or its importance realised. There can be little doubt today that the fault is of great relevance to the evolution of NW

Scotland, probably on a par with the Moine Thrust. The Outer Hebrides Fault Zone has had a much longer and more complex history than the Moine Thrust and many of its problems (e.g. the number, senses of displacement and absolute timing of the phases of deformation) may never be resolved.

This chapter outlines previous work on the fault zone, both land-based and, more recently, sub-surface studies.

2.2 Nomenclature

The existence of the fault zone was first recognised by Jehu and Craig (1923, 1925, 1926, 1927, 1934) although Kursten (1957) appears to have been the first to name it. He refers to the 'Hebridean Thrust', thus establishing a precedent in terminology - all subsequent workers in this area have used the adjective 'thrust' in conjunction with a geographical qualifier.

Dearnley (1962) used the name 'Outer Isles Thrust Plane', which carries the unfortunate implication that the fault zone can everywhere be regarded as a single, continuous, planar feature, which is far from the truth. Hopgood (1971) reverted to Kursten (1957)'s term 'Hebridean Thrust' whilst Francis (1969, 1973) used 'Outer

Hebrides Thrust'. Coward (1969, 1972) termed the zone 'Outer Isles Thrust', thus introducing the name most frequently used in recent literature (e.g. Smythe, 1980; Smythe et al., 1982; Brewer and Smythe, 1984).

Sibson (1977b) used the phrase 'Outer Hebrides Thrust'as he felt "it follow(s) the established mainland practice where the term 'Moine Thrust' refers to a highly complex zone... it is also the most specific geographically. Thus...the name...is used to refer to the whole assemblage of crush zones, thrust planes and mylonite belts which make up the thrust complex."

The fault was originally identified as a thrust because of the presence on South Uist of the granulite-facies Corodale Gneisses to the east of the fault zone, which outcrop at a higher structural level than the lower grade Gray Gneisses to the west (see figure 1.2). Field evidence supports the suggestion of McQuillin and Watson (1973) that the fault may here be exploiting a pre-existing line of density contrast, possibly inherited from the Scourian. This means that the granulites were not necessarily brought up from depth, but may represent an unretrogressed area surviving from the Scourian. In view of the distinct differences in whole rock geochemistry between these two lithologies (see chapter 6), this seems a reasonable possibility.

Sibson (1977b) noted the presence of features indicative of extensional movement; these he attributed to a minor phase of lag sliding following the main thrust-sense motion. More recent field and microstructural evidence (White and Glasser, 1987; also chapters 4 and 5, this thesis) and also seismic interpretations (Brewer and Smythe, 1986) suggest that there has been a considerable element of normal reactivation along the fault zone.

The true extent of the normal reactivation is unknown, but it is likely to have been considerably greater than Sibson (1977b) envisaged. It is inferred elsewhere in this thesis (section 4.6) that extensional displacement exceeded thrust-sense movement, and Wernicke (1986) has gone so far as to infer that the fault zone may never have been a thrust.

Hence it is considered that the term Outer Hebrides Fault Zone is more appropriate. 'Fault' as it is considered to be the most accurate description in the light of current research, and 'Zone' to prevent any assumption that it is a discrete fault plane.

2.3 Land-based Studies

Mapping MacCulloch (1819) was the first person to note the presence of fault rocks on the Hebrides, and Heddle (1888) and Dougal (1928) recorded outcrops of extensively crushed gneiss at various localities. Peach and Horne, the pioneers of NW Scottish structural geology, wrote about the islands in 1930, but had regretably restricted their explorations to Lewis.

The first detailed work on the whole island chain was that produced by Jehu and Craig in a series of maps and reports dated 1923, 1925, 1926, 1927 and 1934. These reports began with a description of the Barra Isles and worked northwards, covering in turn South Uist and Eriskay; North Uist and Benbecula; South Harris;and culminating with North Harris and Lewis. The authors recognised the 'flinty crush phenomena' to be cataclasites, and traced a "belt of crushed and sheared rocks, the base of which rests on a thrust plane" along the length of the islands. It is probable that they favoured a pre-Torridonian age for the fault movement, as they assign the Stornoway Formation (see chapter 3) to the Torridonian.

There were no further investigations until Kursten's (1957) work heralded a new phase of mapping, in which smaller areas were studied in greater detail. More recently, a research group from Imperial College, mostly

under the supervision of the late Janet Watson, have investigated various aspects of Hebridean geology and a number of PhD theses resulted. Amongst these are Hopgood (1964), Myers (1968), Coward (1969), Francis (1969), Graham (1969), Dickinson (1974), Witty (1975), Sibson (1977b), Soldin (1977) and Horsley (1978). Many of these theses touch only marginally, if at all, on the fault zone, exceptions to this being the works of Francis (see also Francis, 1973; Francis and Sibson, 1973).

One result of this areal approach was that conclusions from one area were often applied to other areas, in spite of the inhomogenous nature of the deformation and metamorphism demonstrated by Coward (1973a; 1973b) and Lisle (1974).

The most recent phase of study has been concerned with the Outer Hebrides Fault Zone itself, from both a structural (Sibson 1977a; 1977b) and a geophysical (see section 2.4) point of view. Sibson's work has done much to clarify fault rock nomenclature and the modes of formation of the fault rocks. The now widely-accepted model of a fault zone transecting the continental crust was formulated from his work on the Outer Hebrides.

Petrography There has been a fair amount of work carried out on the petrography of the various supracrustal

complexes and the gneisses, but petrographic studies of the rocks of the fault zone are very limited. Jehu and Craig's series of reports (see last section) contain some painstaking petrological descriptions of the ultracataclasites and pseudotachylytes, although they used the field term 'flinty crush rock' to refer to both. This confusion persisted as recently as Francis (1969) although he recognised the possibility that the pseudotachylytes formed by melting rather than crushing. Coward (1972) mentions a 10 metre thick layer of pseudotachylyte on Ben Kenneth on South Uist; on investigation this proved to be ultracataclasite.

It is now widely accepted that pseudotachylytes are generated by frictional melting resulting from rapid brittle failure (Sibson, 1975a; Passchier, 1982; Maddock, 1986) rather than by mechanical degradation (but see also Wenk, 1978). By their nature, it is often virtually impossible to distinguish ultracataclasites from pseudotachylytes in hand specimen. It is therefore recommended that usage of the name pseudotachylyte in the field is reserved for those rocks which can be seen to possess intrusive features. Even this will not prove entirely satisfactory, as it is possible to find ultracataclasite veins displaying an intrusive geometry (see plate 4.4*c*).

Coward (1969) gives a brief overview of the various fault rocks, despite confusions of terminology as outlined above. Sibson (1977b) presents the classic account of the fault rocks of the Outer Hebrides, although his emphasis was on mapping rather than petrography. His thesis includes some excellent plates, especially of the various mylonites, and gives typical mineral assemblages for the different rock types.

Geochemistry Most geochemical analysis has concentrated on those rocks not affected by the fault zone. Wigley (pers. comm.) has looked at a smaller scale, higher temperature shear zone feature on the northwest coast of North Uist, but his conclusions are not of much relevance to this project. Maddock (1986) has undertaken a detailed study of the composition of the pseudotachylytes and how this varies with their host rock. Jones (pers. comm.) has looked briefly at whole-rock variations across part of the fault zone on Lewis, to see if these could account for differences in seismic reflectivity.

Radiometric dating has been extensively carried out on the Lewisian gneisses. Much of this work has been done on gneisses from the mainland of northwest Scotland, but the ages which have been obtained from the Outer Hebrides are of the same range, suggesting a similar metamorphic

history. Briefly, the gneisses have undergone two main metamorphic events; granulite facies from 2900 - 2200 My and amphibolite facies from 1950 - 1550 My. Radiometric dating of the Lewisian is discussed in more detail in section 3.2, together with possible precursor rocks for the gneisses.

The only radiometric dating to have been attempted on the fault rocks was done for Sibson (1977b) using the K/Ar method. Results are variable, with the pseudotachylytes recording a wide spread of dates (from 2056 $\pm$ 80 to 442 $\pm$ 17 My) and the phyllonites (= c-type mylonites in this case) grouping around 400 My (late Caledonian). The large scatter in pseudotachylyte dates is thought to be due to the quantity of protolith remaining and to incomplete isotopic resetting of the melt phase. The dates from the phyllonites are probably more accurate, although there has been a considerable change in their composition during their formation and this may have affected isotopic ratios. It is possible that Ar/Ar step degassing might give better and more reliable results.

2.4 Sub-Surface Studies

With the current interest in constraining Caledonide basement geology, there have been several geophysical

surveys undertaken in this area. The most important of these are listed in Table 2.1 and will be discussed briefly below. In addition, a relatively recent bathymetric sheet (Roberts et al., 1977) is available, which shows the extent of the various sedimentary basins around the Outer Hebrides. From the bathymetry, the half-graben nature of the basin margins is clear and the location of the Minch Fault can be seen as a series of linear depressions (McQuillin and Binns, 1973).

Binns et al. (1974) have produced an excellent summary of all aspects of the Sea of the Hebrides area for the I.G.S., combining gravity, magnetic, bathymetric, shallow and deep seismic reflection and rock drilling data. More recently, a series of seismic reflection lines (e.g. MOIST, WINCH, DRUM, WISE) have been shot for the British Institutions Reflection Profiling Syndicate, and will be described below.

Gravity and Aeromagnetic Studies Gravity-meter and proton-magnetometer measurements made in the vicinity of the Outer Hebrides reveal gravity lows of as little as 26 mgals over Lewis and Harris (Bullerwell, 1965). These correspond (McQuillin and Watson, 1973) to the location of the late Laxfordian Granite Migmatite complex (as described in section 3.2). An aeromagnetic map of the British Isles, compiled by the I.G.S. (1972), shows a

string of gravity highs running along the eastern seaboard, which has been interpreted as suggestive of dry, dense granulites being more extensive than surface outcrop would indicate (McQuillin and Watson, 1973). Bouguer anomaly studies have also been made more recently by Hussain and Hipkin (1981) for northern Britain; a larger scale map showing the west coast of Scotland and the Hebrides is presented in Brewer and Smythe (1986, Plate 4). They show similar features to those described above.

Conductivity Studies A conductivity traverse running northnorthwest/southsoutheast over the Scottish mainland (see figure 2.1), roughly parallel to the LISPB seismic refraction profile (as discussed in the next sub-section), was undertaken by Hutton et al., 1980. Based on this, they have attempted to construct a two-dimensional model of the mainland crust and mantle across the Caledonides, demonstrating crustal thickening associated with the Caledonian Orogeny, but results so far have been too crude to be widely applicable.

Seismic Studies - On-Land and at Sea Figure 2.1 shows the locations of the relevant seismic studies. Most of these are concerned with imaging sub-sea areas, with the exceptions of the LISPB regional refraction profile (Bamford et al., 1978; Bamford, 1979) which traverses the mainland from Cape Wrath in the north to the Southern

Uplands Fault in the south, and LUST (Hall, 1978), which measured refraction velocities in the extreme NW of mainland Scotland. Also on land, but on a much smaller scale, is a study done by Jones (pers. comm.) across an area of Lewis near Loch Seaforth.

The first two seismic studies mentioned above were concerned with determining basement characteristics (in both cases, Lewisian gneiss), whilst the last imaged a small part of the Outer Hebrides Fault Zone, and is not widely available. It shows poorly resolved east dipping reflectors interpreted as representing the Outer Hebrides Fault Zone. LISPB on the mainland revealed

a) the crustal structure beneath the Caledonian orogenic belt to be asymmetric, with a considerable thickening of crust below the fold belt; and

b) that any Caledonian destructive plate boundary was probably located south of the Southern Uplands Fault (Bamford et al., 1978; Bamford, 1979).

LUST (location on figure 2.1) was undertaken with the aim of demonstrating the presence of granulite facies rocks below the amphibolite facies gneisses of NW mainland Scotland. However, analysis of the results suggests that there is no laterally continuous body of granulite facies rocks, similar to those of the central belt of the mainland Lewisian, existing at depths of less than 4 km

(Hall, 1978). This implies that the granulite facies rocks Harris are not simply the core of a large scale antiformal structure with amphibolite facies rocks flanking it to the north and south.

Of the sub-sea surveys, the Hebridean Margin Seismic Experiment (see figure 2.1) was the earliest to be shot. Interpretations have been made by Armour (1977) and Bott et al. (1979). The profile failed to record any mid-crustal phases. The North Atlantic Seismic Project (figure 2.1), discussed in Smith and Bott (1975), indicated a two-layer crust under the foreland with a Moho depth of 26 $\pm$ 2 km. Sonobuoy refraction profiles (not shown) have been undertaken west of the Outer Hebrides, and results are presented in Jones (1978, 1981), White et al. (1982) and Jones et al. (1984). These profiles show the crust to be mostly Laxfordian, with many offshore faults apparently related to Precambrian shear zones in the basement. These highly foliated belts seem to have facilitated stress relief by normal faulting during Permo-Triassic rifting (Jones, 1981).

The most recent seismic lines to be shot have been the Western Isles Seismic Experiment (WISE), which runs from Barra to Arran (results have not yet been published); the Moine and Outer Isles Seismic Traverse (MOIST); the Western Isles - North Channel (WINCH) deep crustal

reflection profile and the Deep Reflections from the Upper Mantle (DRUM) profile (see figure 2.1 for locations). The results from MOIST, DRUM and the section of WINCH perpendicular to the strike of the Outer Hebrides Fault Zone all show similar features - a section, based on MOIST, is given in figure 2.2, and will be discussed later.

Deep Seismic Reflection Profiles MOIST was the first line to be shot for BIRPS, in 1981 (see figure 2.1 for location). It extends to around 15 seconds two way travel time. The resolution is good, and the trace of the Outer Hebrides Fault Zone shows clearly. The existence of the Flannan Fault (figure 2.2), an upper mantle reflector, was not suspected prior to the MOIST results. Interpretations of MOIST have been made by Smythe (1982); Smythe et al. (1982); Brewer and Smythe (1984); Butler and Coward (1984); Blundell (1984); Blundell et al. (1985); Wernicke (1986) and Enfield and Coward (1987). MOIST suggests that there has been a considerable amount of extensional motion taken up along the Outer Hebrides Fault Zone.

WINCH (figure 2.1) was shot for the BIRPS group in 1982. It extends the work of MOIST and has been discussed by Brewer et al. (1983) and Brewer and Smythe (1986). WINCH supports the MOIST interpretation that normal-sense displacement has occurred along the Outer Hebrides Fault

Zone. The Moho resolves as a series of strong reflections at around 27 km, and its depth appears uniform across the area covered. The Outer Hebrides Fault Zone, and possibly also the Flannan Fault, seems to flatten into the lower crustal reflective layer, suggesting that the lower crust is a region of high strain (Brewer and Smythe, 1986).

DRUM was shot in 1984, also for BIRPS. It runs sub-parallel to MOIST, slightly further to the north and extending somewhat further westwards (figure 2.1). Unlike MOIST, it is an ultra-deep reflection line and was shot and processed to 30 s TWT (approximately 110 km depth). Full results from DRUM have not yet been published, although a preliminary report (McGeary and Warner, 1985) is available.

Characteristics of the Seismic Profiles The seismic profiles resolve four main sets of features. Firstly, there is a series of eastward dipping reflectors (figure 2.2) which correspond, from west to east, to the Flannan Fault, the Outer Hebrides Fault Zone, the Minch Fault and then a package of faults, one of which corresponds to the Moine Thrust. Secondly, above many of the faults are a series of sedimentary basins (figure 2.2). Thirdly the data indicate the presence of a layer of sub-horizontal reflectors at around 9 s two way travel time, interpreted as representing the Moho (figure 2.2). Finally, the

eastern end of the profiles show strong, eastward-dipping reflectors in the upper and middle crust. These have variously been interpreted as representing foliated Caledonian rocks (Butler and Coward, 1984) or as Torridonian sediments overlain by foliated Caledonian rocks (Brewer and Smythe, 1984).

Looking at the faults first, the Flannan Fault is interpreted as a tectonic discontinuity within the upper mantle (McGeary and Warner, 1985; Cheadle et al., 1987). It does not appear to extend into the upper crust within the profile but flattens into the lower crust (Matthews and Cheadle, 1986). The Outer Hebrides Fault Zone, the Minch Fault and the unnamed faults to the east form the western boundaries of a series of sediment-filled half grabens extending under the Minch and the West Orkney Basin. They appear to be gently listric in appearance (figure 2.2), to extend to the surface and to shallow in dip to the east. They have been interpreted by Brewer et al. (1983) and Brewer and Smythe (1984) as reactivated Caledonian thrusts.

The reflectors defining these faults extend to within around 10 km of the Moho, where they probably flatten (Brewer and Smythe, 1984). The westward dip of the sediments and the presence of a tilted top to the basement above the faults suggests that the basins formed in an

extensional environment. The actual position of the Moine Thrust on the sections is debatable, owing to the presence of offshore faults along the north coast of Scotland, which offset its trace. The preferred reflectors resolve as a shallow dipping, slightly planar feature, which also appears to have undergone extensional reactivation.

The sedimentary basins above the half-grabens are up to 9 km deep (figure 2.2). The age of the basin infill is poorly constrained (Binns et al., 1974) as many of the typical sediments are of red-bed facies (e.g. Torridonian, Devonian and Permo-Triassic) which are very similar in appearance, and little commercial drilling has been undertaken. In the east the sediments are Devonian and Permo-Triassic, with Permo-Triassic formations becoming more prevalent westwards (Cheadle et al., 1987). The sediments of the Minch and North Lewis basins are probably Permo-Triassic to Lower Jurassic in age (Binns et al., 1974), although they may have a basal layer of Torridonian sediments (Brewer and Smythe, 1986; Cheadle et al., 1987).

The sediments in the half-grabens dip westwards, as does the top of the basement, suggesting formation in an extensional environment, possibly by Devonian reactivation along earlier Caledonian structures (Enfield and Coward, 1987). The basin infill shows a tendency to young westwards in successive basins, suggesting that

extensional reactivation may have moved progressively west with time.

Of direct interest to this project, the Outer Hebrides Fault Zone resolves as a planar, continuous reflector to within 5 km of the Moho, where it becomes more diffuse. Below the fault, an interpretation suggests that the Moho is offset in a normal sense (Cheadle et al., 1987). It has also been suggested (Peddy, 1984; Brewer and Smythe, 1984) that the fault can be extrapolated to cut the Moho, or to flatten out along the Moho (Enfield and Coward, 1987), whilst Wernicke (1986) has postulated that both the Outer Hebrides Fault Zone and the Minch Fault might extend down through the lithosphere but there is no seismic evidence for this.

Figure 2.1

Locations of deep seismic profiles (dashed lines) and explosion crustal refraction profiles (dotted lines) referred to in table 2.1 and in the text. After Brewer and Smythe (1986) and Smythe (1987).

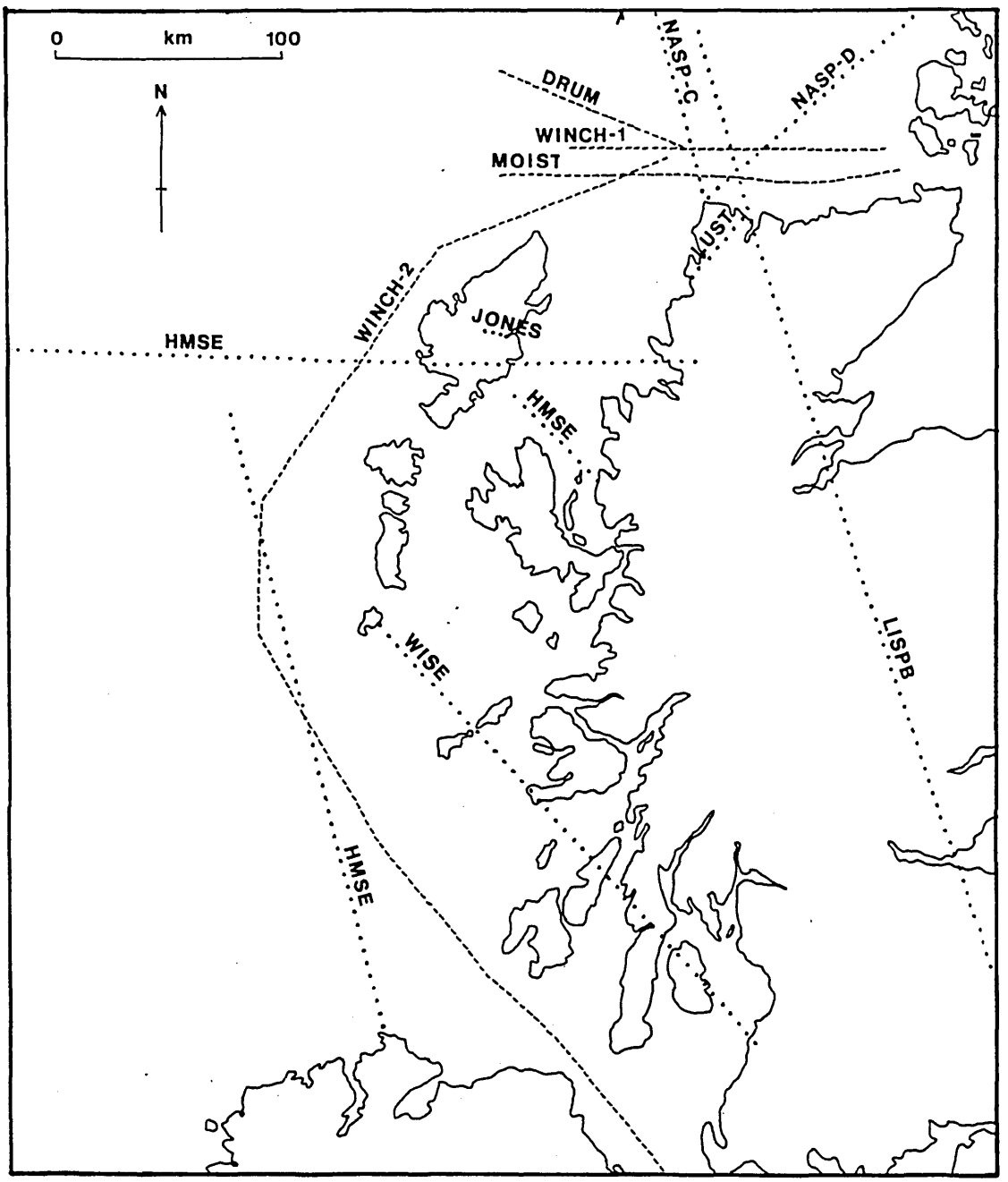

0
km
100
N
DRUM
NASP-C
NASP-D
WINCH-1
MOIST
KUST-3
WINCH-2
JONES
HMSE
HMSE
WISE
LISPB
HMSE

Figure 2.2

An interpretation of the MOIST seismic profile (see figure 2.1 for location), showing the sedimentary basins, their possible infill and the basin bounding faults. FF is the Flannan Fault; OHFZ is the Outer Hebrides FAult Zone; MF is the Minch Fault.

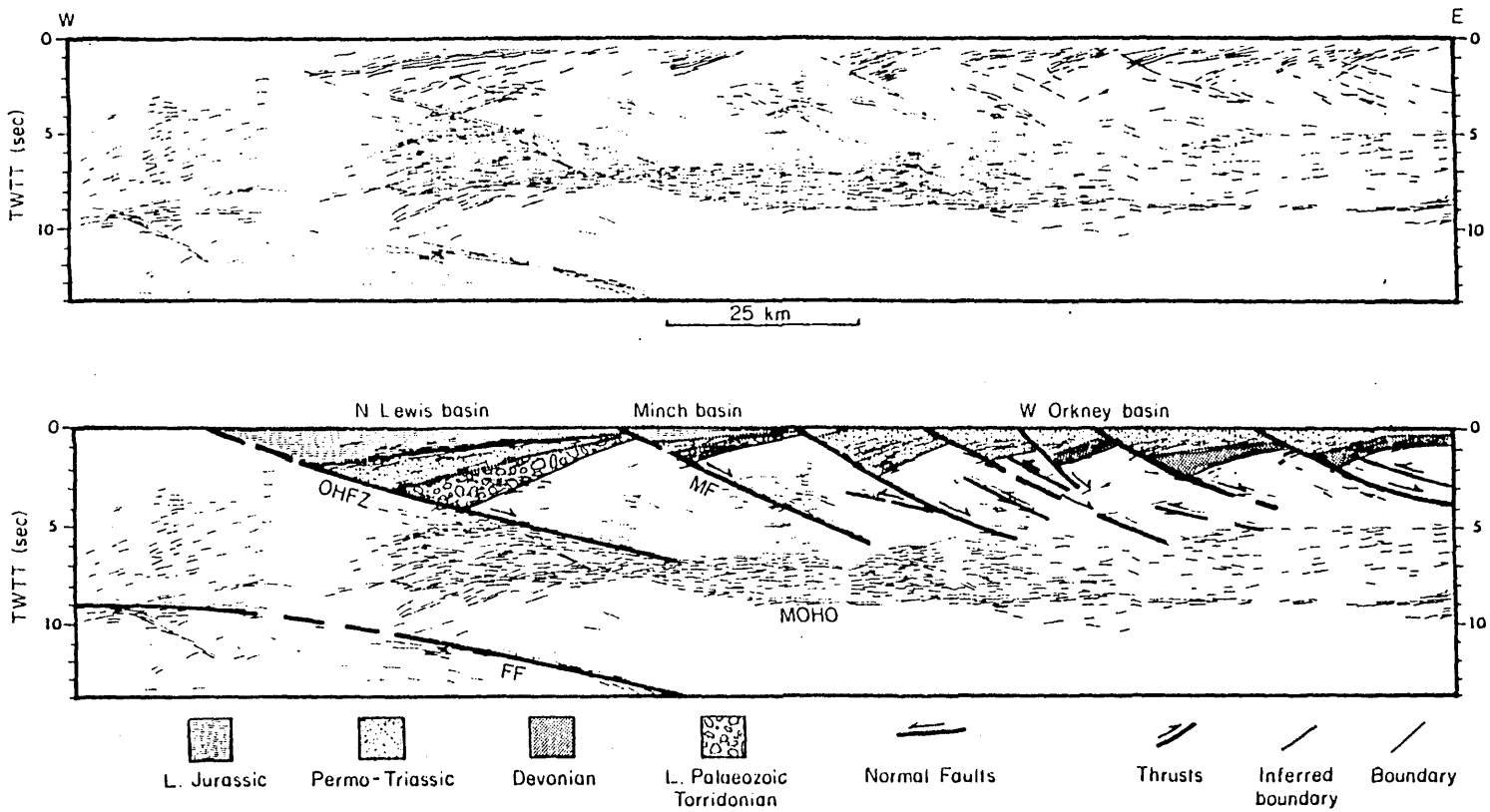

W
E
TWTT (sec)
0
5
10
25 km
N Lewis basin
Minch basin
W Orkney basin
OHFZ
MF
MOHO
FF
L. Jurassic
Permo-Triassic
Devonian
L. Palaeozoic
Torridonian
Normal Faults
Thrusts
Inferred boundary
Boundary

Table 2.1

Table of Geophysical Surveys Concerned with the Outer Hebrides Area and the Nature of the Continental Crust and Caledonian Foreland

Name and Type of Survey	Location	Interpreted/Undertaken
Gravity meter and Proton magnetometer	Outer Hebrides	Bullerwell, 1965
Aeromagnetic map	1:625 000 of Britain	I.G.S., 1972
HMSE (1970)	along continental margin at 58 N between Rockall Trough and the Hebridean Shelf	Armour, 1977 Bott et al., 1979
LISPB (1974)		Bamford et al., 1978 Bamford, 1979
NASP (1975)		Smith and Bott, 1975
LUST (1978) Seismic Refraction	40 km line, Durness to Badcall	Hall, 1978
Sonobouy Refraction Profile	continantal margin west of Hebrides	Jones, 1978, 1981 White et al., 1982 Jones et al., 1984
Conductivity Survey		Hutton et al., 1980
Bouguer Anomaly Map	northern Britain	Hussain and Hipkin, 1981
MOIST Seismic Reflection	roughly east-west off north coast of Scotland	Smythe, 1982 Smythe et al., 1982 Brewer and Smythe, 1984 Butler and Coward, 1984 Blundell, 1984 Wernicke, 1986
WISE	southeast from Barra to Arran	As yet unpublished
WINCH	west and north coasts of Scotland	Brewer et al., 1983 Brewer and Smythe,

		1986
DRUM	east-west off north coast of Scotland	McGeary and Warner, 1985 Cheadle et al., 1987 Smythe, 1987

Chapter 3

General Geology

3.1 Introduction

The Outer Hebrides are composed mainly of highly folded sialic continental crust (basement) with associated supracrustals of Archaean age, and a restricted amount of lithified cover. The nature of the basement, prior to deposition of the supracrustal succession, is uncertain, although both appear to share the same metamorphic history. This combination of metamorphosed basement and supracrustals, together with some basic dykes, is virtually identical to the material forming the Caledonian foreland of mainland Scotland. The Outer Hebrides contains the type locality by which these rocks acquire the name Lewisian - the isle of Lewis.

Briefly, the metamorphism that affects the Hebrides can be split into two distinct episodes; the granulite facies Scourian (after Scourie, NW Scotland) and the amphibolite facies Laxfordian (after Laxford, NW Scotland) with the two events separated in time by the widespread intrusion of basic material - the Scourie dykes (Sutton and Watson, 1951). The lithologies will be described under the divisions of basement, supracrustals and cover, but in view of their similar tectonothermal development, the metamorphism of basement and supracrustals will be discussed together.

A generalised stratigraphy showing the main tectonothermal, intrusive and depositional events affecting the Outer Hebrides is presented in table 3.1

3.2 Lithostratigraphy

Basement Basement of Lewisian age comprises nearly all of the exposure on the Outer Hebrides (Jehu and Craig, 1923; 1925; 1926; 1927; 1934; Peach and Horne, 1930) and is subdivided into amphibolite facies Gray Gneisses and the more restricted higher grade Corodale Gneisses (Dearnley, 1962), whose outcrop is dominantly confined to the east coast of South Uist (see figure 1.2).

Description and Origin of the Gray Gneisses These rocks are compositionally homogenous on a large scale and coarse grained and banded in hand specimen. They bear a quartz - plagioclase - biotite - hornblende assemblage, and exhibit a foliation due to alignmenet of biotite. Within them are patches of metasediments and more basic amphibolites, as well as stringers of granitic and pegmatitic material (Davies et al., 1975).

The origin of the Gray Gneisses is somewhat obscure. Dearnley and Dunning (1968) suggest that they were derived by metamorphism of a greywacke or leptite series. Skinner

(1970) agreed with this interpretation, explaining anomalous whole-rock Rb/Sr values as due to Rb loss during metamorphism and Lowman (1984) has also suggested a sedimentary precursor.

Sheraton (1970), writing about the mainland Lewisian, and Bowes et al. (1971) considered that the Gray Gneisses were derived from a calc-alkaline (basalt-andesite-dacite) volcanic precursor, with only minor intercalations of sediments. Pidgeon and Aftalion (1972) and van Breeman et al. (1971) favoured a plutonic, non-orogenic gabbro-anorthosite-tonalite basement complex. Bridgwater et al. (1973) proposed an elaborate model comprising a granitic-granodioritic-tonalitic basement with a small quantity of basic to intermediate volcanics, intrusions and predominantly chemical sediments. They further suggest that the smaller patches of aluminous rocks present in the southern isles and in South Harris, although usually regarded as of definite metasedimentary origin (Coward et al., 1969), could have had a volcanic precursor.

Consensus of opinion seems to favour an igneous origin for the majority of the Gray Gneiss (Weaver and Tarney, 1980; Park and Tarney, 1987; Fettes and Mendum, 1987), with Holland and Lambert (1973) finding that the bulk composition resembles that of intermediate-acid calc-alkalines, though there is less agreement as to

whether these were volcanic or plutonic. Pidgeon and Aftalion (1972) assign a geochronological significance to discordant U-Pb dates obtained from zircons from Harris and attribute this to a possible plutonic origin. However, it is possible that even if the Gray Gneisses were of primary igneous origin, they were subsequently metamorphosed as reworked sediments. The geochemical evidence does not conclusively preclude any of the above suggestions. However, recent work by Park and Tarney (1987) suggests that rare-earth element patterns indicate magma generation through partial melting of a mafic source under hydrous high pressure conditions, such as would be found in a subduction zone.

Age of the Gray Gneiss As with the origin, there is disagreement as to the absolute age of the basement, and whether or not it suffered a metamorphism prior to deposition of the supracrustals. Earlier workers (Dearnley and Dunning, 1968; Coward et al., 1969; Watson, 1969), basing their conclusions on petrological and structural considerations, inferred a pre-Scourian metamorphic episode (at around 3000 My) affecting the basement. Bridgwater et al. (1973) suggest that this date be pushed back to 3800 My, with deposition of the supracrustals occurring between 3600 - 3300 My.

Isotopic work suggests that there was no great length of time between formation of the Gray Gneiss precursor and the Scourian metamorphism and hence it is very unlikely that a pre-Scourian tectonothermal event took place. Bowes and Hopgood (1973) developed a complicated model involving a pile of volcanics and derived sediments overlying an anorthosite crust and forming immediately prior to the Scourian. Other workers have been rather more cautious in their interpretations. From whole rock Rb/Sr investigations by Moorbath (1973) the precursors of the gneiss probably separated from a previously undifferentiated upper mantle not more than 100 - 200 My before the Scourian. Isotopic ratios rule out the possibility that the Hebridean gneisses could represent reworking of a significantly older basement complex with anything like normal crustal Rb/Sr ratios (Moorbath et al., 1975).

Discordant U-Pb zircon dates (Pidgeon and Aftalion, 1972) have independently pointed to the same conclusion, that the rocks (of probable igneous origin) formed only a short time before the onset of metamorphism. Hamilton et al. (1979) used Pb and Nd-Sm systematics to suggest that the Lewisian gneiss of mainland Scotland separated from the mantle around 2900 $\pm$ 50 My and that around 200 My elapsed before this material was fully stabilised as crust. Because this date falls well into the Scourian (see

table 3.1), and earlier dates for Scourian reworking have been recorded (Moorbath et al., 1969; Pidgeon and Aftalion, 1972; Moorbath et al., 1975), this figure was regarded as too late by the above authors, and a date of around 3100 My was preferred. However, more recent work (Fettes and Mendum, 1987; Park and Tarney, 1987) suggests that Hamilton et al. (1979) were broadly correct, and that dates of around 2900 - 2700 My are acceptable for the formation of the basement precursor.

Description and Origin of the Corodale Gneisses As has been mentioned previously, the outcrop of the Corodale Gneisses is restricted to the east coast of South Uist. For most of this exposure their margins are highly fractured and deformed, due to the action of the Outer Hebrides Fault Zone. In appearance the Corodales are massive, with little evidence of the mineralogical banding typical of their Gray Gneiss counterparts. Folding is rare and mineral fabrics are only locally developed. They are basic in composition. Quartz is uncommon and ferromagnesian minerals (pyroxene, hornblende, some biotite) predominate, sometimes showing exsolution of magnetite-ilmenite phases and iron-ore minerals around grains.

In hand specimen, grains are variable in size, although

generally fine, and are equant to sub-equant. Banding and foliation show limited development. The assemblage is typically plagioclase - diopside - hornblende, although hypersthene may also be present. Coward (1969) considers the Corodale Gneisses may originally have been a layered basic igneous complex, possibly coeval with similar bodies on South Harris. The outcrop pattern does not appear to support this view. They probably represent large pods of a differing composition within the Gray Gneisses, dating from about the same age. There is even less geochemical evidence for the origin of the Corodale Gneisses than there is for the Gray Gneisses.

The Mashed Gneisses It is unclear if this rock unit is a country rock or a fault rock. From field evidence, it would appear to have been a lithological unit distinct from the Gray Gneisses and the Corodale Gneisses, although it has been so highly altered, possibly in connection with an episode of faulting, that its original nature is undetectable. The Mashed Gneisses were so called by Jehu and Craig (1925), and outcrop as highly altered and fractured acidic rocks on the Usinish peninsula, South Uist. Many of the fractures have been cemented shut by quartz and feldspar, although the rock still tends to split along these planes. In hand specimen, the rock is white to pale greenish in colour, and fine grained, with

no obvious internal features other than small-scale fractures.

Supracrustals These metasediments and metavolcanics were deposited on top of, and may have been partially derived from, the pre-existing basement. Outcrop of the supracrustals is confined to two major zones - on South Harris (the Langavat and Leverburgh belts) and in the Ness area - and as smaller patches (mainly metasedimentary) scattered across the islands. Figure 3.1 shows locations of the major outcrops. For a full description of these lithologies on South Harris see Dearnley (1963) and Dickinson (1974). Watson (1969) provides a detailed and comprehensive account of the Ness Assemblage (figure 3.1). The most important of the minor localities are described fully in Coward et al. (1969) and will only be summarised here.

The Langavat and Leverburgh Belts, South Harris

MacCulloch (1819) first noted marble near Rodil, South Harris, thus suggesting the presence of supracrustals in the area, but it was not until 1963 that Dearnley published a general account of the geology of the area. More recent workers have been Myers (1968), Skinner (1970), Dickinson (1974) (who concentrated on the

Leverburgh metasediments) and Dickinson and Watson (1976).

The supracrustals lie in two zones (figure 3.2) parallel to each other, separated by the anorthosite-gabbros and other rocks of the South Harris Igneous Complex (see later). The northernmost of these zones is named the Langavat Supracrustal Series whilst the southernmost is the Leverburgh. They consist mainly of metasediments - quartzites, graphitic schists, kyanite- garnet-pelitic schists - with less abundant fine-grained interbanded amphibolites and ultramafic pods, interpreted as metavolcanics (Fettes and Mendum, 1987).

Both supracrustal successions have been extensively metamorphosed, folded and sheared during the Scourian and Laxfordian metamorphic events. Major dextral shear zones occur within the Langavat and Leverburgh Belts. Together with more minor shears, they form a shear zone some 10 km in width (Graham, 1980), termed the Langavat Shear Zone. It has been suggested (Coward, 1984) that this represents a low-angle lateral ramp, formed in the early Laxfordian, up which the South Harris granulites (see South Harris Igneous Complex) were thrust towards the NW.

This shear zone was reactivated in the late Laxfordian, when further folding gave rise to a steepening of the shear zone and a reversal of the dip-slip movement (see

Coward, 1984). Suggestions that this shear zone correlates along strike with the Laxford (Dearnley, 1962) or Gairloch (Park, discussion on Dearnley, 1962) shear zones on the mainland have been discounted by Coward and Park (1987), who feel that there has been insufficient strike-slip motion between the Outer Hebrides and the Scottish Mainland for this to be possible.

The Ness Assemblage The Ness Assemblage is located on the northern tip of the isle of Lewis (figure 3.1). As with the South Harris Complex (see later), the Ness rocks do not represent a single event in terms of their formational history, and they too occupy a position removed from the main fault zone. The rocks are mostly pelites, semi-pelites, psammites and calc-silicates, with some basic igneous material occurring as metadolerites and amphibolites.

Structurally, the Ness Assemblage occupies the core of a major north plunging antiform. There is an abrupt junction between it and the surrounding Gray Gneiss. Watson (1969) has suggested that this could be due to its relatively high structural position during later metamorphism; this would not favour recrystallisation and would give a different response to regeneration. It is also possible that the layering within the Ness Assemblage and its more

strongly varied lithologies rendered it less competent than the Gray Gneiss, so that deformation exploited the boundary between the two.

Minor Regions of Supracrustals Generally these are small, isolated patches of metasediments, often poorly preserved. Because of their widespread occurrence across the islands, they are of more relevance to this thesis than the larger scale supracrustal complexes which were unaffected by the Outer Hebrides Fault Zone. The existence of supracrustals within the fault zone enables geochemical and microstructural comparisons with unaffected supracrustals to be made.

Metamorphism (granulite and amphibolite facies) and deformation have combined to obliterate any relict sedimentary structures within these metasediments. The most important localities are described by Coward et al. (1969) in their paper on metasedimentary assemblages. The positions of the larger outcrops are shown on figure 3.1. and a brief summary based on the work of Coward et al. (1969), with a few additions, follows:

Lewis and Harris: Many localities have calcareous metasediments and meta-psammites.

North Uist: At Tigharry, quartzites, meta-semi-pelites and an iron-rich band are exposed. At Scolpaig there is a quartz-rich anthophyllite gneiss. In new exposures created by blasting near the Lochmaddy-Sollas road junction are garnet-rich gneisses, and garnet±biotite±hornblende schists.

Gairbh-Eilean: Garnet-biotite gneiss, garnet±biotite±hornblende schists.

Benbecula: At Market Stance there are sillimanite schists, impure quartzites, garnet-rich gneisses and sillimanite-kyanite gneisses.

South Uist: Many localities show development of staurolite gneiss, garnet gneiss, sillimanite-kyanite-anthophyllite gneiss and semi-pelite and hornblende-biotite gneiss.

Barra: A coarse garnet-biotite gneiss outcrops at Scurrival Point.

Age of Supracrustals The only age constraints available are that the supracrustals must post-date the formation of the basement and pre-date the earliest (Badcallian - see next section) metamorphism (c. 2700 My, from Pidgeon and Aftalion, 1972; Moorbath et al., 1969; Moorbath et al.,

1975; Francis et al., 1971; Humphries and Cliff, 1982).

The Scourian Metamorphism The basement and supracrustals have been subjected to several episodes of metamorphism since their formation - see table 3.1 for a summary. Of the early metamorphisms, there was an initial, widespread granulite facies event occurring at around 2700 My. This represents the Badcallian division of the Scourian metamorphism (Park, 1970). The Inverian division (c. 2400 My), as recorded in the Lewisian rocks of mainland Scotland (Evans, 1965; Evans and Lambert, 1974), is of unknown extent in the Outer Hebrides - no dates have yet been obtained that are convincingly Inverian, but the Scourie dykes (see next section) still show the typical mainland signs of having been intruded into warm country rock at depth. Moorbath et al. (1975) have found a loss of radiogenic Ar-40 from minerals around 2100 My, but it is uncertain whether or not this can be attributed to the effects of the Inverian.

The Scourian metamorphism and associated deformation was responsible for the formation of the present day gneisses and their foliation from the basement and supracrustals. Other than this, little is known for certain about the Scourian on the Outer Hebrides, as the overprinting due to later metamorphic episodes has been fairly complete.

The Scourie Dykes The importance of the Scourie dykes lies in the fact that they are the only known chronological and structural 'marker horizon' within the Lewisian. Work undertaken on the Scottish mainland has demonstrated that these dykes represent a suite of tholeiitic composition, forming a swarm throughout the Lewisian complex. To all intents and purposes they are regarded as being of a simultaneous age of intrusion at c. 2200 My ago. However, of those dykes that have been dated on the Hebrides, the dates tend to be somewhat older than those of the mainland - Lambert, Myers and Watson (1970) obtained average dates of 2440 $\pm$ 60 My. Sutton (1963) has suggested that the emplacement of this dyke swarm marked a definite stage in a long-term crustal cycle.

The most comprehensive account of Scourie dykes in the Outer Hebrides has been that of Watson (1968), for the island of Great Bernera, northwest of Lewis. In general, the Hebridean dykes have a west-north-west trend (Watson, 1975) and are steep-sided and discordant, with frequent apophyses. Some show chilling against the country rock, whilst others have amphibolitised margins and granulitic cores; both types, if deformed by later metamorphism, often preferentially develop foliation at their margins. She uses the dykes, predominantly metadolerites (which are

now mainly concordant with the gneissic foliation) to calculate amounts of Laxfordian deformation. In areas of low Laxfordian strain, the dykes may remain discordant, and their central portions bear a granulite facies assemblage which mimics their original sub-ophitic texture.

The difference in facies between the core and the margin of the Scourie dykes led Dearnley and Dunning (1968) to believe that they were subjected to retrogressive metamorphism, causing incomplete conversion to amphibolite facies. O'Hara (1961), referring to dykes on the Scottish mainland, had earlier suggested that partial reconstitution at moderate temperatures and pressures had occurred soon after the intrusion of most of the dykes. Tarney (1963) also noted that earlier members of the mainland swarm tended to be more thoroughly recrystallised and foliated than later members, again pointing to dyke emplacement into warm, deep rock. This raises the possibility that the dykes were injected during the waning stages of the Inverian division of the Scourian (see table 3.1); the Outer Hebrides dykes display similar features.

<u>The South Harris Igneous Complex</u> The South Harris Igneous Complex is marginal to the Outer Hebrides Fault Zone and is little affected by it and hence only a brief description is justified. It occupies a folded,

northwest-southeast trending belt (see figure 3.2) across the southern edge of Harris and is composed mainly of metamorphosed anorthosites, gabbros, tonalites and norites, and has been dated at around 2060 My (Cliff et al., 1983). It has been studied by Dearnley (1963), Livingstone (1963, 1967), Palmer (1971), Skinner (1970) and Witty (1975), who looked at the anorthosites and gabbros.

The Complex was subsequently metamorphosed and folded, giving rise to a major isoclinal antiformal syncline. The anorthosites form the core of this syncline, as shown in figure 3.2, and are surrounded by a marginal gabbroic rim. Remnants of a primary igneous layering can be detected in these anorthosites and gabbros (Witty, 1975), and thus it appears that the Igneous Complex has intrusive origins. The tonalites to the north (occupying a wide belt NW-SE across Harris - see figure 3.2) are thought by Witty (1975) to have been comagmatic with the anorthosite gabbros, and may even have been contemporaneous.

To the south of the anorthosite gabbros, a narrow band of pyroxene granulites (the 'norites' of Dearnley (1963) and Witty (1975) - figure 3.2) outcrops along the coast of South Harris. Their contact with the Leverburgh supracrustals to the north is sharp and Dearnley (1963) interpreted this as due to northeastwards directed

thrusting. However, Palmer (1971) has found supracrustal xenoliths within the pyroxene granulites, indicating forced intrusion. Thus it is possible that the sharpness is due to later folding, resulting in differential strain across the boundary. The northern edge of the Complex (the Langavat belt - figure 3.2) has been interpreted by Coward (1984) as having acted as a low-angle ramp up which the granulites were thrust northeastwards during the early Laxfordian. In the late Laxfordian, this same zone was then reactivated as a dextral shear.

The Laxfordian Metamorphism The Laxfordian metamorphism (1950 - 1750 My) took the form of a retrogressive amphibolite facies event, giving rise to widespread folding. This reworking is of extremely variable intensity - some areas are hardly affected at all and retain their Scourian structures and assemblages; others have had all vestiges of earlier events obliterated. Difficulties arise because of this variability. Hopgood and Bowes (1972) recognised at least six phases of deformation throughout the islands and, despite producing a summary table detailing how these phases affected different areas, ran into problems trying to locate all the fold phases in every locality, and explain changes in orientation and style. More recent work has emphasised the heterogeneity of the deformation (Coward et al., 1970; Coward, 1973a and b; Davies et al., 1975; Watson, 1977) and has restricted itself to describing smaller areas in detail, without trying to erect clumsy regional correlations.

The inhomogeneity of Laxfordian reworking is attributable to ductility contrasts, often inherited from the Scourian (Francis, 1972, 1973; Watson, 1977). It is also possible that with the introduction of a hydrous phase a dramatic increase in ductility would occur. Once amphibolitisation had begun, relatively ductile zones in which the process was more advanced might be expected to undergo strong deformation, whilst the intervening drier

and less ductile rocks suffered less strain.

This would give rise to two distinct styles of reworking; firstly, broad tracts characterised by complex patterns in which Laxfordian structures are superimposed on, and interfere with, those of earlier generations, and secondly, zones with a much simpler structural pattern where earlier features are obliterated. This second type is the 'straight belt' or Laxfordian shear zone of Watson (1977) whilst the first corresponds to the areas of lower finite deformation as described by Coward (1973a and b).

The waning stages of the Laxfordian were marked by cooling and uplift, and varying amounts of jointing resulted (see also section 3.4, and figure 3.6).

<u>The Granite Migmatite Complex</u> Occupying an area of some 220 km^2, the granite migmatite complex (Soldin, 1978) represents the greatest development of late Laxfordian intrusions on the islands. Its position is shown on fig 3.2. Minor areas of migmatitic rocks are also found near Uig, on Lewis, at Garry-a-Siar, Benbecula (Fettes and Mendum, 1987) and near Griminish, North Uist. The complex itself is a large body of granitic material, with diffuse boundaries and associated migmatisation and pegmatisation (Myers, 1968; 1971). Myers (1971) suggests that it formed from a partial melting of the local gneisses, due to an

influx of water and a decrease in hydrostatic pressure. However, Fettes and Mendum (1987) and Fettes et al. (in press) present data on the granite geochemistry that shows that it could not have been derived from local gneisses.

Cover The only lithified cover present in the Outer Hebrides is the Stornoway Formation, a sequence of alluvial and fluvial sandstones and conglomerates (Steel and Wilson, 1975). Its outcrop is restricted to around Broad Bay on the Eye Peninsula, near the town of Stornoway, east Lewis (figure 3.3). The eastern contact of the sediments is unconformable on the Lewisian gneiss, whilst the western margin is bounded by normal faults dipping steeply to the east. These faults are thought to be branches of the Minch Fault system (Jones, 1981), and to have exerted tectonic control on rates of sedimentation. The sediments are therefore both derived from, and deposited against, trapdoor-like fault scarps as a series of fan deposits up to 4000 metres thick. Their red colouration has led to the conclusion that they formed sub-aerially.

It seems probable that the Minch Fault System (see section 3.4) was the dominant structural control in the area at the time of deposition. However, uncertainty exists as to the age of the sediments. They have been correlated with similar deposits in the Torridonian (Jehu

and Craig, 1934), the Old Red Sandstone (Kursten, 1957) and the Permo-Triassic (Steel and Wilson, 1975; Fettes and Mendum, 1987).

Evidence for the age of the formation is sparse - no fossils have ever been recorded from it, perhaps implying a Precambrian age. Clasts of sheared and crushed gneiss, some bearing pseudotachylyte, are common, suggesting that the beds are younger than a major tectonic event. This event is thought to be a movement episode of the Outer Hebrides Fault Zone, correlated as Caledonian by Sibson (1977b) from radio-isotope dating of some fault rocks. Steel and Wilson (1975) found that seismic velocities of the Stornoway Formation are comparable with those of Inner Hebridean Triassic deposits, and significantly different from those of the Torridonian. Sediments from a shallow borehole east of Benbecula and near to the Minch Fault system have been dated as Permian (Binns et al., 1974). In conclusion, a Permo-Triassic age is most likely.

Permian Dykes Scarce dykes of probable Permian age are found in a few localities on the Outer Hebrides. On Barra, there are quartz-dolerites, and on South Uist, there are camptonites and monchiquites. Fettes and Mendum (1987) favour a Permian-Carboniferous age for these dykes, whilst Maddock (pers. comm.) prefers a Permo-Triassic date. The

latter is preferable as it would tie in with continuing Permo-Triassic extension of the Devonian graben structures in the Minch.

Tertiary Dykes The Tertiary dykes on the Outer Hebrides are petrologically identical to those of the mainland, and are predominantly alkali olivine basalts. They trend north-westwards, cross-cutting the foliation of the gneiss, and are concentrated most heavily in southeast Lewis (Nature Conservancy Council, 1977), although a few occur on South Uist. They are thought to have originated from the Tertiary igneous centre on Skye (Macintyre, 1973).

The Madadhs, three islands lying just off the east coast of North Uist at Lochmaddy, appear to be irregular basaltic bodies of Tertiary age. It is thought possible that, rather than radiating out from the igneous centre on Skye, the magma exploited the structural weakness of the Outer Hebrides Fault Zone. Onshore of the Madadh Mor (see figure 4.4 for location) a smaller volume of basic material can be seen exploiting a minor fault plane in this manner. The overall shape of the Madadh outcrops suggests margins parallel to the fault plane orientation - see figure 3.4. It is known (Fettes and Mendum, 1987) that Tertiary sills are common in the Minch sediments, so this

seems a possible explanation of the formation of the Madadhs.

3.3 The Outer Hebrides Fault Zone

This is the major structural feature on the Hebrides as first recognised by Jehu and Craig (1925) (see also chapter 2). The zone strikes approximately north-north-east (figure 3.5) and dips on average at between 20 - 30 degrees east-south-east. It is traceable along most of the east coast of the island chain, although its course is somewhat unclear in the area of central Lewis due to extensive blanket bog coverage and consequent lack of exposure.

The general outcrop pattern (figure 1.2) is of a broad (2.5 to 3.5 km) elongate belt of highly crushed and sheared microbreccia (the 'crush melange' of Sibson, 1977a and b) within which are more highly strained zones of cataclasite and c-type and r-type mylonite (see section 1.6 for a description of fault rock terminology). On South Uist, the highly strained zones were named as distinct 'crush zones' e.g. Eynort, Meall Mhor and Outer Isles Crush Zones (Coward, 1969), but these terms are not used here. Amount and direction of displacement along the fault zone as a whole are debatable, but it seems that at least

one phase of reactivation has occurred.

Fault Rocks The Outer Hebrides are remarkable for containing a wide variety of fault rocks. Essentially the rocks of the Uists were found to display the products of brittle deformation mechanisms (with or without the modifying influence of fluids) whilst some of those of inland Lewis tended towards crystal plastic deformation. One of the major problems in this project lay in attempting to reconcile this wide variation in generative conditions. The distribution of the different styles of fault rocks is also variable. The distribution of the different fault rocks in selected type areas is described in detail in chapter 4, and only a brief description is given here.

In Lewis, from west to east across the fault zone, pseudotachylytes and r-type mylonites crop out inland, with phyllonites and c-type mylonites present towards the coast. Further south, on the Uists, pseudotachylytes and cataclasites occur inland with c-type mylonites again found towards the coast. On South Uist the fault zone exploits the boundary between the Corodale Gneisses to the east and the Gray Gneisses to the west (see figure 4.5). The c-type mylonites of South Uist occur as a discrete band paralleling the overall trend of the fault zone (figure 4.5), whereas those of North Uist form more of an

anastomosing network, sub-parallel to the fault zone (see figures 4.3 and 4.4). In addition, the c-type mylonites on North Uist sometimes dip to the west in the form of antithetic shears (usage as in Gibbs, 1984) to accomodate reactivation.

3.4 Other Faults and Lineaments

Onshore A map of the most prominent lineaments present on the Hebrides is shown in figure 3.6. Onshore, the most important is the northwest trending lineament and crush zone known as the Seaforth Line (Jehu and Craig, 1934). Sibson (1977b) believes that this may offset the base of the Outer Hebrides Fault Zone in a sinistral sense, although this is by no means universally agreed upon (see Davies et al., 1975). Dearnley (1962) maintains the crush zone is aligned with the axis of a Seaforth antiform, but whereas most of the large-scale folds in this area are virtually recumbent, the Seaforth Line appears nearly vertical.

Many other small-scale lineaments are also present, some of which are probably inherited remnants of early Precambrian shear zones (the straight belts of Watson, 1973) and have exerted an influence on subsequent deformation to some extent. Around Stornoway are normal,

half-graben type faults with a downthrow of approximately 3 kilometres to the east. An onshore extension of the Minch Fault System, they control the western margins of the Stornoway Formation and probably represent the original scarps from which the sediments were derived (figure 3.3).

Jointing Within the Hebrides themselves are a number of smaller scale faults and lineaments. The islands are heavily dissected by an extensive joint network which has been exploited during glaciation, giving rise to the heavily indented present-day coastline. The jointing is probably inherited from tectonism and subsequent cooling after the Precambrian metamorphic episodes.

There are three main joint orientations (see figure 3.6); northwest-southeast, northeast-southwest and east-west. A good example of exploitation of these is to be seen in the shape of Loch Seaforth, marked on figure 3.6. A number of the other northwest-southeast joints appear to have been reactivated as faults, often with a sinistral strike-slip sense of displacement (see Fettes and Mendum, 1987).

Offshore The chief structural feature is the Minch Fault System (figure 3.5). The existence of such a dislocation was first postulated by Dearnley (1962) who required the

presence of a sinistral wrench fault to account for displacements of zones which he recognised on the Hebrides and was attempting to correlate with the Scourian and Laxfordian zones of northwest mainland Scotland. The presence of these zones on the islands has since been largely discredited, but geophysical work (McQuillin and Binns, 1973; Binns et al., 1974) has subsequently confirmed the existence of the Minch Fault.

The fault system consists of a number of sub-parallel, normal, half-graben type structures, downthrown to the east (figure 3.3). Although the origins of the Minch Fault System may go back to the Precambrian, extensive reactivation last occurred during Permo-Triassic rifting (Jones, 1981). Recently interest has been revived in the possibility of some strike-slip motion occurring along the fault (Lisle, 1986) as a means of explaining apparent discrepancies in the locus of extrapolated Scourie dykes on the Hebrides when compared to that of the mainland.

To the west, roughly parallel to the Outer Hebrides Fault Zone, runs the Flannan Thrust. It lies approximately 20 km offshore of Lewis and its presence has only been detected by interpretation of seismic profiles (see section 2.4; Smythe et al., 1982; Brewer and Smythe, 1984; Blundell, 1984). Motion along this fault has been interpreted by the above mentioned authors as being

thrust-sense, and opinion is divided as to whether it cuts and offsets the Moho or flattens out along a crust-mantle detachment.

3.5 Tectonic Setting

The Outer Hebrides were originally part of the Precambrian North Atlantic craton, a large crustal expanse that once included the Rockall Plateau and parts of Greenland and North America. This craton was roughly triangular in shape and was enclosed by early Proterozoic mobile belts (Bridgwater et al., 1973; Watterson, 1978). These belts may have served to localise later deformation, and have probably influenced evolution of the area ever since.

From the late Precambrian to mid-Palaeozoic times the islands behaved mainly as a horst block marginal to troughs flanking Iapetus in mainland Scotland. After the closure of Iapetus in Siluro-Devonian times they became part of the Caledonian foreland. From the late Palaeozoic onwards the tectonic history of the islands has been governed by events connected with the opening of the Atlantic Ocean:- volcanism and rifting (resulting in the formation of the Minch) to the east, sea-floor spreading to the west (Watson, 1977). During this time, the Outer

Hebrides continuing to act as a relatively stable block. The fault-bounded margins of this horst are thought to have exerted strong controls on the location of present-day coastlines.

The eastern horst margin is defined by the presence of two tectonic features - the Outer Hebrides Fault Zone and the Minch Fault System (figures 2.2 and 3.5). The Minch Fault System marks the western edge of a graben that forms the sediment-filled Minch Basin and Sea of the Hebrides Basin. To the east of these basins lies the Caledonian Orogen, with the orogenic front defined on land by the Moine Thrust Zone (figure 3.5).

To the west of the Hebrides lies the Flannan Trough (figure 3.5), which is also a graben structure (from the seismic work of Jones, 1981). Further west, the Caledonian foreland is bounded by the passive continental margin of the Rockall Trough (figure 3.5), which formed during the early stages of the formation of the North Atlantic.

Ages of the Basins The ages of the basins are poorly controlled, due to a lack of commercial drilling in the area, and because of the similarity in appearance of the different lithologies (Binns et al., 1974; Chesher et al., 1983). The Flannan Trough to the west of the islands

contains Permo-Triassic and younger sediments, suggesting that its formation is related to the North Atlantic opening. The general trend of the basins to the east (figure 3.5) shows that their structure was probably controlled by an underlying Caledonian framework (see section 2.4). The MOIST seismic reflection profile (Smythe et al., 1982) supports the idea that many of these basins formed by extensional reactivation of Caledonian features. Brewer and Smythe (1986) point out that the sediments in the deepest parts of the basins are undated, and it is therefore possible that some of the basins are immediately post-orogenic in age, or conversely as old as Torridonian (c. 1000 My ago).

Figure 2.2 presents an interpretation by Cheadle et al. (1987) of the DRUM seismic line. This shows that the eastern basins are Devonian and Permo-Triassic in age, whilst Permo-Triassic sediments are more abundant westwards. The Minch and North Lewis basins are probably Permo-Triassic to lower Jurassic in age (Binns et al., 1974) but may be floored by Torridonian sediments. The faults controlling the basins have been interpreted as reactivated Caledonian thrusts (Brewer et al., 1983; Brewer and Smythe, 1984).

Formation of the Outer Hebrides Since the Laxfordian, the

Outer Hebrides have never accumulated much in the way of sedimentary cover, thus reflecting their horst block status. This has been attributed to high bouyancy due to the unusually acid (and therefore low density) nature of the basement which is seen in the field (Watson, 1977). Jones (1981) has also inferred the presence of a dominantly granitic basement from the low seismic refraction velocities which have been recorded offshore.

Data from WINCH (Brewer and Smythe, 1986) and earlier studies have shown, firstly, that the deepest part of the Minch Basin is generally east of the middle portion of the Hebrides, where the topography is highest (Smythe et al., 1982) and secondly, that the throw on the Minch Fault decreases abruptly north and south of the islands. This raises the possibility (Brewer and Smythe, 1986) that the Outer Hebrides are the isostatically uplifted footwall to the Minch Fault System, the hanging wall being delineated by the Minch and Sea of the Hebrides Basins (see figure 3.5). Basin infills are Late Palaeozoic and Mesozoic in age and it is likely that this reflects the age of fault movement and uplift.

Summary The Outer Hebrides contain many faults and joints, of either Precambrian or Caledonian age. Evidence suggests that many of the earlier structures have been

reactivated in the Caledonian or during the Permo-Triassic, or both. The presence of so many fractures means that there will nearly always be one orientated favourably for reactivation (White et al., 1986), making it highly unlikely that any new faults (ie. later than Caledonian) would have formed.

Figure 3.1

Map showing areas of supracrustals on the Outer Hebrides. The thin line shows the trace on land of the westernmost limit of deformation associated with the Outer Hebrides Fault Zone. L-S = Lochmaddy - Sollas road junction; S = Scolpaig; T = Tigharry; G-E = Gairbh-Eilean; MS = Market Stance; SPt = Scurrival Point

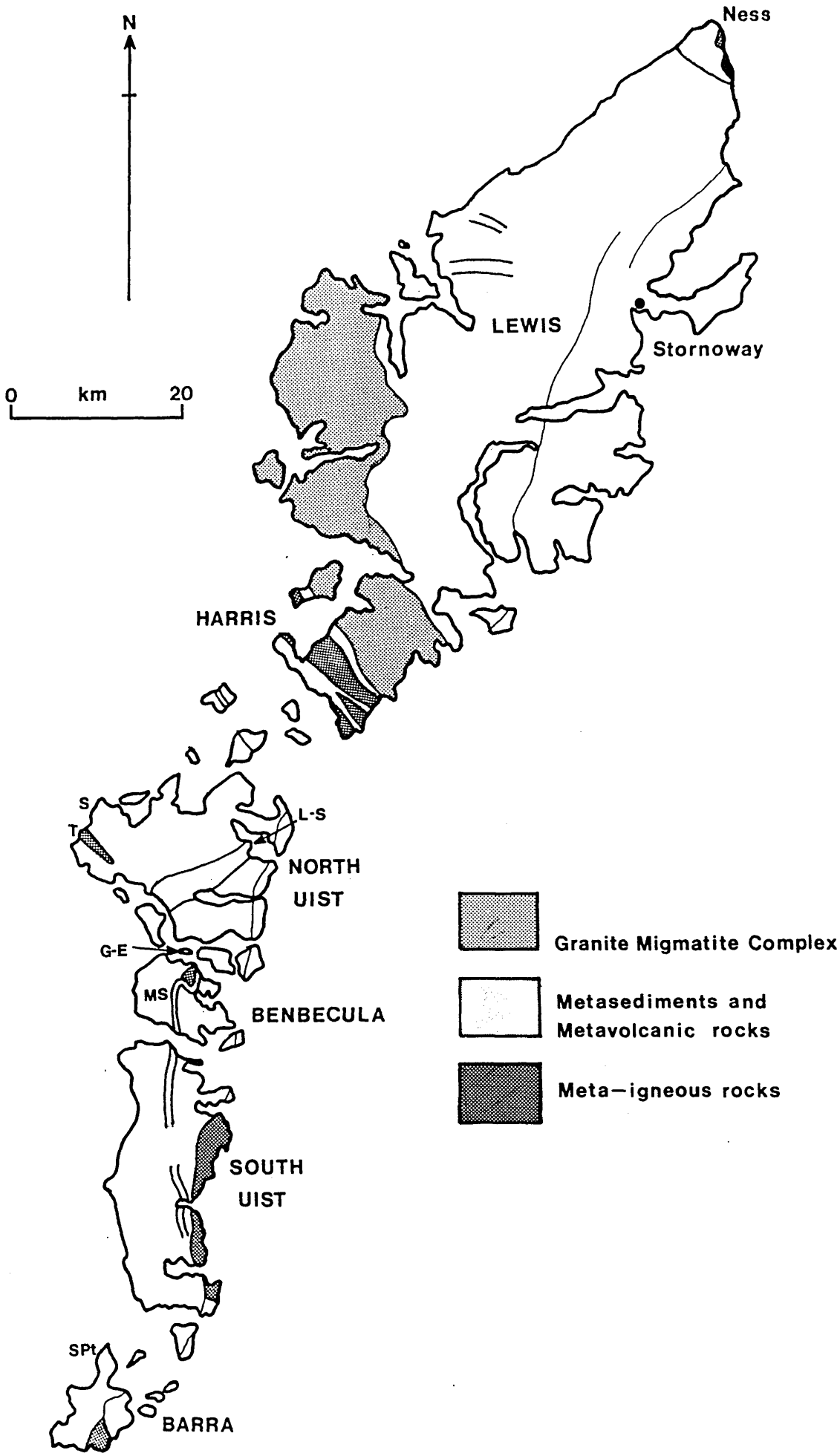

N
Ness
LEWIS
Stornoway
0 km 20
HARRIS
S
T
L-S
NORTH
UIST
G-E
MS
BENBECULA
SOUTH
UIST
SPt
BARRA
Granite Migmatite Complex
Metasediments and
Metavolcanic rocks
Meta—igneous rocks

Figure 3.2

Simplified map of the geology of South Harris, showing the supracrustals and the South Harris Igneous Complex. After Dickenson (1974).

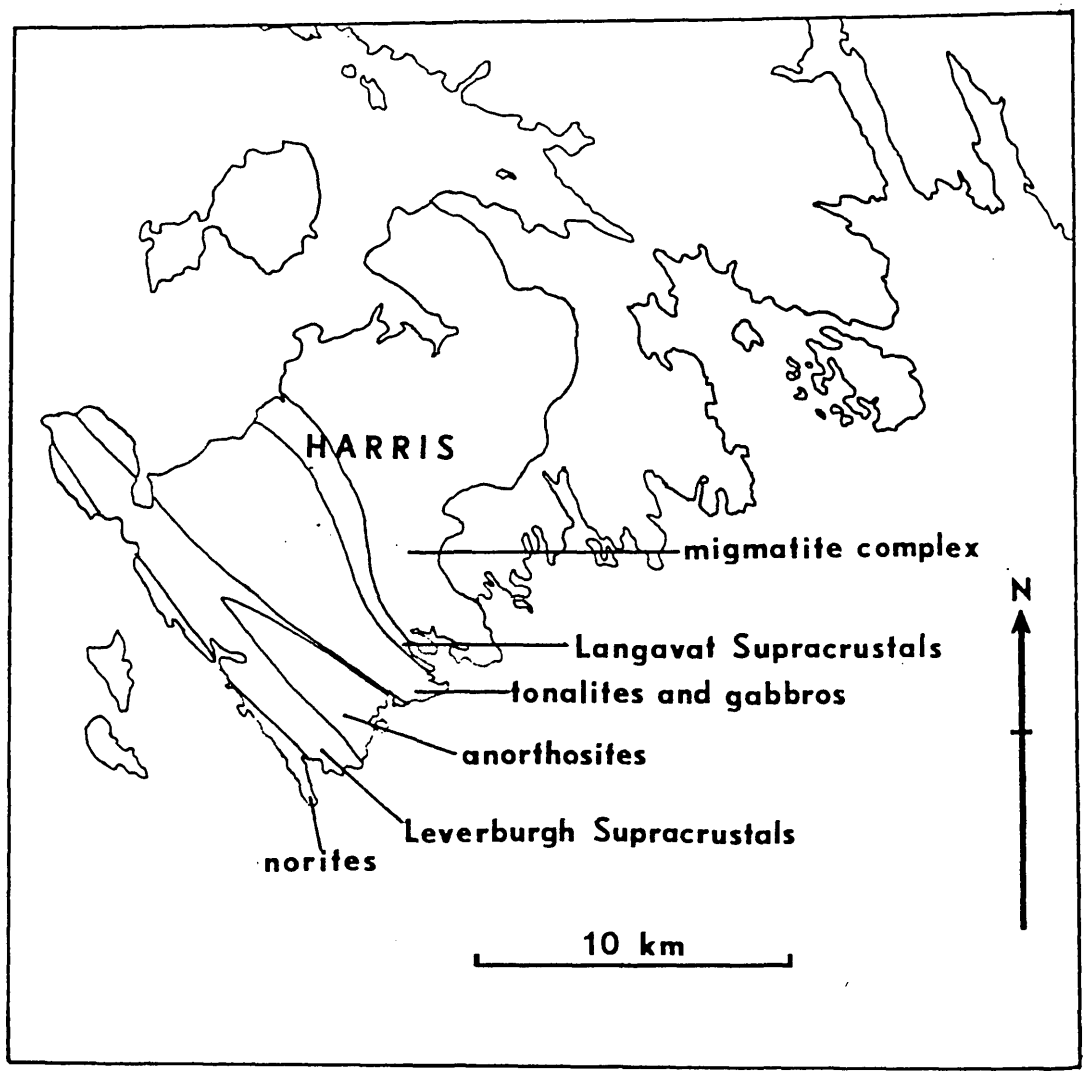
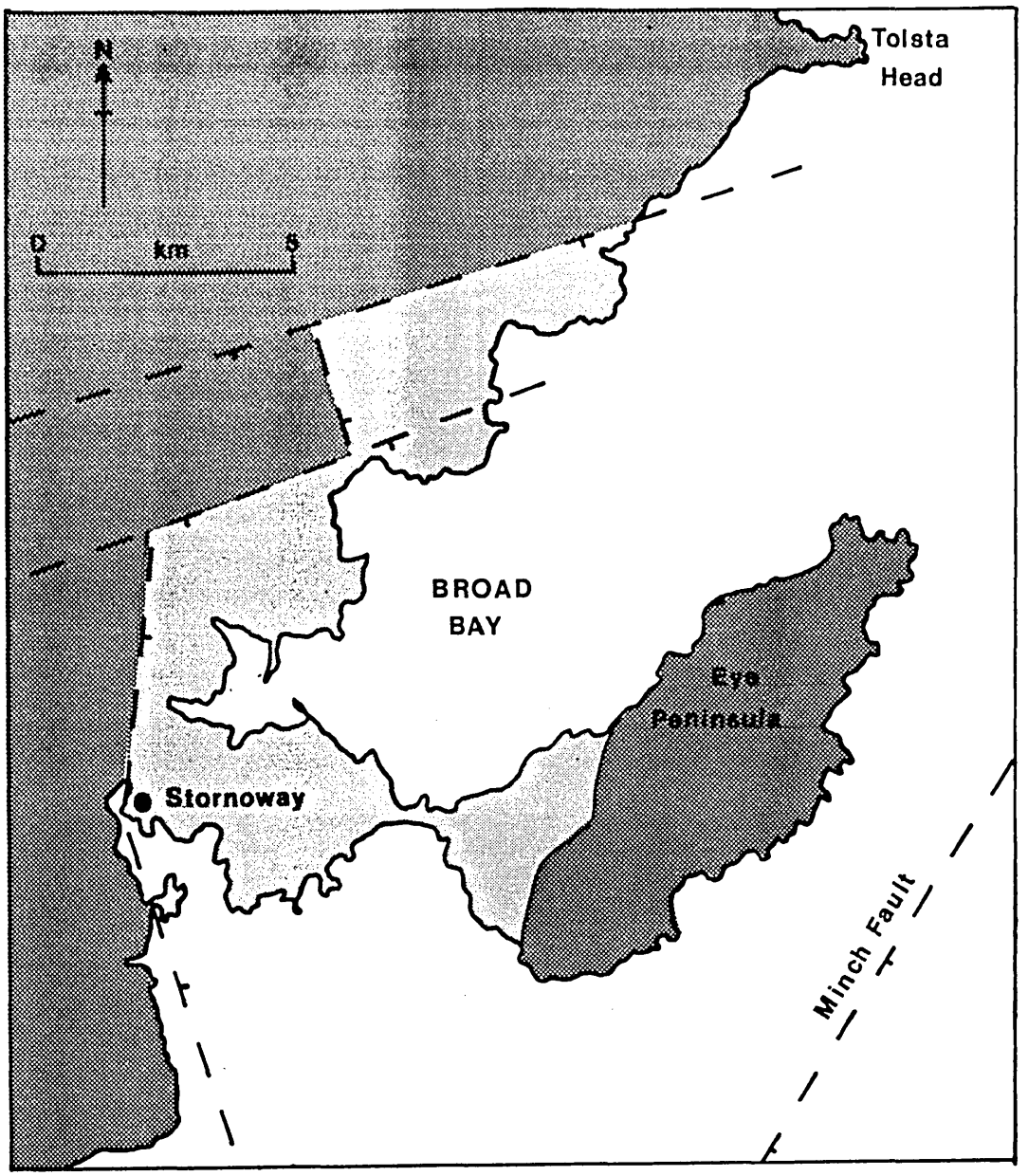

HARRIS
migmatite complex
Langavat Supracrustals
tonalites and gabbros
anorthosites
Leverburgh Supracrustals
norites
N
10 km

Figure 3.3

Location of the Stornoway Formation and its bounding faults. After Steel and Wilson (1975).



Stornoway Formation

Gray Gneiss

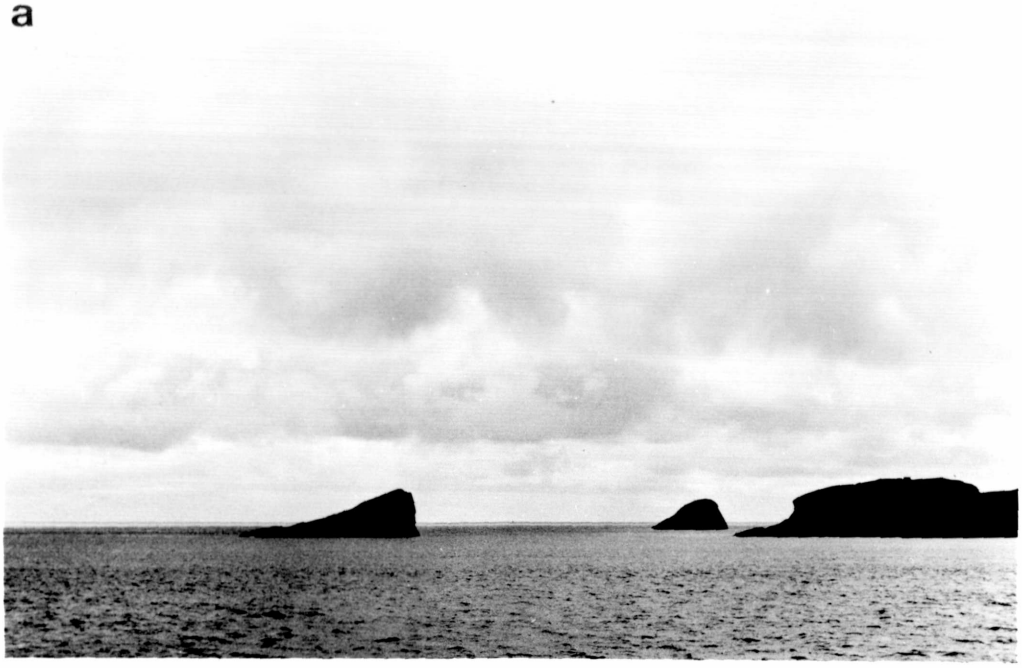
Major bounding fault (tick on downthrown side)

Unconformity

Figure 3.4

Photograph of the Madadh Mor (*a*), with sketch (*b*) showing suggested mode of formation by injection of basaltic magma along a fault plane (indicated by thin lines).

a



b

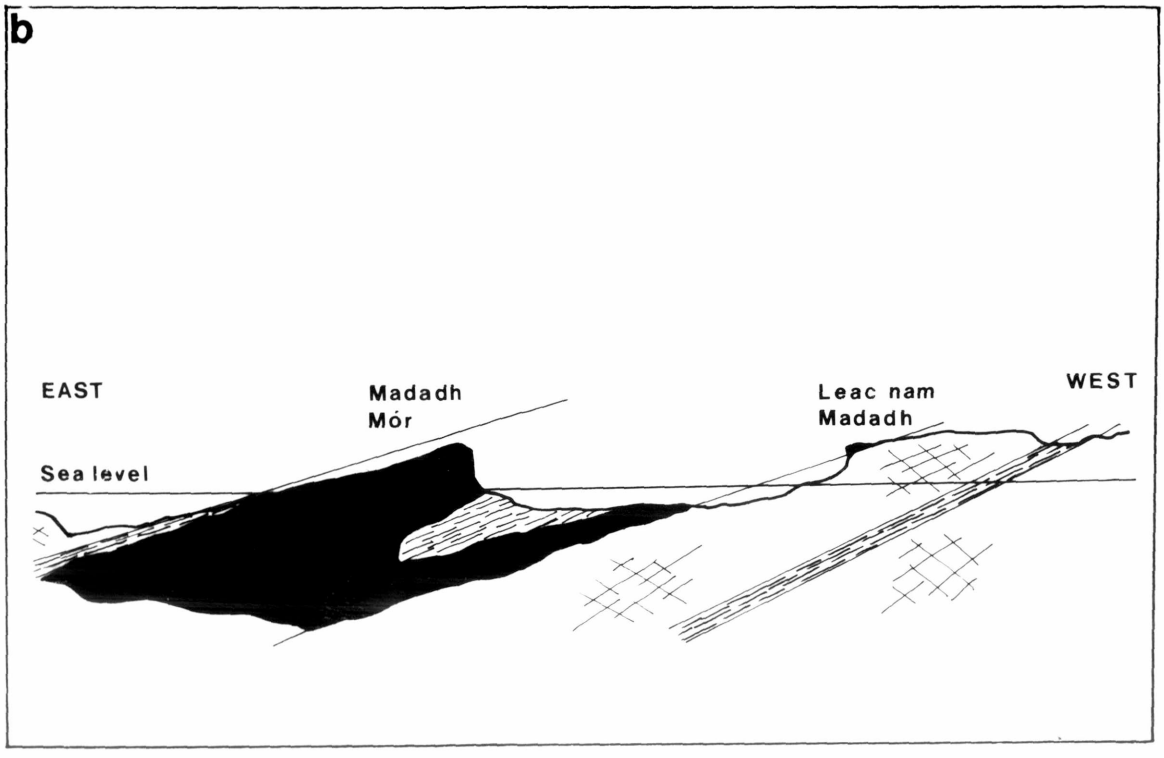


Figure 3.5

Map showing the horst status of the Outer Hebrides block, and the sub-parallel relationships between the Moine Thrust, Minch Fault, Outer Hebrides Fault Zone (OHFZ) and the various troughs and basins. After Brewer and Smythe (1986).

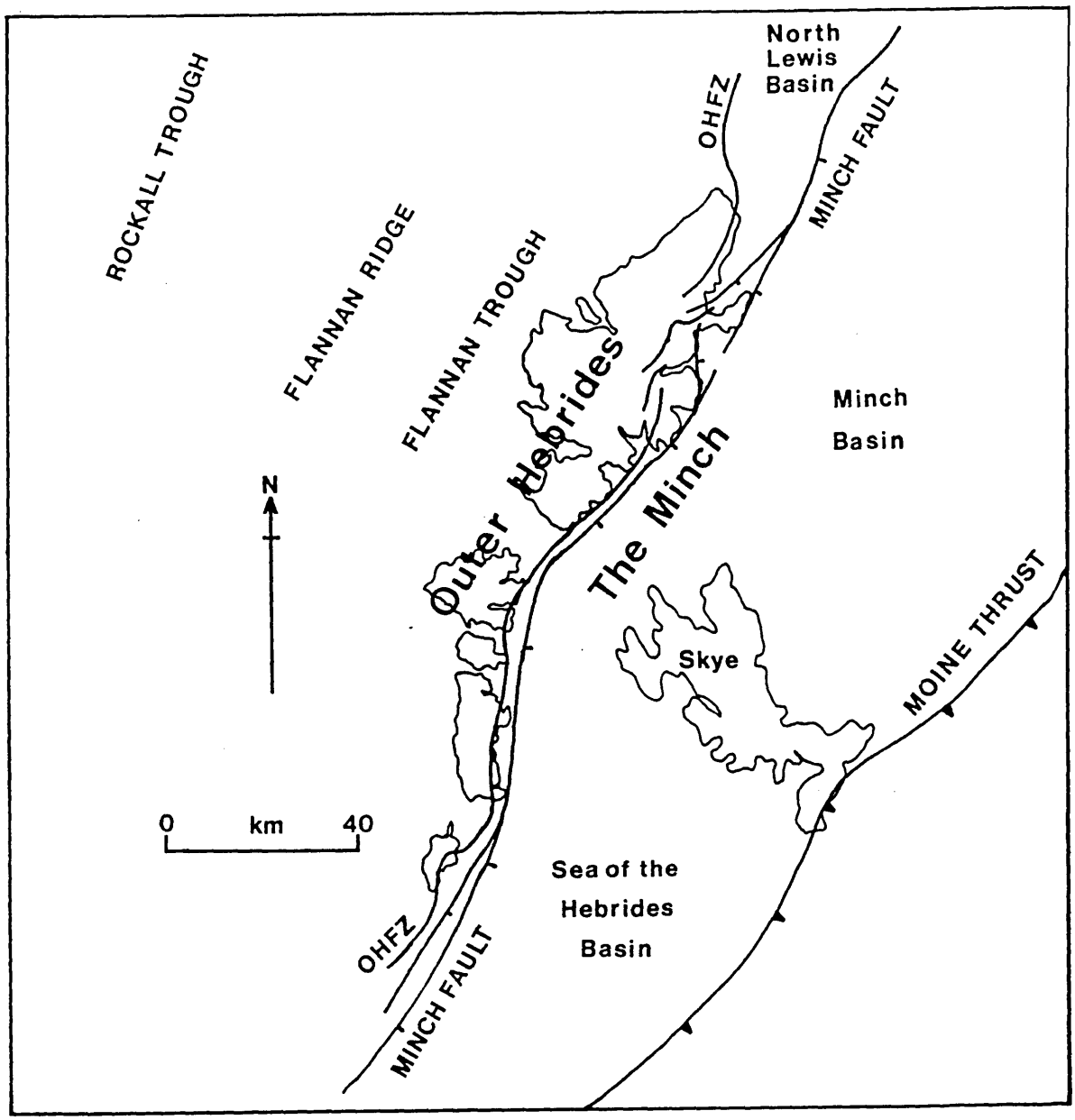

ROCKALL TROUGH
FLANNAN RIDGE
FLANNAN TROUGH
OHFZ
North
Lewis
Basin
MINCH FAULT
Outer Hebrides
The Minch
Minch
Basin
N
Skye
MOINE THRUST
0 km 40
Sea of the
Hebrides
Basin
OHFZ
MINCH FAULT

Figure 3.6

Lineament map of the Outer Hebrides, after Jehu and Craig (1934); Watson (1977); Sibson (1977); McQuillin and Watson (1973); Jones (1981)

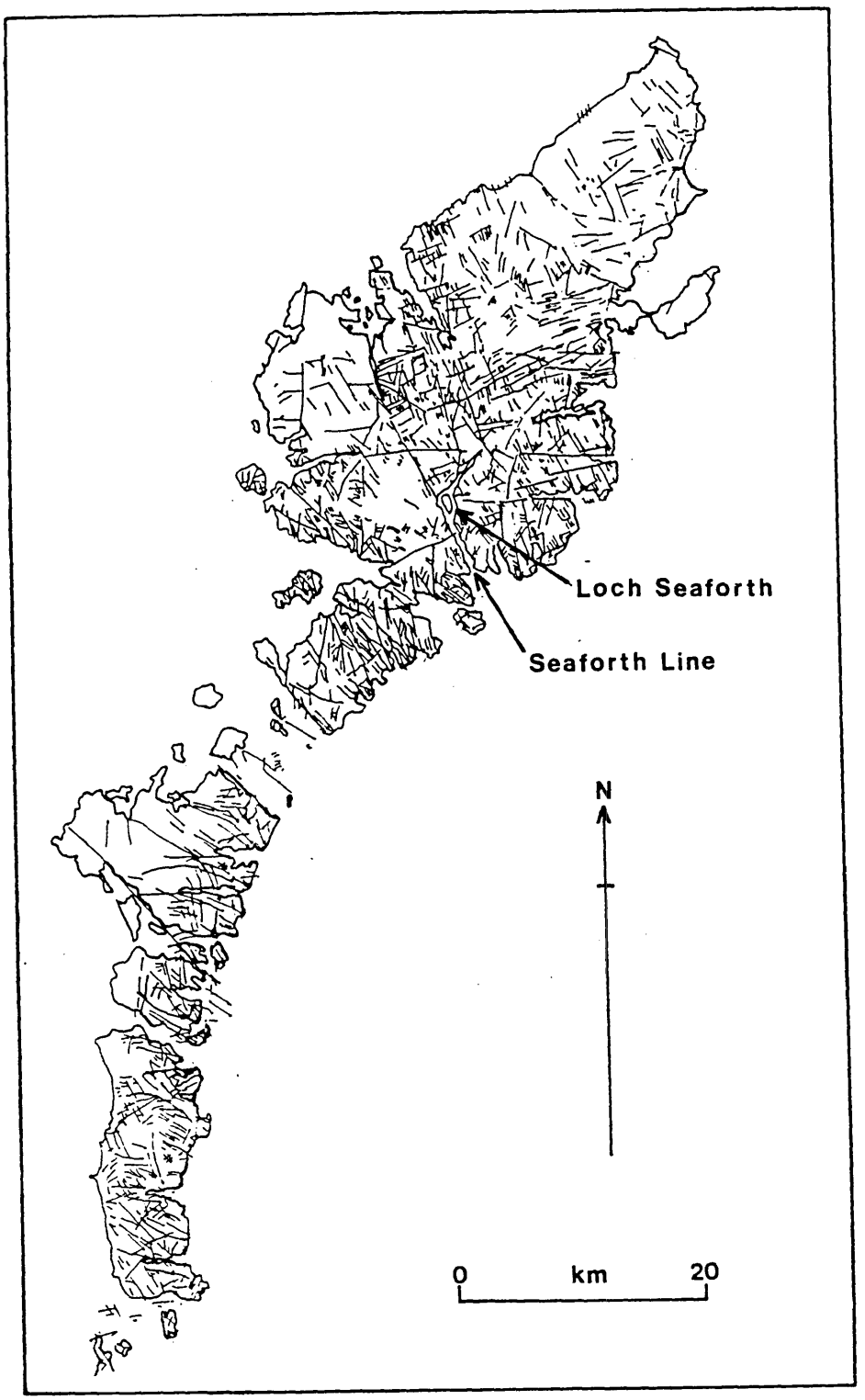

Loch Seaforth
Seaforth Line
N
0
km
20

Table 3.1

Main Tectonothermal, Intrusive and Depositional Events Affecting the Outer Hebrides

Tertiary	Dyke intrusion	c. 65 M.y.
Permo-Triassic	?Deposition of Stornoway Formation; some dyke intrusion	280-195 M.y.
Laxfordian	Folding, retrogression to amphibolite facies. Inhomogenous in effect. Formation of South Harris Igneous Complex	1950-1550 M.y.
Scourian/ Laxfordian Boundary	Intrusion of basic rocks, now metadolerites and amphibolites (Scourie dykes)	2200 M.y.
Inverian	Widespread metamorphism to granulite facies, pegmatite injection	2400-2200 M.y.
Badcallian		2900-2700 M.y.
	Deposition of supracrustals	?
	Formation of basement precursor	<3100 M.y.

Chapter 4

Field Studies

4.1 Introduction

Field mapping was concentrated in areas (see figure 1.3) selected for the likely degree of exposure and geological interest (with the aid of Ordnance Survey 1:50 000 sheets, Sibson's (1977b) thesis maps and the B.G.S. geological and tectonic maps). Sibson's maps were of limited use in the field as they omit both topography and streams. His mapped lithological boundaries are mostly accurate, except in areas of poor exposure where such boundaries are open to conjecture, and thus the mapping undertaken represents, for the most part, a re-interpretation of his work.

A series of sampling traverses was also undertaken, concentrated on the Uists, and designed to collect information about areas not mapped in this project. Their locations are shown in figure 1.3. The main purpose of these traverses was to obtain specimens for geochemical analysis, but data about outcrop patterns, structures and microstructures were also collected. These helped in interpretation of the mapped areas, construction of cross-sections and in studying systematic variations in fault rock type.

Lithological units mapped in the field have been changed slightly from those used by Sibson (1977b), as it was thought possible, and important, to distinguish between r-

and c-type mylonites (i.e. mylonites formed dominantly by recrystallisation and cataclasis respectively - see section 1.6 for discussion of fault rock terminology); these have different appearances in the field. In hand specimen, c-type mylonites are of greenish colouration, are generally fine grained, with scarce clasts of a larger size than those in the r-type mylonites and are usually poorly foliated. The foliation is defined by alignment of mineral grains, mostly chlorite and mica, with some clay and amphibole.

The r-type mylonites have a banded appearance, and a medium grain size; mineral grains are usually evident without recourse to a hand lens. Foliation is well-developed and defined by grain shape, mostly quartz and feldspars. A quartz stretching lineation is frequently present, whereas lineations in the c-type mylonites are scarce and, if present, usually due to the intersection of foliation or shear planes.

Table 4.1 presents a summary of the fault rocks found on the Outer Hebrides, and gives an idea of the north/south and east/west variations in deformation style. Briefly, the fault zone is marked by a broad band of microbreccia (see section 1.6 for description of all fault rocks) extending roughly NNE/SSW, which contains fractures orientated parallel to this trend and dipping moderately

east or west. Within this are developed more highly cataclased zones, in the form of c-type mylonite bands. These bands generally parallel the microbreccia fracture trend, and may dip either to the west or the east.

Most of the fractures in the microbreccias are laterally discontinuous, although occasionally they coalesce and form a major discontinuity through the microbreccia. These may dip either east or west, with the eastward dipping set predominant. The angle of dip of these large-scale fractures and the easterly-dipping mylonite bands shows a decrease towards the east (see cross sections in figure 4.7).

In the north, r-type mylonites occur to the west (see table 4.1), with microbreccias, phyllonites and c-type mylonites developing eastwards. In the south, there are microbreccias and c-type mylonites, with wide zones of ultracataclasite and pseudotachylyte developed on South Uist (table 4.1). Along the length of the fault zone, minor pseudotachylyte occurs west of the limit of microbreccia and mylonite formation, and there is a tendency for stronger alteration of both the microbreccias and the mylonites towards the east. Dolerite dykes of Tertiary age cut the fault rocks in many areas.

This chapter describes in detail the features and

structures seen in the field in each area. These will be interpreted in chapter 7, which aims to establish the relationships between the areas, and the controls on styles of deformation and fault rock distribution patterns. In this chapter, individual areas mapped will be described in geographical sequence, starting in the north and working southwards. This will be followed by a brief resume of the sampling traverses.

4.2 Malasgair and Shiltenish

Geographical Introduction The area mapped is around 6 km^2 and is shown in figure 4.1. It is bounded to the north by Loch Erisort, to the south by the Seaforth River and Loch Sgibacleit, to the east by the northwards trending arm of Loch Sgibacleit and Cnoc a' Charnain (to the west of the Habost village) and to the west by Seaforth Head and the settlement of Shiltenish. Exposure is patchy; it is poor or non-existent in the blanket bog between Cnoc a' Charnain and Loch Clach na h-Iolaire and along the valley of Abhainn Chleiteir, but is reasonably good on the slopes of Malasgair and along the coast of Loch Erisort.

Geological Introduction The outcrop is predominantly intact, well-banded Gray Gneiss, with a north-south trending, eastward dipping foliation. It is disrupted by

r-type mylonite and ultramylonite bands in approximately parallel orientations to the gneissose foliation, and pseudotachylyte is extensively developed, especially west of Malasgair. The boundaries between the mylonites and the Gray Gneiss are often gradational (plate 4.1*a*).

To the east of the mapped area, the r-type mylonites become phyllonitic, and the gneiss grades into microbreccia. R-type mylonites die out further east and microbrecciation becomes more intense. Alteration becomes stronger, and c-type mylonite bands develop nearer the coast. A late stage fault, trending E-W, cuts all the earlier structures and may be related to pervasive smaller-scale fracturing in the gneisses and pseudotachylytes.

Intact Rock The Gray Gneiss possesses a strong foliation and fine mineral banding where this has not been overprinted by later deformation associated with formation of the Outer Hebrides Fault Zone. It typically contains a quartz - plagioclase - hornblende - biotite $\pm$ alkali feldspar assemblage. Stringers of basic and acid material are common, probably representing remnants of Scourie dykes and pegmatites respectively. The foliation in general trends north-south, although it does swing NW-SE about the south end of Loch na Craoibhe, then round NE-SW to the north of it, as shown in figure 4.1.

Faults The orientation of the gneissose foliation was favourable for reactivation during deformation. Faulting has occurred preferentially parallel or sub-parallel to the foliation, and tends to follow the foliation as it curves round (figure 4.1). This results in a component of strike-slip movement along such fault segments, as revealed by shear band orientation and asymmetry of folds in the r-type mylonites. The fault planes, as far as can be detected, seem to be impersistent along strike, and tend to stack in groups, as on the western slopes of Malasgair (figure 4.1). There is a general tendency for the fault plane dip to decrease towards the east; see the cross-section presented in figure 4.7.

Away from the faults, the gneiss often has a blocky appearance (plate 4.1*b*), due to the presence of numerous near vertical, east-west trending fractures, which may be infilled with quartz. A second set of fractures, roughly parallel to the gneissose foliation, is less well developed, and probably pre-dates the vertical set, as it is sometimes offset. Together, these sets of fractures combine to produce a localised microbreccia, similar to that found further to the east and on North and South Uist.

Fault Rocks Possibly because of the favourable

orientation of the gneissose foliation for reactivation in this area, development of Gray Gneiss microbreccia is not so great as it is further to the south, where the foliation is orientated more orthogonally with respect to the fault zone. The most abundant fault rock product is r-type mylonite, which occurs in narrow bands parallel, or at a low angle, to the gneissic foliation.

R-Type Mylonite Plate 4.1*a* shows a transition between gneiss and r-type mylonite. Such boundaries tend to be gradational, except where modified by later movement. The plate also shows a blocky zone between the two, and a slight angular difference between the mylonitic and the gneissic foliations. The r-type mylonites commonly display a quartz stretching lineation on the foliation surfaces, plunging generally to the SE or ESE at angles between 5 and 23 degrees (figure 4.1). Small-scale asymmetric folding of the mylonitic foliation (plate 5.11*d*) may be developed, indicating a reverse sense of shear. The r-type mylonites are not affected by fracturing to any great extent, and this could be due to their relatively high competence or small grain size.

Occasionally, the r-type mylonite bands are disrupted by low angle faults, which result in offsets between the stacks of mylonite (see figure 4.1). Less often, the margin between the Gray Gneiss and an r-type mylonite band

is reactivated by an eastward dipping fault, making it appear more sharply in the field than the usual gradational boundary. Internal disruption of the mylonites is rare, but does occur at high angles to the foliation towards the eastern edge of their outcrop, in the Creag na h-Uamha region.

Pseudotachylyte This is common, and is concentrated in areas where there are numerous stacked faults. It seems as if these faults acted as loci of rapid brittle failure, resulting in the generation of the pseudotachylytes. This mode of failure may help to explain why the fault planes are so discontinuous. The pseudotachylyte is rarely fresh; plate 4.1*c* shows an exception where the pseudotachylyte is still black in colour.

More typically, the pseudotachylyte is weathered to a dark brownish colour and is heavily fractured (plate 4.1*d*). The veins often have a patchy distribution, with thick (up to 10 cm), discontinuous patches next to thinner, more persistent veins. Altogether, pseudotachylyte can locally account for up to 40 % of an exposure. The fractures in the pseudotachylyte have the same orientations as those in the gneiss (i.e. sub-vertical, striking east-west), but tend to be much better developed and more closely spaced (plate 4.1*d*), suggesting a difference in competence between the two rock

types.

Clearly, most of the brown pseudotachylytes predate both orientations of fractures, and it is thought that they represent a very early phase of deformation. This is supported by the folding of some of the veins, as shown in plate 4.2*a* and 4.2*b*, which may be interpreted as due to Laxfordian reworking (section 7.3).

East of Malasgair/Shiltenish A brief reconnaissance was made eastwards outside of this area, to the coast around the villages of Cromore and Marvig. Here, the style of deformation is much more like that seen further south on the Uists, with bands of c-type mylonite set in a region of microbreccia (see table 4.1). Injection veins of ultracataclasite appear, usually semi-concordant with the gneissose foliation. The microbreccia itself becomes more finely laminated and green in colour, with the mineral grains streaked out, especially towards the c-type mylonite bands. These bands weather out strongly, making it easy to detect their outcrop, but hard to sample.

Between the Malasgair/Shiltenish area and this area, the r-type mylonites become altered and greenish in appearance. They appear to have been statically retrogressed to form phyllonites (as defined in section 1.6). It is usually possible to distinguish remnant

features of r-type mylonites within them, such as traces of ribbon grains, and lineations often remain visible.

4.3 Scalpay

Geographical Introduction The island of Scalpay, about 4 km by 3 km in lateral extent, lies in East Loch Tarbert, southeast of Tarbert itself. Relief is generally low, with the exception of Ben Scoravik at 104 m (figure 4.2). Exposure is poor over the boggy central part of the island, but elsewhere is moderate, and is aided by the presence of several small but excellent quarries.

Geological Introduction The west of the island is composed of folded Gray Gneiss. This is separated from a broad zone of c-type mylonites, forming the whole of the remainder of Scalpay, by two NE/SW trending, eastwards dipping faults. The area between the two faults is essentially Gray Gneiss, but with some signs of microbrecciation. The easternmost of the faults has c-type mylonite present along it, whilst above it to the east, the Gray Gneiss grades rapidly into the broad zone of c-type mylonite, which becomes progressively more strongly deformed eastwards.

Basic pods are present within the Gray Gneiss and some have become caught up in the deformation which formed the c-type mylonites (figure 4.2). The deformation seems to

have left them relatively untouched, apart from shearing at their margins. A late stage, gouge-bearing fault cuts the island WNW/ESE.

Intact Rock The Gray Gneiss on Scalpay is lithologically similar to that seen in the Malasgair-Shiltenish area (figure 4.1), except that there seems to be rather more pegmatitic material present, and concentrations of basic pods, some of which became incorporated into the c-type mylonites. The gneissose foliation trends generally south-east/north-west at the western end of the island and dips gently to moderately southwards (although there has been some moderate folding), but above the westernmost of the two NE/SW trending faults (figure 4.2) it runs more northeasterly, dipping moderately east.

Faults Three major faults are present on Scalpay (see cross section in figure 4.6). Two are associated with the Outer Hebrides Fault Zone, whilst the third is a late stage feature and will be described later. The two earlier faults trend NE/SW, and have moderate dips (around 40 degrees) to the east. The westernmost of the two separates intact Gray Gneiss below from slightly deformed microbreccia above, whilst the easternmost is overlain by microbreccia grading rapidly into c-type mylonites. This second fault has moderate developments of c-type mylonite along its length, especially at its southern end (figure

4.2).

Because of the similarity in orientation between the faults (both in the Malasgair/Shiltenish area and the eastern fault on Scalpay) and the foliation plane of the parent gneiss, it is thought that they may be reactivating the gneissose foliation. They also appear to have had some control over coastlines, especially where the easternmost one runs along the Or Eilean peninsula (figure 4.2).

Fault Rocks The gneiss above the westernmost of the NE/SW trending faults is affected by crushing, fracturing and some alteration, and grades into microbreccia, similar to that developed in the Uists (see later). Above the eastermost NE/SW trending fault, the microbreccia grades rapidly into c-type mylonite, whose foliation roughly parallels that of the parent gneiss. Of the fault rocks present on Scalpay, c-type mylonite is the most abundant. The microbreccia was probably the earliest to form, followed by the c-type mylonites, with the gouge along the late stage fault being the last.

C-Type Mylonite The c-type mylonites lie above the easternmost of the NE/SW trending faults (figure 4.2). They become more pervasive and the mylonitic foliation becomes stronger towards the eastern coast. The foliation trends NE/SW across the island and dips vary between 45

and 20 degrees, with the lower figures generally in the east (see cross section in figure 4.6). In the region of Eilean Glas and Meall Challibost (figure 4.2) there are numerous metabasite pods, which have been sheared out into lenses along the plane of the c-type mylonitic foliation.

A well-developed shear band foliation is present in these rocks, indicating a somewhat oblique (downwards to the east) sense of shear, with indeterminate components of sinistral and down-dip movements. Where the shear band foliation cuts the mylonitic foliation, it gives rise to a weak intersection lineation.

There is also a mineral alignment lineation present on the foliation planes of the c-type mylonites. Sibson (1977 b) describes this as a quartz stretching lineation, but quartz is virtually absent in these rocks (at least in grains large enough to be seen in hand specimen), and the lineation appears to be due to preferential growth of new minerals during the mylonitisation process.

In appearance, the c-type mylonites are intensely green in colour and extremely altered. They appear to be composed mainly of clay minerals, epidote and micas, although it is difficult to distinguish individual grains even with the aid of a hand lens. The best developed c-type mylonites occur as a massive unit with a true

thickness of at least 1050 metres on the eastern side of the island but, as they are fairly soft, they tend to weather out so exposure is not always good.

The best three-dimensional exposure is obtained in the quarry marked on figure 4.2, where the rocks are also extremely fresh. Here there are two sets of c-type mylonite bands around 10 - 20 cm thick. Set 1 dips moderately to the northwest, and represents a shear band foliation. Set 1 is offset by set 2 (see plate 4.2*c*), which dips at around 20 degrees to the east-south-east. Both sets contain well-developed sense-of-shear indicators, such as shear bands and asymmetric crenulations.

The steeper dipping set 1 c-type mylonites have gradational boundaries over 0.5 metres, with less well developed c-type mylonites to either side containing numerous small scale folds and kinks, whose asymmetry suggests dextral displacement along strike. The bands of c-type mylonites are composed of dark green material with a good, slightly undulating foliation. Within the bands are down-dip verging folds, indicating normal movement; the folds range from open (plate 4.2*d*) to tight in interlimb angle. Normal sense shear bands are also present, giving rise to a strike parallel intersection lineation.

Set 1 c-type mylonite bands are displaced in a sinistral sense by those of set 2 (plate 4.2*c*). The latter are grey in colour, and have distinct boundaries. The planar c-type mylonitic foliation is only well developed at the margins of the bands, and small grains of quartz and feldspar can be identified within them. Elsewhere within them a shear band foliation predominates, splitting the rock into a series of lenses, and indicating a sinistral sense of shear (plate 4.3*a*). It is thought that these bands represent a relatively late stage, local feature and are not of any widespread importance.

An interesting feature of the c-type mylonites on Scalpay lies in the opportunity to examine the effects of deformation on different rock types. Plates 4.3*b* and *c* show the responses of more basic rocks to the deformation. In plate 4.3*b*, deformation can be seen to be exploiting the boundary between a basic pod and the Gray Gneiss. The resulting c-type mylonite is extremely well foliated with numerous small scale crenulations. It appears to have mostly formed from the Gneiss, leaving the basic pod virtually untouched. Plate 4.3*c* shows a completely different response, with a boudinaged Scourie dyke taking on a mylonitic foliation whilst the Gray Gneiss has fractured into blocks which have then been rotated.

Both orientations of c-type mylonite bands have been offset by the late stage fault, which in places exploits the boundary between Gray Gneiss and more pegmatitic material.

The Late Stage Fault This fault runs WNW/ESE across the island from the North Harbour to Scoravick, dipping at around 60 degrees to the south. A sinistral offset of approximately 270 metres is apparent along it from the displacement of earlier features. About 10 cm of foliated gouge has been generated along the fault; this is very soft and weathers out easily. The presence of the gouge along this fault was probably an influence over the formation of the inlet known as North Harbour (figure 4.2). It is thought that the fault continues west-north-westwards and transects Harris through the isthmus on which Tarbert is situated. Thus it appears that it has exerted strong control over the location of present-day coastlines.

Gouge The gouge (plate 4.3*d*) has been generated in a zone along the fault described above. It is soft, fissile and shaley in appearance, green-gray in colour, incohesive and strongly foliated. Its thickness is variable from about 15 cm down to 3 cm, as the boundaries of the zone undulate. Extensive alteration of the original Gray Gneiss to clay minerals has occurred during its formation. Features

within the gouge include shear bands (plate 4.3*d*), asymmetric folds and quartz-infilled tension gashes. Although there is some ambiguity of sense of shear, overall displacement was probably sinistral - this is consistent with the observed offset of larger-scale features across the fault.

4.4 Crogary na Hoe and North Lee

Geographical Introduction Crogary na Hoe and North Lee are sited on large promontories on the eastern coast of North Uist. Although mapped separately (see figures 4.3 and 4.4) the two areas are lithologically and structurally similar and so will be described together. In combination, an area of some 12 km^2 was studied. Exposure is generally better in the North Lee block, as the topography is greater. The Crogary na Hoe region is mostly poorly exposed, due to extensive glaciation. The rocks that do outcrop tend to have been planed smooth, so that a somewhat two-dimensional picture is all that can be obtained. The sea cliffs in the east of the area afford good exposure but access is difficult.

Geological Introduction Deformation associated with the faulting is confined to the east of a line running from the island of Orasay in Bagh Chaise, through a point to

the east of the island of Flodday in Loch nam Madadh (all marked on figure 4.3), through Baigh Aird nam Madadh and on to the reservoir between North and South Lee (figure 4.4).The gneiss in the west of this line is relatively intact.

Eastwards, a wide zone of microbreccia develops, within which are slightly anastomosing c-type mylonite bands and discrete fault planes. These trend NE/SW with shallow dips to either east or west. The microbrecciation of the rock between the c-type mylonite bands becomes more intense eastwards, whilst the dip of the mylonite bands decreases (see cross sections Crogary na Hoe, Beinn Grotta and North Lee in figure 4.6). Discrete fault planes also occur within the microbreccia, where fractures have coalesced to allow finite displacement. Thus the general outcrop pattern is one of fault-bounded wedges of microbreccia separated by subparallel zones of more intense alteration and deformation represented by the c-type mylonite bands.

Intact Rock The rocks to the west of the limit of deformation are typically Gray Gneiss with the usual scattering of metabasite dykes and, to a lesser extent, pegmatitic material. The gneisses are generally more massive in this area than on Lewis and Scalpay, with mineral banding and gneissose foliation poorly developed. In the Loch Portain area (figure 4.3) the foliation trends

east-west, whereas at North Lee it runs more north-south.

Pods of metasediments are recognisable on the promontory of Rubha Mor (between Bagh Caolas an Eilein and Bagh Aird nam Madadh, north of North Lee (figure 4.4)), and in new exposure created by re-alignment of the A865 and A867 roads at Strumore, just outside Lochmaddy village (NGR NF 9098 6915) (outside area shown on figure 4.4). In these localities, a better foliation is developed and the rocks contain varying proportions of quartz, feldspar, hornblende, biotite and garnet. As far as can be seen, the foliation in these metasedimentary pods is concordant with that of the Gray Gneisses to either side of them.

The Strumore outcrop shows signs of deformation associated with faulting, with grain size reduction visible on some foliation planes, which appear to have accomodated small amounts of slip. In places, it is evident that fluid has passed along these slip planes, for the rock may be heavily epidotised and development of iron sulphide mineralisation is apparent.

Metabasites are found in small patches throughout the Lochportain region (figure 4.3), but are most concentrated in the areas east of Loch Hacklett and between Loch na Dubhcha and Loch Smallag. Figure 4.3 shows the localities, although the metabasite pods themselves are too small to

be shown. They are concordant with the surrounding Gray Gneisses and are composed almost entirely of very slightly altered hornblende.

Faults There are two main types of mappable faults in these areas, both occurring within the microbreccias: Discrete fault planes and late stage faults which cut across the earlier structures at a high angle. The late stage faults will be discussed later in this section. All the discrete faults trend generally NE/SW, striking and dipping (i.e. NW or SE) sub-parallel to the c-type mylonite bands. Together the mylonites and the discrete faults form an anastomosing network of failure surfaces, dissecting the already fragmented microbreccias into a series of elongate blocks (figures 4.3, 4.4).

The discrete faults manifest themselves as planes where the fractures within the microbreccias are very closely spaced or where they have coalesced to form a laterally continuous plane along which movement has been concentrated. They appear in the field as narrow zones traceable over considerable distances. They are often filled with fine crush breccia, and this has a tendency to weather out, leaving notches (in a manner similar to that shown in plate 4.5*b*). The outcrop of these faults tends to be restricted to the western edge of the microbreccias (see figures 4.3 and 4.4), although occasional examples

are found linking or truncating c-type mylonite bands in both localities. In some localities, notably north-east of North Lee (figure 4.4), an appreciable thickness of ultracataclasite (up to 15 metres) has been generated.

The relationship between the c-type mylonite bands and the discrete faults is unclear. In some localites (e.g. west of Creag Scalan, figure 4.3) the c-type mylonites terminate against them, whilst in others (e.g. west of Scor na Caillich, figure 4.4; west of Crogary na Hoe, figure 4.3) the faults appear to run into the mylonite bands with no disruption. It appears that motion can be transferred from the faults into the bands quite easily in some cases, whereas in others movement has been localised onto the fault plane segments after formation of the c-type mylonites.

Fault Rocks These are essentially confined to the area east of the line through Bagh Chaise, Flodday (figure 4.3), Bagh Aird nam Madadh and the reservoir (figure 4.4), with the exception of small amounts of pseudotachylyte, which extend westwards across much of North Uist, and the cataclasis already noted in the Strumore area.

Microbreccia East of the line delimiting the deformed area, the gneisses become cataclased and slightly altered in appearance. Two sets of gently undulating,

cross-cutting fractures appear as one progresses eastwards. Both sets are near horizontal, but dip gently in opposing directions (i.e. roughly to the east/southeast and west/northwest). Spacing between them is variable, from millimetres to metres, and they are generally better developed, and the degree of associated brecciation is stronger, to the east.

These fractures represent the 'early cataclastic foliation' of Sibson (1977b), and he termed the rock containing them 'crush melange'. Slight displacement has occurred along some of the fractures, and this results in the rock being split into a series of rhombs, as shown in plate 4.4*a*. The fractures themselves may have cataclased material present along them, whilst the intervening rhombs invariably show signs of cataclasis.

The size and shape of the rhombs varies with the spacing of the two fracture sets, from large blocks several metres across to tiny fragments. Often, they have been slightly rotated, and small offsets can be detected across the fractures, as seen by displaced markers, e.g. ultracataclasite veins. The rhombs are cemented together by minute veins of quartz, often barely visible in the field (see plate 4.4*b*). The fractures merge in places to form the discrete failure surfaces mentioned above, mapped as 'topographic thrusts' by Sibson (1977b).

C-type Mylonites Moving eastwards, the crushed material infilling the fractures in the microbreccia begins to show signs of alteration. Further east, the crushed material becomes more strongly altered, and alteration begins to affect the fracture walls, giving a wider zone of alteration. The altered material then begins to take on a crude foliation. It becomes dark green in colour and ultimately develops into c-type mylonite bands, whose orientations parallel those of the fractures. These c-type mylonites tend to weather along their foliation planes, resulting in slight iron staining.

The most prevalent c-type mylonite bands are those dipping to the east or southeast (see figures 4.3 and 4.4), with the northwest dipping set taking on a subordinate role, possibly as accomodation structures. The angle of dip of the east/southeast dipping bands tends to decrease towards the east - see the cross-sections for Crogary na Hoe, Beinn Grotta and North Lee presented in figure 4.6.

The bands have gradational boundaries, with alteration and foliation becoming more intense towards their centres. In hand specimen, the c-type mylonites appear to be composed mainly of alteration products; chlorite, epidote, clay minerals and micas, although the grain size is often

small. Foliation varies from barely detectable to good, although it is never as well developed as in the Scalpay c-type mylonites. Lineations are rare but can be found in the coastal exposures east of Crogary na Hoe. Of these, the majority are intersection lineations where the two fracture or foliation planes cross, but rare stretching lineations on eastward dipping foliation surfaces indicate a transport direction parallel to the downdip direction of these foliations.

The most notable features of the c-type mylonites are their sense of shear indicators. Marginal curve-in of foliation, shear-band orientation, asymmetry of crenulations and small-scale folds (plate 4.4*d*) and displacement of markers all give consistently normal senses of movement, for both orientations of c-type mylonite bands. The motion taken up by the mylonite bands of North Uist appears to have been extensional, and accomodated by dip-slip movement. There is no evidence for any component of oblique motion, as seen on Scalpay (section 4.3).

Ultracataclasite Two distinct varieties of ultracataclasites are found in the Crogary na Hoe/North Lee area. Firstly, there is a dark, indurated material which achieves thicknesses of up to 15 m along discrete fault planes in the microbreccias (as mentioned in the

'faults' sub-section). Secondly, there is a pale greenish, altered material which is present as small veins within the microbreccias throughout much of the area.

The first type is of limited extent, confined to the northwest slopes of North Lee (figure 4.4), between the peak and Bagh Aird nam Madadh. The outcrops follow the same north/northeast trend as the fractures and c-type mylonite bands, and appear to have been generated along discrete fault planes within the microbreccias. The rock is dark in colour, indurated and massive. A considerable amount of strain energy must be stored in it, as it tends to fracture explosively when hammered. Late stage jointing has split the ultracataclasite into a series of near cubic blocks.

The second type of ultracataclasite occurs as veins, injected both into the rhombohedral microbreccia fragments and along fractures. They are often green in colour, suggesting heavy alteration, and 'flow' textures (possibly fluxion structures) are sometimes visible within them. Vein orientation tends to be controlled by the microbreccia fractures. Where the ultracataclasite is injected into rock fragments, it seems to be exploiting pre-existing cracks.

Plate 4.4*c* shows a banded green ultracataclasite vein,

parallel to the eastward dipping set of fractures, which has been transected by the westward orientated set and then pulled apart. From observation of similar veins, in varying orientations, it seems that the two fracture sets formed early on, followed by the generation and injection of the ultracataclasite veins. At a later date, extensional reactivation occurred, at least on a local scale, fragmenting the veins, offsetting them in a normal sense and pulling the vein fragments apart. The spaces between individual fragments then became infilled with crushed material, possibly by a process of cataclastic flow (plate 4.4*c*).

The dark ultracataclasites were almost certainly generated along the discrete fault planes as they formed. Why they should be restricted to the one locality is unknown. The greenish ultracataclasite was probably generated along the smaller fractures in the microbreccias, with some of it then being injected into barren cracks to form veins. It appears to predate c-type mylonite formation (and some of the fracturing - see above), but has been heavily altered subsequently, possibly by the same event that caused widespread alteration in the microbreccias and gave rise to the c-type mylonites. Thus it seems that both varieties of ultracataclasite represent fairly early events in the deformation history.

Other Fault Rocks Southeast of Beinn Grotta (figure 4.3) a most unusual lithology occurs at the contact between c-type mylonite below and microbreccia above. Illustrated in plate 4.5*a*, this rock parallels the eastward dipping foliation in the c-type mylonite, and consists of a badly weathered, iron-stained rubble-like material with blocks of altered microbreccia up to 60 cm in length sitting randomly in a matrix of soft, ochre-coloured clay-like matter. The lower boundary of this zone is sharp, whilst the upper is only marginally less so. It appears to be a zone of brecciation that has subsequently acted as a conduit for fluids and has undergone intense alteration.

Late Stage Faults Two late stage, vertical faults occur in the area (see figures 4.3 and 4.4). The largest of these trends southeast through the valley between North and South Lee (figure 4.4), and appears to offset the c-type mylonite bands sinistrally by around 150 metres. The other runs from Loch Scalan (figure 4.3) eastnortheastwards to the sea, and also has a sinistral displacement of indeterminate, but probably small, magnitude.

These faults are considered to be late stage because they cut and displace earlier features, and because of their different trend and/or vertical dips. The direction

of displacement across them is sinistral, whereas all the earlier faults show dip-slip (or slightly oblique) movement, where this can be ascertained.

4.5 Usinish

Geographical Introduction Usinish differs from the previously studied areas in that it is structurally much simpler, in terms of mappable features, and lithologically more complex. The area mapped (figure 4.5) runs along the southern shores of Loch Skipport and out to the lighthouse on the Usinish promontory. Mapping coverage was restricted by lack of exposure away from the coast, with the exception of Ornish and Maol Martaig. On Maol Martaig, individual NNE trending fault planes weather out to give rise to distinct gullies (plate 4.5*b*); these are the 'topographic fault planes' of Sibson (1977b). The fault planes dip at around 40 degrees for the westernmost ones, shallowing to about 20 degrees eastwards (figure 4.5).

Geological Introduction The host rocks are different from those in the areas described previously. The intact rocks in the west are the standard Gray Gneisses and above the westernmost fault (figure 4.5) they show the usual signs of microbrecciation. Above these lies the more basic Corodale Gneiss, and above this lies the acidic Mashed Gneiss unit (figure 4.5).

Microbrecciation in this area is confined to the Gray

Gneiss. Both this and the Corodale Gneiss show development of discrete fault planes, which trend roughly northnortheast and have variable eastward dips (see cross section in figure 4.6). Late stage faults cut and displace the discrete faults in a sinistral sense. A c-type mylonite band separates the Corodale Gneiss from the Mashed Gneiss.

Intact Rock In this area, there is some difficulty in deciding exactly what constitutes intact rock. The Gray Gneisses are relatively straightforward; they are only intact to the west of the limit of microbreccia formation, as in the areas already described. However, the Corodale Gneiss lies to the east and structurally above this limit of deformation, yet remains for the most part undeformed, save for some discrete faults and some pseudotachylyte development. The Mashed Gneiss also is a separate lithological unit, but is so altered, whether by fluids related to the faulting or to some prior event, that its origins are obscure.

Intact Gray Gneiss The Gray Gneisses west of the limit of deformation are quartzo-feldspathic and poorly banded. Their foliation trends northwesterly and is not well developed. To the east of Loch Bein (figure 4.5) a patch of equigranular, coarse-grained hornblende and feldspar rock is found within the microbrecciated area, which is

devoid of any trace of foliation or banding, and appearing massive. Its metamorphic history is unknown.

Corodale Gneiss Above the Gray Gneiss, and separated from it by an eastward dipping fault plane, lies the Corodale Gneiss. As described in Chapter 3, the Corodale Gneiss is more basic than the Gray Gneisses and has a pyroxene-bearing assemblage. In general it is fine grained in this area, although occasional patches of coarse pyroxenite (grains up to 1 cm) are found. The Corodale Gneiss weathers to a rusty brown colour, and is often heavily jointed in random orientations. The western outcrops are reasonably fresh, whilst those to the east may be altered. They then have a more greenish colouration and epidote is visible in hand specimen. Pseudotachylyte occurs sporadically throughout the Corodale Gneiss.

Mashed Gneiss The rock unit that occupies the Usinish peninsula (figure 4.5) was named 'Mashed Gneiss' by Sibson (1977b). Its exposure is poor, and the rocks are so heavily altered and brecciated that structural relationships are almost impossible to observe. It has been brecciated, and has undergone heavy alteration, possibly syn- and post-tectonically. The resultant melange was then further broken up by a phase of jointing, much of which appears to have been subsequently recemented. It is not known whether the jointing represents a phase of

uplift post-dating the brecciation and alteration, or if it represents reactivation of a pre-existing set of joints.

In appearance, it is a white or pale green, strongly altered, acidic rock. It is extensively fractured, and has weathered to leave hackly, jagged surfaces. It contains no obvious internal structures apart from the fractures; even grain size is often indeterminate. The assemblage appears to contain quartz, feldspar and some epidote, and sometimes chlorite. It has been affected by the faulting, which probably caused some brecciation and much alteration within it, but how badly it was cataclased and/or altered prior to this is unknown.

It is possible that the Mashed Gneiss was derived by excessively strong alteration of Gray Gneiss by fluids from the fault zones, i.e. it represents 'end-member' altered Gray Gneiss microbreccia. The geochemical evidence (chapter 6) supports this, as the compositions of the Mashed Gneiss broadly coincide with those for the Gray Gneiss derived altered microbreccias. Furthermore, fluid content and alteration within the deformed rocks of the fault zone show a general increase towards the hanging wall. The Mashed Gneiss is the highest structural unit exposed on the Outer Hebrides, and is certainly the most strongly altered. However, there is no field or thin

section evidence for the relative timing of the brecciation and alteration episodes.

However, the Mashed Gneiss does not appear to show any of the usual deformation features typical of the Gray Gneiss (i.e. no pervasive fracture system or discrete fault planes visible). It is probable that the extensive alteration has annealed or sealed up these typical features.

In conclusion, it is thought that the Mashed Gneiss represents a cataclased and altered rock unit, possibly derived from Gray Gneiss, which has been heavily affected by hydrothermal fluids, and later fractured by reactivation along joint planes.

Faults The early faults are discrete fault planes within the microbreccias and the Corodale Gneiss. They trend NNE and dip between 42 and 27 degrees to the east. The dip of these faults shallows to the east (see the Loch Skipport/Usinish cross-section in figure 4.6). The faults within the microbreccias form splays, branching northwards from a single plane in the south. They are accompanied by moderate amounts of cataclasis.

The fault that acts as the boundary between the

microbreccia and the Corodale Gneiss (figure 4.5) is marked by strong cataclasis. Grain size reduction is severe, with dark ultracataclasite, similar to that of the North Lee area (section 4.4, figure 4.4) formed locally. The cataclasis extends up to 20 m wide in places, although the thickness is laterally variable and exposure generally poor. Most of the larger fragments in the crushed material appear to be of Gray Gneiss/microbreccia origin, suggesting that the Corodale Gneiss acted as a virtually inert pod during deformation.

The discrete faults within the Corodale Gneiss are similar to those in the microbreccias, though laterally less continuous (figure 4.5). They are the only large-scale response to deformation within this rock unit. Extensive microbrecciation has not occurred in the Corodale Gneiss, although small amounts of crush breccia have been generated along the faults.

Fault Rocks The fault rocks are generally similar to those in the areas already described, with the possible exception of the Mashed Gneiss, though to what extent this can be termed a fault rock is debatable. Microbreccia, c-type mylonite, pale green and dark ultracataclasite and pseudotachylyte all occur.

Microbreccia Microbrecciation is similar to that in the

Crogary na Hoe/North Lee areas (figures 4.3 and 4.4). Pervasive fracturing and crushing has occurred, with these becoming stronger to the east. Alteration, both of the fracture infills and the rock fragments between the fractures, also becomes slightly stronger eastwards, towards the Corodale Gneiss.

C-Type Mylonite Only one c-type mylonite band occurs. It runs almost north/south along the coast in the northern part of the area, but to the south it separates the Corodale Gneiss from the Mashed Gneiss on Usinish (figure 4.5). Its dip varies from around 70 degrees in the north to 20 degrees in the south, and it is lithologically similar to the c-type mylonites of Scalpay and North Uist. Sense-of-shear indicators (tight asymmetric folds) suggest predominantly normal, dip-slip movement.

The extreme variability in the dip of this c-type mylonite band is a unique feature. The dip appears to progressively steepen to the north (figure 4.5). It is suggested that, during the initial stages of deformation, cataclasis occurred along the boundary between the Mashed Gneiss and the Corodale Gneiss. Subsequent further deformation and alteration allowed this cataclased material to develop into a c-type mylonite. The present outcrop pattern of the mylonite band therefore probably reflects that of the original Corodale Gneiss/Mashed

Gneiss boundary.

Ultracataclasite As described for the North Uist area (section 4.4), two types of ultracataclasite occur. However, here their development seems to be strongly controlled by host rock type. Development of small amounts of pale green ultracataclasite veining (similar to those described on North Uist - section 4.4) is confined to the microbreccias, where it is common. The dark, indurated variety of ultracataclasite outcrops as small pods along the discrete fault planes present in the microbreccias and the Corodale Gneiss.

Pseudotachylyte Two types of pseudotachylyte were briefly mentioned in section 4.2. Both types are present here, but are very much better developed. The first type appears to be confined to the Corodale Gneiss, which, in places, contains large concentrations of pervasively distributed pseudotachylyte veining (plate 4.5*c* and *d*). This pseudotachylyte is brown in colour and not very fresh. It is frequently fractured, giving an appearance similar to those on Malasgair, Lewis (section 4.2). The fractures are probably due to cooling and/or uplift.

The second type of pseudotachylyte is the more typical black, fresh, unfractured type which is common throughout the islands. It is found here in the Gray Gneiss, the

microbreccias, and the Corodale Gneiss. It has not been seen in the Mashed Gneiss, although this may be due to obliteration by the extensive alteration which has affected this unit.

It is thought that these two types of pseudotachylyte may represent two separate events in the tectonic history of the area. The brown type, being less fresh and more affected by fracturing, probably represent an early phase of deformation during which the Corodale Gneiss underwent some internal disruption, giving rise to pseudotachylyte. This subsequently became fractured and altered as it cooled and was uplifted. This may have occurred as early on as during post-Laxfordian cooling.

The second phase of pseudotachylyte generation, producing the black, fresh, undeformed material, obviously postdates this, and may be related to the event which gave rise to the microbrecciation of the Gray Gneisses.

Late Stage Faults Four late stage faults occur in the Loch Skipport/Usinish area. They are all sub-vertical, and record sinistral displacements. Three of the four, those to the north, trend NW/SE (figure 4.5), whilst the fourth strikes more NE/SW. All four of the faults displace the boundary between the microbreccias and the Corodale Gneiss.

The Area to the North Across Loch Skipport from the Usinish locality lies East Gerinish, which affords some excellent exposures of the contacts between various lithologies. Plate 4.5*e* shows a tectonic contact between an altered pegmatite sheet, similar in appearance to the Mashed Gneiss, and a basic dyke of Scourian age. The contact is extremely sharp, and has been heavily sheared. Plate 4.5*f* depicts the closest juxtaposition observed in the field of the Gray Gneiss and the Corodale Gneiss. This contact is also sheared, suggesting that deformation is exploiting boundaries between rocks of differing competences.

4.6 The Sampling Traverses

The traverses were undertaken to follow as near as possible a line at right angles to the strike of the fault zone (as determined from Sibson (1977b)) from the east coast into the footwall of the fault. Samples could not be taken at regular intervals as this would have resulted in missing many of the rock types - they often occur as rather narrow bands - and because of irregularities in exposure. Instead, samples were collected wherever there was an obvious change in fault rock type. Some fault rocks are softer than others, notably the c-type mylonites, and

tend to weather out, so to avoid sample bias heavily in favour of the more resistant fault rocks, it was sometimes necessary to leave the line of the traverse and move along strike to find a suitable exposure before rejoining the traverse.

Figure 4.6 illustrates cross sections drawn along all the lines of sampling, some of which coincide with the mapped areas (see figure 1.3 for locations of the traverses). Where this is not the case, an additional cross section of the mapped area has been included. The variable nature of the faults is also displayed, from the discrete, single plane to the c-type mylonite belt within the wide zones of crushing represented by the microbreccias. The sections show across strike (east-west) variations in host lithologies and fault rock types. Taken together, they enable comparisons of the same features to be made along strike.

It is important to realise that there is no real control at depth on these sections, other than that which can be obtained from seismic surveys, eg. the MOIST and WINCH profiles (figure 2.2). Such surveys reveal much about the sub-surface structure of the Outer Hebrides Fault Zone, but the features it resolves are of a larger scale then those mapped on land. It seems probable that what is shown on these surveys as a single fault plane at depth is the

same structure that is observed on land as an assemblage of numerous different elements.

It is known from seismic profiles that individual fault planes observe a listric or ramp-flat geometry at depth, and it is possible that the majority join some form of sole fault at depth. Within the scale of the field observations, however, the fault rock bands and faults are essentially planar and are represented on the cross-sections as such.

The most notable feature of the sections is the marked decrease eastwards in the angle of dip of the fault planes. This geometry does not fit the classic imbricate or duplex models for thrust fault development, where the earlier faults become part of the hanging wall as the fault propagates into its footwall. In this situation, the dip of the earlier faults should steepen as they become back rotated by movement along the sole fault. The shallowing in dip actually observed suggests the contrary, that the fault system developed in an extensional regime.

It is possible that the faults propagated initially as a thrust zone. In this case, in order to achieve the observed geometry, displacement due to normal reactivation would have had to be greater than the initial thrust displacement. This hypothesis is considered unlikely,

however, as it would be difficult to normally reactivate *every* element within the fault system, yet sense-of-shear indicators are almost entirely consistent with extension. Possible histories for the development of the fault zone as a whole will be discussed further in chapters 7 and 8.

Another feature revealed by the cross-sections is the virtual lack of deformation within the Corodale Gneisses - see the sections for Loch Skipport and Ben na Hoe. Deformation seems to have been concentrated at the margins of the Corodale unit, leaving the bulk of it intact, save for jointing and some early-formed pseudotachylyte.

Also brought out by the sections is the variability of fault plane dips within the general pattern of the decrease in dip eastwards. It is apparent that the individual fault planes, c-mylonites and cataclasite bands cannot in reality be regarded as planar. From seismic studies to the north, it is thought that the fault zone contains several lateral ramps (Enfield, pers. comm.). This may help to explain the somewhat arcuate trace of the fault zone on land.

The implication of the presence of lateral ramps is that some of the cross-sections, apparently drawn perpendicular to the strike of the fault zone and displaying the true dip projection, may, in fact, be sub-parallel or slightly

oblique to a lateral ramp, so the section will not be accurate. Several of the generally available seismic lines for the area (e.g. MOIST, parts of WINCH) intersect the fault zone at laterals, which may partly explain some discrepancies (as mentioned earlier) between seismic and field observations.

4.7 Summary

A summary of the fieldwork observations is given in table 4.1, showing main east to west and north to south variations in deformation style across and along the strike of the fault zone. The main north-south variation is reflected in the confinement of crystal plastic deformation to Lewis, with the outcrop of the r-type mylonites. To the east of these, and everywhere else on the islands, the deformation is predominantly brittle, with the formation of microbreccia, cataclasite and c-type mylonite. East -west variations are more pronounced, with microbrecciation and alteration becoming stronger eastwards, and the formation of c-type mylonite bands.

The general outcrop pattern, going west to east, is as follows. West of the limit of deformation, there is intact Gray Gneiss, which usually has slight quantities of fresh pseudotachylyte veining. Eastwards, the Gray Gneiss begins to show signs of cataclasis; this marks the limit of

deformation or base of the fault zone. Above this, the Gneiss becomes microbrecciated, with development of brecciated rhombohedral fragments separated by fracture planes along which cataclasis proceeded further. In places these fractures link up to form more continuous fault planes which transect the microbreccia into a series of elongate, sub-parallel blocks up to 1 km wide. Ultracataclasite may form locally along these fault planes.

Eastwards, fracturing and cataclasis of the microbreccias becomes more intense. Finer grained material generated along the fractures is injected into barren fractures to form ultracataclasite veins. The material infilling the fractures begins to show signs of alteration. The alteration begins to affect the fracture walls and, in combination with continued deformation, ultimately results in development of the c-type mylonite bands to the extreme east. Further deformation, possibly localised onto the c-type mylonite bands, produces normal sense-of-shear indicators.

There are fault rocks on the Outer Hebrides which have not been formed as part of this process. These are the r-type mylonite, the phyllonite, the brown pseudotachylyte and the gouge. The r-type mylonites are thought to have formed at an early stage in the history of the islands,

and they may outcrop west of the limit of deformation, as defined by the microbrecciation. From textural and mineralogical evidence (see chapters 5 and 6), it appears that the r-type mylonites formed in amphibolite facies conditions, and are hence much earlier than the bulk of the deformation. They are probably Laxfordian in age, and related to the metamorphism.

The phyllonites represent retrogressed r-type mylonites. The timing of the retrogression is unknown, but probably post-dates initial r-type mylonite formation as the resultant mineral assemblages are of lower grade than amphibolite facies.

For reasons already mentioned in section 4.5, it seems that the brown pseudotachylyte is a distinct phase from the black material which is found throughout the islands. The brown pseudotachylyte appears to be confined to areas on Lewis, where its outcrop seems to be related to that of the r-type mylonites, and South Uist, where it occurs within the Corodale Gneiss. It is also thought to represent an early event, whereas the black pseudotachylyte probably formed in relation to the microbrecciation episode.

The gouge is only found on Scalpay, and has been generated along what is undoubtedly a late-stage fault. As

such, it postdates the microbrecciation episode, although the fault itself may be reactivating an earlier feature.

Figure 4.1

Field map of the Seaforth Head area - Malasgair and Shiltenish, Isle of Lewis.
The dip of the gneissose foliation and the fault planes are indicated by the number of ticks on the symbols (ticks to down dip side): Single tick - <30 degrees, double ticks - 30 to 60 degrees.

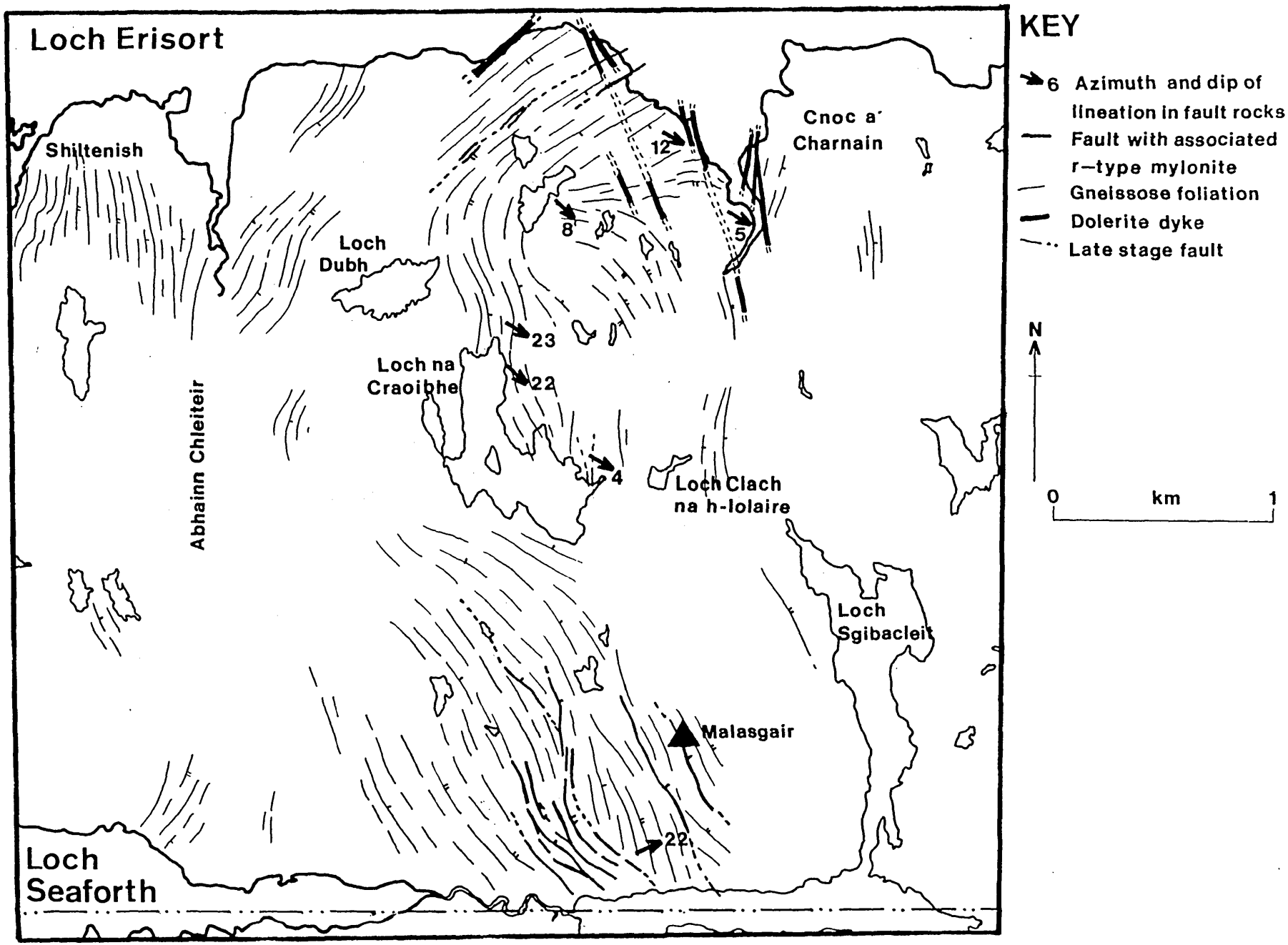

Loch Erisort
Shiltenish
Loch Dubh
Cnoc a' Charnain
12
8
5
23
22
Loch na Craoibhe
Abhainn Chleiteir
4
Loch Clach na h-Iolaire
Loch Sgibacleit
Malasgair
22
Loch Seaforth
KEY
6 Azimuth and dip of lineation in fault rocks
Fault with associated r–type mylonite
Gneissose foliation
Dolerite dyke
Late stage fault
N
0
km
1

Figure 4.2

Field map of the island of Scalpay, off Harris.
The dip of the gneissose foliation is indicated by the number of ticks on the foliation symbols (ticks to down dip side): Single tick - < 30 degrees, double ticks - 30 to 60 degrees, treble ticks - >60 degrees.

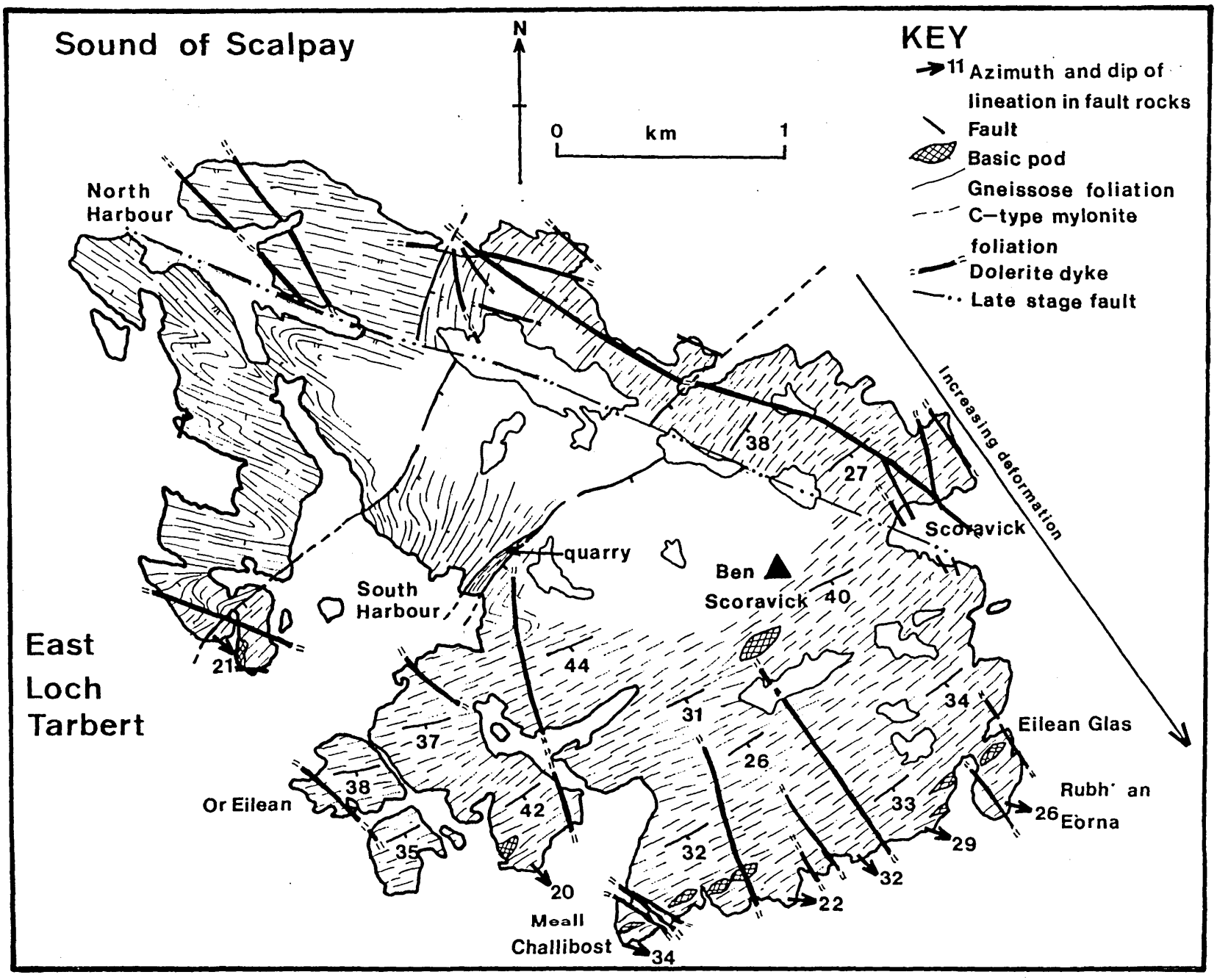

Sound of Scalpay
N
0 km 1
KEY
11 Azimuth and dip of lineation in fault rocks
Fault
Basic pod
Gneissose foliation
C–type mylonite foliation
Dolerite dyke
Late stage fault
Increasing deformation
North Harbour
South Harbour
East Loch Tarbert
quarry
Ben Scoravick
Scoravick
Eilean Glas
Rubh' an Eòrna
Or Eilean
Meall Challibost
21
38
27
44
40
31
34
37
26
38
42
33
35
32
29
20
22
32
34
26

Figure 4.3

Field map of the Crogary na Hoe area, North Uist.
The dip of the microbreccia foliation is indicated by the number of ticks on the foliation symbols (ticks to down dip side): Single tick - <30 degrees, double ticks - 30 to 60 degrees, treble ticks - >60 degrees.

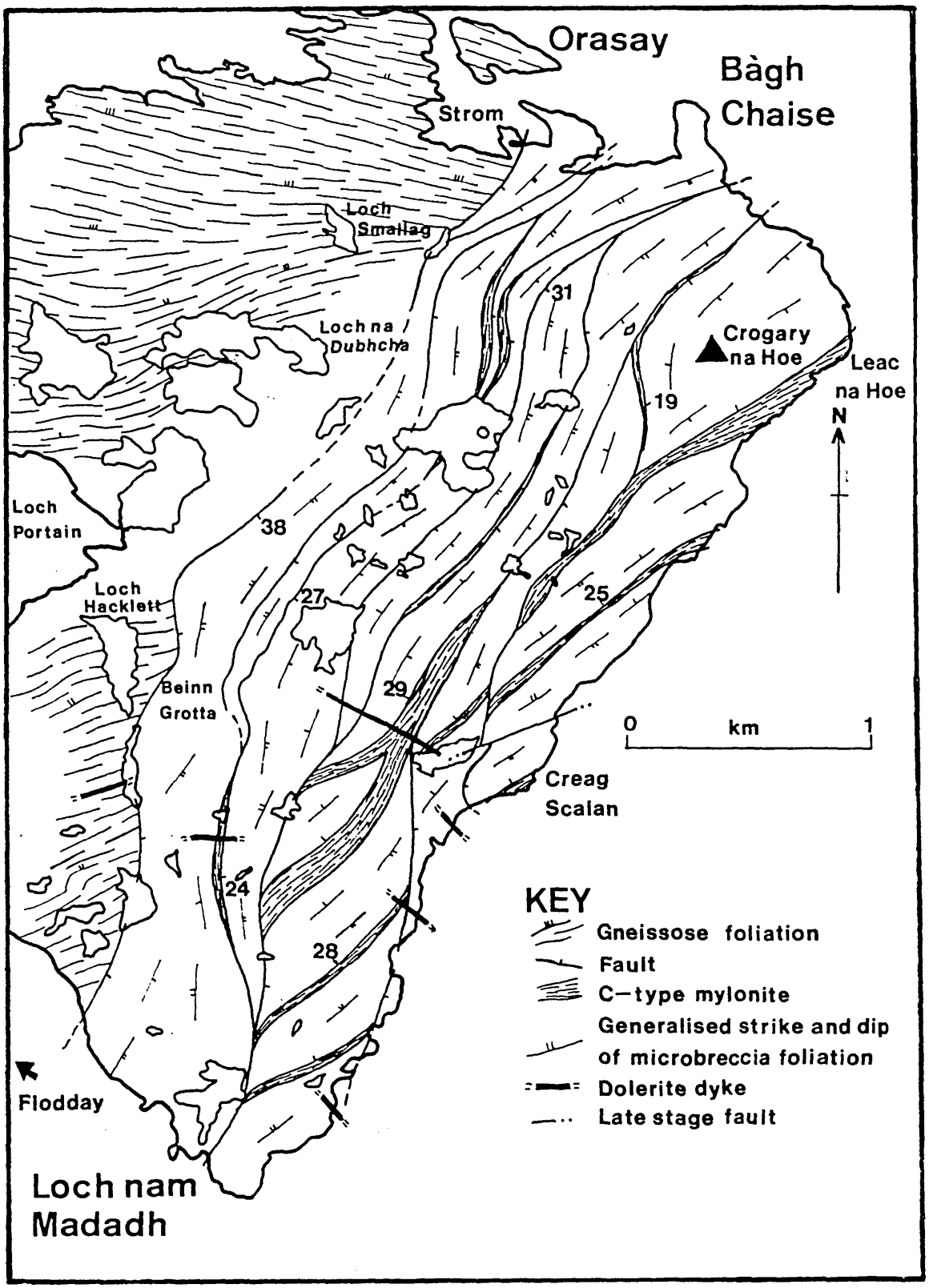

Orasay
Bàgh Chaise
Strom
Loch Smallag
Loch na Dubhcha
31
Crogary na Hoe
Leac na Hoe
19
N
Loch Portain
38
Loch Hacklett
27
25
Beinn Grotta
29
0 km 1
Creag Scalan
24
28
Flodday
Loch nam Madadh
KEY
Gneissose foliation
Fault
C–type mylonite
Generalised strike and dip of microbreccia foliation
Dolerite dyke
Late stage fault

Figure 4.4

Field map of the North Lee area, North Uist.
The dip of the microbreccia and gneissose foliations are indicated by the number of ticks on the foliation symbols (ticks to down dip side): Single tick - <30 degrees, double ticks - 30 to 60 degrees.

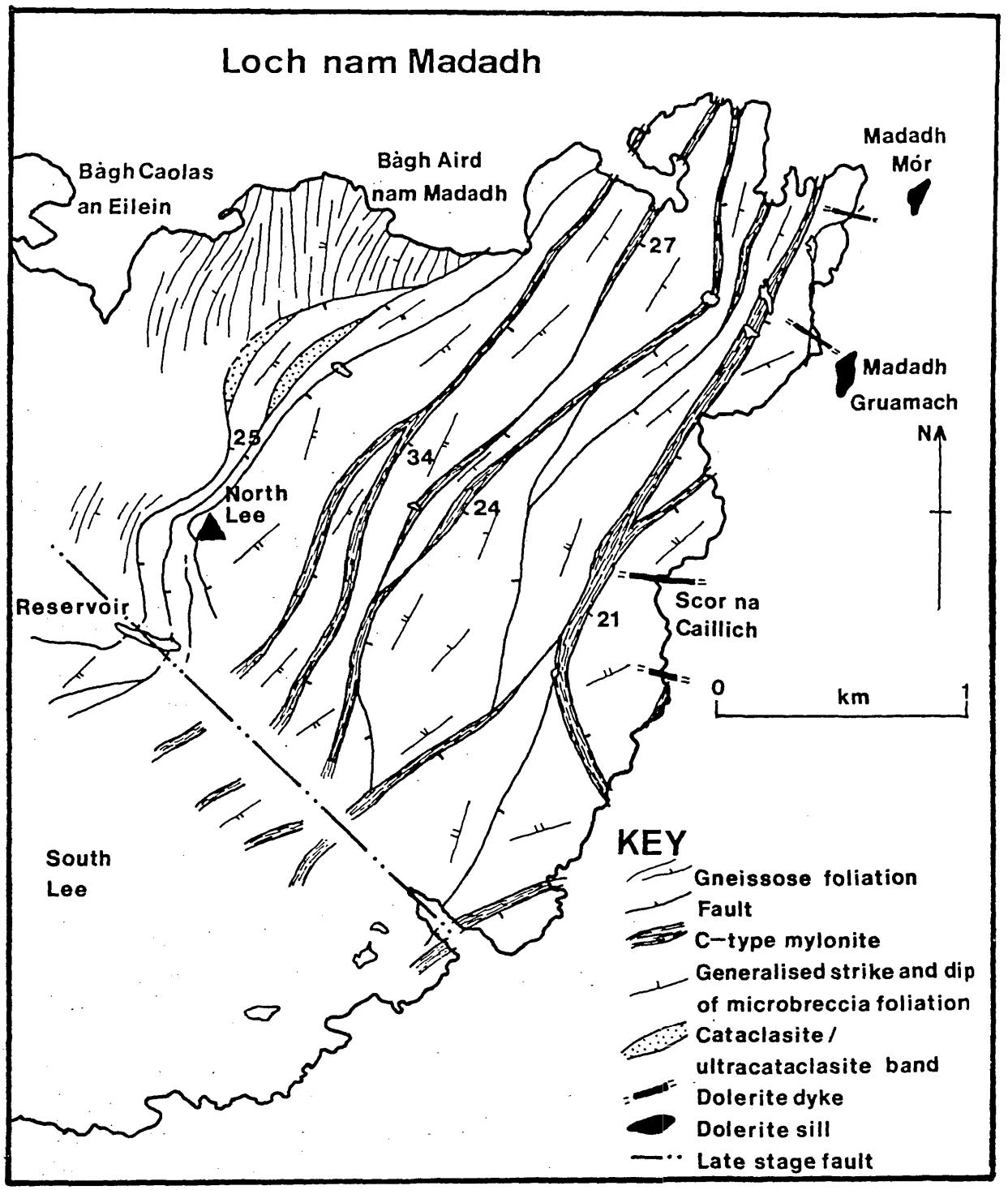

Loch nam Madadh
Bàgh Caolas an Eilein
Bàgh Aird nam Madadh
Madadh Mór
Madadh Gruamach
NA
27
25
34
24
21
North Lee
Reservoir
Scor na Caillich
South Lee
0
km
1
KEY
Gneissose foliation
Fault
C–type mylonite
Generalised strike and dip of microbreccia foliation
Cataclasite / ultracataclasite band
Dolerite dyke
Dolerite sill
Late stage fault

Figure 4.5

Field map of the Usinish area, South Uist.
Heavy stipple represents Corodale Gneiss, light stipple represents Mashed Gneiss and no ornament represents Gray Gneiss.
The dip of the microbreccia and gneissose foliations, and the fractures in the Mashed Gneiss, are indicated by the number of ticks on the symbols (ticks to down dip side): Single tick - <30 degrees, double ticks - 30 to 60 degrees, treble ticks - >60 degrees.

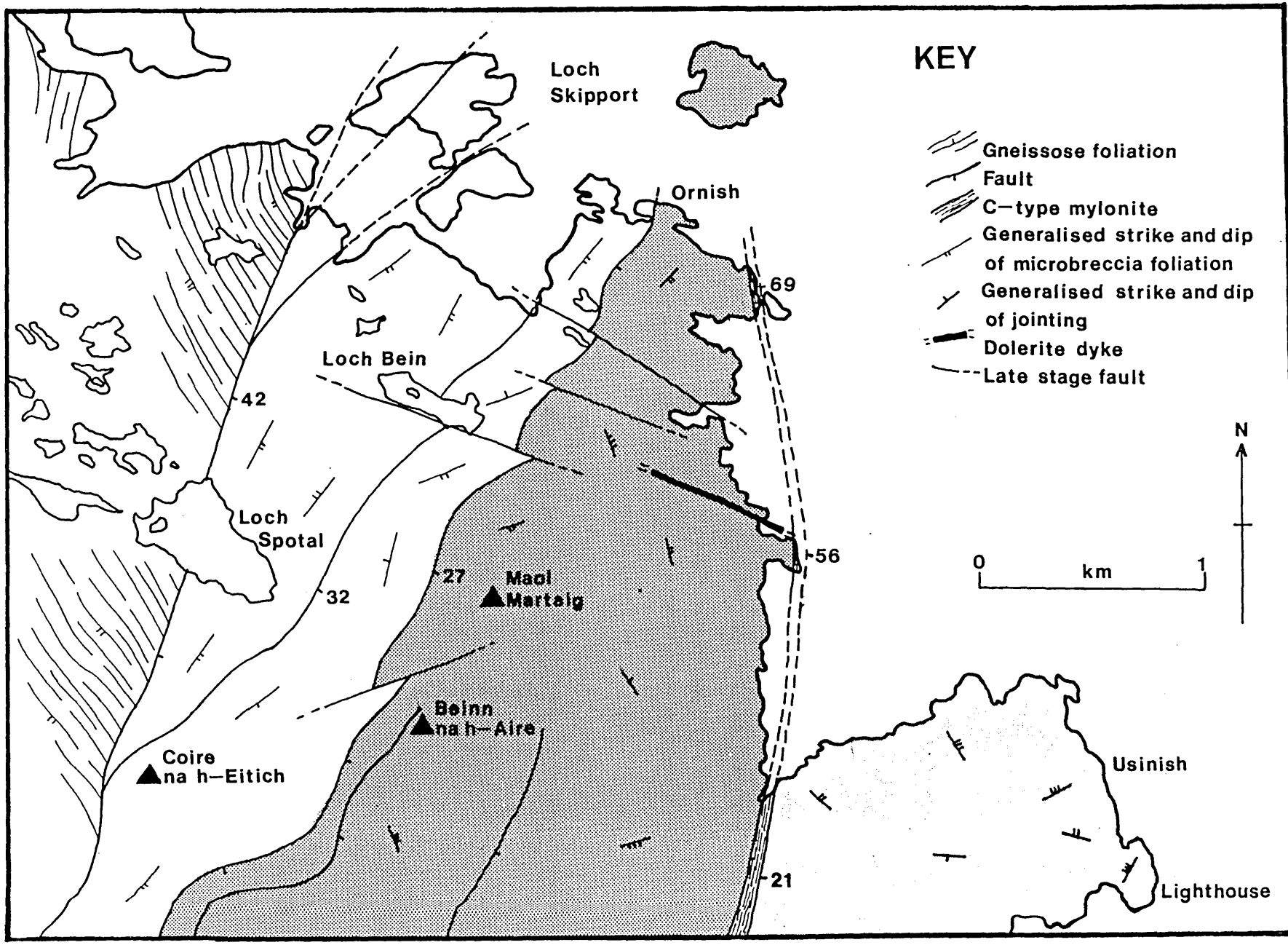

KEY
Gneissose foliation
Fault
C–type mylonite
Generalised strike and dip of microbreccia foliation
Generalised strike and dip of jointing
Dolerite dyke
Late stage fault
N
0
km
1
Loch Skipport
Ornish
Loch Bein
Loch Spotal
Maol Martaig
Beinn na h–Aire
Coire na h–Eitich
Usinish
Lighthouse
42
32
27
69
56
21

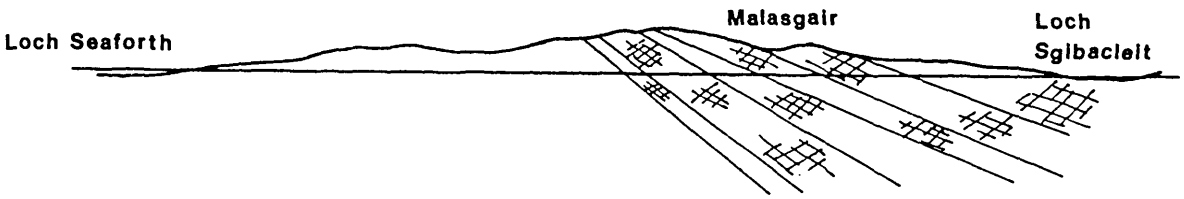
Figure 4.6

Cross-sections drawn along the sampling traverses. Cross-hatching = microbreccia, close cross-hatching = basic pods, dashes = c-type mylonites, heavy stipple = Corodale Gneiss, light stipple = Mashed Gneiss, random dots = ultacataclasite bands. Discrete lines represent individual fault planes. All fault planes have a down dip sense of movement.

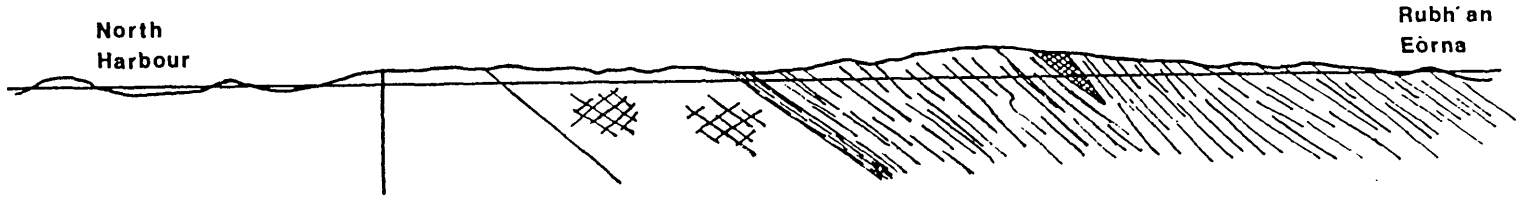
Vertical scale = horizontal scale = 1:25 000 (4 cm to 1 km).

The locations of the sampling traverses are given in figure 1.3.

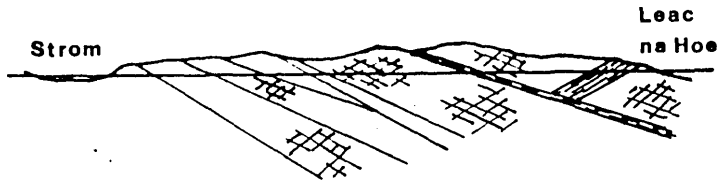
MALASGAIR / SHILDENISH



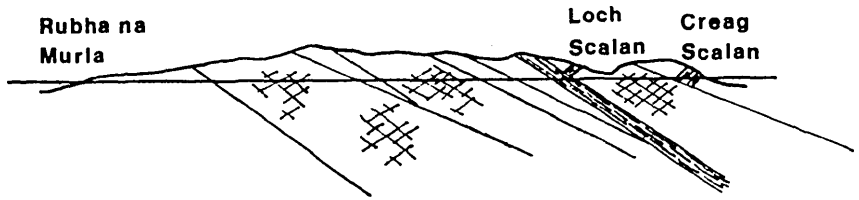
SCALPAY



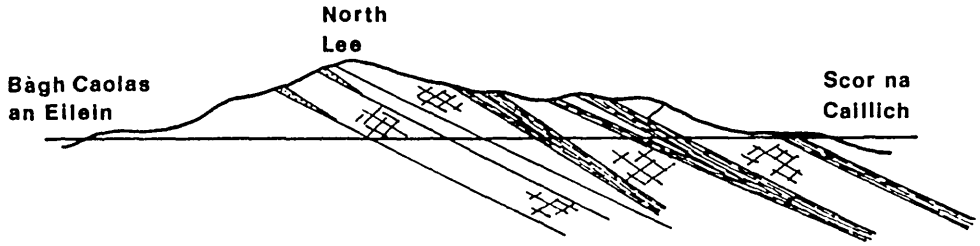
CROGARY NA HOE



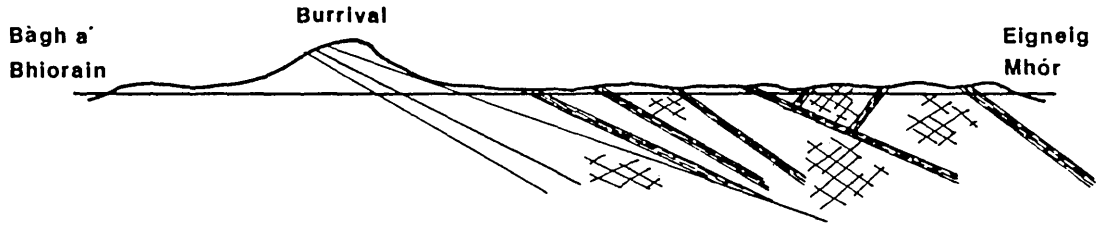
BEINN GROTTA



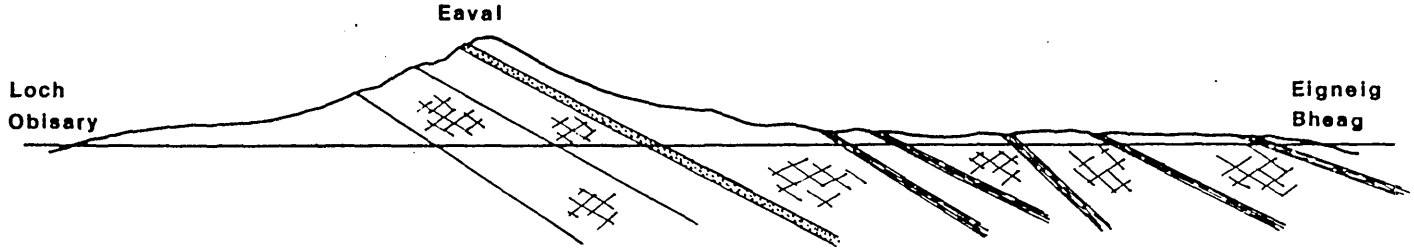
NORTH LEE



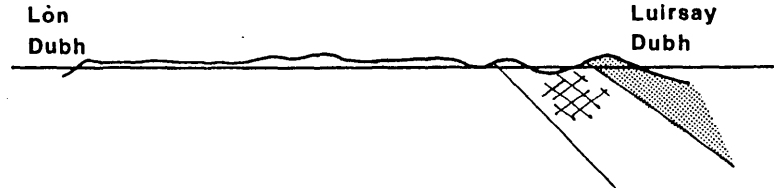
BURRIVAL



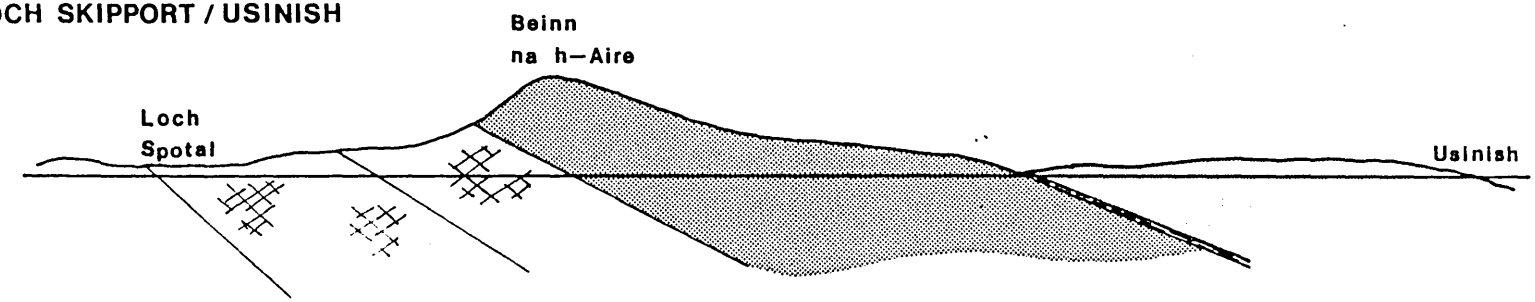
EAVAL



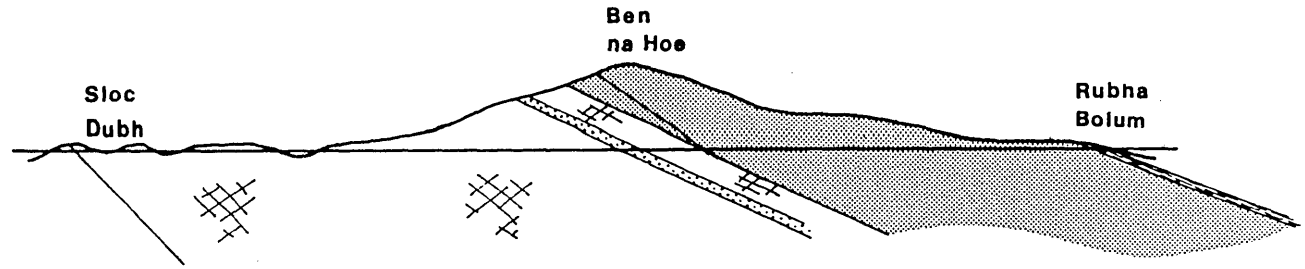
EAST GERINISH



LOCH SKIPPORT / USINISH



BEN NA HOE



NORTH GLENDALE



Table 4.1

Area	West of margin of deformation	At margin of deformation	Within margins of deformation
Central Lewis	R-mylonitic fabric (amphibolite facies) common in gneisses. Minor thrust faults with psueotachylite/ R-type ultramylonite	Zone of microbreccia marks fault zone. Roughly coincident with the NW limit of (hydrothermal) alteration.	Microbreccia and c-type mylonite alteration of variable intensity to east. Early r-type mylonites locally altered to phyllonites. (Coherent acid gneisses found extensively in both Central and South Lewis.
South Lewis	Localised early r-type mylonite to the north. C-type mylonites to the east. Thrust faulting localised at margins of granite sheets	Pseudotachylite developed along minor faults. R-type mylonites spatially coincident with pseudotachylite development. Some microbreccia.	Microbreccia with areas of altered microbreccia. C-type mylonite bands developed, some showing tight chevron folds and strong foliation, indicating normal sense of shear.
Harris	Effects largely absent. Minor pseudotachylite and minor thrusts associated with granites. Local brecciation and alteration extending to NW	Minor pseudotachylite. Some microbreccia formed in anorthosite.	C-type mylonites on Scalpay, especially evident in acid rocks. General brecciation and alteration
North Uist	Pseudotachylite and microbreccia. Localised alteration	Wide zone of altered microbreccia. C-type mylonites in Loch Portain and Lee areas.	Microbreccia with minor pods of coherent gneiss. C-type mylonites abundant, with local tight chevron folding

Area	West of margin of deformation	At margin of deformation	Within margins of deformation
South Uist	Minor pseudotachylites	Thick pseudotachylite/ ultracataclasite zones.	Granulite facies rocks contain minor pseudotachylite. Slightly altered c-type mylonites developed from acid gneisses. Alteration stronger to east.
Barra	Sporadic pseudotachylite	Pseudotachylite marks the fault front.	Granulite facies rocks with few fault features. C-type mylonites may lie offshore to east, where there are deep channels in the sea floor.

Modified from Fettes and Mendum (1987)

Plate 4.1

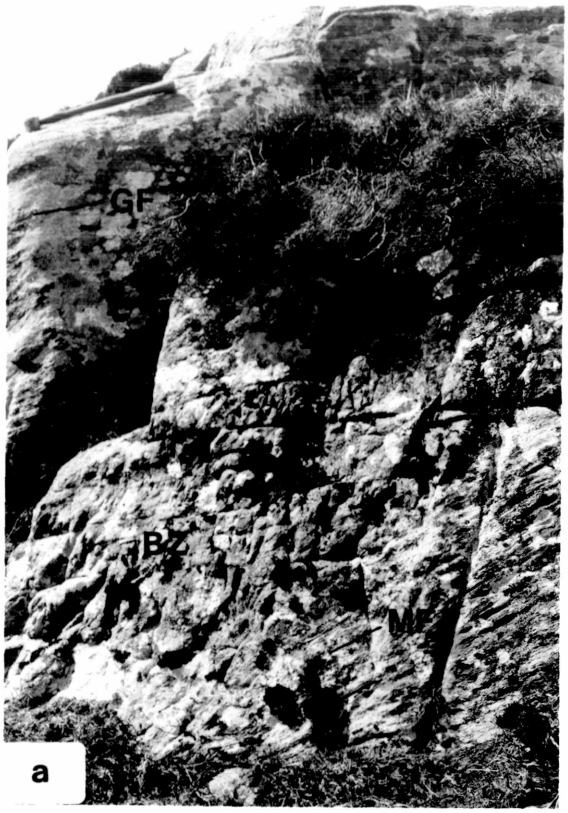
Field photographs from Malasgair and Shildenish, Lewis.

a Transition zone between Gray Gneiss (*top of photograph*) and r-type mylonite (foreground). The boundary is gradational, and marked by a blocky zone (BZ) of microbreccia. The gneissose foliation (GF) dips at a low angle towards the bottom left, whilst the mylonitic foliation (MF) dips in the same direction but more steeply. Beinn Mheadhonach, Shildenish, Lewis. GR NB 2982 1955

b Characteristic brecciated, blocky appearance of the Gray Gneiss microbreccia away from the faults, due to extensive fracturing. The appearance is very similar to that of the blocky zone shown in plate 4.1*a*. Loch na Craoibhe, Shildenish, Lewis. GR NB 3022 1829

c Black pseudotachylyte in Gray Gneiss. The 'Y' shape is formed by an injection vein branching off a generating surface. Mullach Breac Malasgair, Lewis. GR NB 2996 1675

d Typical appearance of pseudotachylyte on Lewis. The pseudotachylyte is brown in colour and heavily fractured. Most of the fractures run near vertical, and are very closely spaced. Mullach Breac Malasgair, Lewis. GR NB 2998 1674


GF
BZ
a


b


OLYMPUS
c


d

Plate 4.2

Field photographs of Malasgair, Lewis, and Scalpay, Harris.

a Tight folding of a brown pseudotachylyte vein (P) in Gray Gneiss microbreccia. Note the vertical fracturing through both this vein and that shown in plate 4.2*b*. Mullach Breac Malasgair, Lewis. GR NB 2996 1675

b Folding of a brown pseudotachylyte (P) in Gray Gneiss microbreccia, with later extensive fracturing. Mullach Breac Malasgair, Lewis. GR NB 2996 1675

c C-type mylonite bands in Gray Gneiss microbreccia. Two sets of mylonite bands are present; one set represents a shear band foliation and dips moderately from top right towards lower left (M1), whilst the second (M2) truncates the first and represents the mylonitic foliation. It runs horizontally across the plate. Roadside quarry exposure, South Harbour, Scalpay, off Harris. GR NG 2241 9566

d Down dip verging asymmetric open fold from the M1 mylonite set (see plate 4.2*c*), indicating dextral shear. The pencil points in the down dip direction. Roadside quarry exposure, South Harbour, Scalpay, off Harris. GR NG 2241 9566



a



b



c



d

Plate 4.3

Field photographs from Scalpay, Harris.

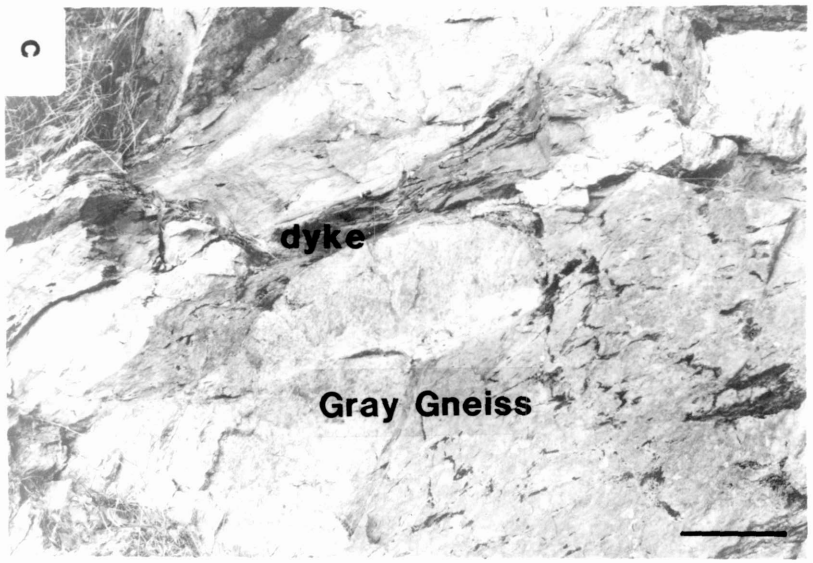
a Close-up of a c-type mylonite of the M2 mylonite set (see text and plate 4.2*c*). A shear band foliation (S_b) predominates, indicating sinistral sense of shear. Roadside quarry exposure, South Harbour, Scalpay, off Harris. GR NG 2241 9566

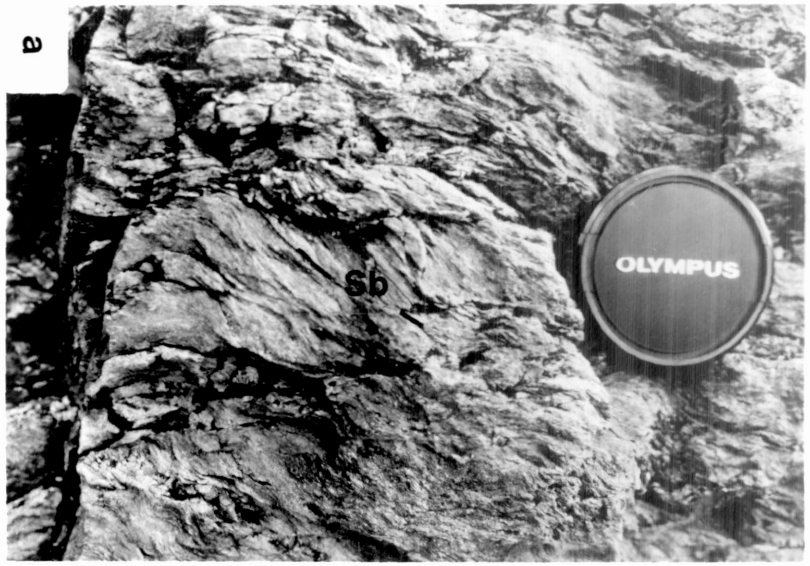
b Exploitation of the boundary between a basic pod and the Gray Gneiss (lower part of photograph) by deformation. This has resulted in formation of a well-foliated c-type mylonite, which displays numerous small scale crenulations. Roadside quarry exposure, South Harbour, Scalpay, off Harris. GR NG 2241 9566

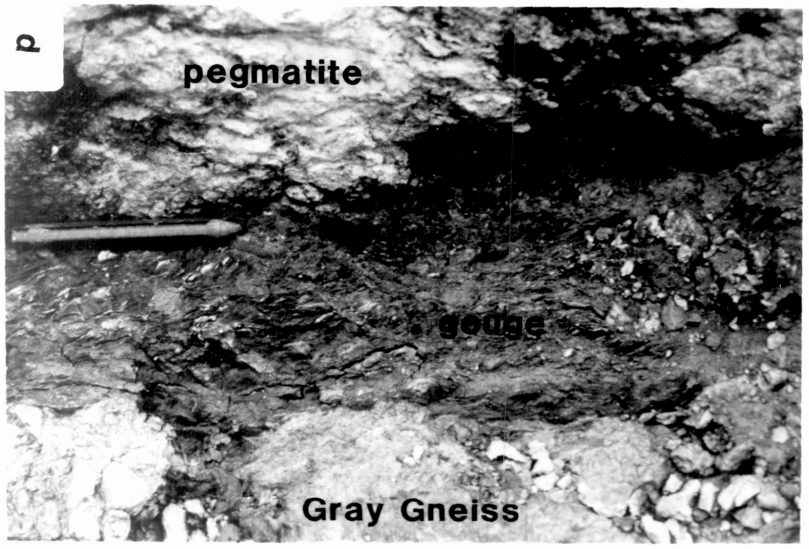
c Deformation being accomodated by development of foliation in a boudinaged Scourie dyke, whilst the surrounding Gray Gneiss has fractured into blocks and rotated. Scale is 20 cm in length. Roadside quarry exposure, South Harbour, Scalpay, off Harris. GR NG 2241

9566

d Development of gouge at the boundary between the Gray Gneiss and a pegmatite sheet, showing poorly developed shear bands. North Harbour, Scalpay, off Harris. GR NG 2180 9675


c
dyke
Gray Gneiss


a
Sb
OLYMPUS


d
pegmatite
gouge
Gray Gneiss

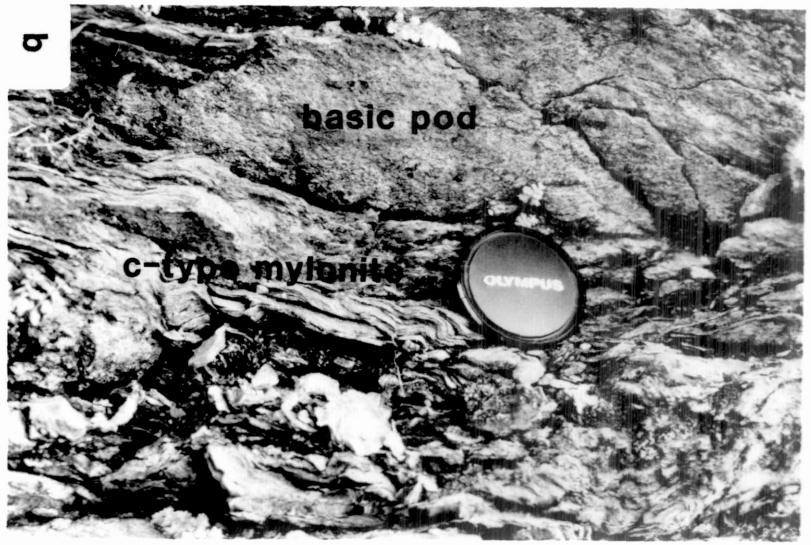

b
basic pod
c-type mylonite
OLYMPUS

Plate 4.4

Field photographs from Crogary na Hoe and North Lee, North Uist.

a Characteristic rhombohedral relationship of the two fracture sets (marked in foreground) in Gray Gneiss microbreccia. Loch Scalan, Crogary na Hoe, North Uist. GR NF 9664 7068

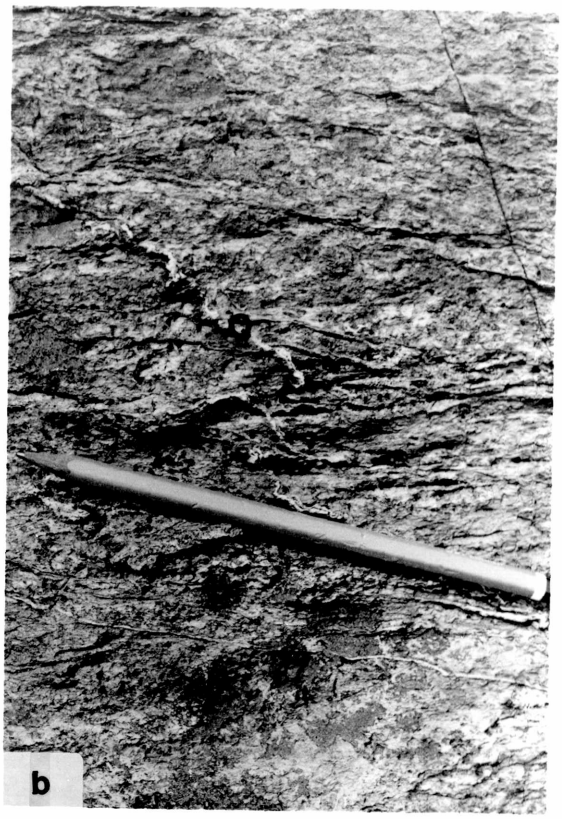
b Thin veins of quartz (Q) cementing rhombohedral fragments of Gray Gneiss microbreccia together. The veins themselves have been offset by continuing movements along the fractures. Crogray na Hoe, North Uist. GR NF 9796 7246

c Banded ultracataclasite vein, in Gray Gneiss microbreccia, parallel to east dipping fracture set, which has been transected by the west dipping set, then pulled apart. Crushed material has infilled the spaces between the vein fragments. Crogary na Hoe, North Uist. GR NF 9767 7222

d Small scale chevron fold with down-dip vergence in c-type mylonite, indicating dextral shear. North Lee, North Uist. GR NF 9442 6590



a



b



c



d

Plate 4.5

Field photographs from North Uist and Usinish, South Uist.

a Badly weathered, rubble-like material containing blocks of altered microbreccia, lying between c-type mylonite (in foreground) and Gray Gneiss microbreccia (top of plate). Loch Scalan, Crogary na Hoe, North Uist. GR NF 9639 7059

b Individual fault planes outcropping as notches on the hillside to the right of the plate. They weather out as the brecciated material formed along the fault planes is relatively soft. Maol Martaig, South Uist. GR NF 8357 3752

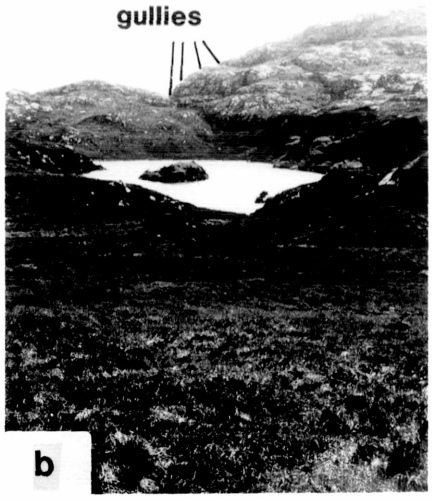
c Brown pseudotachylyte veining (P) in Corodale Gneiss, showing partial incorporation into the Gneiss. Meall Mhor, Ben na Hoe, South Uist. GR NF 8163 2724

d Large pod of broken-up brown pseudotachylyte (P) in Corodale Gneiss. Rubha Rossel, Loch Skipport, South Uist. GR NF 8572 3660

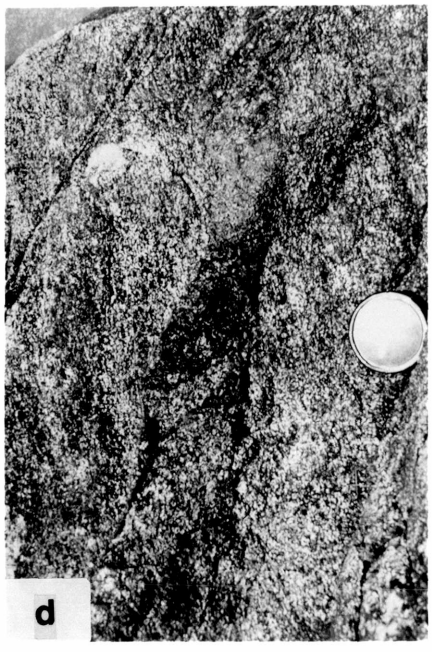
e Tectonic contact between a basic (?Scourie) dyke and brecciated pegmatitic material (possibly Mashed Gneiss) above. Rubha Caolas Luirsay, East Gerinish, South Uist. GR NF 8587 4004

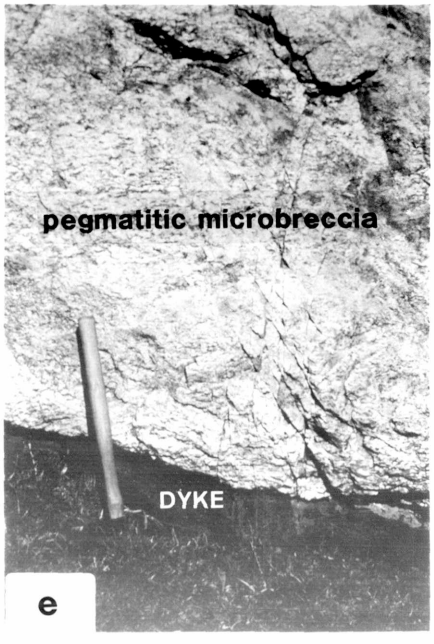
f Closest juxtaposition seen of a contact between Gray Gneiss and the Corodale Gneiss, with a gap of around one metre covered by vegetation. From looking at the exposure margins, the contact would appear to have been heavily sheared. Rubha Caolas Luirsay, East Gerinish, South Uist. GR NF 8585 4002

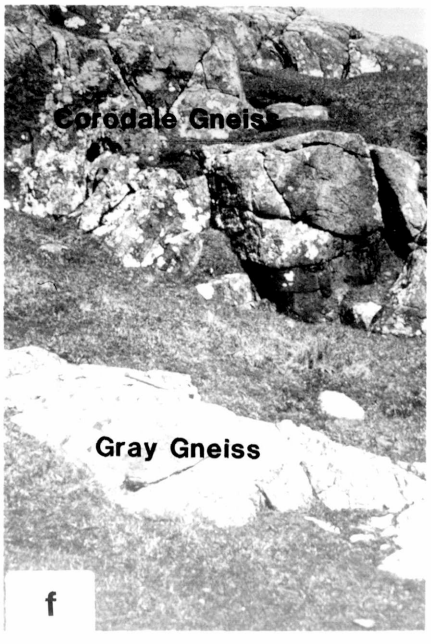

microbreccia
altered and brecciated material
c-type mylonite
a


gullies
b


c


d


pegmatitic microbreccia
DYKE
e


Corodale Gneiss
Gray Gneiss
f

Chapter 5

Microstructures

5.1 Introduction

This chapter describes the textures and microstructures of samples observed by optical and electron microscopy techniques. Samples have been subdivided into the categories proposed in chapter 1 (section 1.6) for this purpose. For each rock type, a description of its characteristic features is presented, together with any inferences that can be drawn about its conditions of formation. Field relations are taken into consideration in inferring these conditions. Mention will be made of atypical specimens where these occur, and variations of the same rock type within different areas will be described.

Many of the fault rock types grade into one another, and this means that any attempt to subdivide them may result in somewhat arbitrary distinctions between those that lie on or near boundaries of the classification. For this reason, type samples will be concentrated on, to give a clear picture of the range of characteristic features of each rock type. It is important to realise, however, that the majority of specimens do not show such obvious textures, and it is only after close study of many such samples that it is possible to assign them to a particular fault rock type.

To enable useful comparisons to be made, and to give an indication of the extent of deformation, this chapter begins with a brief description of the country rocks outcropping away from the areas affected by faulting, and then describes the fault rocks. Optical and SEM micrographs (all SEM micrographs are in back-scattered mode) are used to illustrate various microstructural features.

5.2 Country Rocks

Gray Gneisses Typically medium grained, they contain a quartz - potassium feldspar - plagioclase ± hornblende ± biotite assemblage. The majority of the Gray Gneisses (c. 85 %) are acid-intermediate in composition, grading continuously through basic (c. 14 %) to strongly basic compositions (less than 1 %). The average Gray Gneiss contains around 35 % quartz, 30 % potassium feldspar, 15 % plagioclase and 15 % hornblende.

Plate 5.1a shows the characteristic features of a biotite-bearing Gray Gneiss. Mineralogical banding is apparent in some sections, and foliation, where developed, is defined by a grain shape preferred orientation of biotite, and to a lesser extent, hornblende. Commonly, a

crystallographic preferred orientation is developed, especially for the more basic gneisses. If biotite is present, as in the metasediments, it forms small, acicular grains (plate 5.1*a*), giving a very pronounced grain shape preferred orientation.

Grain shape for all other constituents (quartz, potassium feldspar, plagioclase, accessory phases) tends to be equant, with good 120 degree triple junctions, giving an equigranular texture. Feldspars tend to be slightly altered, especially the alkali feldspars, and hence appear cloudy in thin section compared to the quartz (e.g. plate 5.1*a*). In the acid rocks, the typical Gray Gneisses, quartz tends to show evidence of minor deformation in the form of strain shadowing or deformation bands (plate 5.1*c*); these are interpreted as due to post-metamorphic cooling.

In the hornblende-rich rocks, the amphibole usually develops to a larger grain size (plate 5.1*b*), up to 1.5 cm. Blebs of feldspar are usually still present, and epidote veining is common. This is thought to be a late-stage feature associated with the fluids introduced during faulting.

The Altered Gray Gneisses The classification of this rock

type is problematical, as it is not clear if it should be classed as a fault rock or not. The predominant process is generally one of static retrogression, but invariably some grain cracking is also present, suggesting that deformation was not entirely absent during their formation.

Typically, the altered Gray Gneisses show cracking on a grain scale (plate 5.3*a*), in a similar style to impingement cracks. These cracks exploit crystallographic weaknesses, such as cleavage planes, within the minerals to give a complex set of cracks within each grain. Fluid can pass into the rock along these cracks, and has deposited opaque phases in the form of iron oxides along them, giving them a heavily-outlined appearance (e.g. upper left corner of plate 5.3*a*).

Corodale Gneiss These are medium to fine grained, pyroxene-bearing rocks, generally more basic than the Gray Gneisses, but varying from virtually pure pyroxenite to intermediate-basic in composition. The pyroxenes are often replaced by amphiboles, although it is hard to tell at what stage in their history this happened. Plate 5.1*d* shows the characteristic appearance of the Corodale Gneiss.

The pyroxenes are mostly diopside-rich, with rarer occurrences of hypersthene. Under crossed polars, many of the diopsides show exsolution lamellae and twinning. Opaque minerals are present along many of the pyroxene grain boundaries, mainly as iron pyrites or ilmenite (plate 5.2*a*). It is uncertain whether these grain boundary phases are a primary feature or due to later alteration. Quartz, where present, shows slight strain shadowing. Features of post-metamorphic deformation are usually absent, save for ubiquitous minor alteration and occasional microfractures (plate 5.1*d*).

Mashed Gneisses The difficulty in classifying the Mashed Gneiss was discussed in chapter 4. It seems clear that they were originally a rock type in their own right prior to deformation, so they will be discussed here. The assemblage comprises quartz and plagioclase, with some potassium feldspar, epidote and chlorite. In thin section, this rock type consistently shows more evidence of deformation than the previous two. Some sections are so severely brecciated, altered and veined (plate 5.2*b*) that it is impossible to discern anything of their original nature. The veins, as shown in the plate, are often disrupted or offset by other veins, which are in turn offset themselves.

More typically, deformation is less severe than this, with quartz being strongly strained and deformation bands developing, whilst plagioclase shows deformation lamellae and microfaulting (plates 5.2*c* and *d*). The alkali feldspar grains show a different response to deformation, with the development of transgranular cracks.

Most samples of Mashed Gneiss are very strongly altered, with almost complete sericitisation of potassic feldspars, and partial alteration of almost all other minerals, so that it is only possible infrequently to observe the deformation features described above. Micro-cracking and fracturing are pervasive, with alteration along fractures generally more severe than in the adjacent rock, suggesting that incoming fluid has travelled along such dilatational features (and possibly also along grain boundaries). Fragmentation of grains is common and incipient fragmentation is shown in the alkali feldspars in plate 5.2*d*. If this process continues it eventually gives rise to ultracataclastic patches, as shown in plate 5.2*b*.

The Fault Rocks

5.3 The Microbreccias

General Description The microbreccias are essentially cataclasites in that they are formed by cataclastic processes, although the process of grain size reduction has not gone very far. The microbreccias consist typically of angular fragments of intact gneiss (varying in size from centimetres to hundreds of metres) separated by fractures or narrow zones of cataclasite (see section 1.6). Fragments commonly show relative displacement and rotation, although no consistent sense of movement can be obtained. Two types of microbreccias are recognised here, microbreccias and altered microbreccias. The distinction is based largely on the extent of feldspar alteration. The microstructures of both types are similar, as they formed under similar conditions of deformation, although there is a tendency for the microstructures of the altered microbreccias to be obscured by strong alteration. These microbreccias are gradational between slightly cataclased country rock, and either c-type mylonite or altered cataclasite.

The majority of the microbreccias are derived by cataclasis of Gray Gneiss, although minor amounts have formed from the Corodale Gneiss. This is thought to reflect the relative abundances and relative ease of deformation of the two parent rocks (see section 7.5). With increasing deformation, a microbreccia will become a cataclasite, whilst with increasing alteration and

deformation, an altered microbreccia will become a c-type mylonite.

The generation of a microbreccia from intact Gray Gneiss is dominantly a cataclastic process. Initially, the rock is traversed by numerous fractures, often with varying amounts of cataclasis associated. The fractures are usually orientated parallel to the present fault plane orientation, or in an antithetic orientation to it. They tend to group into splays, giving rise to a foliated appearance in the rock.

As deformation proceeds, the material within and adjacent to the fractures becomes finer grained, through continuing cataclasis. The fractures can act as channels along which fluids can pass, and this, together with the grain size reduction which gives a higher grain boundary area, allows reaction and alteration to occur more readily. The feldspars begin to alter to sericite, and the amphiboles to a mixture of chlorite and epidote (with increasing alteration an altered microbreccia will be produced). Once alteration begins, shearing can occur more easily as:

a) The material along the fractures is now weaker, having

altered from feldspars and mafic minerals to micas

and

clay minerals.

b) The minerals take on a preferred orientation if alteration occurs whilst deformation is still operative.

In this situation the fractures become marked by a band

of aligned platey minerals, resulting in the development

of a reaction enhanced foliation.

c) Strain softening occurs.

d) The presence of fluids help to reduce friction.

e) Reduced grain size enables grain boundary sliding to

occur.

If fluid does not penetrate into the microbreccias, dry cataclasis becomes the dominant process, leading to the development of cataclasites or ultracataclasites, as described in section 5.4. These in turn may be statically (or more rarely, dynamically) altered by fluids after their formation, giving rise to altered cataclasites.

Microfracturing The microfractures in the microbreccias are generally impersistent and die out laterally, often within the area of a thin section, i.e. they are trans-granular. They may occur as single fractures, but most commonly they are found in splays (plates 5.3*b* and 5.4*c*), where they may give rise to a weak foliation. Two orientations of microfracture splays (the fault plane parallel and the antithetic) are frequently seen (plates 5.3*c* and 5.4*d*).

Displacement along microfractures or splays is often hard to determine, owing to the general grain size reduction in the area. In the coarser grained and less-deformed microbreccias it is sometimes possible to match up mineral grains or other features across the microfractures. The 'sliver' texture displayed in plates 5.5*b* and 5.5*c* is characteristic of the less deformed microbreccias, where they have been split into a series of wedges and slivers by the microfracture splays. The wedges and slivers are seen to have been displaced in various directions, often with an oblique motion. No consistent overall direction of displacement has been obtained for them.

The microfractures may become reactivated and infilled with various materials. Sometimes these take the form of

injection veins of ultracataclasite, but more commonly they are filled with epidote, opaques or quartz (plate 5.4*b*). Evidence for various phases of fracturing and infilling are observed by cross-cutting relationships.

Other Deformation Features Formation of trans-granular cracks is not the only response to deformation that is shown by the microbreccias. Intra-granular cracking is also common. Plate 5.4*c* illustrates this feature in quartz. Plate 5.5*a* shows a quartz grain with strain shadowing, probably resulting from post-metamorphic cooling (i.e. it is an inherited strain feature). The deformation associated with microbreccia formation is thought to have occurred at too low a temperature for such crystal plastic features to have formed.

Superimposed on this strain shadowing is a brittle response to deformation in the form of thin cataclastic bands, visible optically as bright lines across the grain. As cataclasis proceeded, the small grains that have been generated rotate, and become optically mis-aligned with the host grain, so that they are clearly visible under crossed polars. The generation of cataclastic bands similar to those shown in plate 5.5*a* is contemporaneous with formation of the microfracture splays.

In response to the brecciation, biotite accomodates deformation by kinking and sliding along its cleavage planes, and finally fracturing (plate 5.5*f*). Alteration, mainly to illite, is common along the cleavage planes, which allows the kinking to be imaged clearly. Ilmenite becomes severely fractured, with the deformation again exploiting the cleavage planes, although no displacement usually occurs (plate 5.5*e*).

Alteration The most common pathway for incoming fluids is along the microfractures. This may result in formation of epidote, iron oxides and iron sulphides along the microfractures (plates 5.3*c*, 5.3*d* and 5.4*d*), giving them a darker appearance than the surrounding microbreccia. Alternatively, and more commonly, the fluids deposit quartz or alkali feldspar along fractures (plate 5.5*d*), which effectively cements them shut. Alteration also gives rise to 'blurring' of grain boundaries. Their indistinct nature can be seen in plates 5.3*c* and 5.3*d*.

Another common feature is for several phases of fracturing and infilling to have occurred. Earlier fractures tend to be infilled by phases (e.g. epidote and opaque phases) that are more mafic than the later ones (typically quartz and feldspar) (plate 5.4*b*). These later veins are thought to represent a late stage in the

evolution of the fault zone, as silica-bearing excess fluids moved from the c-type mylonites into the microbreccias, depositing quartz and cementing the fracture systems. This idea is supported by the geochemical evidence and will be discussed in chapter 6.

Fluids may also move along grain boundaries, causing alteration there too. This in turn can lead to other pathways for further deformation to exploit, leading eventually to development of a c-type mylonite band (see section 5.7). If alteration continues without further deformation, as often happens in the microbreccias once deformation has been partitioned onto developing c-type mylonite bands, then an altered microbreccia will form (plate 5.3*d*). Deformation may then, in turn, become partitioned into narrow zones within the altered microbreccia (plate 5.4*a*).

5.4 Cataclasites

The cataclasites vary in intensity of deformation from strongly deformed microbreccias (those showing severe grain size reduction and few relict fragments) to ultracataclasites. In this section, the rocks that will be described are those cataclasites in which grain size reduction has played an important role during deformation. Of these, the Outer Hebridean cataclasites mostly fall into the field of ultracataclasites (as defined in section 1.6). They are thought to represent rocks where deformation has proceeded beyond the microbreccia stage, possibly due to localisation of strain in some way. They appear to be derived originally from Gray Gneiss, as this rock type is the host.

The ultracataclasites are generally grey or grey-green in colour, with those in the Eaval area (North Uist) being more intensely green. In thin section, this green colour appears to reflect post-tectonic retrogression. The ultracataclasites generally occur as injection veins in the microbreccia, and are often fractured and offset. Occasional brownish-black ultracataclasites (the 'flinty crush rock' of Jehu and Craig (1925)) are also found. These too usually occur as injection veins and are heavily iron-stained, hence their colouration. The ultracataclasites contain small, angular to sub-rounded

clasts (generally less than 1 mm in diameter) of quartz and, more rarely, sericitised feldspar, set in a fine grained matrix with a random fabric (plate 5.6*a*). Late fracturing is common, and narrow veins of quartz occasionally cut the fractures (plate 5.6*a*).

The matrix itself is extremely fine grained (less than 5 microns) and possesses a random fabric (plate 5.6*b*). Frequently, the matrix is too fine to obtain reliable analyses of constituents, even using scanning electron microscopy. Where it is not, the matrix is composed of quartz, sericite, chlorite and epidote. It is thought that this assemblage reflects post- (or possibly syn-) tectonic alteration.

A common feature within the ultracataclasites is the injection of matrix material into fractures in the clasts (plate 5.6*c*). This results in plucking off of fragments of clasts, and their assimilation into the matrix. The characteristic amorphous nature (even at high magnifications) of the ultracataclasite matrix and the replacement of original minerals by opaque phases within the dark-coloured ultracataclasites is also seen in plate 5.6*c*.

5.5 Gouges

Gouges were only found on Scalpay, along the north-dipping, south-south-east trending fault that traverses the island (section 4.3 and figure 4.2). They are green-grey in colour, incohesive, and possess well-developed foliation and shear bands. They are mainly composed of clay minerals, and X-Ray Diffraction was utilised to identify the individual phases. These were found to be biotite, paragonite, kaolinite, muscovite, potassium feldspar, plagioclase and brookite.

The incohesive nature of the gouge makes sectioning difficult, and resin impregnation under vacuum is required. Hence, thin section observation is limited. Relatively few clasts are present, usually of quartz, and the matrix grain size is small (around 70 microns) as a result of extensive syn-deformational recrystallisation or alteration. A marked foliation is present along which the gouge tends to crack during impregnation and sectioning (plate 5.6*d*).

5.6 Pseudotachylyte

It is not proposed to describe the pseudotachylytes in much detail here as this would duplicate the work of Maddock (1986), who has gone into the subject in great

depth. However, it is felt necessary to emphasize some points he has not covered. Two types of pseudotachylyte are found in the Outer Hebrides; a fresh, black, undeformed phase as found almost everywhere and a brownish, extensively fractured phase, as found at Malasgair on Lewis, and in the Corodale Gneisses of South Uist. Both types occur along generating surfaces and as injection veins.

The fresher pseudotachylyte is so fine grained and dark in colour that little can be told about the matrix in optical thin section. All that can be seen are sub-rounded clasts of host rock, or grains of quartz and feldspar (plates 5.7*a* and 5.7*b*), and occasional traces of flow-banding or chilled margins. Many different types occur within the subdivisions of generating surfaces and injection veins. The classification of Sibson (1977b) has been used here.

Quasi-conglomerates, zones in which pieces of host rock have been spalled off by plucking and thermal shattering and now act as clasts set within a matrix of pseudotachylyte, are found throughout the Uists. The host rock is generally Gray Gneiss, and rotation of the clasts within the quasi-conglomerates (as seen by angular discordance between the foliation traces of the clasts) is common (plate 5.7*a*). Later shearing is often localised at

the boundaries between gneissose clasts and pseudotachylyte (plate 5.7*a*).

Pseudotachylyte formed along generating surfaces tends to display slightly different characteristics. The uppermost margin of the pseudotachylyte is generally flat, with frequent evidence of chilling or flow-banding against the host rock. The lower boundaries often have numerous small injection veins coming off them, exploiting fractures in the Gneiss and giving a 'whiskered' appearance (plate 5.7*b*). The generating surfaces do not appear to follow any apparent pre-existing feature within the Gneiss, but tend to cut across them.

Using the back-scattered detector, the matrix can be resolved as being composed of acicular, randomly orientated grains suggestive of a devitrification texture (plate 5.7*c*). It appears that this texture consists of quartz, acicular mica (mostly biotite) and amphibole (mostly hornblende), and feldspar, with occasional opaques. Comparing this with the SEM micrograph of an ultracataclasite at similar magnification presented in plate 5.6*b*, the differences between the two textures are apparent. The ultracataclasite consists of mostly subrounded clasts on various scales, whereas the pseudotachylyte has a more crystalline appearance. Although ultracataclasites that have been statically

retrogressed may show similar textures to those seen in the pseudotachylytes, the field relations usually make it possible to distinguish between these rock types.

The second type of pseudotachylyte, the dark brown type found in the Corodale Gneiss and in parts of Lewis, is generally altered and featureless (plate 5.7*d*), except for fractures, even when looked at in the SEM. One sample studied appeared to show remnant traces of recrystallisation, with subhedral grains of biotite and amphibole visible, suggesting that the pseudotachylyte formation could have occurred under high temperature (?amphibolite facies) conditions. The extent of the alteration also suggests that the brown pseudotachylyte is an older phase than the black pseudotachylyte, pre-dating the arrival of fluids in the rocks. The presence of fractures offsetting pseudotachylyte veins, or cutting both gneiss and pseudotachylyte, supports this, as they suggest subsequent deformation.

5.7 C-type mylonites

Most of the foliated fault rocks on the Outer Hebrides are found, on inspection of the thin sections, to be dynamically retrogressed c-type mylonites as described in section 1.6. These are a sub-group of the rocks described

by Sibson (1977b) as phyllonites.

As has already been described (section 5.3), the c-type mylonites in the Outer Hebrides have developed by further grain refinement and alteration from the microbreccias. In general, initial c-type mylonite development involves pods of microbreccia becoming isolated from each other by continued alteration and development of shears along the original fracture splays, resulting in lenses of microbreccia surrounded by c-type mylonite. It is highly retrogressed, and bears complex mineral assemblages. Typical minerals present are small quantities of quartz, potassium feldspar, plagioclase feldspar, one or more amphiboles (usually hornblende and/or actinolite), muscovite, biotite, epidote, apatite, sphene, Fe-oxides, Fe-sulphides, ilmenite, rutile (or some other polymorph of TiO_2), chlorite and other clay minerals.

It is unlikely that all of these minerals would be present in any one sample, but it is rare to find less than ten phases in a c-type mylonite. Some of the minerals are inherited from the host rock (e.g. quartz, feldspar), others are formed by *in situ* alteration of the inherited minerals (chlorite, epidote, sericite), whilst yet others are found in greater abundance than in the host rock (ilmenite, TiO_2, apatite) and growing as the bulk chemistry of the rock is altered by ingress of fluids. For

more details of bulk chemical changes, see chapter 6.

The stages in the textural development of a c-type mylonite from a microbreccia are shown in the series of optical micrographs presented in plate 5.8. The first micrograph, plate 5.8*a*, shows a typical microbreccia with a splay of microfractures running diagonally across the centre. Slight alteration has occurred along the microfractures, which have an anastomosing nature, and the feldspars and amphiboles in the rock between the fractures show signs of alteration.

Plate 5.8*b* shows the next stage in the development of a c-type mylonite, in a more quartz-rich rock, which has an above average amount of biotite present (c. 10 %). Alteration and precipitation of opaques along the microfractures are more pronounced, and the fractures are beginning to develop from discrete surfaces into wider zones of shearing. These 'shears' can still be seen to consist of several closely spaced microfractures, but the deformation is beginning to localise into them, with relatively intact lenses of the host rock in between. The mica and feldspar in these intact lenses shows some alteration. Earlier deformation, probably during formation of the initial microbreccia, has resulted in preferential crushing of the biotites (e.g. plate 5.8*b*).

The microfracturing becomes progressively more pervasive, as shown in plate 5.8*c*, where the incoming fluids and continuing deformation have taken advantage of an initially highly fractured microbreccia. Individual microfractures can still be picked out, but the process of amalgamation into shear zones has gone further than in plate 5.8*b*. Quartz is the only mineral present unaffected by alteration; the remainder have degenerated to a fine grained mixture of chlorite, epidote and other alteration products, within which the original grain boundaries are virtually indistinguishable.

The final stage in the development of a c-type mylonite is when individual microfractures can no longer be distinguished (plate 5.8*d*). The alteration of the original minerals has gone to completion, and growth of new minerals has occurred. Little remains of the original microbreccia texture in the unsheared, altered portions of the rock.

The resultant c-type mylonites contain scarce, sub-rounded clasts of quartz and feldspar, rather than ribbon grains (indicating cataclastic, not crystal plastic, deformation). The clasts are set in a matrix of fine-grained alteration products and other minerals as listed above. The matrix foliation varies from almost non-existent to good. Epidote veining is common.

The foliation is mainly due to the presence of minerals aligned along fractures or a grain shape preferred orientation (plates 5.9*c* and 5.9*d*), although a poorly developed crystallographic preferred orientation occasionally exists too, most commonly in phyllosilicate-rich samples. This is because mica has a grain shape that tends to coincide with its crystallographic orientation. It is common for a shear band foliation to form in addition to the mylonitic foliation (plate 5.9*d*). Where neomineralisation has been locally extensive, as in the growth of clusters of epidote or opaque minerals, both of these foliations may be deflected (plate 5.9*c*).

The development of a foliation defined by the neo-minerals in these rocks suggests that the c-type mylonites are undergoing syn-deformational alteration, although some growth could be mimetic along fractures. Even in a well developed c-type mylonite, the grain size remains very variable, again suggesting that cataclasis, alteration and neo-mineralisation were all operating concurrently. The textures and microstructures developed within the c-type mylonite bands are very variable, and the more notable features are illustrated in plates 5.9 and 5.10.

The most commonly observed microstructures are lenses of

microbreccia separated by more strongly sheared c-type mylonite (plate 5.9*b*). Some late stage fracturing and veining can be seen in the central portion of the micrograph, disrupting the c-type mylonitic foliation. In contrast, plate 5.9*a* shows a clast of c-type mylonite which has been fractured due to later brecciation. The clast is now set within microbreccia, and its margins have been sheared. This indicates that, although most deformation was taken up by the c-type mylonite bands after their formation, this was not always the case.

The variation in the textures and microstructures of the c-type mylonites is due to their complex deformation history. Some of the microstructures are inherited from the microbreccias, others develop due to the mylonite forming processes. They include;

a) development of foliation

b) displaced markers (e.g. grains, veins of ultra cataclasite), offset across fractures

c) shear fractures within relatively hard porphyroclasts (e.g. garnet - plate 5.10*c*))

d) rotation of mineral fragments formed by tensile fracturing (plate 5.10*d*)

e) mica fish

f) folding of mylonitic foliation (plate 5.10*a*),

banding or
veining (plate 5.10*b*)

g) shear bands and curve-in of foliation at the margins of
the mylonite bands.

These features for the most part are best developed in the more hydrated, highly altered c-type mylonites. An additional common feature in the highly altered c-type mylonites is the presence of opaques with a striped appearance (plate 5.10*d*) and it is thought that these form by replacing original biotite. It is reasonable to suppose that the mica is replaced first along its cleavage. If the replacement process does not go to completion, then the resulting opaque grain will have a stripey appearance.

In addition to these, a number of rarer features have also been observed. Amongst these are pulling apart of epidote veins to give a boudinage effect (plate 5.10*e*) and the formation of complex intergrowths of opaque minerals, such as TiO_2, ilmenite and magnetite (plate 5.10*f*).

5.8 R-type mylonites

Mineralogically, the r-type mylonites are very similar to the Gray Gneisses, typically bearing an assemblage of

quartz - plagioclase - potassium feldspar - hornblende - biotite, with garnet commonly present in more mafic specimens. They range in degree of deformation from protomylonites to ultramylonites - see section 1.6 - although the latter are relatively rare (plate 5.12*c*). Most samples display a strong foliation, with clasts of plastically deformed quartz and/or feldspar, with the clast tails drawn out parallel to the foliation. The protomylonites (plate 5.11*a*) show incipient development of quartz ribbon grains. Strong crystallographic and grain shape preferred orientations are present in the mylonites - see the quartz c-axis fabric presented in figure 5.1. The asymmetric shape of many of the augen suggest a reverse sense of shear (plate 5.11*b*).

Two foliations are generally present in the r-type mylonites, the mylonitic foliation (S_m) and a shear band foliation (S_b), which help to define the clast shapes (plate 5.11*b*). The relationship between these two foliations also indicates a reverse sense of movement. An apparent foliation may also be present in some samples, due to alignment of clast margins. Shear folds are found occasionally.

In addition to the crystal plastic deformation of the quartz and feldspar, plastic deformation of mafic minerals is also seen (e.g. the amphiboles in plate 5.11*c* and

5.12*a*). Recrystallisation of many of the minerals (including static recrystallisation) has occurred, especially in the clast tails and ribbon grains. Plate 5.11*d* shows an ultramylonite, showing extreme ductile deformation. Grain size reduction has occurred due to dynamic recrystallisation processes, and elongate grains are extensively developed. Biotite appears to have undergone more static recrystallisation (plate 5.12*b*), and only displays a weak preferred orientation. This is probably because it continued to recrystallise after cessation of deformation.

The ductility and style of deformation present in these rocks suggests that formation of the r-type mylonites took place at deeper crustal levels than for the other fault rock types. The similarity in mineral assemblage between the Gray Gneiss and the r-type mylonites suggests that they formed under similar conditions. It is thought probable that the mylonites were created during the amphibolite-facies Laxfordian event, as a shear zone within the gneiss. It is also possible that such a shear zone dates back to the Scourian, and was reactivated during the Laxfordian.

5.9 Phyllonites

The phyllonites are formed by retrogression of r-type mylonites, and on the Outer Hebrides are found exclusively on the eastern side of Lewis. The textures and microstructures of these are totally different from those displayed in the c-type mylonites. Remnant quartz ribbon grains can still be seen, and the alteration products have a larger grain size than in the c-type mylonites, and are more sub-equant, with no optical or grain shape preferred orientation (5.12*d*). They have frequently been brecciated and have then undergone static rather than dynamic retrogression.

5.10 Conditions of Deformation

Microbreccias These display the results of cataclastic deformation, typical of low pressure and temperature. The large amount of dilation that appears to have accompanied their formation (as indicated by the pervasive sub-horizontal microfracturing - see figure 7.3) also suggests that they formed at high crustal levels. These conditions would have been initially dry, although hotter fluids undoubtedly entered the rocks along the fractures at a later date, giving rise to the altered microbrecias and, with continued deformation, the c-type mylonites.

Cataclasites Conditions of deformation were probably

broadly similar to those given above. Cataclasite genesis could have been at a slightly deeper level, as there is less dilatancy. However it is thought more likely that this merely reflects the more intense deformation that they have undergone, as supported by the finer grain size. Some of the cataclasites have been hydrothermally altered, suggesting initially dry deformation with subsequent ingress of fluids either throughout the rock or along specific zones.

Gouges The gouges formed by cataclasis, again probably at similar crustal levels to those outlined above. Initial cataclasis may have been dry, but the gouges undoubtedly continued deforming at a similar temperature, under wet conditions, as indicated by the alignment of neo-minerals. From the resultant mineral assemblage, they are thought to be of lower greenschist facies.

Pseudotachylyte It is difficult to estimate the conditions of formation of this fault rock type, as it can form under a wide range of pressures and temperatures. It can form below the brittle/crystal plastic transition in the crust (Maddock, 1986) if strain rates are high enough. The presence of chilled margins on some of the veins suggests intrusion into cooler host rock, but it is thought that the temperature difference necessary to produce this effect may be as low as several hundred

degrees. The only conclusion that can be drawn with certainty is that they formed in a high strain environment, although there is some evidence for the brown phase having formed at high temperatures (see section 5.6).

C-type mylonites These are thought to have formed under similar conditions to the microbreccias and cataclasites, with deformation continuing as the rocks became wetter and more alteration products formed. Sense of shear indicators suggest that they formed in an extensional environment. The temperature and pressure were low, although the incoming fluids could have been warmer than the surrounding microbreccias (see section 6.6). The mineralogy suggests that the fluids were around 300 degrees, or lower greenschist facies.

R-type mylonites The presence of crystal plastic deformation and the more ductile response to deformation in these fault rocks suggests that they formed at deeper crustal levels (high pressure and temperature relative to the other fault rocks). Similarities in the mineral assemblage of the Gray Gneiss and these rocks suggest that they formed under similar conditions, i.e. lower amphibolite facies metamorphism, probably during the Laxfordian metamorphic episode. They formed in a compressional regime, as indicated by their

microstructures.

Phyllonites These reflect static retrogression of r-type mylonites. Their mineral assemblages suggest formation under wetter conditions and cooler temperatures than those of r-type mylonite formation. Many of them have subsequently been brecciated under conditions similar to those of microbreccia formation.

Figure 5.1

Quartz c-axis fabric for 200 grains from an r-type mylonite from Shiltenish, Lewis, indicating dextral shear. Contours are at 3, 5, 7, 9, 11 and 13 times uniform distribution.

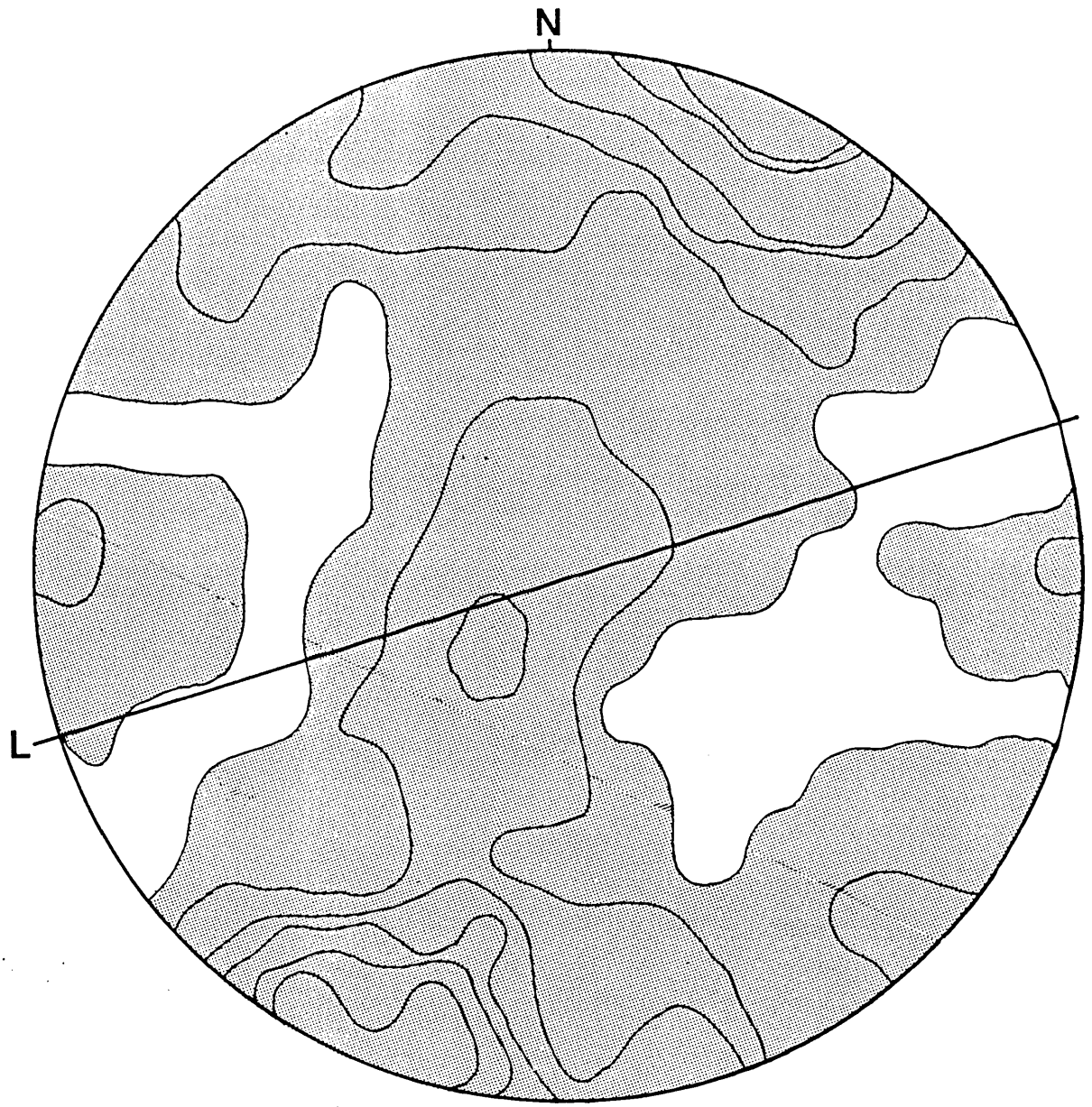

N
L

Plate 5.1

Photomicrographs of the textures and microstructures exhibited by the country rocks. The external diameter of the scale ring is 3 mm.

a Optical micrograph of a typical biotite-bearing Gray Gneiss texture, showing foliation as defined by mineralogical banding and alignment of acicular biotite (B). Quartz (Q) appears clear against the cloudy altered alkali feldspar (KF) and plagioclase (P). Hornblende (H) is also present. Metasedimentary Gray Gneiss, plane polarised light. Sample from Ardivachar Point, South Uist. GR NF 7421 4679

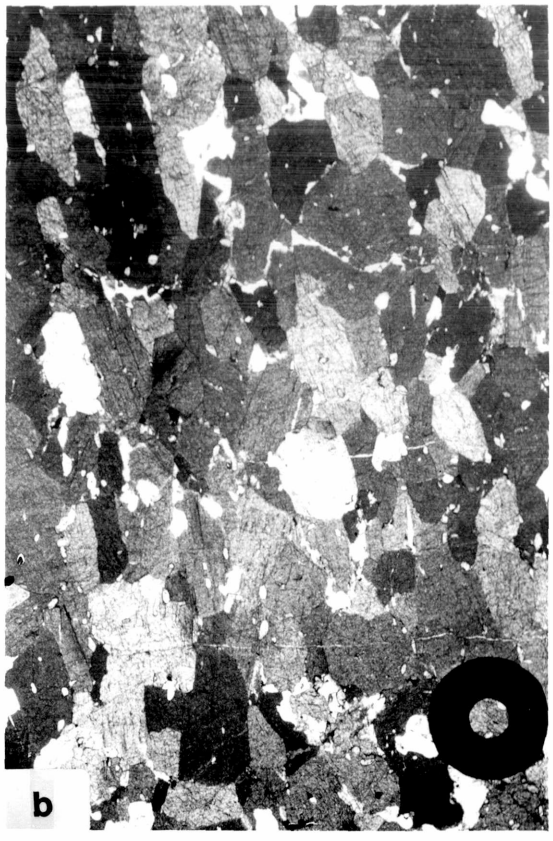
b Optical micrograph of a typical amphibolitic Gray Gneiss texture, with development of larger grain size than in the more acid Gray Gneiss. Small inclusions of quartz and feldspar are present within the amphibole grains. Later veining of epidote runs across the sample. Basic Gray Gneiss, plane polarised light. Sample from Strumore, North Uist. GR NF 9093 6919

c Optical micrograph of deformation bands in quartz (Q), interpreted as resulting from post-metamorphic cooling. Quartz-rich Gray Gneiss, crossed polars. Sample from North Lee, North Uist. GR NF 9290 6665

d Optical micrograph of a typical Corodale Gneiss texture, with diopsidic pyroxene (D) and quartz (Q). Grain size is relatively small, and the rock is here traversed by poorly developed microfractures. Intermediate/basic Corodale Gneiss, plane polarised light. Sample from Eaval, North Uist. GR NF 9194 5864



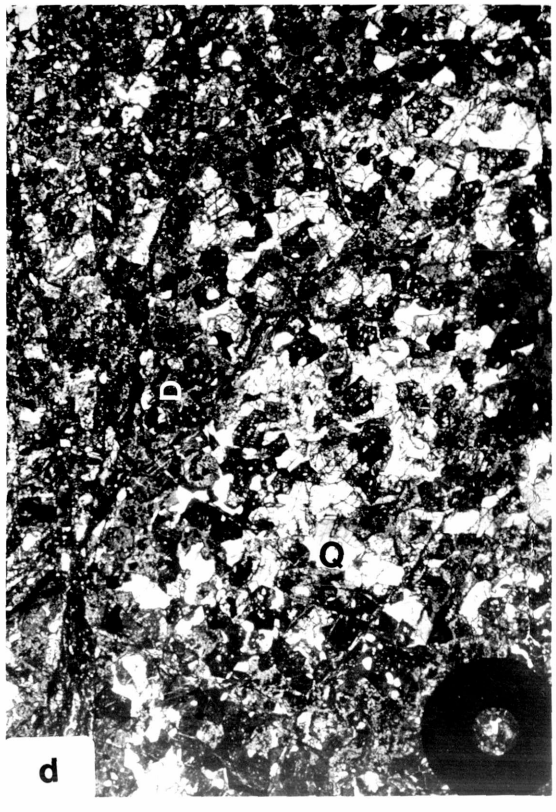
a



b



c



d

Plate 5.2

Photomicrographs of the textures and microstructures exhibited by the country rocks.

a Back-scattered electron micrograph of grain boundary phases in a Corodale Gneiss. The grain boundary phases are iron pyrite and ilmenite, and are visible as bright rims around grains of slightly altered pyroxene (grey phase) and plagioclase (dark phase). Scale bar represents 100 microns. Altered Corodale Gneiss from Loch Bein, South Uist. GR NF 8544 3667

b Optical micrograph showing a severely cataclased Mashed Gneiss. Pervasive alteration and quartz veining are present. Scale ring is 3 mm in external diameter. Cataclased Mashed Gneiss, crossed polars. Sample from adjacent to lighthouse on Usinish peninsula, South Uist. GR NF 8581 3538

c Optical micrograph of deformation features in feldspar, showing kinking and bending of deformation lamellae and

twin planes in plagioclase, resulting in an undulose appearance. Scale bar is 5 mm. Mashed Gneiss, crossed polars. Sample from Creag Dhughaill, Usinish peninsula, South Uist. GR NF 8715 3527

d Optical micrograph of kinked deformation lamellae in plagioclase, with reverse displacement microfaults. The rock shows transgranular cracking, with fractures (arrowed) propagating into alkali feldspar and quartz grains adjacent to the plagioclase. Scale bar is 5 mm. Acid Mashed Gneiss, crossed polars. Sample from Creag Dhughaill, Usinish peninsula, South Uist. GR NF 8715 3527


a


b


c


d

Plate 5.3

Photomicrographs of textures and microstructures in the altered Gray Gneisses and the microbreccias. The scale ring is 3 mm in external diameter.

a Optical micrograph of an altered Gray Gneiss, showing intragranular fracturing, which exploits crystallographic weaknesses (e.g. the feldspar grains, bottom left). The upper left corner of the micrograph shows heavy outlining of grains due to deposition of opaque phases along the grain boundaries. Altered Gray Gneiss, plane polarised light. Sample from Loch Marulaig, South Uist. GR NF 8232 1591

b Optical micrograph of a microbreccia, showing grouping of parallel microfractures producing a foliation. The feldspar and amphibole between the fractures are slightly altered. Gray Gneiss microbreccia, plane polarised light. Sample from Loch Scalan, Beinn an Fhaireachaidh, North Uist. GR NF 9616 7091

c Optical micrograph of a microbreccia split into rhombs by the strong development of two fracture sets (arrowed), running approximately parallel to the diagonals of the micrograph. In the field the fractures are orientated parallel to, and antithetic to, the fault plane. They are picked out by deposition of opaques and alteration along their length. Note also the now indistinct nature of the grain boundaries. Gray Gneiss microbreccia, plane polarised light. Sample from Loch na Creige, Crogary na Hoe, North Uist. GR NF 9642 7228

d Optical micrograph of an altered microbreccia. Microfractures (running obliquely across the centre) have heavy development of opaque phases and epidote. Away from the microfractures, grain boundaries have become obliterated as the rock underwent extensive alteration to a fine grained mixture of chlorite, sericite, epidote, opaques and unidentified clay minerals. Altered Gray Gneiss microbreccia, plane polarised light. Sample from Caolas Mor, Loch Skipport, South Uist. GR NF 8011 2910

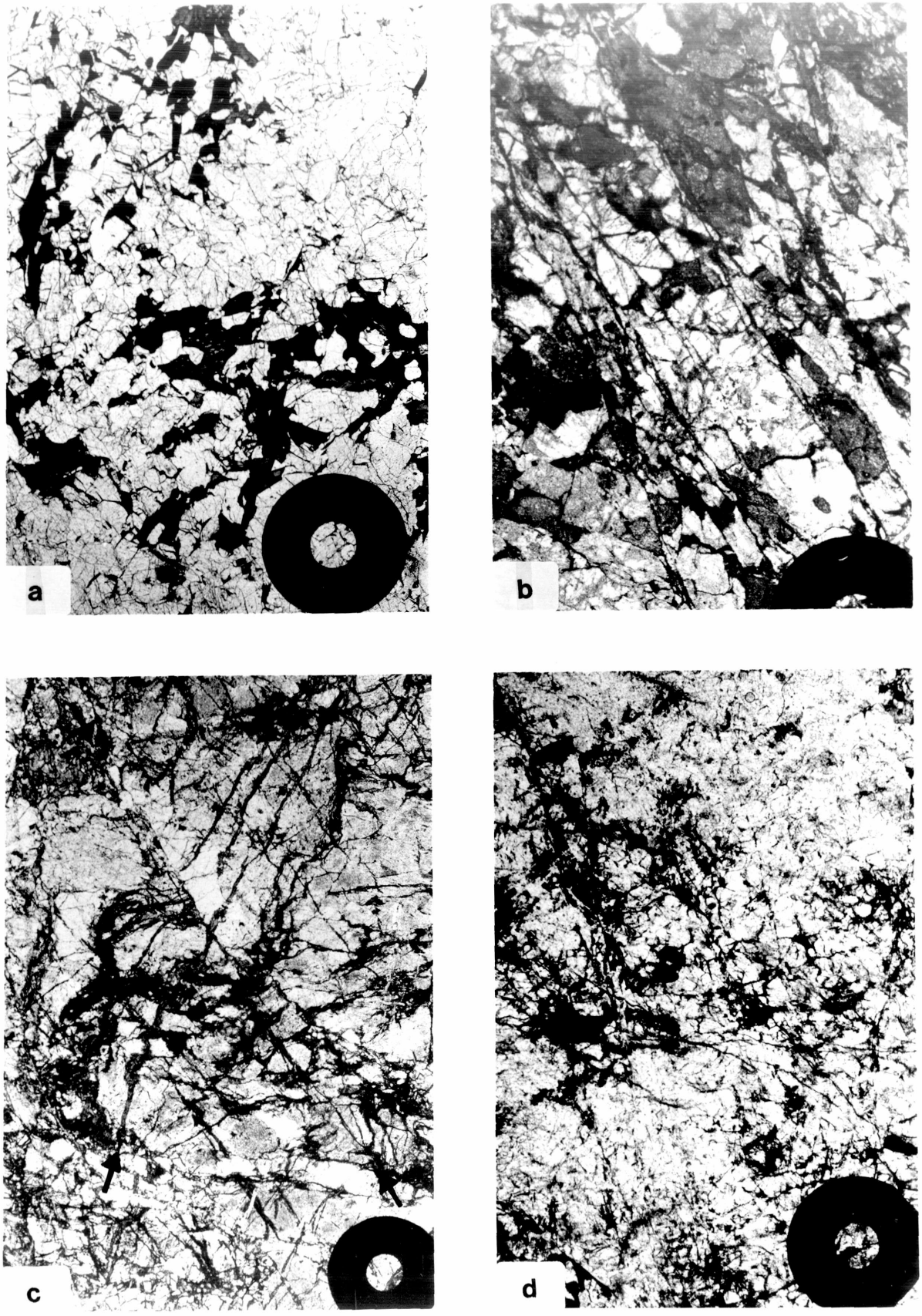

a
b
c
d

Plate 5.4

Photomicrographs of textures found within the altered Gray Gneiss microbreccias.

a Optical micrograph of an altered microbreccia, showing partitioning of deformation and alteration. Remnants of the two microfracture sets can be seen in the shape of the margins of the quartz clasts in the lower part of the micrograph. The originally more mafic central portion has undergone extreme alteration, and is beginning to shear along a zone from upper left to lower right. The heavy line running down the centre of the micrograph is an artifact produced during sectioning. The scale bar is 5 mm. Altered Gray Gneiss microbreccia, plane polarised light. Sample from coast opposite Dun Mhic Laitheann, Crogary na Hoe, North Uist. GR NF 9762 7305

b Optical micrograph of an altered microbreccia showing extensive veining of epidote (dark) and quartz (light). The epidote appears to represent an early phase of veining, which was then brecciated. Quartz has later

infilled earlier-formed fractures, which were dilating due to reactivation. Scale ring is 3 mm in external diameter. Extensively veined altered microbreccia, plane polarised light. Sample from Loch na Cointich, Crogary na Hoe, North Uist. GR NF 9637 7226

c Back-scattered electron micrograph of an altered microbreccia texture. Fracturing of the quartz (dark phase), alteration of the feldspar (medium gray phase altering to a slightly darker grey - sericite - along grain margins, fractures and cleavages), deposition of opaque material (bright phase) and grain size reduction along microfractures running across the micrograph can all be seen. Scale bar is 100 microns. Altered Gray Gneiss microbreccia from Strumore, North Uist. GR NF 9092 6907

d Back-scattered electron micrograph showing strong alteration of the microbreccia, and the presence of opaque phases along both fracture orientations. Compare with the optical micrograph of a similar rock shown in plate 5.3*c*. Scale bar is 100 microns. Altered Gray Gneiss microbreccia from Rubha Rossel, Loch Skipport, South Uist. GR NF 8572 3660


a


b


c


d

Plate 5.5

Photomicrographs of microstructures found within the altered Gray Gneiss microbreccias.

a Optical micrograph of a strain-shadowed quartz grain which has undergone subsequent brittle failure, manifested as cataclastic bands running at a low angle across the grain. Continued deformation has rotated the sub-grains within the bands, causing them to become optically mis-aligned with their host. Scale ring is 3 mm in external diameter. Altered Gray Gneiss microbreccia, crossed polars. Sample from Maol Martaig, Loch Skipport, South Uist. GR NF 8465 3699

b Optical micrograph of a microfracture splay showing development of the characteristic 'sliver' texture common in the microbreccias. Scale ring is 3 mm in external diameter. Altered Gray Gneiss microbreccia, crossed polars. Sample from Hartavagh, South Uist. GR NF 8262 1558

c Optical micrograph of a 'sliver' texture disrupting an

amphibole grain (dark phase). Scale ring is 3 mm im external diameter. Altered Gray Gneiss microbreccia, plane polarised light. Sample from Hartavagh, South Uist. GR NF 8262 1558

d Back-scattered electron micrograph of a healed microfracture within a quartz grain (dark phase). Alkali feldspar (grey) and opaque phases (bright) have been deposited along the microfracture, cementing it closed. Scale bar represents 100 microns. Altered Gray Gneiss microbreccia from Sloc Dubh, Ben na Hoe, South Uist. GR NF 7991 2907

e Back-scattered electron micrograph of an original ilmenite grain (light) set in quartz (dark), showing heavy fracturing exploiting the cleavage planes during microbrecciation. Scale bar is 100 microns. Altered Gray Gneiss microbreccia from Strumore, North Uist. GR NF 9092 6907

f Back-scattered electron micrograph of a primary biotite grain (light) showing bending of the cleavage planes and alteration (dark grey) along them. Just to the right of the centre, the biotite has been unable to accomodate deformation by kinking or sliding along the cleavages, and has failed across the cleavage. Scale bar represents 100 microns. Altered Gray Gneiss microbreccia from Crogary na

Hoe, North Uist. GR NF 9732 7273


a


b


c


d


e


f

Plate 5.6

Photomicrographs of the textures and microstructures characteristic of the ultracataclasites and gouges.

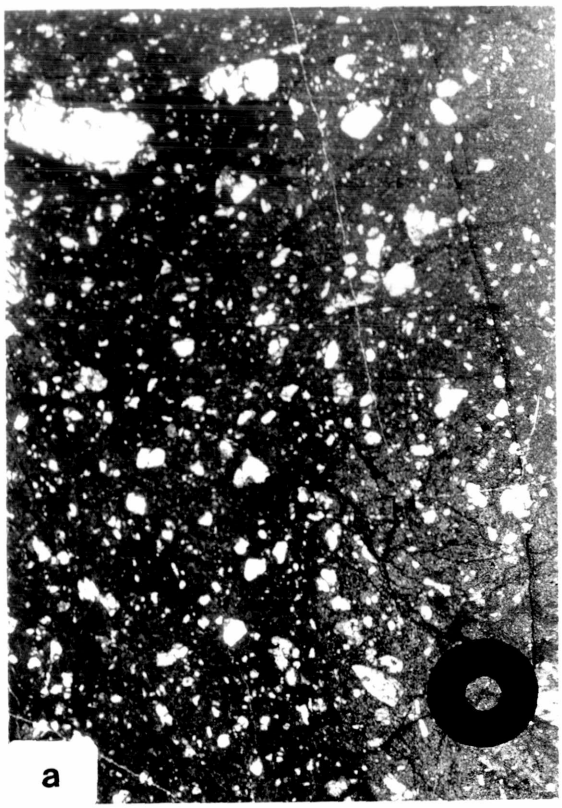
a Optical micrograph of a typical cataclasite texture. Clasts of quartz and feldspar are set in a fine grained matrix, which has undergone later fracturing. Scale ring is 3 mm in external diameter. Cataclasite, plane polarised light. Sample from Maol Martaig, Loch Skipport, South Uist. GR NF 8489 3695

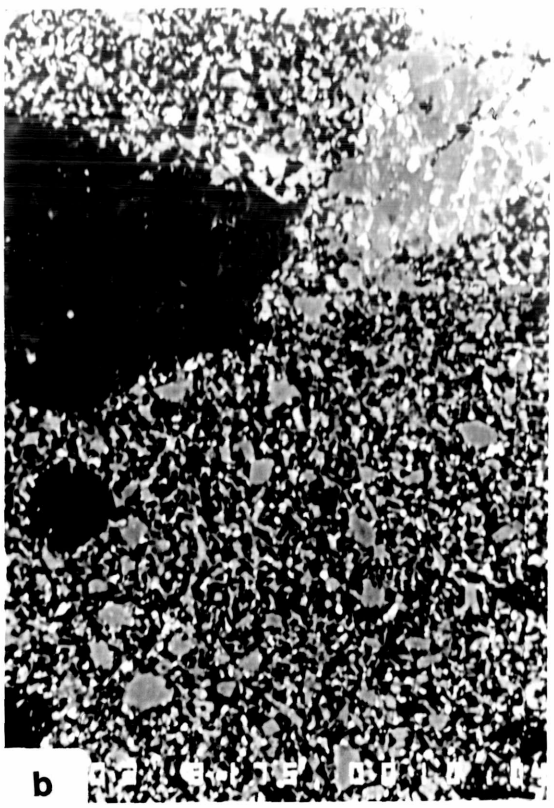
b Back-scattered electron micrograph of an ultracataclasite, showing the similarity of the textures regardless of scales. The dark clast is quartz, whilst the grey one in the top right is a feldspar altering to sericite. Note the extremely fine grain size and random fabric of the matrix material. Scale bar is 10 microns. Ultracataclasite from Beinn na h-Aire, North Uist. GR NF 8989 5859

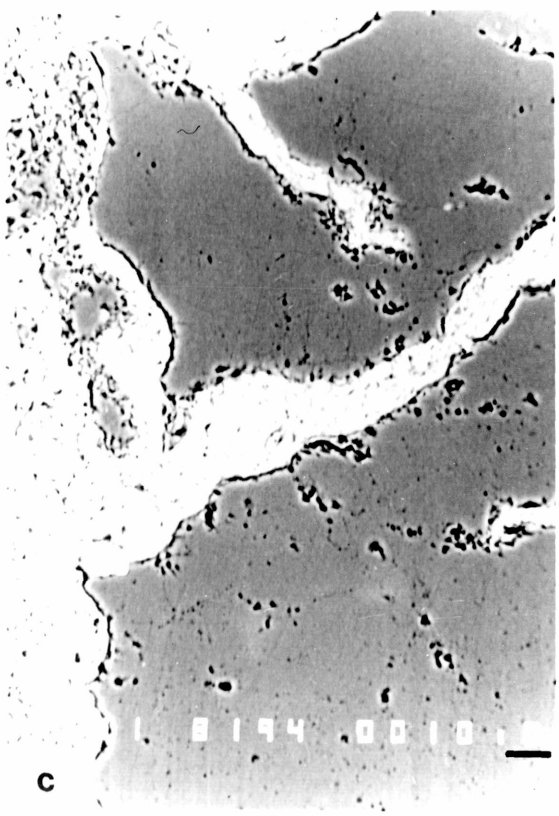
c Back-scattered electron micrograph of a dark coloured

ultracataclasite ('flinty crush rock', which shows as light coloured material on the micrograph) injecting into fractures in a quartz grain (dark material). This results in plucking off of fragments and their subsequent assimilation into the matrix (incipient in the fragment in the upper left of the micrograph). Scale bar is 10 microns. Ultracataclasite from Crogary na Hoe, North Uist. GR NF 9771 7257

d Optical micrograph of a gouge, showing the characteristic textural features - remnant clasts of quartz set in a fine grained, heavily altered matrix. The light coloured bands are due to the impregnating material used in the preparation of the sections, which have impreganated along the foliation and the shear band foliation. Scale ring is 3 mm in external diameter. Gouge, plane polarised light. Sample from North Harbour, Isle of Scalpay, off Harris. GR NG 2180 9675


a


b


c

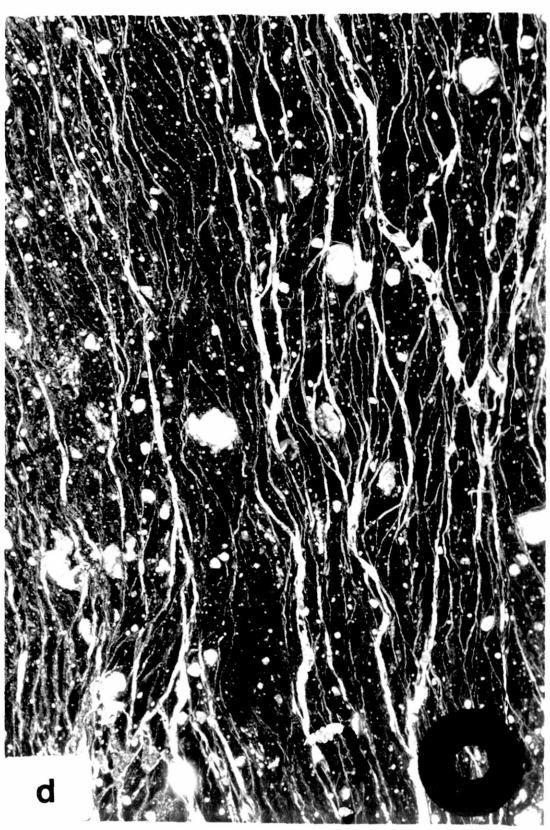

d

Plate 5.7

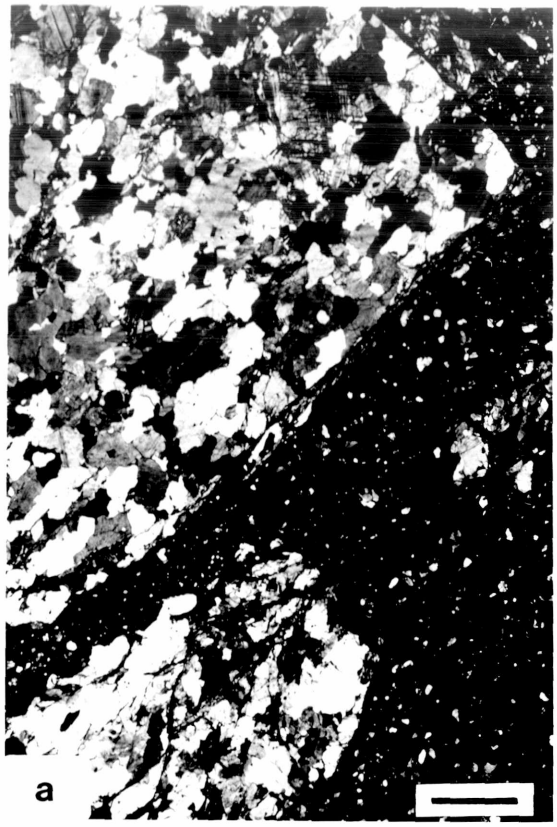
Photomicrographs of the characteristic textures and microstructures of the pseudotachylytes.

a Optical micrograph of black pseudotachylyte veins containing sub-rounded clasts of quartz and feldspar, forming part of a quasi-conglomerate. The gneissose clasts have been rotated, as is evident from the foliation within them. Later shearing has been localised at the boundaries of the gneissose clasts. Scale bar represents 2.5 mm. Quasi-conglomeratic pseudotachylyte in Gray Gneiss, crossed polars. Sample from Ardivachar Point, South Uist. GR NF 7391 4606

b Optical micrograph of a black pseudotachylyte formed along a generating surface. Small scale injection veins exploit fractures in the gneiss below the generating surface, whilst the upper boundary remains smooth. Scale bar is 2.5 mm. Pseudotachylyte vein in Gray Gneiss, crossed polars. Sample from Rubha Ardvule, South Uist. GR NF 7121 2955

c Back-scattered electron micrograph of a black pseudotachylyte, showing a devitrification texture composed of randomly orientated, acicular grains of mica and amphibole (two brightest phases), with feldspar (grey) and quartz (dark). Compare with plate 5.6*b*, an ultracataclasite matrix at similar magnification. Scale bar represents 10 microns. Pseudotachylyte in Gray Gneiss from Loch Skipport, South Uist. GR NF 8483 3696

d Optical micrograph of an altered pseudotachylyte, as typically seen in within Corodale Gneiss. It has a murky appearance compared to the black pseudotachylyte, with the clasts appearing less distinct due to alteration (compare with plate 5.7*a*). Fractures cut through it (top of micrograph). Scale ring is 3 mm in external diameter. Pseudotachylyte in Corodale Gneiss, plane polarised light. Sample from Ben na Hoe, South Uist. GR NF 8163 2724


a


b


c


d

Plate 5.8

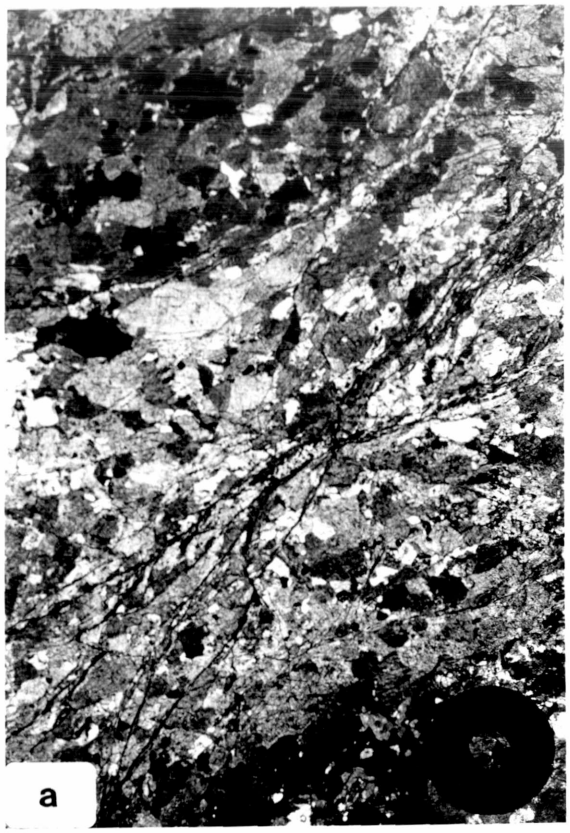
Photomicrographs showing development of c-type mylonite textures from altered microbreccias. Scale ring is 3 mm in external diameter.

a Optical micrograph of a microbreccia, showing alteration along an anastomosing microfracture splay (running diagonally across the centre of the micrograph, from top right to bottom left). The phases between the microfractures are beginning to alter. Amphibole rich Gray Gneiss microbreccia, plane polarised light. Sample from Maol Martaig, Loch Skipport, South Uist. GR NF 8475 3697

b Optical micrograph showing stronger alteration along microfractures, which are beginning to coalesce to form shear zones, and to show precipitation of opaque phases along their length. Brecciation of biotite has occurred. Gray Gneiss microbreccia, plane polarised light. Sample from Strumore, North Uist. GR NF 9093 6918

c Optical micrograph showing more pervasive microfractures and their progressive coalescence into zones of shearing. The microfractures show strong alteration. All phases away from the microfractures, except quartz, now show signs of alteration to a fine grained material, mostly composed of chlorite and epidote. The original grain boundaries have been virtually obliterated. C-type mylonite, plane polarised light. Sample from Burrival, North Uist. GR NF 9103 6163

d Optical micrograph of a fully developed c-type mylonite, showing a shear zone parallel to the long dimension of the micrograph - individual microfractures are no longer distinguishable. Alteration of the original minerals has gone almost to completion, and growth of new minerals has occurred. The resultant texture is one of sub-rounded quartz clasts in a fine-grained matrix of alteration products, which displays a variable intensity of foliation. C-type mylonite, plane polarised light. Sample from mainland north of Floddaybeg, North Uist. GR NF 9187 5864


a


b


c


d

Plate 5.9

Photomicrographs of textures found within the c-type mylonites.

a Optical micrograph of a clast of c-type mylonite which has undergone later brecciation and is now set within a microbreccia. Later shearing has exploited the boundary between the mylonite clast and the microbreccia. Scale ring is 3 mm in external diameter. Gray Gneiss microbreccia with block of c-type mylonite, plane polarised light. Sample from Eaval, North Uist. GR NF 9191 5859

b Optical micrograph of a more typical relationship between microbreccia and c-type mylonite. Pods of microbreccia remain relatively unaltered and undeformed as the shears take up most of the deformation. Late stage fracturing and veining is evident. Scale ring is 3 mm in external diameter. Gray Gneiss microbreccia, plane polarised light. Sample from Loch Skipport, South Uist. GR NF 8494 3692

c Back-scattered electron micrograph showing characteristic alignment of chlorite grains (grey phase) within the c-type mylonites. Their alignment marks the mylonitic foliation in the top portion of the micrograph, whilst the lower portion shows the foliation curving around a clast and into parallelism with the mylonitic foliation. Epidote and opaque phases (bright phases) replace original minerals. Scale bar is 10 microns. C-type mylonite from Creag Scalan, Crogary na Hoe, North Uist. GR NF 9649 7071

d Back-scattered electron micrograph showing curve-in of the shear band foliation (running diagonally bottom left to upper right) to the mylonitic foliation (running vertically up the plate). The foliation is marked by acicular grains of chlorite and amphibole in a matrix of feldspar and apatite. Scale bar is 10 microns. C-type mylonite from Mol a Tuath, Usinish, South Uist. GR NF 8572 3547

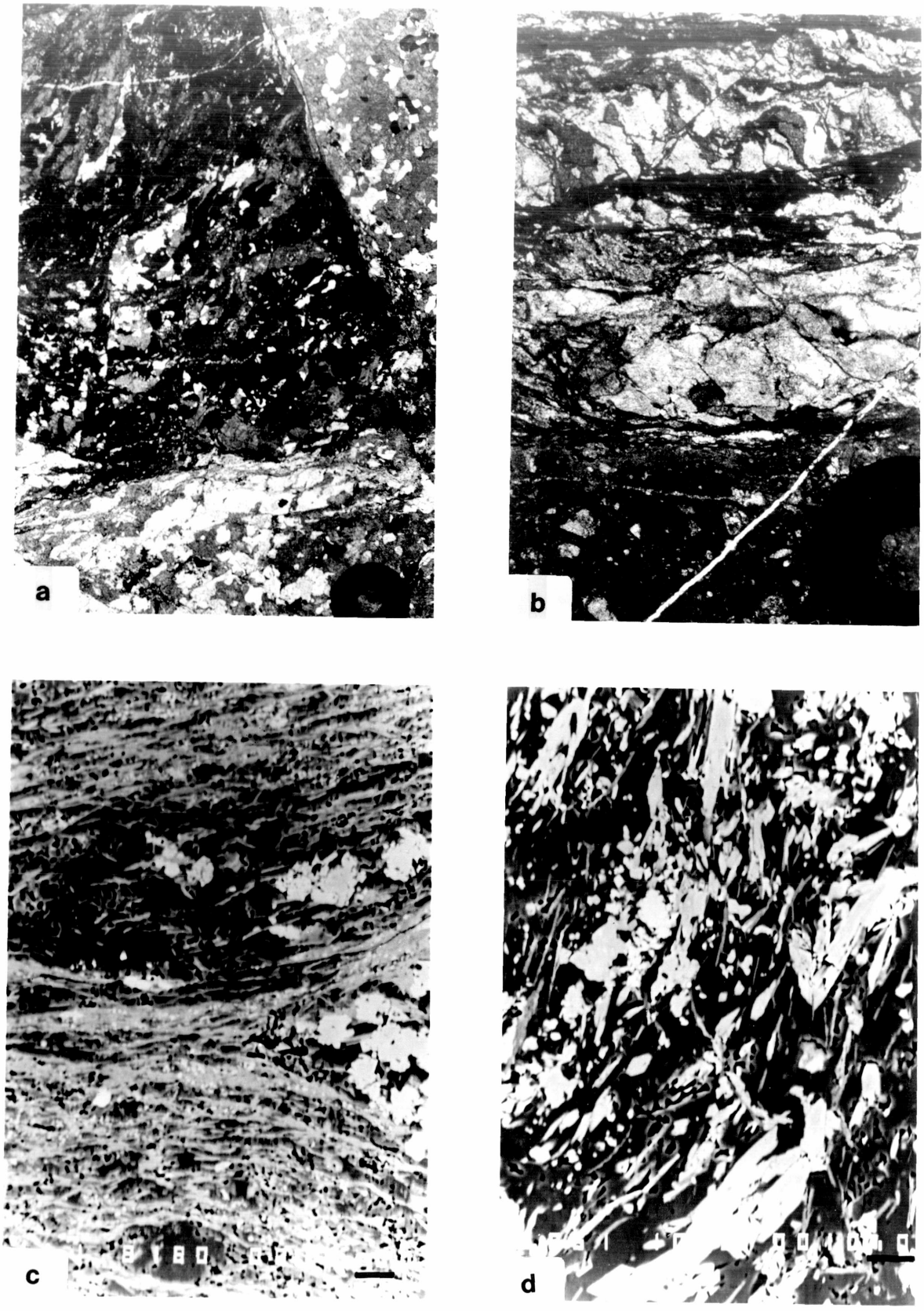

a
b
c
d

Plate 5.10

Photomicrographs of characteristic microstructures found within the c-type mylonites.

a Optical micrograph of asymmetric crenulation developed in the mylonitic foliation, as a result of dextral shear. Scale ring is 3 mm in external diameter. C-type mylonite, crossed polars. Sample from Loch an Tomain, Burrival, North Uist. GR NF 9207 6158

b Optical micrograph of an epidote vein (upper part of micrograph) which has been crumpled by strong localised compression across the foliation. Scale ring is 3 mm in internal diameter. C-type mylonite, plane polarised light. Sample from coast adjacent to Dun Mhic Laitheann, Crogary na Hoe, North Uist. GR NF 9777 7299

c Optical micrograph of a shear fractured garnet porphyroclast, which has been offset along fractures, set within a weaker matrix of altered feldspar. Scale ring is 3 mm in external diameter. C-type mylonite, plane

polarised light. Sample from Scor na Caillich, North Lee, North Uist. GR NF 9523 6649

d Optical micrograph showing tensile fracture in an opaque phase (centre of micrograph). Ultracataclastic material infills the gaps where the opaque has been pulled apart. Above and to the right is a striped opaque, thought to represent replacement of a micaceous phase. Scale ring is 3 mm in external diameter. C-type mylonite, plane polarised light. Sample from Partachal, North Lee, North Uist. GR NF 9449 6592

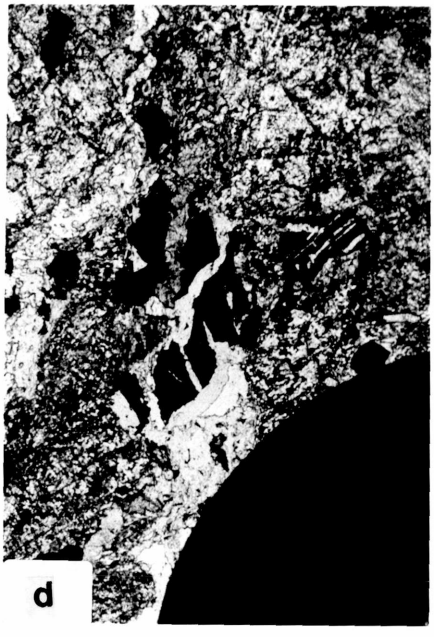
e Back-scattered electron micrograph of a foliation-parallel pulled apart epidote vein (bright phase, marked E), with the gaps infilled by fine grained cataclastic material. Scale bar is 100 microns. C-type mylonite from Creag Scalan, Crogary na Hoe, North Uist. GR NF 9649 7071

f Back-scattered electron micrograph of an opaque phase showing a complex intergrowth of TiO_2 (dark grey), ilmenite (medium grey) and magnetite (bright). The TiO_2 and the ilmentite appear to be intergrown along a top right to bottom left orientation, whilst the magnetite runs at a high angle to this. Scale bar is 10 microns. C-type mylonite from the Usinish peninsula, South Uist. GR NF 8572 3547


a


b


c


d


E
e

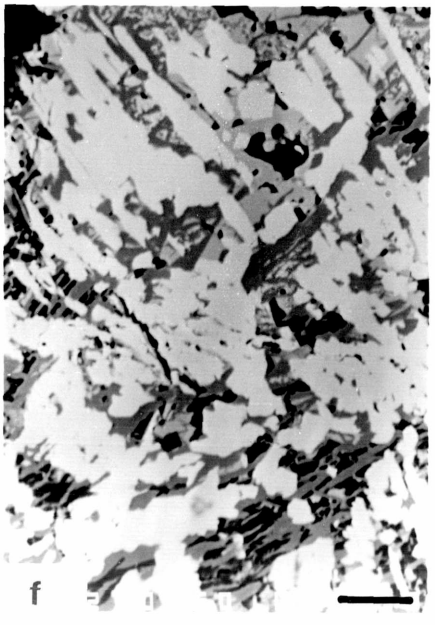

f

Plate 5.11

Photomicrographs of textures and microstructures found within the r-type mylonites. Scale ring is 3 mm in external diameter.

a Optical micrograph of a protomylonite showing incipient development of ribbon grains of quartz. Foliation has been disrupted by later high-angle fracturing. R-type protomylonite, plane polarised light. Sample from Loch Mor an Iaruinn, Shildenish, Lewis. GR NB 2998 1927

b Optical micrograph showing asymmetric augen of quartz and feldspar, defined by the presence of the mylonitic foliation (S_m) and a shear band foliation (S_b). R-type mylonite, plane polarised light. Sample from Loch na Craoibhe, Malasgair, Lewis.
GR NB 2972 1877

c Optical micrograph showing crystal plastic behaviour of the mafic minerals (dark phases), in this case, amphibole, and quartz. Specimen has subsequently been affected by

high-angle fracturing. R-type mylonite, plane polarised light. Sample from Loch na Craoibhe, Malasgair, Lewis. GR NB 2984 1884

d Optical micrograph of extreme ductile behaviour of all minerals. A small scale sinistral sense fold is present in the foliation, in the bottom centre of the micrograph. Ultramylonite, plane polarised light. Sample from north of Loch Sgibacleit, Malasgair, Lewis. GR NB 3119 1679

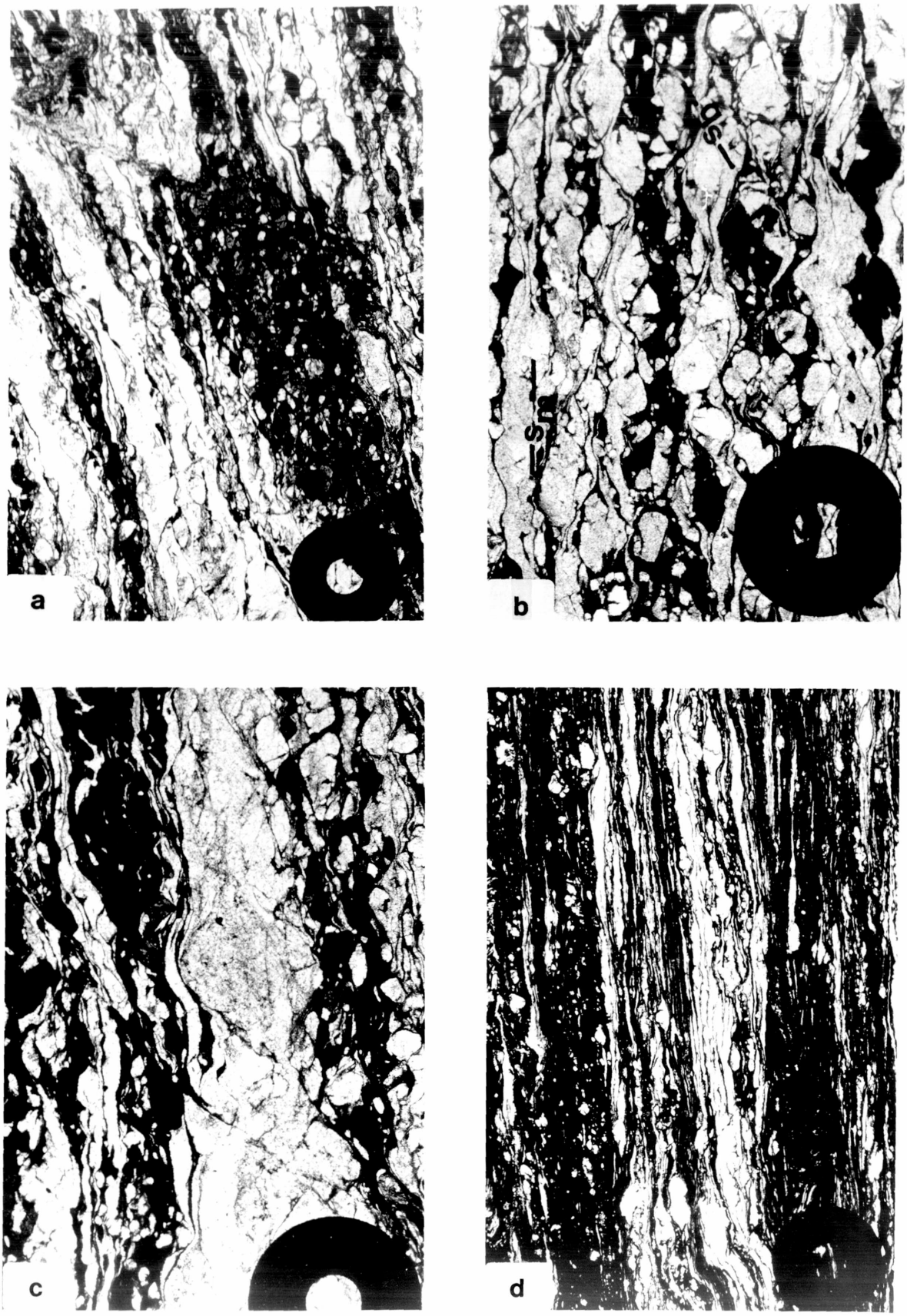

a
b
c
d

Plate 5.12

Photomicrographs of textures and microstructures found within the r-type mylonites - continued

a Back-scattered electron micrograph showing ribbon grain development of quartz (dark phase) and amphibole (bright phase). Scale bar is 100 microns. R-type mylonite from Malasgair, Lewis. GR NB 3012 1691

b Back-scattered electron micrograph of a mafic band from plate 5.12*a*, but at higher magnification. Grains of quartz and feldspar define the foliation (darker phases) whilst biotite (bright phase) displays only a weak preferred orientation. Scale bar is 10 microns. R-type mylonite from Malasgair, Lewis. GR NB 3012 1691

c Back-scattered electron micrograph of an ultramylonite, showing the ultrafine grain size present. Scale bar is 100 microns. R-type ultramylonite from Cleite Catriona, Eishken, Lewis. GR NB 3157 1163

d Back-scattered electron micrograph of an altered and brecciated *r*-type mylonite. Scale bar is 100 microns. Phyllonite from Cnoc a' Charnain, Lewis. GR NB 3270 1641


a


b


c


d

Chapter 6

Geochemical Studies

6.1 Introduction

This chapter will discuss results and interpretations of the analytical work undertaken during the course of this project. The data are presented in a series of Appendices at the end of this thesis, and include amphibole analyses obtained by electron microprobe energy dispersive spectral (EDS) analysis, using a Jeol 733 Superprobe (Appendix I), whole rock analyses by Inductively Coupled Plasma (ICP) techniques (Appendix II), Fe^{2+} determinations by wet chemistry (Appendix III) and density determinations (Appendix IV). Each Appendix contains a full description of the method used, together with any notes and information on problems encountered.

The majority of the rock types studied were Gray Gneiss and its derivatives, and, to a lesser degree, the Corodale Gneiss. Samples showing a clear deformation history were assigned to one of a number of categories by inspection of thin sections, dependent on the nature of the source rock (e.g. Gray Gneiss, Corodale Gneiss) where this could be ascertained, the degree of retrogression and alteration, and the degree and style of deformation.

The categories are; intact Gray Gneiss, Corodale Gneiss, Mashed Gneiss, microbreccias with their retrogressed and altered equivalents, cataclasites, c-type mylonites,

r-type mylonites, gouges, pseudotachylytes and phyllonites (see chapter 5 for a description of each rock type). Subdividing the samples in this manner has disadvantages, primarily in the difficulty of drawing a distinction between the different fault rock types. This was particularly true for the gradational division between the microbreccias and the c-type mylonites, necessitating a somewhat arbitrary dividing line to be drawn. This may partially explain why some of the results are not as conclusive as they might otherwise have been.

Very few cataclasites and ultracataclasites have been analysed owing to difficulties in separating them cleanly from their host. Gouges and phyllonites were not studied, as their outcrop is so restricted and impersistent, and their development so variable, that it was felt impossible to obtain representative samples (X-ray diffraction was applied to a gouge specimen and the results given in section 5.5). For the geochemistry of the pseudotachylytes, see the exhaustive account of Maddock (1986).

Measurement of Fluids

The accurate determination of fluid content is one of the main problems in investigating the chemical changes occuring in the rocks. The techniques used, and the

problems associated with each, are discussed in Appendix II, together with a comparison of the results obtained. Figures for fluid content quoted in this chapter were obtained by loss on ignition (LOI).

6.2 Description of the Bulk Chemistry of the Major Rock Types

As very lttle work has been done previously on the characterisation of the geochemistry of the Outer Hebridean country rocks (Gray Gneiss, Corodale Gneiss and Mashed Gneiss), it is proposed to briefly describe the geochemical characteristics of each. This is particularly relevant as it will form a basis for comparison with the fault rock compositions.

The rocks were analysed for 10 major elements: SiO_2; Al_2O_3; total Fe expressed as Fe_2O_3; MgO; CaO; Na_2O, K_2O, P_2O_5; TiO_2 and MnO, and 11 trace elements: Ba, Be, Co, Cr, Cu, La, Ni, Sr, V, Zn and Zr, this being the range analysed as standard by the ICP. Major elements are expressed throughout in terms of weight percent oxide, traces in parts per million. A full tabulation of the results described below is given in Appendix II, and a comparison of the average compositions of the main rock types is presented in table 6.1.

The Country Rocks

The Gray Gneiss

The Gray Gneiss varies in composition from acid to basic, with the acid types being dominant. An average of all Gray Gneiss analyses is shown in table 6.1, whilst figures 6.1*a* and *b* show the ranges of major and trace elements respectively for selected Gray Gneiss samples, i.e. those that have been ascertained, on the basis of thin section inspection, to be completely unaltered and unaffected by the faulting. Variation in SiO_2 (figure 6.1*a*) is largely due to the differing modal proportions of quartz and feldspar relative to amphibole and biotite. The relatively high levels of some trace elements are also accounted for by the mineralogy. Ba goes into the feldspars, whilst Sr goes into apatite, an accessory phase in the Gray Gneiss.

The Corodale Gneiss

An average analysis for the Corodale Gneiss is shown in table 6.1. Figures 6.1*c* and *d* illustrate the ranges of the major and trace elements respectively. Due to difficulties in obtaining fresh specimens, the results from only four Corodale Gneiss samples have been used. Their bulk chemistry appears to fit well with the mafic mineralogy

observed in hand specimen and thin section. Two samples of altered Corodale Gneiss were also analysed, and the range of values obtained is given in figures 6.1*c* and *d*, for comparison.

The relatively high values for LOI are thought to be due to the incipient slight alteration present in many of the specimens, evident as reaction rims of amphibole around many of the pyroxene grains, and sericitisation of the feldspars. One sample of Corodale pyroxenite was also analysed (column 3, table 6.1). This was much fresher, and had a volatile content of only 0.96. It may be that there was a scarcity of fluid, or that the fluids did not have access to the pyroxenite, which has prevented it from retrogressing. The pyroxenite is likely to have been relatively impermeable, so that fluids would have had restricted access.

The Mashed Gneiss

An analysis for the average Mashed Gneiss composition is given in column 4 of table 6.1. The Mashed Gneiss has a restricted outcrop on the Usinish peninsula, South Uist, and tends to be badly weathered. Because of this, only four samples obtained were suitable for analysis, and the results show considerable variation (see average analysis presented in table 6.1, and the ranges in figures 6.1*c* and

d).

The Fault Rocks

The Altered Gray Gneiss

Although not actually fault rocks, these are mentioned here as it is likely that their alteration was associated with the faulting. An average analysis of altered Gray Gneiss is presented in table 6.1. The ranges for Si, Al, Mg and Ca are greater than those for Gray Gneiss (see figures 6.1*c* and *d*), as a result of varying degrees of alteration.

The Microbreccias

These are more difficult to characterise than the country rocks as the processes that have acted upon them have led to a greater variation in composition, even more so than for the altered Gray Gneiss. This is because differing degrees of crushing, alteration and retrogression have occurred within them.

Microbreccia Derived from the Gray Gneiss

The microbreccias derived from the Gray Gneiss have been

split roughly into two groups, depending on the extent of alteration. The groups were defined on the arbitrary basis of the extent of feldspar alteration visible in thin section.

a) Relatively Unaltered Microbreccia

The compositions of these fault rocks show some significant differences when compared with those of the Gray Gneiss (compare columns 1 and 6 in table 6.1). Ranges for major and trace elements are given in figures 6.1*a* and 6.1*b*, and are broadly similar to those for Gray Gneiss. Levels of SiO_2 show a decrease, whilst Fe_2O_3, MgO, CaO and Na_2O show slight elevations, whilst LOI shows a larger increase. Trace element variations are slight (figure 6.1*b*), with Cr, Ni and Sr being the most notable exceptions, with considerably higher levels than are found in the Gray Gneiss.

b) Altered Microbreccia

These microbreccias are very similar in composition to the relatively unaltered microbreccias (compare columns 6 and 7 of table 6.1), although they are quite different to the Gray Gneiss. It seems that the major element trends in

geochemical differences between the Gray Gneiss and the relatively unaltered microbreccias are continued as the latter become altered microbreccias. Silica levels continue to fall in general, although the range of values becomes much wider. This dramatic widening of ranges of almost all elements characterises the altered microbreccias, as figures 6.1*a* and *b* show.

Considering the average analyses presented in table 6.1, the general differences in chemistry between the altered microbreccias and the Gray Gneiss are the already-mentioned decrease in SiO_2, together with increases in Fe_2O_3, MgO, CaO, Na_2O, K_2O, TiO_2 and LOI. Trace element levels show similar increases to those noted for the unaltered microbreccias, although, in addition, there has been a rise in Ba levels.

The Corodale Derived Microbreccia

Corodale-derived microbreccias are fairly scarce, so fewer samples have been analysed. Thin sections reveal that they tend to be fresh, so they have not been subdivided into altered and unaltered categories. The most important major element changes that occur as a Corodale Gneiss becomes a microbreccia (compare columns 2 and 8, table 6.1) are increases in SiO_2, Na_2O and K_2O and

decreases in Fe_2O_3, MgO and CaO. Trace elements show decreases in Cr, Cu, Ni, Sr, Zn and a large decrease in V, and large increases in Ba and Zr. Ranges of values are shown in figures 6.1*c* and *d*.

Summary of Geochemical Changes from Country Rock to Microbreccia

There seems to have been a continuing process producing microbreccia from parent rock (as represented by samples showing varying intensity of deformation). From this, it is to be expected that one end of the range for the microbreccias should broadly coincide with the values for their parent (i.e. Gray Gneiss or Corodale) - see figures 6.1*a* to *d*. In general, this appears to hold true for the Gray Gneiss series, but not for the Corodale Gneiss and derivatives. This may be partly because their restricted outcrop meant that only a small number of samples could be analysed, giving a high probability that the samples are unrepresentative.

The most important conclusions regarding microbreccia formation are:

1) The average geochemical changes shown as a Gray Gneiss undergoes microbrecciation tend to be the opposite

of those shown by the Corodale Gneiss undergoing similar deformation. For example, the Gray Gneiss shows increases in Fe, Mg and Ca and decreases in Si, whilst the Corodale Gneiss shows decreases in Fe, Mg and Ca and increases in Si.

2) The ranges of values increase during the microbrecciation process, i.e. the microbreccias have a more variable composition than their parent rocks. This is best seen in the Gray Gneiss to Gray Gneiss microbreccia transition.

3) The ranges of values for Gray Gneiss derived altered microbreccias are larger than those for Gray Gneiss derived unaltered microbreccias (see figure 6.1*a* and *b*). They also tend to show a displacement in the opposite sense, e.g. the Gray Gneiss has a Fe_2O_3 range of 2 to 5 and the microbreccia shows a wider range of higher values (2.8 to 6.8); the altered microbreccias show a wider yet range of lower values (0.2 to 5.5). This is not always reflected in the average analyses shown in table 6.1, where there appears to be a straightforward decrease in silica levels along the series, and is thought to reflect the influence of more than one process within the altered microbreccias, that is, alteration as well as deformation.

The Ultracataclasite and Cataclasite

It is not proposed to go into much detail about the composition of these rocks, for the reason already mentioned in the introduction to this chapter. They generally have a range of major and trace elements that is similar to that of the Gray Gneiss from which they are derived. Those that show a greenish appearance in hand specimen were found to be heavily altered on inspection of their thin sections. For more details of their compositions, refer to Appendix II.

The C-Type Mylonite

These are developed gradationally with increasing deformation and alteration from the Gray Gneiss derived microbreccias, as far as can be ascertained from field and thin section evidence. Because of this gradation, an arbitrary boundary between the two was established at the point where the amphiboles originally present in the parent gneiss have completely broken down. An average analysis is presented in column 9 of table 6.1; compare this with column 1, Gray Gneiss. Ranges of values are presented in figures 6.1*a* and *b*.

Of all the fault rocks, the c-type mylonites show the widest range of values, and the largest changes in composition relative to the Gray Gneiss. SiO_2 decreases by an average of 6 %, and K_2O decreases slightly, whilst Fe_2O_3, MgO, MnO, CaO, Na_2O, P_2O_5, TiO_2 and LOI show increases, LOI markedly so. Trace elements show decreases in levels of Ba, Co and Zr, increases in Zn and Sr, and strong increases in Cr, Ni and V.

The overall geochemistry of the c-type mylonites indicates a fairly mafic composition, as suggested by the mineralogy (see section 5.7). The LOI measurements support the thin section observations of the presence of many hydrous phases. Composition of these mylonites is very similar to that of the green altered cataclasites (although the latter are not generally quite so mafic), suggesting that alteration is an important process in the formation of the c-type mylonites.

The R-Type Mylonite

This is similar in composition to the Gray Gneiss and an average analysis is given in column 9 of table 6.1. Ranges of values are shown in figures 6.1*a* and *b*; these are also similar to those for the Gray Gneiss. MgO and Ba are the only constituents present in significantly different

amounts, with an increase in MgO and a decrease in Ba. In addition, Cr shows a slight increase, and K_2O, TiO_2, and Sr show slight decreases, but these are thought to be due to sample bias rather than any real difference.

6.3 Bulk Chemical Changes

Variations in composition, as noted above, are present between the fault rocks and their parent gneisses which can, in part, be related to the degree of deformation and associated influx of fluids. These will be looked at in more detail here, for both the Gray Gneiss and the Corodale Gneiss derived fault rocks.

The most immediate problem with looking at chemical variations is that of the dilution effect, whereby an addition (or loss) in the level of one element will produce an apparent decrease (or increase) in the remaining elements by dilution (or concentration). This effect is especially noticeable where the element whose level is changing is present in large amounts. Any variation in the level of this element will induce a larger relative variation in the levels of those elements present in smaller amounts. If more than one element varies in level, then this produces further variations in the levels of the other elements present, and it becomes

difficult to distinguish between real and apparent element variations. In addition, this effect will tend to swamp any real changes in the level of those elements present in small quantities.

To show that variations are real and not simply due to the above effect, graphs are presented with annotated lines showing theoretical dilution trends for comparison.

Bulk Changes in the Gray Gneiss-derived Fault Rocks

For almost all plots there is an overall trend for Gray Gneiss and r-type mylonites to occupy similar fields, with the microbreccia field lying within or slightly removed from this area, and grading into the field occupied by the c-type mylonites. The general trends with increasing deformation are for a large decrease in SiO_2, and moderate to large increases of Fe_2O_3, MgO, P_2O_5, TiO_2, MnO and LOI. CaO and Na_2O show a wider range in values compared to Gray Gneiss, whilst K_2O and Al_2O_3 remain fairly constant (for a graphical representation of these changes, see figure 6.1).

The main differences are, therefore, that the r-type mylonites show little chemical variation, the microbreccias show some variation, and the c-type

mylonites show the greatest variation, relative to parent Gray Gneiss.

The most highly altered of the microbreccias do not conform to this general pattern. In thin section, they are seen to be traversed by minute veins, mainly of quartz but with smaller amounts of alkali feldspar, in addition to fractures and associated alteration. Because of this, they frequently show higher levels of silica and K_2O. Levels of Na_2O are similar, or slightly lower, than those of the Gray Gneiss, but the large increase of SiO_2 gives a dilution effect which may mask an actual rise of Na with respect to the Gray Gneiss. Probably because of this dilution effect, the other elements all show apparent decreases in concentrations.

The remainder of this section will concentrate on the geochemical relationships between the Gray Gneiss, the r-type mylonites, the c-type mylonites and the strongly altered microbreccias. Most of the graphical representations used to demonstrate the chemical variations will be normalised in some fashion in an attempt to avoid the problem of the dilution effect, as noted above.

Variation of LOI with SiO_2 (figure 6.2) indicates definite fields for each rock type. The general trend is

for SiO_2 to show an inversely proportional relationship to LOI. R-type mylonites have very similar SiO_2 and fluid contents to the Gray Gneiss, suggesting little chemical change took place during amphibolite facies mylonitisation, i.e. it was an essentially isochemical process.

The c-type mylonites show a decrease in SiO_2 and increasing LOI relative to the Gray Gneiss. The thin sections suggested that this might be the case, as there is little quartz present and many hydrous phases. The microbreccia field also shows high levels of LOI, but the inverse relationship breaks down here, as it has higher levels of silica.

A normalised plot of LOI against Fe_2O_3 is presented in figure 6.3. Again, the rock types occupy clearly defined fields, with a general directly proportional trend. The Gray Gneiss and the r-type mylonites once more overlap, with the c-type mylonites showing higher Fe_2O_3 and higher LOI. The altered microbreccias occupy the lower end of the Fe_2O_3 scale, extending upwards to occupy a wide range. This plot once more shows that there is no significant variation between the Gray Gneisses and the r-type mylonites, whereas the c-type mylonites show an increase of total iron with LOI, as do the microbreccias. A similar pattern is observed for MgO, as shown in figure 6.4.

Variation in LOI against Al_2O_3 is shown in figure 6.5. It can be seen from this (and also by looking at figure 6.1) that Al_2O_3 has a relatively restricted range and does not show much variation between rock types. This suggests that Al remains approximately constant across the range of Gray Gneiss derived fault rocks. This assumption was used, in conjunction with other evidence, to calculate the mass balance equations presented in section 6.5.

Trace Element Changes in the Gray Gneiss-derived Fault Rocks

So far, only the major element distributions between fault rock types have been discussed. From the averages in table 6.2, and the ranges presented earlier in this section, it can be seen that the only trace elements displaying significant variations are Ba and Sr. Plots of Ba and Sr against SiO_2 are shown in figures 6.6 and 6.7 respectively. The patterns are similar to the major element variations; the r-type mylonites show similar values to the Gray Gneiss, whilst the altered microbreccias tend to have slightly higher levels of the trace elements.

The c-type mylonites show the strongest trend, with enrichment in Ba and Sr. The trend is much stronger for Sr than for Ba, with the majority of c-mylonites having

higher levels of Sr than the Gray Gneiss, whilst only a few possess more Ba. It is thought that this elevation of trace element content is for the same reasons that they show elevated levels of certain major elements, such as Fe_2O_3 and MgO; that is, that these elements have been brought into the rocks by a fluid phase. The only other trace elements to show a significant variation are the levels of Cr (figure 6.8) and V in the c-type mylonites, which respectively show average increases of 300% and 50 % over the Gray Gneiss levels.

General Summary and Conclusions from Bulk Chemical Changes in the Gray Gneiss-derived Fault Rocks.

R-type mylonites show very similar values to the Gray Gneiss for all elements, implying that their formation was an isochemical process. With progressive deformation and alteration from Gray Gneiss through microbreccia to c-type mylonite, there is a general trend for an increase in Fe_2O_3, MgO, LOI, Ba and Sr, and a decrease in SiO_2. Al_2O_3 levels remain approximately constant.

It appears possible that there has been an ingress of fluid into the c-type mylonites, which removed silica as it passed through. The fluid then passed into the microbreccias, causing some alteratiom, though not as extensive as that caused in the c-type mylonites. As it

passed through the microbreccias, the fluid, possibly cooling, redeposited the silica it had dissolved from the c-type mylonites. This would account for the patterns displayed in figure 6.2.

The directly proportional relationship between iron and LOI for the c-type mylonites and the microbreccias suggests that Fe in some form may have been brought into the rocks by the fluids responsible for the increase in LOI. This idea of introduction of Fe and Mg into the fault rocks together with the fluid will be discussed in more detail in the mass balance section. The pattern of elements when compared to Gray Gneiss is very similar to that displayed by the c-type mylonites, suggesting that some of the same processes may have been operating.

It is possible that the Mashed Gneiss (sections 4.5, 5.2, 6.2) was derived by excessively strong alteration of Gray Gneiss by fluids from the fault zones, i.e. it represents 'end member' altered Gray Gneiss microbreccia. The geochemical evidence supports this, as the compositions of the Mashed Gneiss broadly coincide with those for the Gray Gneiss derived altered microbreccias. Furthermore, fluid content and alteration within the deformed rocks of the fault zone show a general increase towards the hanging wall. The Mashed Gneiss is the highest structural unit exposed on the Outer Hebrides, and is

certainly the most strongly altered.

Major and Trace Element Changes in the Corodale-derived Fault Rocks

The only fault rock derived from the Corodales is a microbreccia, which is scarce and usually not very well developed, owing to the relative competence of the Corodale Gneiss compared to the Gray Gneiss. It rarely shows any degree of alteration, whereas the undeformed Corodale Gneiss that were collected frequently exhibited signs of alteration. Furthermore, as so few samples could be obtained, the number of analyses performed are really too few to be representative, so that differences in composition between the rocks may only be apparent.

SiO_2, Al_2O_3, Na_2O, K_2O and P_2O_5 all show average increases from the levels present in undeformed Corodale Gneiss, while Fe_2O_3, MgO, MnO, CaO and TiO_2 levels drop, MgO and CaO dramatically so (figure 6.1*c*). Trace element levels generally show small average variations: Ba and Zr increase by around 50 %, and Sr by around 10 %. All other trace elements remain at similar levels to those present in the undeformed Corodale Gneiss, with the exceptions of Cr, Cu and V, which show decreases of approximately 60 - 70 % (figure 6.1*d*).

It is interesting to compare the changes in levels of trace and major elements from undeformed rock to microbreccia for the Gray Gneiss and the Corodale Gneiss. Figures 6.9*a* and *b* show a graphical representation of these changes. Since microbreccia formation has occurred at high crustal levels, it is unlikely that any high temperature mechanism (e.g. diffusion) has played a part in modifying bulk compositions. As fluid content increases in the microbreccias, it seems reasonable to conclude that fluids might be the modifying influence.

Examination of figure 6.9 reveals an unexpected relationship between the comparative changes in the microbreccias relative to their parent rocks. Elements that decrease in abundance from the Gray Gneiss to the Gray Gneiss-derived microbreccias show an increase in the Corodale microbreccias relative to the Corodale Gneiss. Conversely, elements that increase from Gray Gneiss to Gray Gneiss-derived microbreccia decrease from Corodale Gneiss to corodale Gneiss microbreccia (Compare also columns 1, 2, 5 and 7 of table 6.2.).

One explanation for these reverse trends could be attributed to some sort of mechanical mixing of the two starting rock types during deformation. However, the outcrop patterns and lack of any field relationship between these rock types and the microbreccias makes this

unlikely.

An alternative explanation could be that some sort of homogenisation process was operating, with an external source of fluid tending to buffer the microbreccia compositions towards a composition intermediate between the two starting compositions. Again, this would necessitate an intimate field relationship between the two starting compositions. Such a relationship is absent.

6.4 Fe^{2+} determinations

FeO values were determined for a variety of rock types, and the data are presented in Appendix III. Figure 6.10 presents this data as a proportion of FeO + Fe_2O_3 for the different rock types. Only a few samples have been analysed for the Corodale Gneiss. It should be noted that several samples showed values for FeO that were higher than the total iron as measured by ICP. These rocks were two samples of strongly altered Gray Gneiss microbreccia, together with a metasediment, not shown on figure 6.10. All of these samples contained iron sulphides and it is thought that this has affected the accuracy of the Fe^{2+} determination technique. For comparison purposes, the FeO content of two basic Gray Gneiss was also determined. They were both amphibolites, and gave strongly reduced values when compared to the more acid Gray Gneiss.

From the analyses that were performed, it can be seen that all rocks of Corodale derivation possess very similar $FeO/FeO + Fe_2O_3$ ratios, suggesting that despite the low number of samples analysed, the figures obtained are representative. The value for altered Corodale Gneiss is slightly higher than that for unaltered Corodale Gneiss, suggesting that some reduction of Fe has occurred, whereas that for the Corodale microbreccias is almost the same as that for the Corodale Gneiss, implying no significant change in oxidation state during the microbrecciation process. In a similar fashion to the Corodale Gneiss, the altered Gray Gneiss show a slight reduction when compared with the Gray Gneiss.

The Gray Gneiss-derived microbreccias are significantly oxidised, possibly due to weathering effects - as they contain so many open microfractures, it is easy for alteration to occur once they are exposed. The altered Gray Gneiss-derived microbreccias show relatively strong reduction, in a similar manner to the altered Corodale Gneiss and altered Gray Gneiss. This is possibly because one of the effects of the altering fluids is to cause reduction of the iron. However, if the iron sulphide-bearing samples are excluded, the value for $FeO/FeO + Fe_2O_3$ comes down to 0.6, making the ratio for the altered microbreccias similar to that for the

unaltered microbreccias.

The r-type mylonites also show a reduction when compared to the Gray Gneiss. Possibly this is connected to the effects of the mylonitisation, which may have involved small quantities of fluid, on the basis of the loss on ignition measurements. Certainly, there is no field or microstructural evidence to support any post-tectonic episode of fluid ingress which could have brought about later reduction. However, the majority of the Gray Gneiss analysed was from North and South Uist, and it is possible that the oxidation state of the parent Gray Gneiss on Lewis, further to the north, was lower. Also, there are numerous patches of metasediments and meta-igneous rocks in the vicinity of the r-type mylonites. As these have been found to have high $FeO/FeO + Fe_2O_3$ ratios, it is possible that portions may have been incorporated into the mylonites at the time of their formation, thus affecting their Fe^{2+}/Fe^{3+} ratio. This possibility is remote, as such inclusion would also affect the mylonite bulk chemistry.

In contrast to the reduced state of the r-type mylonites, the c-type mylonites show oxidation when compared to their parent rocks, to around the same levels displayed by the Gray Gneiss microbreccias. It is thought that this is related to the ingress of fluids during their formation.

In summary, straightforward alteration of either Corodale or Gray Gneiss results in reduction of iron. Microbreccia formation results in no real change for the Corodale Gneiss, and oxidation for the Gray Gneiss-derived samples. Alteration of the Gray Gneiss microbreccias results in no further change, and the same is true for c-type mylonitisation. It is thought that these oxidation reactions are due to later weathering and do not necessarily reflect the composition of any fluids present at the time of deformation. R-type mylonites are significantly reduced compared to the Gray Gneiss, and the reason for this is unknown.

6.5 Mass Balance Calculations

As noted above (section 6.3), comparison of straight oxide variations does not allow the effects of dilution or concentration to be considered, nor does it allow any estimate of the likely volume changes associated with chemical change since variation in density is not considered. To overcome these problems, mass balance calculations were performed following the method of Gresens (1967).

Gresens (1967) formulated a general set of equations

that allows the actual gains and losses of volume and individual component oxides that occur during a reaction to be calculated in terms of the bulk chemistry and specific gravity of the starting and finishing compositions. To this end, density determinations were carried out (Appendix IV), to be used in conjunction with the whole rock chemical results. Twenty samples were chosen as being typical representatives of their type, all of Gray Gneiss derivation. Their densities were measured in duplicate or triplicate, and the mean was used for the purposes of the mass balance calculations (Appendix IV).

The Gresens' (1967) method works by initial calculation of the gradient of a line for each component oxide assuming arbitrary values for volume changes, and extrapolating to find the point where it cuts a line representing zero gain or loss of that element. Once this composition-volume diagram has been plotted, these intersections are examined, and a volume factor is chosen for calculation of a balanced equation.

In simple cases, it can be assumed either that there has been no change in volume with reaction (isovolumetric) or that the amount of one or more of the component oxides has remained broadly constant (isochemical). There is no reason to assume that either of these cases applies to the Outer Hebrides fault rocks for the following reasons. The

isovolumetric case is unlikely as the rocks formed in a deformational environment. Because of the complex chemistry and nature of the fault zone and its rocks, it is not obvious that specific elements have necessarily remained immobile (isochemical), so we have to constrain the volume factor used to balance reactions using field, mineralogical and textural evidence from the fault rocks.

The constraints used in selecting the volume factor are discussed below. This will not be the same for all the fault rock types, owing to differences in their conditions of formation. Representative graphs and the resultant equations for gains and losses of component oxides for the selected volume factor are also reproduced.

Limitations

There are limitations when applying mass balance calculations, both in the techniques and the rocks. Firstly, the density determinations do not take porosity into account, i.e. the presence of microscopic pores or open fractures will return a apparent density which is lower than the true density. Secondly, the complex history of some of the fault rock types means that there may have been several phases of alteration, and it may be impossible to separate the effects of the phases. Those presented below are thought to represent only one phase of

bulk compositional change. The method also relies on identification of the correct parent rock to give meaningful results. For the fault rocks considered here, Gray Gneiss is thought to be the parent.

Altered Gray Gneiss The composition-volume diagram for a typical Gray Gneiss-altered Gray Gneiss reaction is presented in figure 6.11. It can be seen that, within the broad range of volume factors of 0.2 to 1.2, there are general clusterings of component oxide lines (where they cut the line of zero gains/losses) around volume factors of 0.4 (Fe_2O_3, MgO, TiO_2 and P_2O_5) and 1.0 (SiO_2, Al_2O_3 and Na_2O). Those oxides with the lower values are present in relatively small quantities, so the volume factor of 1.0 is considered more appropriate. Supporting evidence for choosing this volume factor comes from the textural evidence of thin sections, which suggests that there was no significant volume change (i.e. a volume factor of 1.0) associated with the alteration, as there was no accompanying deformation. Additionally, Al is generally regarded as relatively immobile under such low temperature conditions, and its component oxide line returns a value of 1.0 too.

The balanced equation resulting from using this volume factor is presented in the caption to figure 6.11, and requires the addition of small amounts of iron, magnesium,

sodium, potassium, titanium and fluid (as represented by loss on ignition). It also requires removal of silica, aluminium and calcium. Essentially, the alteration process is making the Gray Gneiss more mafic in composition.

The Altered Microbreccia Figure 6.12 presents the composition-volume diagram for microbreccia derived from Gray Gneiss. As with the altered Gray Gneiss, there seems to be two clusters of component oxide lines. These occur at volume factors of 1.1 and 1.7, within a range of 0.4 to 1.8. From thin section examination, it is known that microbrecciation involves a volume increase (although this may not be fully reflected in the density determinations - see above) and addition of SiO_2 in the form of quartz veining along some of the microfractures.

The volume factor of 1.1 gives more reasonable figures for the quantity of SiO_2 which must be added than does a factor of 1.7, and also allows for the relative immobility of Al. The balanced reaction resulting is given in figure 6.12, and, as expected, gives addition of moderate amounts of silica, although the amount of fluid (as represented by LOI) is not as high as might be expected.

The R-Type Mylonites Looking at the composition-volume diagram for a typical Gray Gneiss/r-type mylonite pair (figure 6.13), it can be seen that all the component oxide

lines cross the gain-loss zero line between volume factors of 0.6 and 1.1, with no significant clustering. This represents a fairly tight range of volume factors when compared to the diagrams for other fault rock/parent pairs, and suggests that little chemical change has occurred during the reaction. This agrees with the thin section mineralogical and textural evidence (section 5.8). The densities of the r-type mylonites (Appendix IV) are slightly greater than those for Gray Gneiss. Since it is thought that these mylonites formed in a compressional environment, conditions might be expected to favour mineral reactions which lead to an increase in density.

Thus, r-type mylonite formation is expected to involve almost no chemical change and a density increase. Taking a volume factor of 1.0 gives a balanced equation (figure 6.13) which minimises chemical change, and allows Al to remain immobile.

The C-Type Mylonites These rocks have much more variable compositions and consequently, the composition-volume plots show more variation. For this reason, two plots are presented, in figures 6.14 and 6.15. The component oxide lines cover a wide range of values, mostly cutting the zero gains/losses line at volume factors of 1.0 or less. Figure 6.14 shows clustering of component oxide lines at volume factors of around 0.5 and 1.0. Figure 6.15 shows no

evidence of clustering, and the component oxide lines are widely scattered.

In selecting volume factors for the calculation of balanced equations for these rocks, there are several problems. From thin section study, it is thought that the chemical changes involved in c-type mylonite formation are more extreme than those producing the other rock types. The c-type mylonites are more mafic in appearance than their parent Gray Gneiss, and contain an abundance of opaque phases, so their formation involved removal of SiO_2 and/or addition of Fe_2O_3 and MgO, so the selected volume factor must lie between the intercepts of these lines with the line of zero gains/losses. Additionally, the thin sections show the presence of many hydrous phases, so the selected volume factor must allow for the addition of fluid. However, this does not narrow the range of possible volume factors by very much.

Field evidence suggests that the c-mylonites formed in an extensional regime. However, because strain was accomodated on the fault planes along which the c-type mylonites were forming, there would have been local compression. This is supported by the increase in density recorded in Appendix IV. It seems likely that a volume decrease occurred during their formation, as the majority of volume factors are less than 1.0. This would provide a

mechanism for an increase in density, but still leaves a wide range of values to choose from. The selection of the volume factor for Al, based on its immobility, is probably not valid, as there has been break-down of feldspar during c-type mylonite formation.

This leaves a range of possible volume factors of 0.6 to 1.0 for both figures 6.14 and 6.15. The balanced equations presented alongside the figures utilise values of 0.9 and 0.8 respectively, in order to minimise chemical changes. Interestingly, selection of any volume factor within the range given above does not greatly affect the balanced equations, other than to change the amounts of silica by a few grams.

In conclusion, there is a volume decrease in c-type mylonite formation, and chemical changes which involve addition of small quantities of Fe_2O_3, MgO, K_2O, TiO_2 and LOI, and removal of large quantities of SiO_2 and small amounts of Al_{2o3} and Na_2O.

Summary and Discussion The mass balance calculations have shown that most of the variations in bulk chemistry described in section 6.3 can be regarded as real. The assumption of Al_2O_3 as immobile appears to be justified for all rock types except the c-type mylonites, whilst SiO_2 is seen to be the most mobile component, followed by

Fe_2O_3.

Alteration unaccompanied by deformation, as in the altered Gray Gneiss, seems to be an isovolumetric process. The chemical changes are similar to those seen for the c-type mylonites, suggesting that perhaps the sample of altered Gray Gneiss came from adjacent to a c-type mylonite band.

The essentially dilational altered microbreccias show a volume increase, which is to be expected in view of their microfracturing. The r-type mylonites are isovolumetric and involve very little chemical change. The c-type mylonites show large volume decreases, and the most striking changes in bulk chemistry. The presence of a fluid phase is unquestionnable, as the changes in bulk chemistry correlate well with the calculated and measured values for loss on ignition. It seems as if the fluid phase acted as a transport medium, carrying component oxides between the microbreccias and the c-type mylonites.

The possibility has been raised that the difference in composition of the c-type mylonites when compared to the Gray Gneiss is due to derivation from bands of more basic rocks. This is thought improbable on several counts. Any such band would have to run across all the pre-existing structures in the area, hence it is improbable that it

could have been a Scourian or Laxfordian feature. The trend of the fault zone is such that it is unlikely to represent failure along a Tertiary dyke, which trend more-or-less perpendicular to the c-type mylonite bands.

Furthermore, in at least one locality there are Tertiary intrusives injected up the fault planes, and, though it is difficult to be certain of their exact relationship to each other, the Tertiary intrusives certainly post-date c-type mylonite formation. Modelling the generation of c-type mylonites from more basic gneiss results in extremely small values for the volume factors, and necessitates moving around large quantities of most component oxides.

There is one other possibility to explain the variation in composition of the c-type mylonites and the altered microbreccias from the Gray Gneiss. From the mass balance calculations presented in section 6.5, it can be seen that small amounts of Fe, Mg and other elements are 'left over' after formation of the altered microbreccias from Gray Gneiss. These elements correspond broadly to those which must be added to the Gray Gneiss to result in c-type mylonite. It therefore seems plausible that some sort of exchange has occurred between the altered microbreccias and the c-type mylonites during their formation.

This is considered improbable for two reasons. Firstly, the ratios of the excess elements is incompatible with this idea. Secondly, it is hard to envisage a driving force for deriving such different rock types from a common parent at low temperatures and pressures. In addition, since the data for the altered microbreccias have been obtained from the density as measured from one sample, it does not seem wise to place too much emphasis on the results.

The balanced equations for c-type mylonites require addition of Fe and Mg, and removal of silica. Those for altered microbreccias require addition of silica. It seems from this, and also from field relations, that transport of silica occurred from the forming c-type mylonites into the fracture system of the microbreccias, by means of solution in a warm, predominantly aqueous fluid phase and subsequent precipitation. It is also suggested that the same fluid introduced the Fe and Mg into the c-type mylonites during their formation. Such a fluid could have come from a magmatic source - this idea is discussed more fully in section 6.6. Discrepancies in the relative abundances of c-type mylonite and altered microbreccia can be explained as the change in bulk chemistry is more extreme in the scarcer c-type mylonites than it is in the volumetrically more significant altered microbreccias.

6.6 Temperature, Quantity and Composition of the Fluid Phase

From the results of the mass balance calculations, the presence of a fluid phase passing through the fault rocks and causing changes in the bulk chemistry is indisputable. This section proposes to investigate the nature and properties of this fluid in more detail. Obviously, as there are so many 'unknowns' involved, the calculations presented are very approximate, but it was felt that they were still worth including, to give a rough idea of the quantities of fluid involved.

Fluid Temperature The fluid can be assumed to have been an aqueous based phase, as the reactions that occur during the formation of the fault rocks mostly involve hydration. For this reason also, fluids can be assumed to have been absent from the r-type mylonites, as they show no significant change in mineral assemblage and will not be discussed further here. This implies that the fluid was absent during the early deep-level phases of deformation, and only became available in quantity later in the evolution of the fault zone. At this time, upper crustal conditions would have prevailed, i.e. relatively low temperatures and pressures.

The major problem lies in the origins of the fluid. One

possibility is that it came from within the Gray Gneiss itself. This is considered to be unlikely, as the fluid content of the Gray Gneiss is relatively low, suggesting that it would be difficult to generate the required amount of fluid *in situ*. A further line of evidence for external derivation lies in the mass balance calculations, which point towards addition of certain elements into the c-type mylonites, indicating a source from outside the rocks themselves.

Starting with the assumption of an externally derived aqueous fluid, bearing no impurities in the simplest case, it is introduced into the contemporaneously-forming fractures in the Gray Gneiss microbreccias. Initially, the fluids permeate through the most continuous fractures, or along the most strongly deformed or brecciated zones. As deformation continues with the ingress of the fluid, bands of c-type mylonite begin to form. The continuing deformation causes further grain size reduction, which simultaneously promotes the growth of alteration products and neo-mineralisation.

The temperature of the Gray Gneiss is presumably fairly low at this time, as the deformation is brittle. Formation of the microbreccia fracture system has been inferred to have taken place at high crustal levels under conditions of shallow overburden (see chapter 7), say, around 5 km

deep. Assuming a geothermal gradient of 23 C/km (see Shankland and Anders (1983), writing about the Basin and Range Province) then temperatures would have been in the region of 115 degrees. This depth corresponds to a pressure of around 2.5 kb.

Attempts were made to find a geothermometer that can be applied to the c-mylonite assemblage, to try to pin down the temperature of formation. Unfortunately, this was not possible for several reasons. Firstly, no minerals were present without the wide pressure-temperature stability range already mentioned - all occupy approximately the same area in P-T space.

Secondly, as ilmenite is an abundant phase in many of the c-mylonites, it was hoped to use the magnetite-ilmenite geothermometer, but magnetite is extremely rare. Thirdly, no characteristic amphiboles are developed within the c-type mylonites - at middle-upper greenschist facies, the development of actinolitic amphiboles might be expected, but as these are absent, all that can be said is that the rocks were formed at temperatures below this. The amphiboles that do occur in the c-type mylonites are partially altered remnants of those from the Gray Gneiss. Finally, there is no evidence to suggest that these mylonites reached equilibrium with the fluids.

The assemblages generated within the c-type mylonite bands extend up to lower greenschist facies, and nearly all of the minerals have a wide pressure-temperature stability field. The typical assemblage comprises (in no particular order) relict alkali feldspar, plagioclase, quartz, hornblende, biotite, and new sericite, apatite, chlorite, epidote, ilmenite, TiO_2 (as rutile, anatase or brookite), magnetite, sphene, iron sulphide, iron oxide and iron hydroxide. Thus we have microbreccia formation at around 115 degrees centigrade and 2.5 kbars, and c-type mylonite formation at around 250-350 degrees C and similar pressures. If this temperature discrepancy is real, then the fluid phase has to be warmer than the microbreccias, and to come from deeper crustal levels or from a magma system, or both. In any case, it is unlikely to be a pure phase.

A further line of evidence in support of the existence of a temperature difference lies in the fact that SiO_2 has been removed from the c-type mylonites and added to the altered microbreccias. Quartz is most soluble at higher temperatures and pressures; as there is no evidence that any great pressure difference exists across the fault zone, it is likely that temperature is the dominant control. Thus the fluid has passed through the c-type mylonite bands dissolving silica, to cool and redeposit it

in the altered microbreccias.

The possibility exists that fluids played a greater part in the formation of the fault rocks. An increase in fluid pressure could cause brittle deformation in a previously plastic regime, leading to brecciation. Depressurization would result, and precipitation of silica from pore fluids could then result. This is thought to be unlikely, as microbreccia formation appears to have been relatively anhydrous. Furthermore, this would not explain the large chemical changes that occur during c-type mylonite formation.

Fluid Quantities In a system as complex as the Outer Hebrides Fault Zone, any calculations of fluid flow will be very approximate, as has already been stated, so to some extent the starting parameters for such calculations are academic. However, to keep things simple, the initial calculations of quantity will be made on the basis that the fluid contains no impurities, it will be calculated both for a fluid at the same temperature as the Gray Gneiss and for a fluid capable of causing lower greenschist facies alteration.

The assumptions made in making the calculations were as follows:

a) The most important assumption is that the fluid

reaches saturation with respect to SiO_2. This is unlikely to be so in reality, therefore the figures calculated for fluid quantities will be minimums.

b) The fluid was a relatively pure phase when it was introduced into the microbreccias. This assumption is probably not correct on several counts:

(1) The fluid has almost certainly brought elements such as Fe and Mg, in some form, in with it and added these to the c-type mylonites. It has been shown that the solubility of SiO_2 in aqueous solutions is virtually independent of the concentration of dissolved salts (Siever (1962), Greenberg and Price (1957), and Krauskopf (1956)), so this need not be of great concern.

(2) The fluid may also contain other dissolved elements, such as sulphides or chlorides in various forms, which may affect its pH. This is highly likely as many of the c-type mylonites and altered microbreccias contain pyritic or chlorine-bearing phases. However, Alexander et al. (1954) have shown that the solubility of silica appears to be essentially independent of the pH of aqueous solutions for most of the range of geological interest.

(3) The fluid may already contain some quartz in solution on its' introduction to the c-type mylonites. If this is the case then obviously it will be less able to dissolve SiO_2 from the fault zone, making the calculated figures too small. It is unlikely that the incoming fluids

contained much dissolved silica, as then an equilibrium might have been reached, where precipitation and dissolution would have balanced. This is clearly not the case as so much silica has been removed from the c-type mylonites.

c) The depth (and hence pressure - 5 km and 2.5 kb respectively) of microbreccia formation has been inferred correctly. This will have little effect on the calculations, as it is only above 350-400 C that the solubility of quartz becomes strongly pressure sensitive. An error in estimating depth of brecciation will not, therefore, have much effect on the computed figures.

d) The temperatures used in the calculations (115 and 300 C) are in the right region.

e) The average loss of silica from the reaction Gray Gneiss microbreccia --> c-type mylonite is correct. From the mass balance calculations, it is known that the average c-type mylonite loses 16 g of SiO_2 per 100 g (160 g per 1 kg) of starting composition.

Assuming a temperature of 115 C, and a pressure of 2.5 kb, the value for solubility of quartz is 0.06 g/l (from data presented by Holland and Malinin, 1979). This yields a value of 2666 litres of fluid to remove the necessary

quantity of silica from one kilogram of rock. From the same data source, the solubility of quartz at 300 C (a convenient 'midway' figure for lower greenschist facies) and 2.5 kb is around 12 g/l, giving a value of 13 litres/kg rock.

These values for fluid quantities are minimum estimates, as mentioned above, on the assumption that the fluids are saturated with respect to quartz. Fournier and Rowe (1966) have shown that above 180 C, geothermal waters are saturated with respect to silica, but there is no evidence here to suggest that the fluids in this case were necessarily in equilibrium with quartz.

From the above calculations, the 300 C figure is preferred for several reasons: The available field and microscope evidence suggests that the fluid was at a higher temperature than the microbreccias, and it is obviously less of a problem to move the smaller amount of fluid required at this temperature through the rock. For a rough 'guesstimate' of fluid quantities involved, the minimum volume of fluid that must pass through is equal to thirty-five times the rock volume.

The remaining problem from the calculations is how to move this quantity of fluid through the rock. A temperature gradient would have existed, which would have

provided a driving mechanism. However, an additional mechanism, given that the fluid was contemporaneous with the deformation, is one of seismic pumping. The extensional environment giving rise to the c-type mylonites would have been accompanied by large amounts of seismic activity, as it was at high crustal levels. Because of the undulose character of the fault planes, this would have created an environment of alternating dilatational and compressional regions, so seismic pumping seems a likely mechanism.

Composition and Source of the Fluids From the compositional and mineralogical changes observed in the fault rocks, it can be inferred that the fluid is dominantly H_2O, containing sulphides, chlorides and iron and magnesium salts, together with lesser amounts of phosphorous, calcium and titanium.

The problem remains concerning the origin of the fluid. In view of the type of dissolved elements that must have been present, it seems probable that the fluids were derived from a basic magmatic source. The presence of Tertiary dykes intruded up the fault zone in several places suggests that there may be some connection between the two. The intrusions themselves are not deformed to any great degree, as far as can be ascertained from their inaccessible exposure, although they do appear to be

altered. This suggests that they were intruded at a late stage, after most of the tectonism had ceased, but whilst circulation of magmatic fluids was still strong. It is therefore hypothesised that Tertiary magmatic fluids may have been responsible for causing the lower greenschist facies alteration within the c-type mylonites. The deformation environment during the Tertiary was one of extension, with Atlantic rifting beginning, so this would fit with the normal senses-of-shear observed in the c-type mylonites.

In bringing about this alteration, the fluids have precipitated amounts of dissolved Fe, Mg, S, P, Cl, Ca and Ti, many of which became incorporated into new minerals within the c-type mylonites. Most of these new minerals present no strong preferred orientation, suggesting that they may have formed post- tectonically. The older, altered minerals do tend to possess a grain shape preferred orientation, suggesting that they deformed as they were being altered. Thus it appears that the fluid was present both syn- and post-tectonically.

The excess fluids passing into the c-type mylonite bands, whilst depositing the elements mentioned above, dissolved appreciable quantities of silica, with minor amounts of K_2O and Na_2O. This ties in well with thin section and microprobe evidence of feldspar breakdown. The

fluid then passed into the fracture systems in the microbreccias, depositing the dissolved SiO_2 and the alkalis as it cooled into the fractures, effectively sealing them. This gives rise to the more cohesive nature observed in the altered microbreccias, with rhombohedral blocks of rock cemented together by thin veins of quartz, and occasionally feldspar.

There is one other possibility to explain the variation in composition of the c-type mylonites and the altered microbreccias from the Gray Gneiss. From the mass balance calculations presented in section 6.5, it can be seen that small amounts of Fe, Mg and other elements are 'left over' after formation of the altered microbreccias from Gray Gneiss. These elements correspond broadly to those which must be added to the Gray Gneiss to result in c-type mylonite. It therefore seems plausible that some sort of exchange has occurred between the altered microbreccias and the c-type mylonites during their formation.

This is considered improbable for two reasons. Firstly, the ratios of the excess elements is incompatible with this idea. Secondly, it is hard to envisage a driving force for deriving such different rock types from a common parent at low temperatures and pressures. In addition, since the data for the altered microbreccias have been obtained from the density as measured from one sample, it

does not seem wise to place too much emphasis on the results.

Summary The microbreccias formed from the Gray Gneiss during cataclasis in a compressional regime. Some time after this, and still under the same conditions of low overburden, the deformation environment changed to one of extension. At around the same time, a hot fluid (c. 300 C) became available, probably associated with a basic magma on the basis of the impurities contained within it. The fluid and magma may have been Tertiary in age, as an extensional deformation environment existed at this time, and Tertiary magmatism was present in the area.

The fluids passed up the fractures in the rock as deformation continued, giving rise to the c-type mylonites by hydration reactions and depositing their impurities. Deformation began to be localised into the mylonite bands, as they became a weak, easily deformable material: Old minerals retrogressed and altered, and completely new ones began to form, due to the deposition of the impurities and the changing bulk chemistry. Simultaneously, the fluids were dissolving out silica and breaking down feldspar, weakening the c-type mylonites still further and leaving them with the bulk composition now observed. This process reached the stage now seen after the passage of a minimum fluid volume to rock ratio of 35:1.

The fluid that passed through the c-type mylonites then passed into the microbreccias, causing wisespread alteration. The fluids were cooling by this time, and began to redeposit the dissolved silica, along with minor amounts of Na in fractures within the breccias.

The apparently high mobility of all elements in certain of the fault rocks, in particular the c-type mylonites, is an important feature. It must influence isotope ratios, and hence casts some doubt on the validity of the K-Ar radio-isotopic dating that has been done on the fault rocks (Sibson, 1977 b). In addition, it suggests that further dating programmes utilising other isotopic systems (e.g. Rb-Sr) are probably not worthwhile.

6.7 Amphibole Compositions

The compositions of amphiboles from a selection of rock types were determined by electron microprobe energy dispersive analysis, using a JEOL 733 Superprobe. The results are given in Appendix II. Insufficient analyses were done to allow detailed interpretation. Graphs of $Mg/(Mg + Fe^{2+})$ v. Si were plotted for fault rocks of both Corodale Gneiss (figure 6.16) and Gray Gneiss (figure 6.17) derivation. Nomenclature is after Leake (1978). No analyses for c-type mylonites have been included, as the

amphiboles in these are relict from the parent Gray Gneiss and have undergone alteration.

Analyses from Corodale Gneiss, Corodale Gneiss derived-microbreccia and amphibolitic Corodale Gneiss showed the majority of the amphiboles to be calcic and to occupy a wide range of compositions. They are actinolites, actinolitic hornblendes, magnesio-hornblendes, tschermakitic hornblendes, ferroan pargasites and magnesian hastingsites. Additionally, scarcer Fe-Mg-Mn amphiboles (cummingtonites) and sodic-calcic amphiboles (ferro-richterite) were found; these are not considered further.

It can be seen from figure 6.16 that calcic amphiboles from Corodale Gneiss amphibolites have higher $Mg/(Mg + Fe^{2+})$ ratios than those from the more typical Corodale Gneiss. The Corodale Gneiss itself contains amphiboles of types I, II and III (as defined on figure 6.16). The Corodale Gneiss-derived microbreccias only contain types I and II, but this probably reflects lack of data rather than any significant variation. The amphiboles from the microbreccias plot in similar areas to those of the same type from the Corodale Gneiss, although they do seem to have slightly higher $Mg/(Mg + Fe^{2+})$ ratios. Type I amphiboles from all three rock types plot coincidentally, although those from the Corodale Gneiss show a wider

range, though this may reflect the more numerous analyses.

A similar graph is presented for rocks of Gray Gneiss derivation (figure 6.17). These were Gray Gneiss, altered Gray Gneiss, microbreccia, altered microbreccia and r-type mylonite. Almost all amphiboles analysed were calcic, and they cover a more restricted range than those for the Corodale suite, comprising magnesio-hornblende, edenitic hornblende, ferroan pargasitic hornblende, ferroan pargasite and magnesian-hastingsitic hornblende. Several analyses of Fe-Mg-Mn amphiboles (cummingtonites) were also obtained.

The amphiboles for all rocks of Gray Gneiss derivation do not show any great variation in Si content or Mg/(Mg + Fe) ratio (figure 6.17). The exception to this tight clustering is for some amphiboles from altered microbreccias to tend towards higher values for Si and Mg/(Mg + Fe). In conclusion, microbrecciation, alteration and r-type mylonitisation are all processes which do not seem to affect the composition of the amphiboles in fault rocks of Gray Gneiss derivation. In the case of the first two processes, this is due to temperature and pressure being too low to allow recrystallisation of amphiboles. For r-type mylonitisation, conditions would have allowed recrystallisation. However, formation of r-type mylonites from Gray Gneiss was an essentially isochemical process,

occurring under identical conditions to those forming the Gray Gneiss. Because of this, chemical differences between the amphiboles of Gray Gneiss and r-type mylonites would not be expected.

Figure 6.1

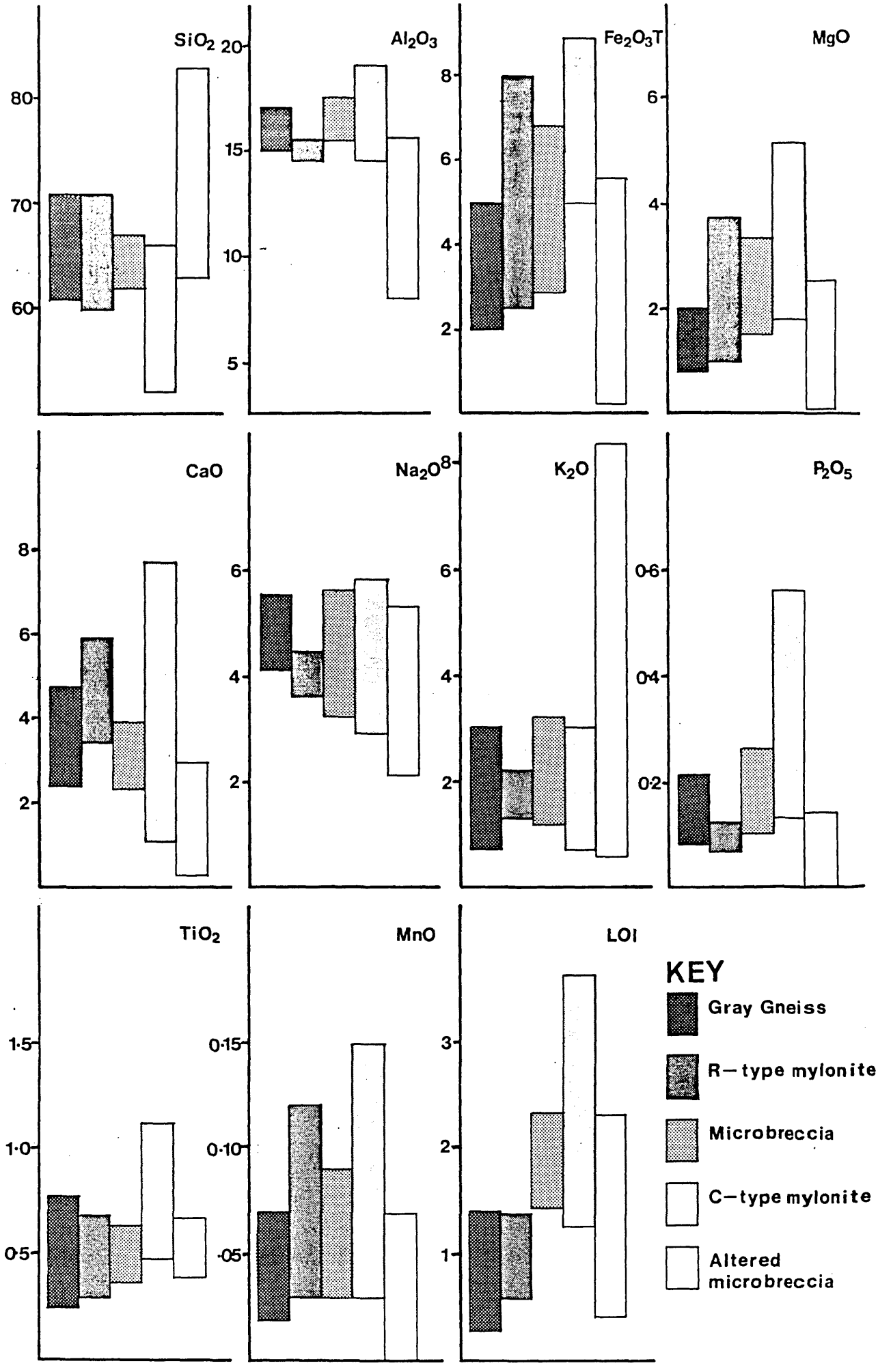
Ranges of composition for selected rock types.

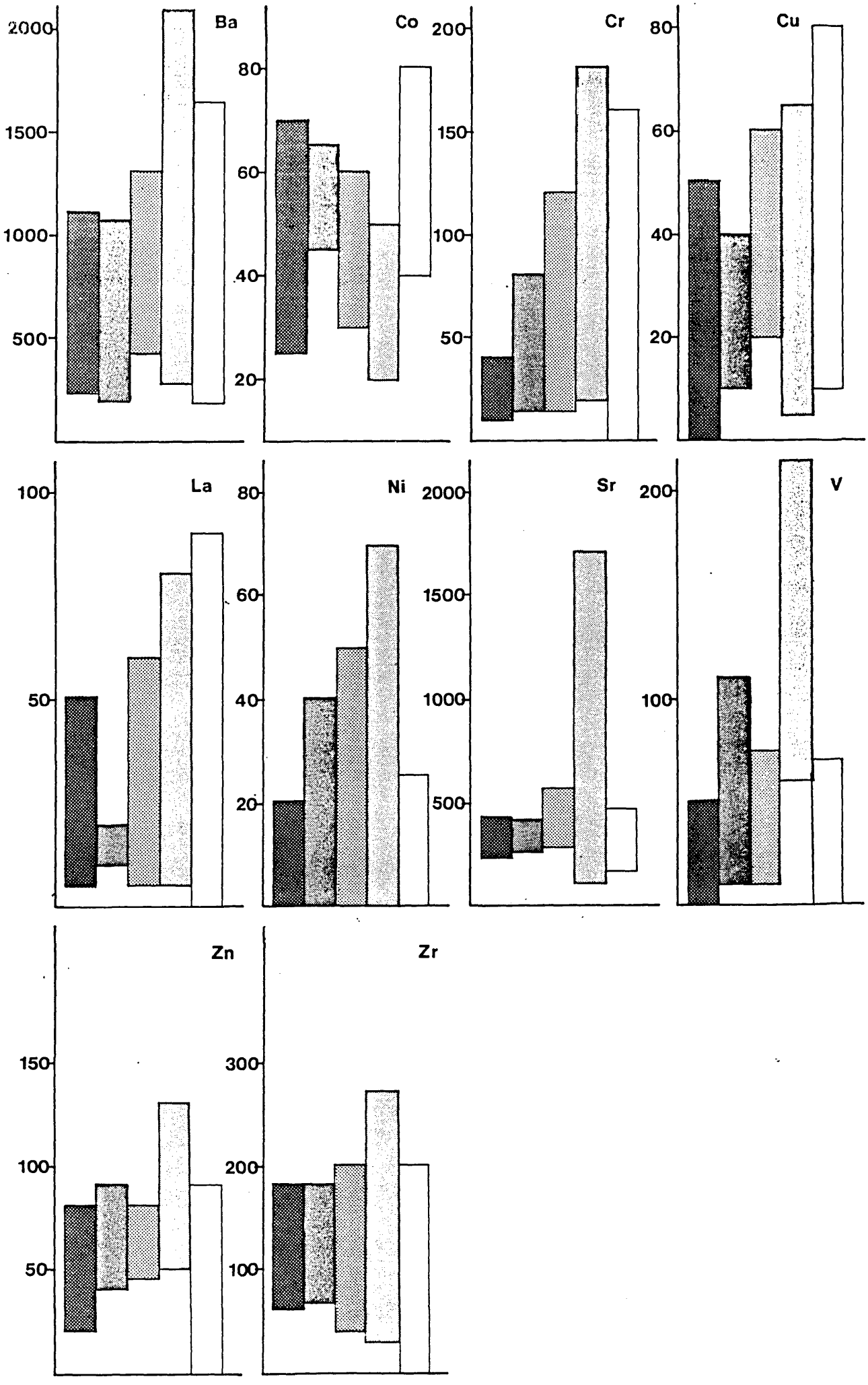
a Major element in weight percent oxide for Gray Gneiss and fault rocks of Gray Gneiss derivation.

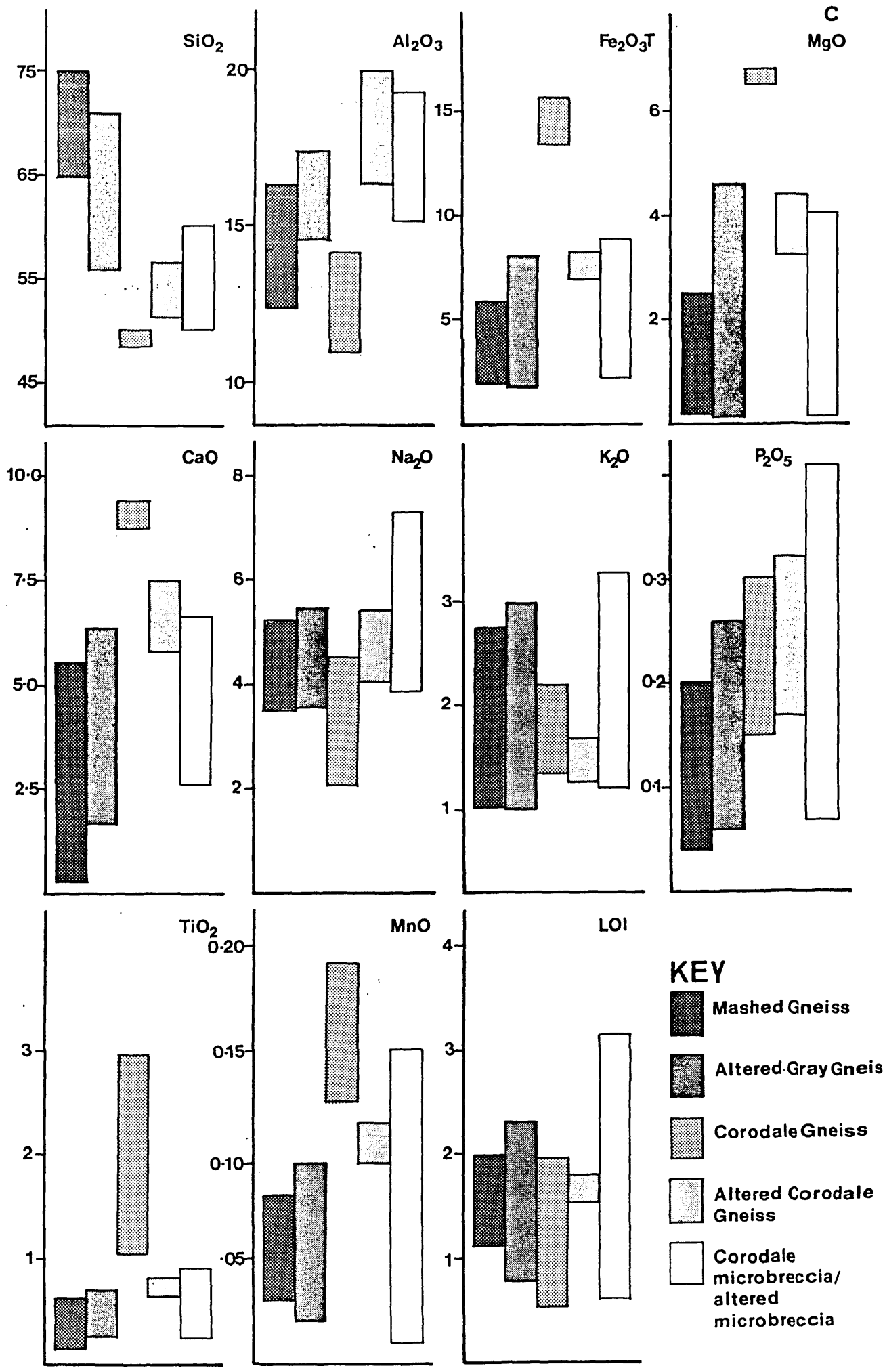
b Trace elements in parts per million for Gray Gneiss and fault rocks of Gray Gneiss derivation.

c Major element in weight percent oxide for Mashed Gneiss, altered Gray Gneiss, Corodale Gneiss and fault rocks of Corodale Gneiss derivation.

d Trace elements in parts per million for Mashed Gneiss, altered Gray Gneiss, Corodale Gneiss and fault rocks of Corodale Gneiss derivation.


SiO2
80
70
60
Al2O3
20
15
10
5
Fe2O3T
8
6
4
2
MgO
6
4
2
CaO
8
6
4
2
Na2O
8
6
4
2
K2O
6
4
2
P2O5
0·6
0·4
0·2
TiO2
1·5
1·0
0·5
MnO
0·15
0·10
·05
LOI
3
2
1
KEY
Gray Gneiss
R—type mylonite
Microbreccia
C—type mylonite
Altered microbreccia


Ba
2000
1500
1000
500
Co
80
60
40
20
Cr
200
150
100
50
Cu
80
60
40
20
La
100
50
Ni
80
60
40
20
Sr
2000
1500
1000
500
V
200
100
Zn
150
100
50
Zr
300
200
100


C
SiO_2
75
65
55
45
Al_2O_3
20
15
10
Fe_2O_3T
15
10
5
MgO
6
4
2
CaO
10·0
7·5
5·0
2·5
Na_2O
8
6
4
2
K_2O
3
2
1
P_2O_5
0·3
0·2
0·1
TiO_2
3
2
1
MnO
0·20
0·15
0·10
·05
LOI
4
3
2
1
KEY
Mashed Gneiss
Altered Gray Gneis
Corodale Gneiss
Altered Corodale Gneiss
Corodale microbreccia/ altered microbreccia

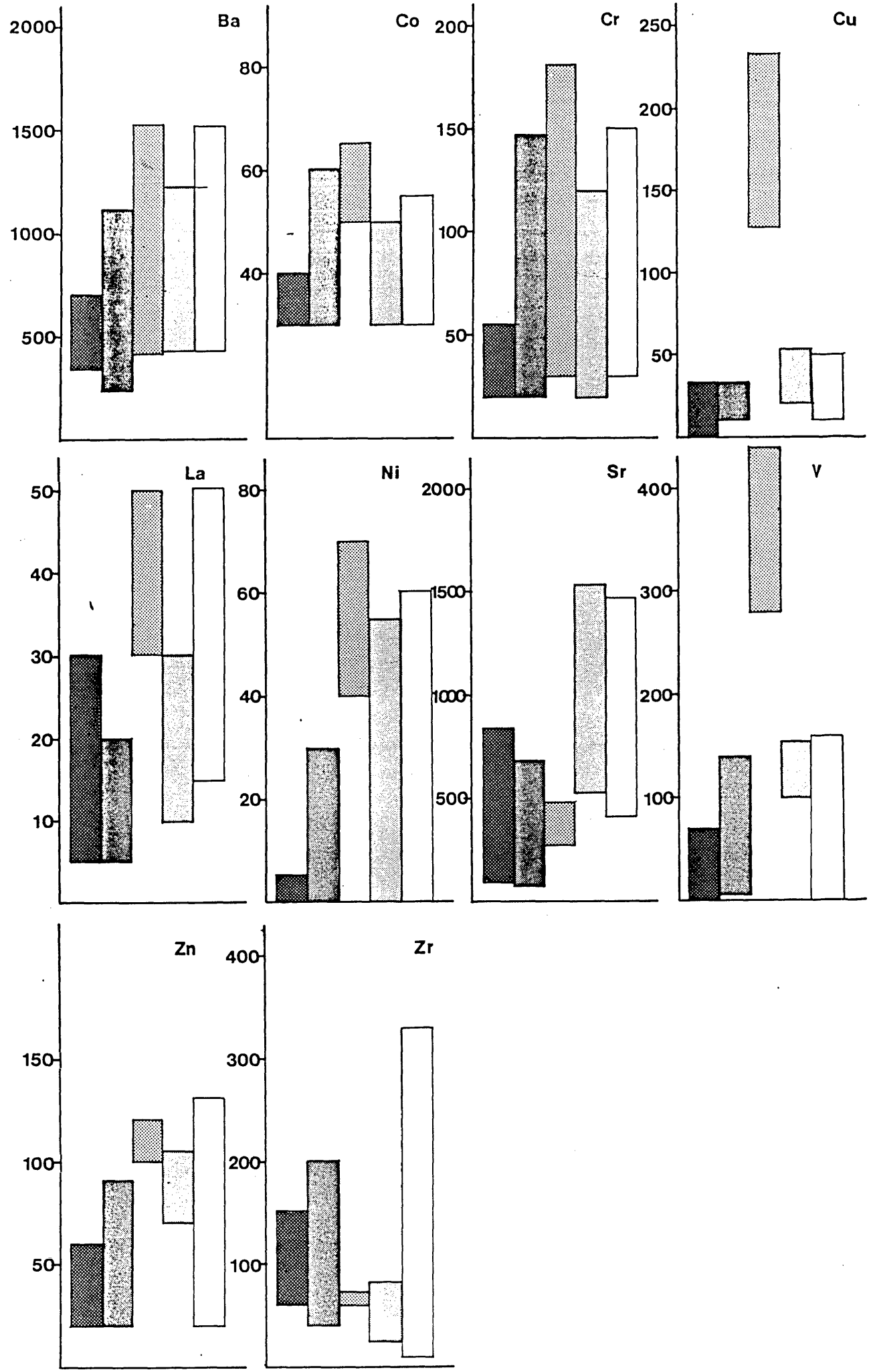

Ba
2000
1500
1000
500
Co
80
60
40
Cr
200
150
100
50
Cu
250
200
150
100
50
La
50
40
30
20
10
Ni
80
60
40
20
2000
1500
1000
500
Sr
400
300
200
100
V
Zn
400
150
100
50
Zr
300
200
100

Figure 6.2

Variation of LOI with SiO_2 for fault rocks of Gray Gneiss derivation. Lines show theoretical dilution trends.

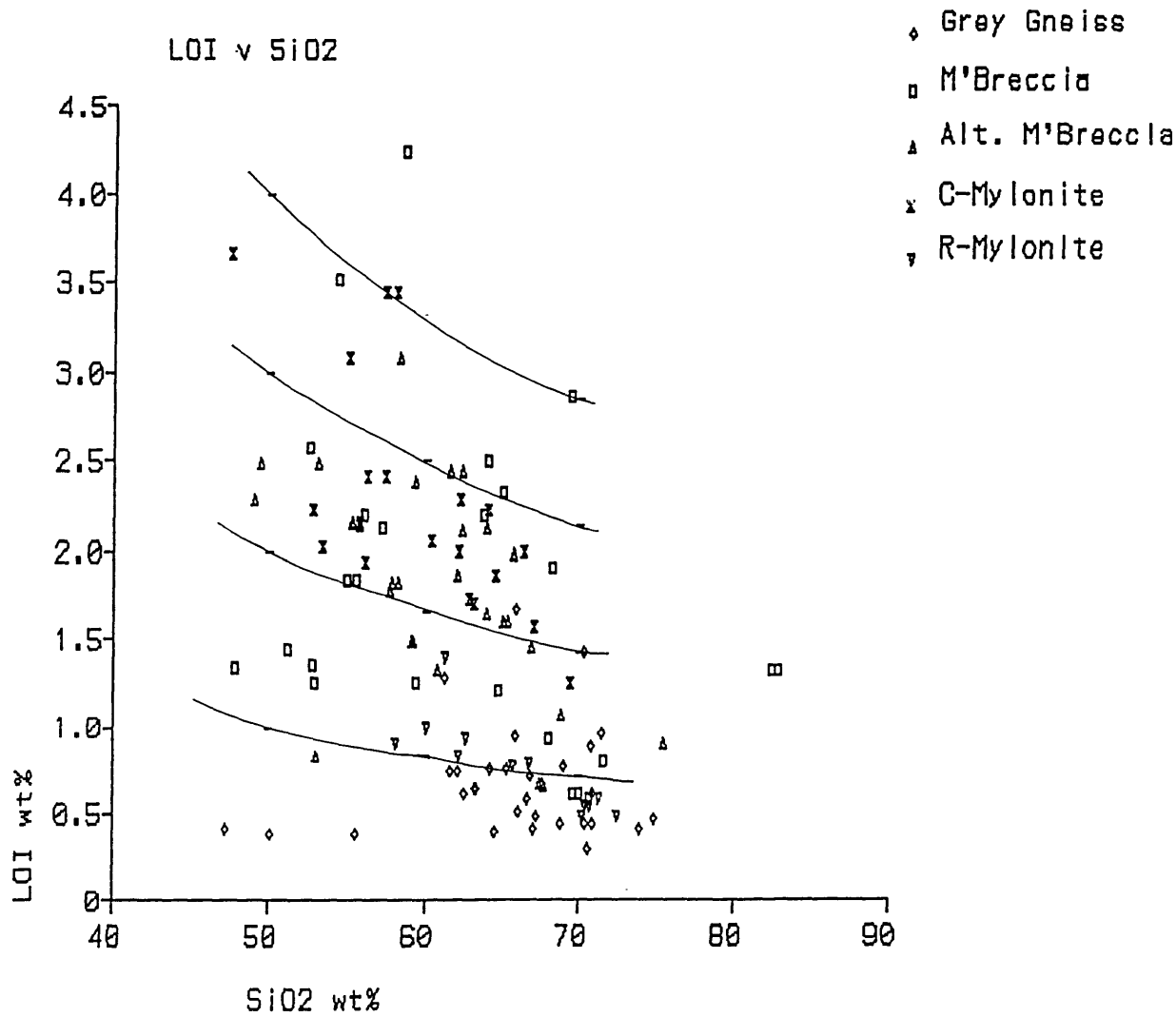

LOI v SiO2
Grey Gneiss
M'Breccia
Alt. M'Breccia
C-Mylonite
R-Mylonite
LOI wt%
SiO2 wt%
4.5
4.0
3.5
3.0
2.5
2.0
1.5
1.0
0.5
0
40
50
60
70
80
90

Figure 6.3

Variation of LOI with Fe_2O_3 T for fault rocks of Gray Gneiss derivation. Lines show theoretical dilution trends.

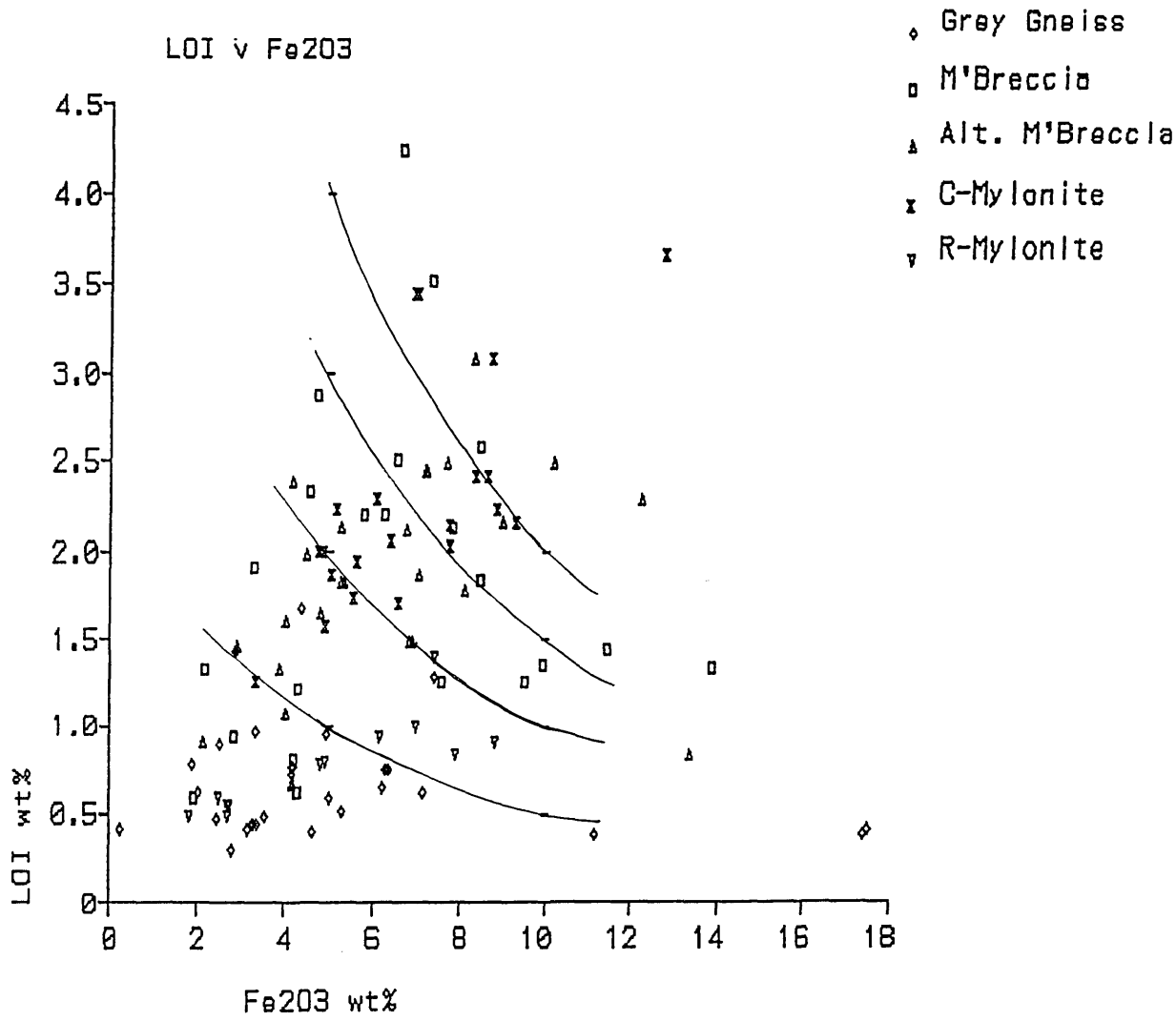

LOI v Fe203
Grey Gneiss
M'Breccia
Alt. M'Breccia
C-Mylonite
R-Mylonite
LOI wt%
Fe203 wt%
0
0.5
1.0
1.5
2.0
2.5
3.0
3.5
4.0
4.5
0
2
4
6
8
10
12
14
16
18

Figure 6.4

Variation of LOI with MgO for fault rocks of Gray Gneiss derivation. Lines show theoretical dilution trends.

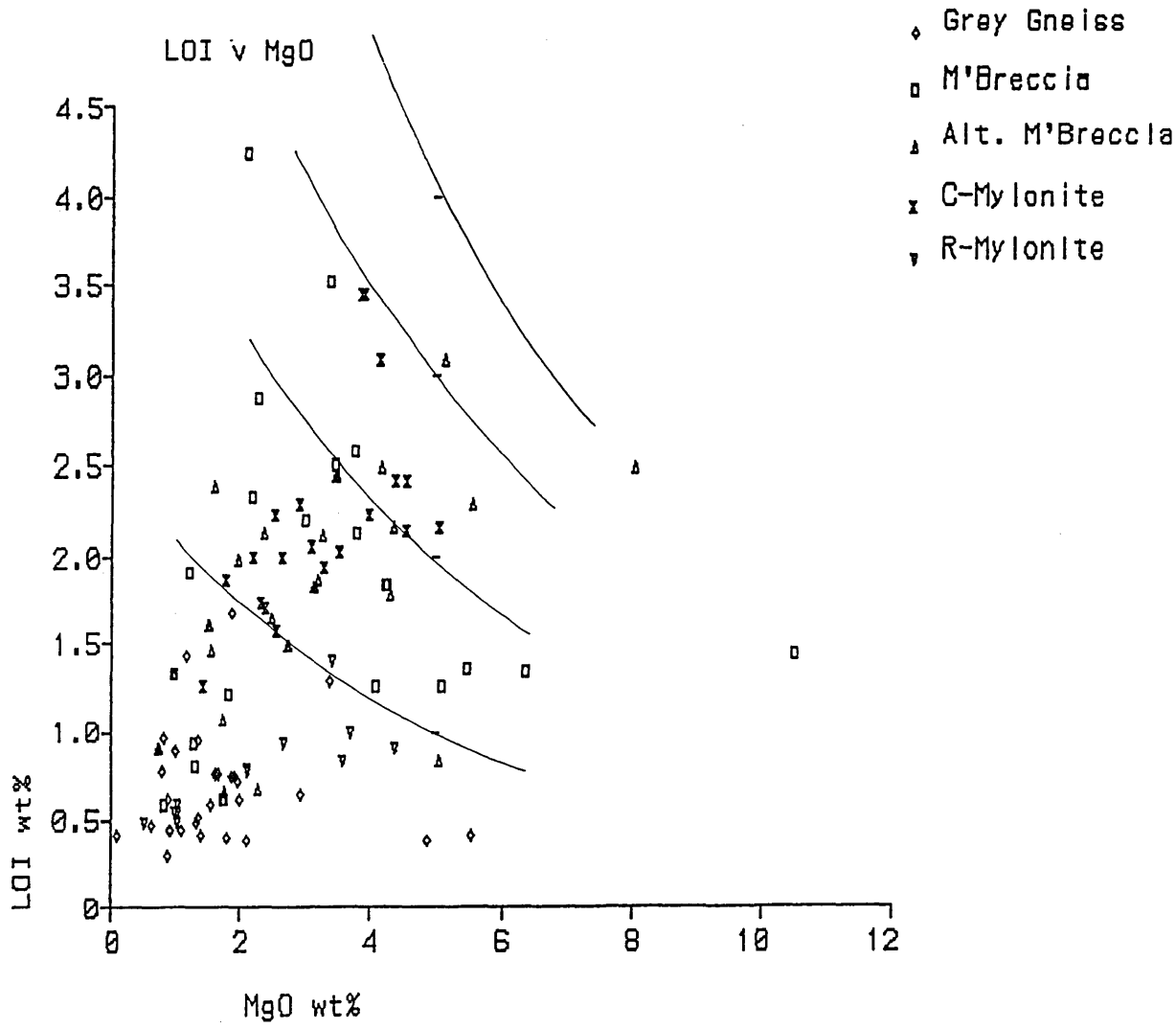

LOI v MgO
Grey Gneiss
M'Breccia
Alt. M'Breccia
C-Mylonite
R-Mylonite
LOI wt%
MgO wt%
0
0.5
1.0
1.5
2.0
2.5
3.0
3.5
4.0
4.5
0
2
4
6
8
10
12

Figure 6.5

Variation of LOI with Al_2O_3 for fault rocks of Gray Gneiss derivation. Lines show theoretical dilution trends.

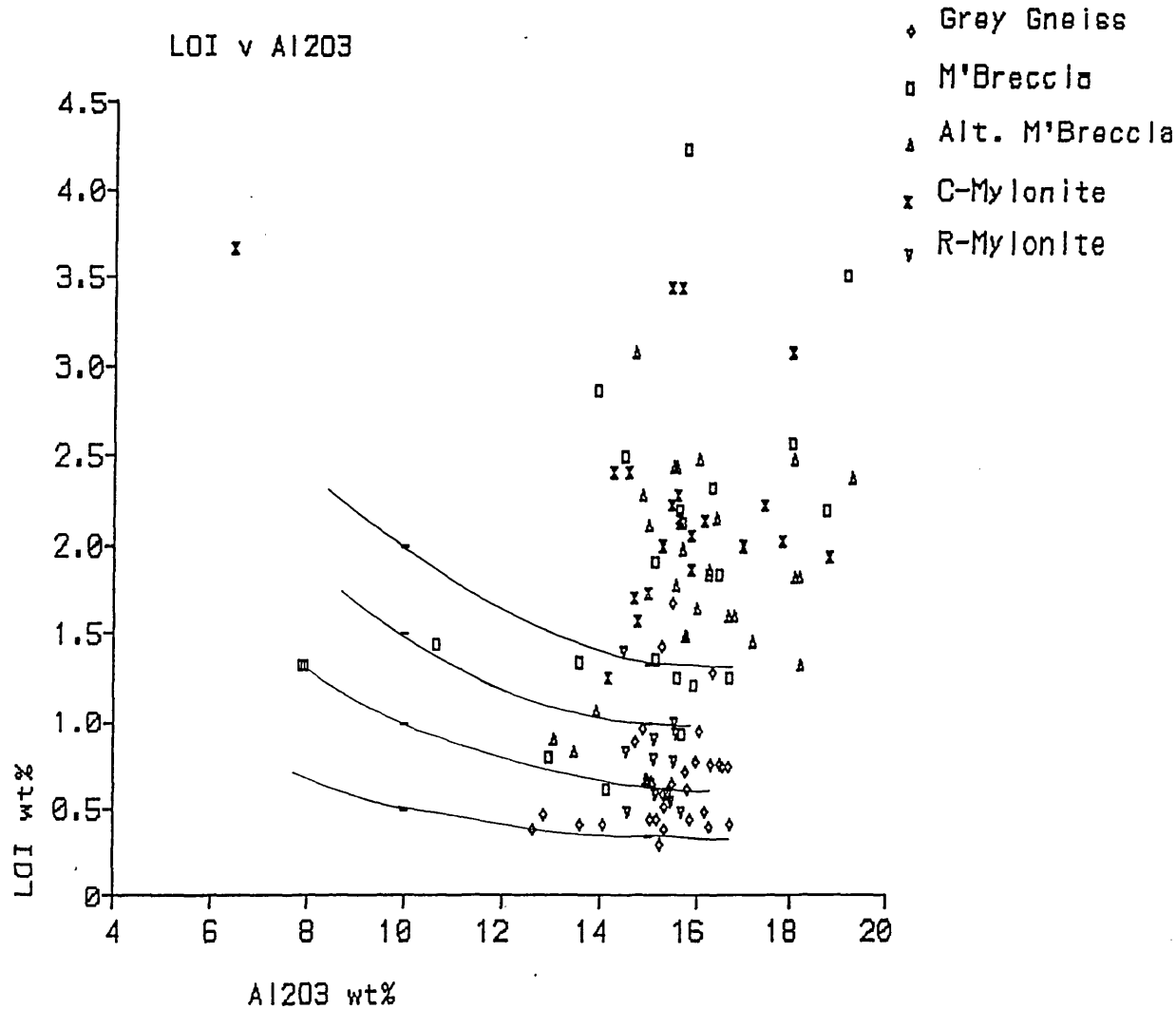

LOI v Al203
Grey Gneiss
M'Breccia
Alt. M'Breccia
C-Mylonite
R-Mylonite
LOI wt%
Al203 wt%
0
0.5
1.0
1.5
2.0
2.5
3.0
3.5
4.0
4.5
4
6
8
10
12
14
16
18
20

Figure 6.6

Variation of Ba with SiO_2 for fault rocks of Gray Gneiss derivation. Lines show theoretical dilution trends.

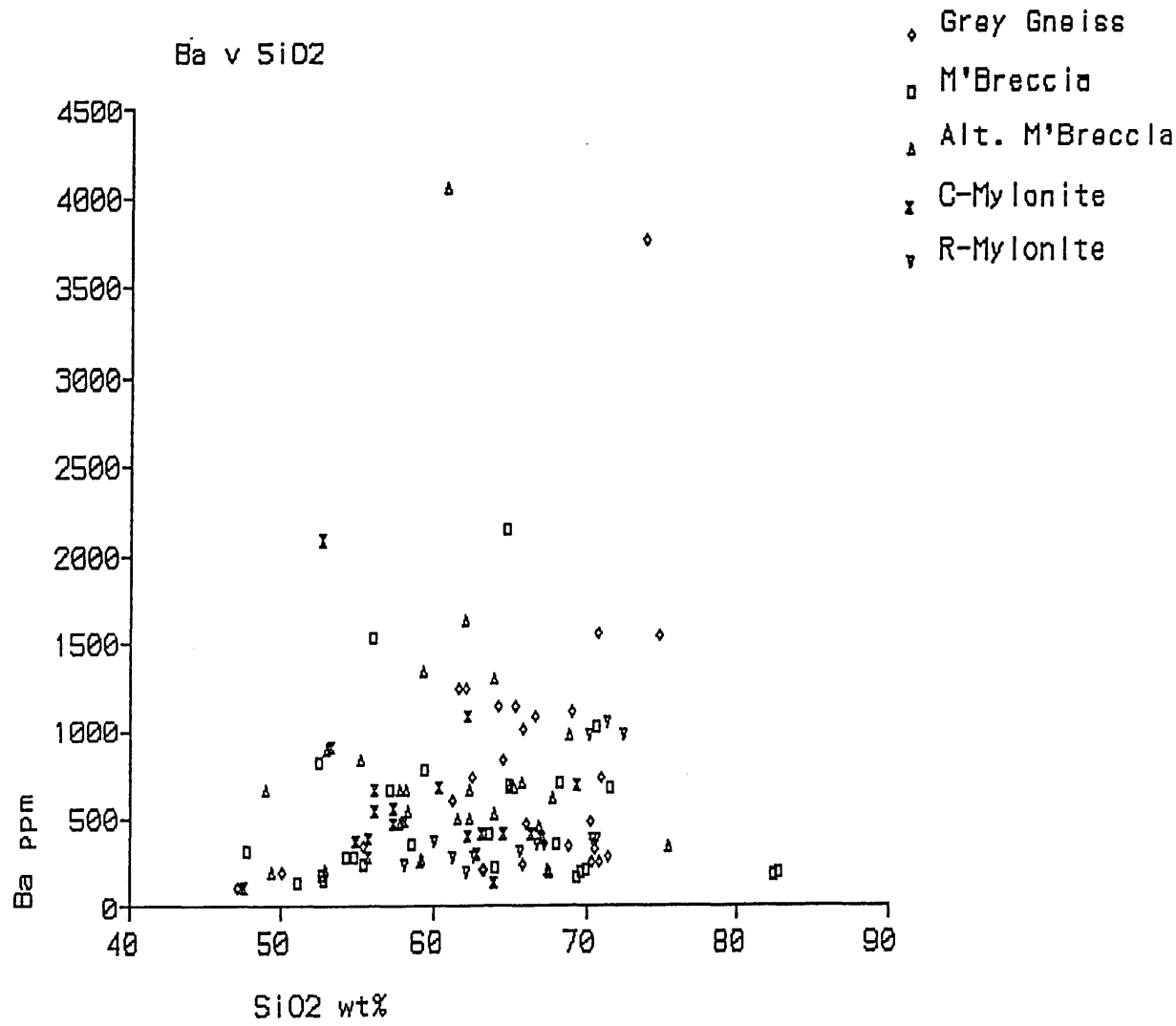

Ba v SiO2
Grey Gneiss
M'Breccia
Alt. M'Breccia
C-Mylonite
R-Mylonite
4500
4000
3500
3000
2500
2000
1500
1000
500
0
Ba ppm
40
50
60
70
80
90
SiO2 wt%

Figure 6.7

Variation of Sr with SiO_2 for fault rocks of Gray Gneiss derivation. Lines show theoretical dilution trends.

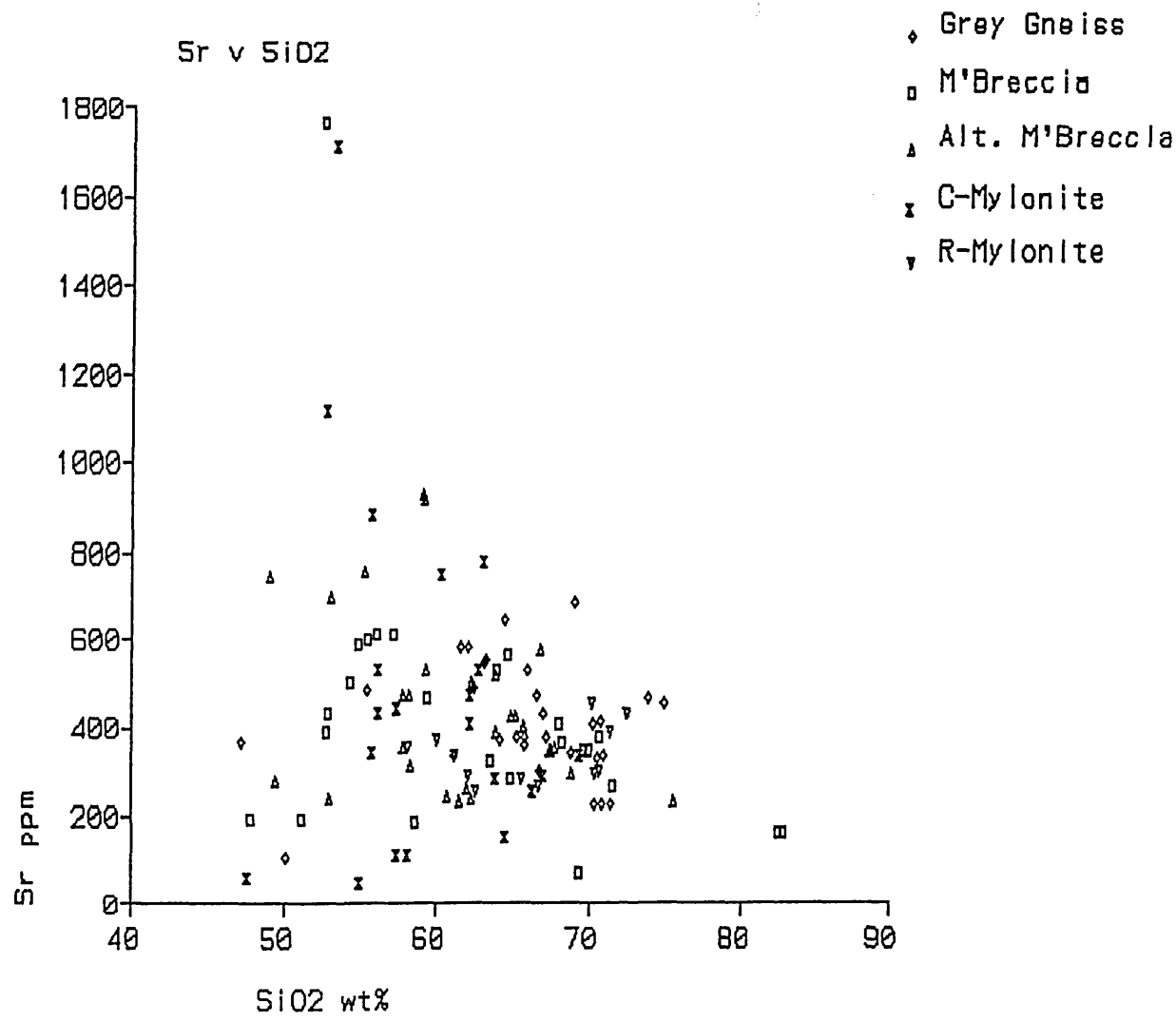

Sr v SiO2
Grey Gneiss
M'Breccia
Alt. M'Breccia
C-Mylonite
R-Mylonite
1800
1600
1400
1200
1000
800
600
400
200
0
Sr ppm
40
50
60
70
80
90
SiO2 wt%

Figure 6.8

Variation of Cr with SiO_2 for fault rocks of Gray Gneiss derivation. Lines show theoretical dilution trends.

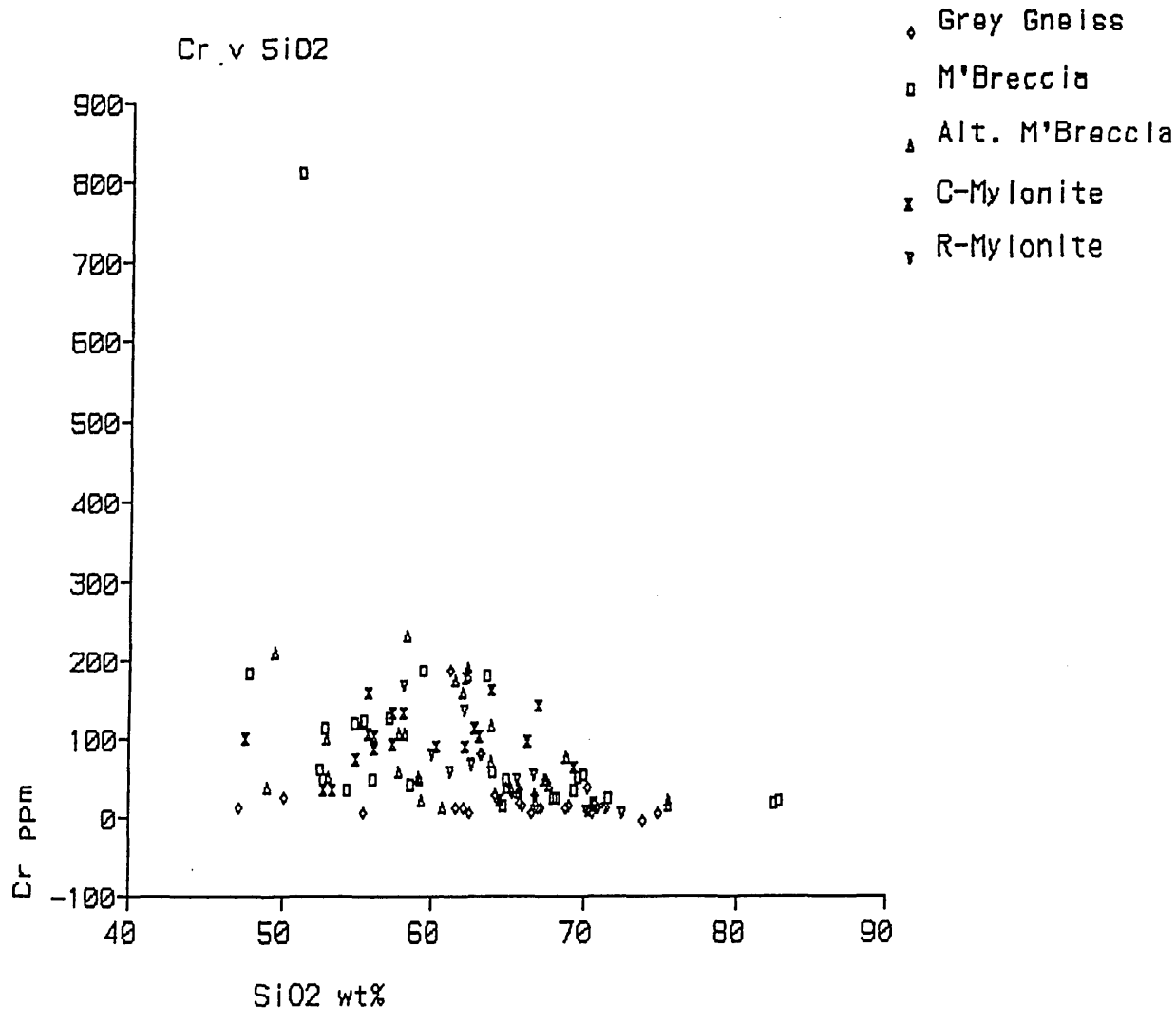
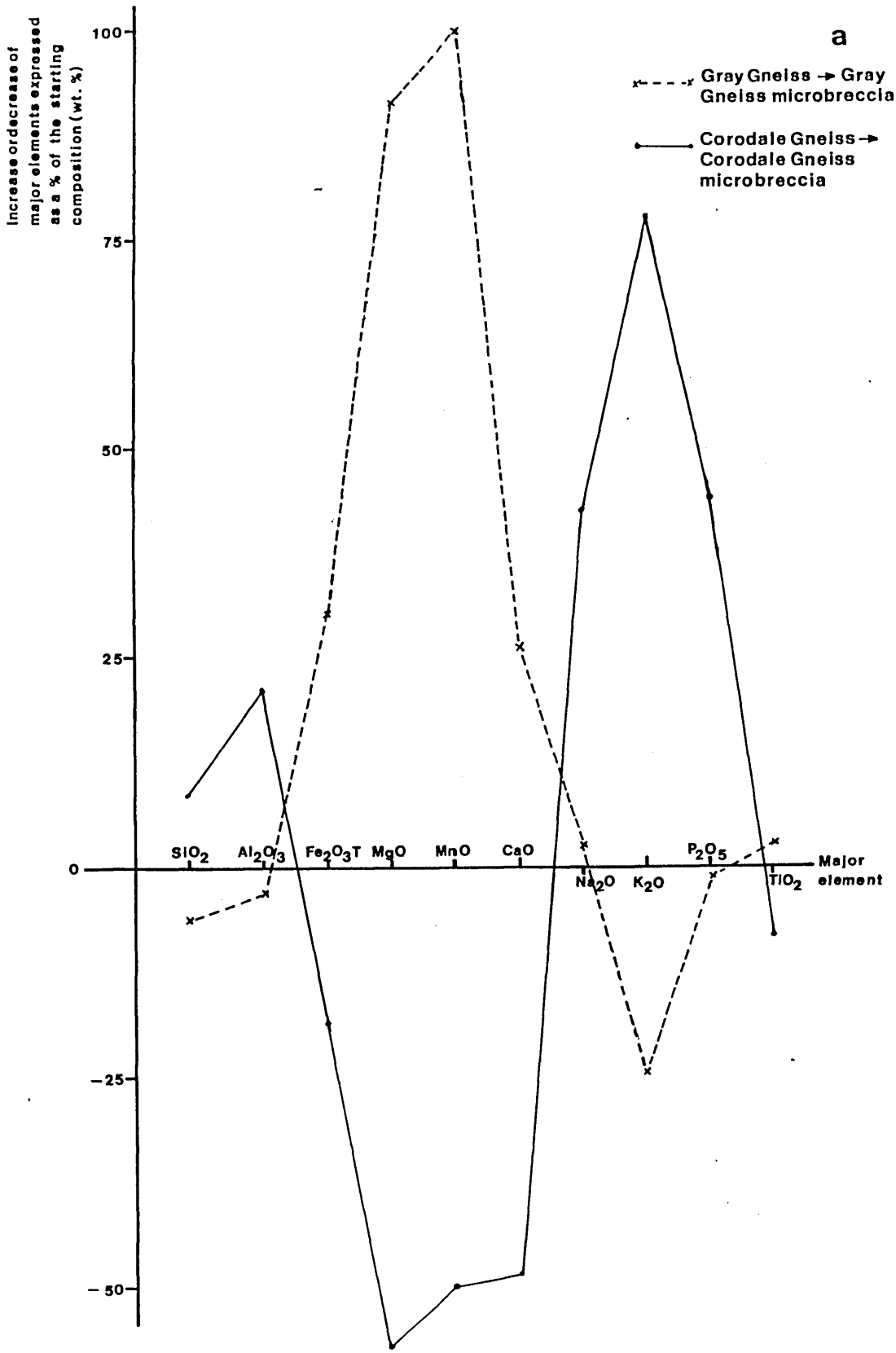

Cr v SiO2
Grey Gneiss
M'Breccia
Alt. M'Breccia
C-Mylonite
R-Mylonite
900
800
700
600
500
400
300
200
100
0
-100
Cr ppm
40
50
60
70
80
90
SiO2 wt%

Figure 6.9

Variation of elements with microbrecciation.

a Variations of major element abundance between microbreccias and their parent rocks.

b Variations of trace element abundance between microbreccias and their parent rocks.


a
Increase or decrease of major elements expressed as a % of the starting composition (wt. %)
100
75
50
25
0
-25
-50
Gray Gneiss → Gray Gneiss microbreccia
Corodale Gneiss → Corodale Gneiss microbreccia
SiO2
Al2O3
Fe2O3T
MgO
MnO
CaO
Na2O
K2O
P2O5
TiO2
Major element

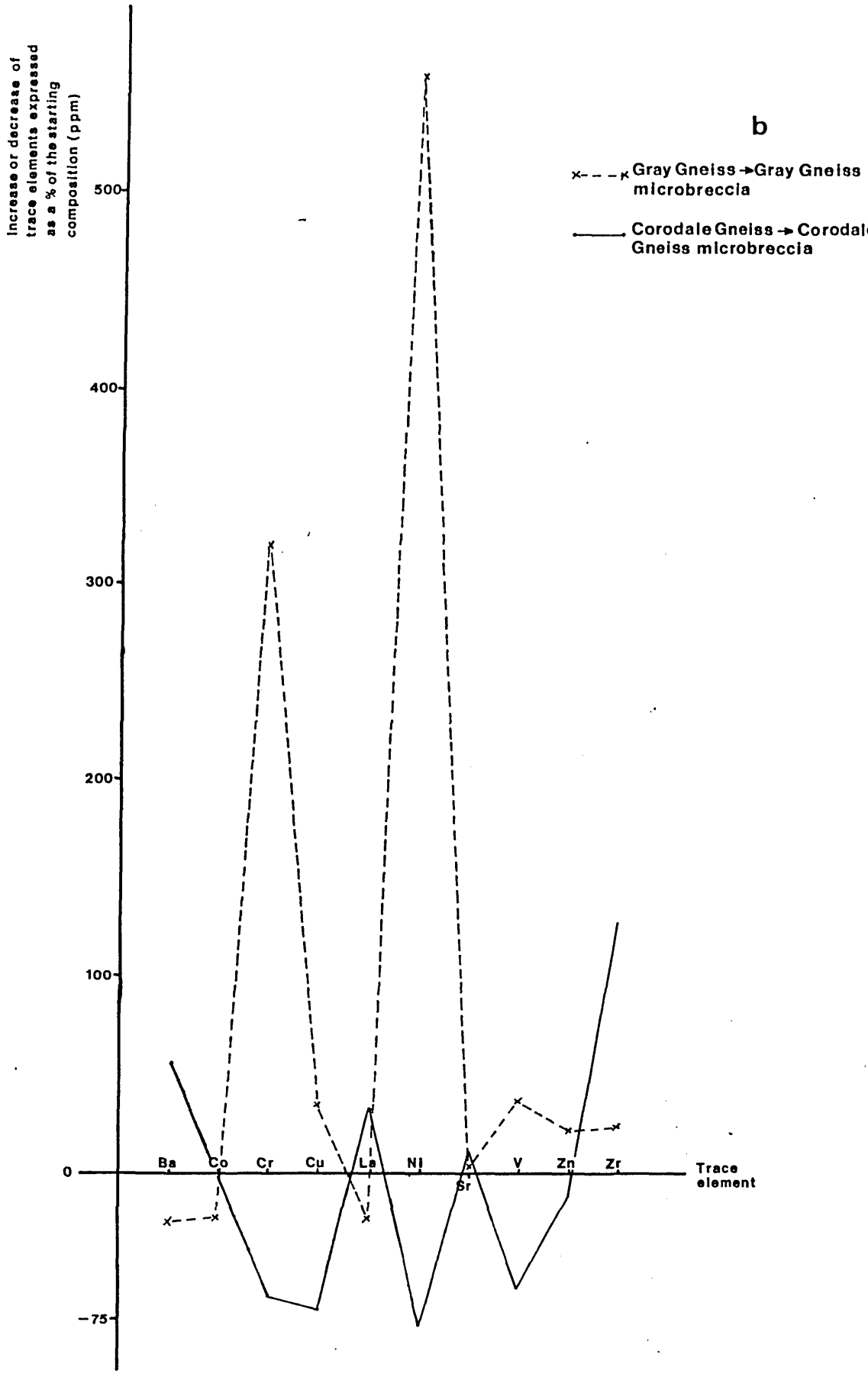

b
Gray Gneiss → Gray Gneiss microbreccia
Corodale Gneiss → Corodale Gneiss microbreccia
Increase or decrease of trace elements expressed as a % of the starting composition (ppm)
500
400
300
200
100
0
−75
Ba
Co
Cr
Cu
La
Ni
Sr
V
Zn
Zr
Trace element

Figure 6.10

Ranges of values for $FeO/(FeO + Fe_2O_3)$ for selected samples of Corodale Gneiss, Gray Gneiss and derived fault rocks. Bars on the bar chart represent average values, numbers represent the number of samples in each category.

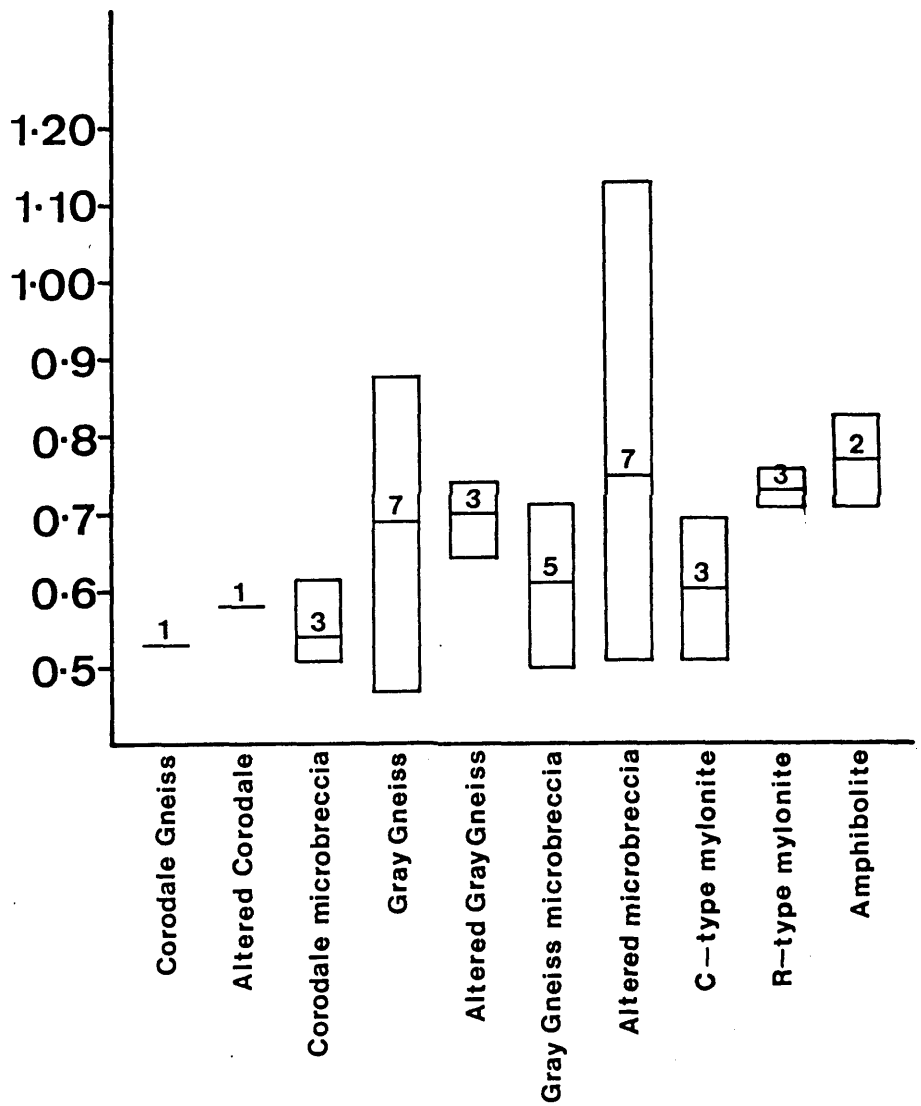

1·20
1·10
1·00
0·9
0·8
0·7
0·6
0·5
1
1
3
7
3
5
7
3
3
2
Corodale Gneiss
Altered Corodale
Corodale microbreccia
Gray Gneiss
Altered Gray Gneiss
Gray Gneiss microbreccia
Altered microbreccia
C–type mylonite
R–type mylonite
Amphibolite

Figure 6.11

Composition-volume diagram of samples of Gray Gneiss and altered Gray Gneiss.

Samples used : CR03, NT01.

Balanced equation, using a volume factor of 1.0 :

100g CR03 + 3.24g Fe_2O_3T + 1.63 MgO + 0.32g Na_2O + 0.33g K_2O + 0.05g P_2O_5 + 0.42g TiO_2 + 1.63g LOI

==> 4.07g SiO_2 + 0.27g Al_2O_3 + 0.63g CaO + 102.50g NT10

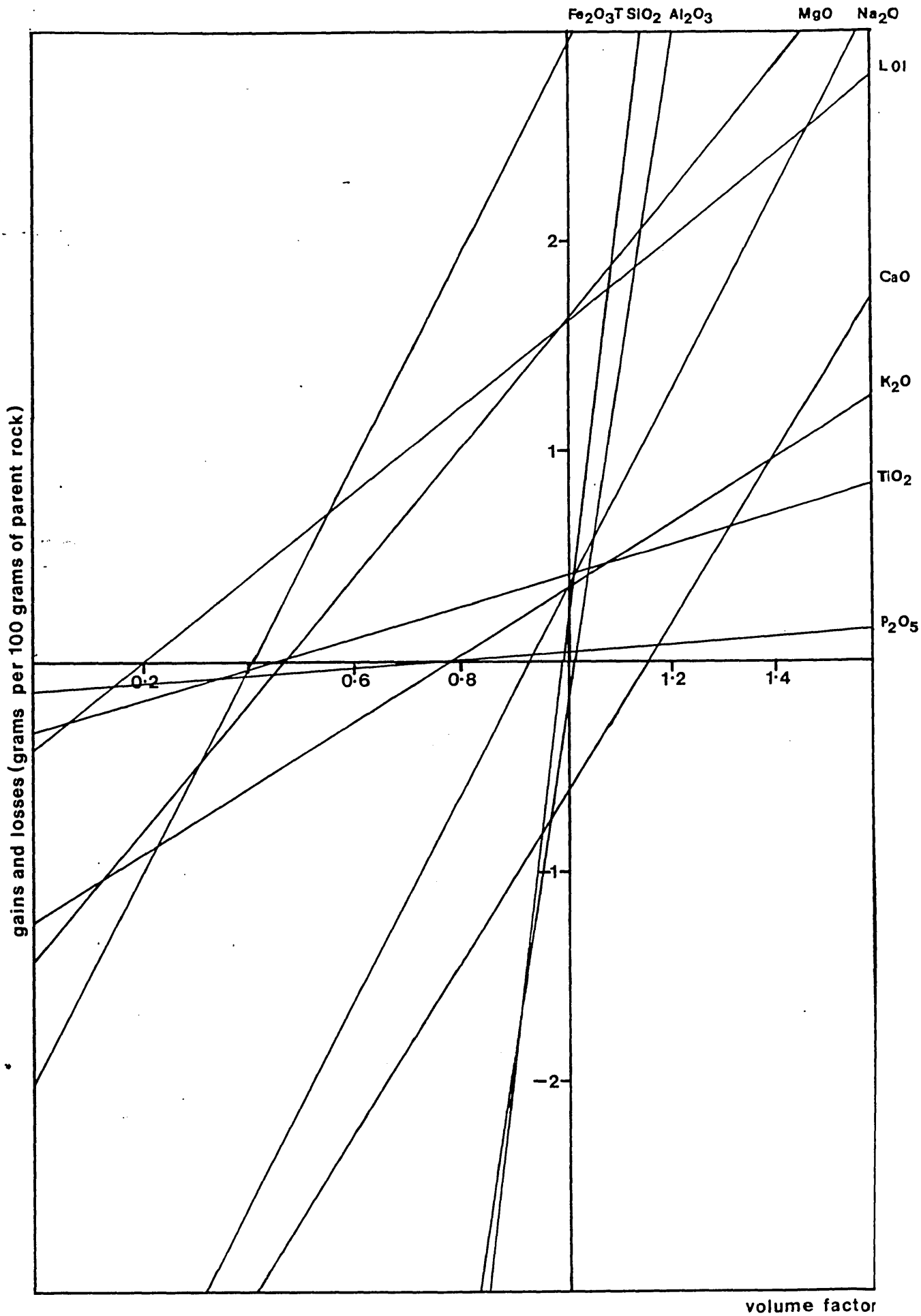

Fe_2O_3T SiO_2 Al_2O_3 MgO Na_2O
LOI
CaO
K_2O
TiO_2
P_2O_5
2
1
−1
−2
0·2
0·6
0·8
1·2
1·4
gains and losses (grams per 100 grams of parent rock)
volume factor

Figure 6.12

Composition-volume diagram of samples of Gray Gneiss and Gray Gneiss derived microbreccia.

Samples used : CR03, M03c.

Balanced equation, using a volume factor of 1.1 :

100g CR03 + 9.57g SiO_2 + 0.02g Na_2O + 2.03g K_2O + 0.22g LOI

==> 0.05g Al_2O_3 + 1.07g Fe_2O_3T + 0.52g MgO + 1.79g CaO + 0.03g P_2O_5 + 108.55g M03c

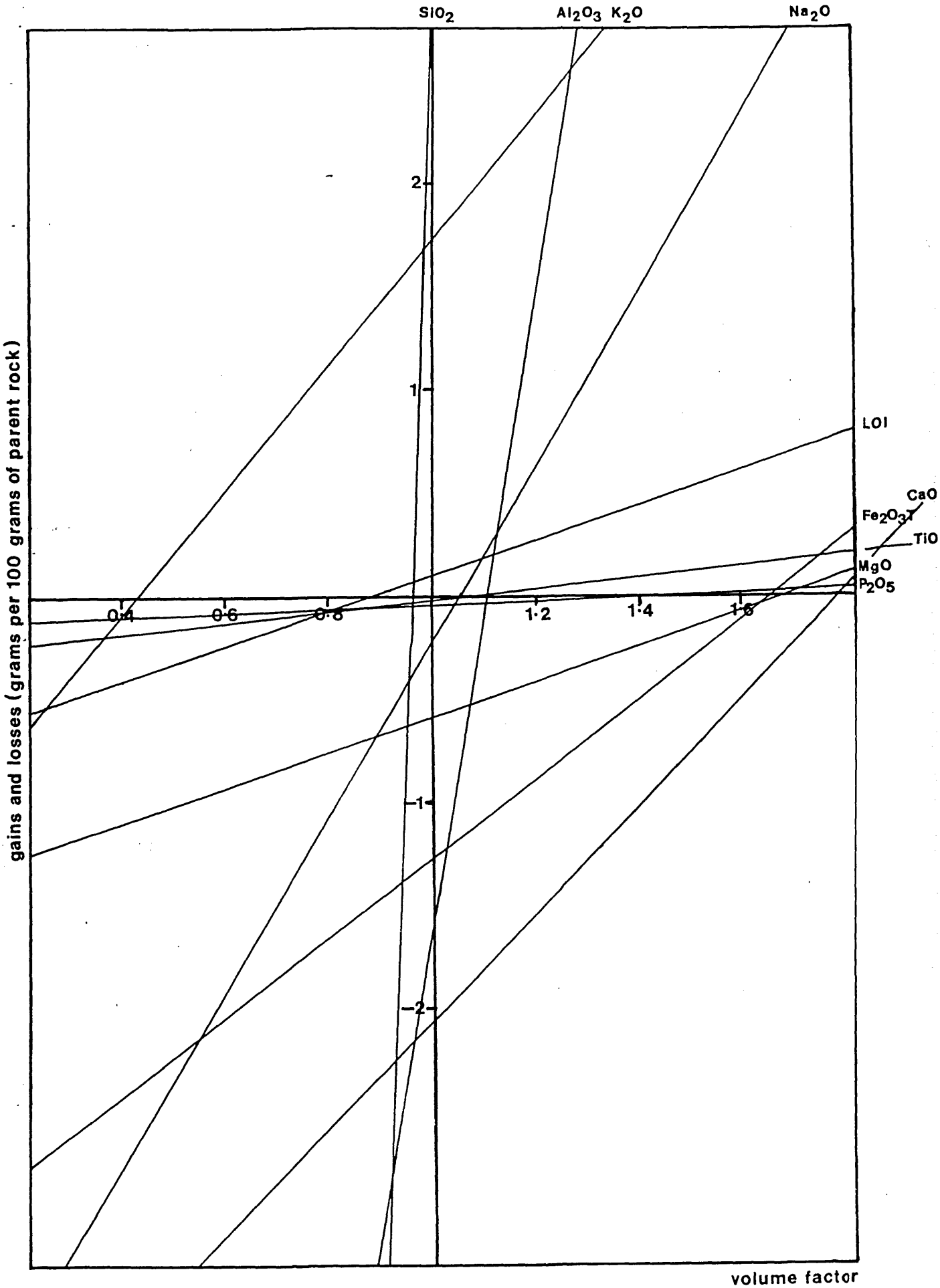

SiO2
Al2O3
K2O
Na2O
2
1
−1
−2
LOI
CaO
Fe2O3T
TiO
MgO
P2O5
0·4
0·6
0·8
1·2
1·4
1·6
gains and losses (grams per 100 grams of parent rock)
volume factor

Figure 6.13

Composition-volume diagram of samples of Gray Gneiss and r-type mylonite.

Samples used : ARDPT02, M05b.

Balanced equation using a volume factor of 1.0 :

100g ARDPT02 + 0.49g SiO_2 + 1.36g Fe_2O_3T + 0.84g MgO + 0.36g CaO + 0.21g K_2O 0.31g LOI

==> 0.16g Al_2O_3 + 0.38g Na_2O + 0.02g P_2O_5 + 0.06g TiO_2 + 102.83g M05b

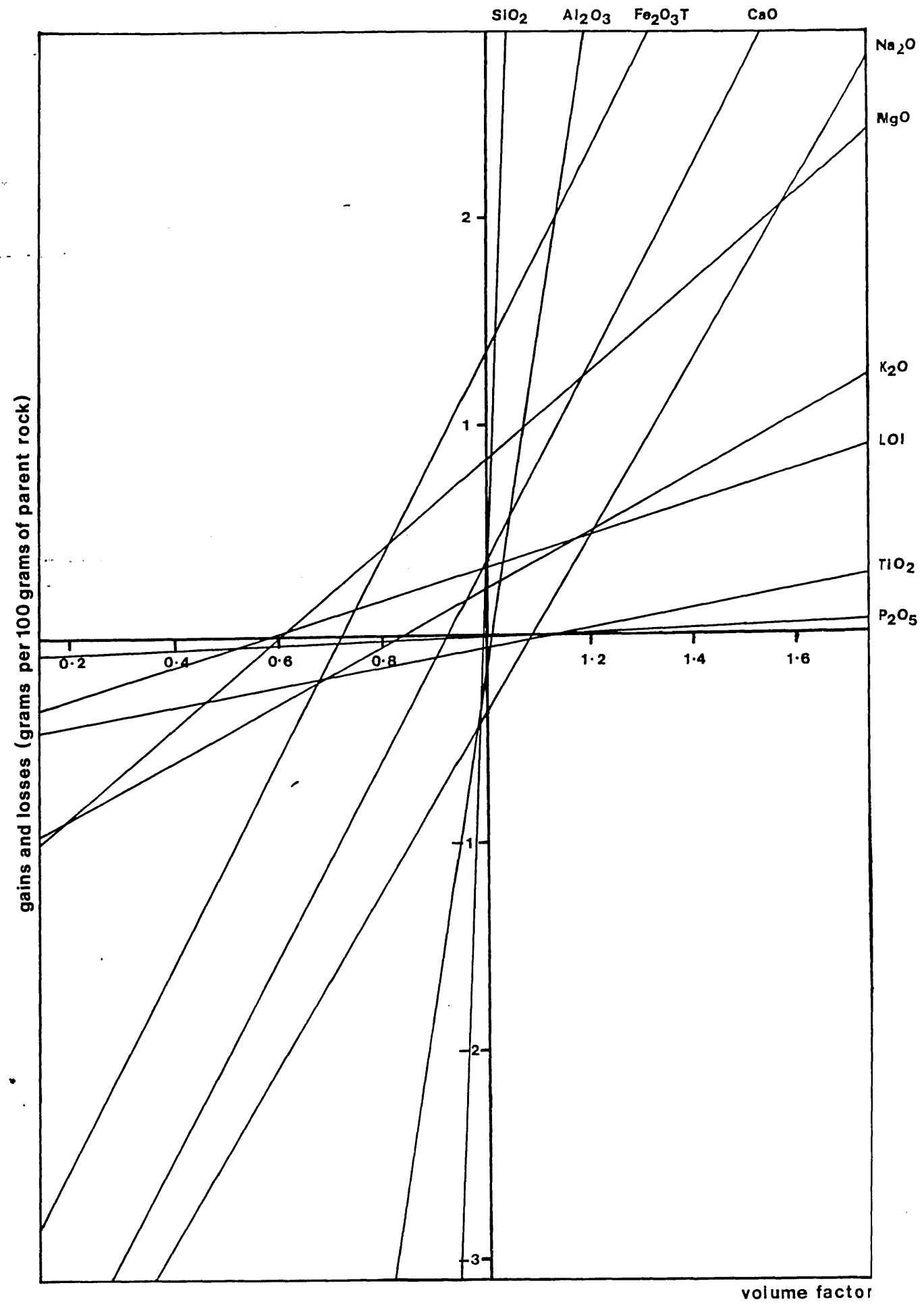

SiO2
Al2O3
Fe2O3T
CaO
Na2O
MgO
K2O
LOI
TiO2
P2O5
2
1
-1
-2
-3
0·2
0·4
0·6
0·8
1·2
1·4
1·6
gains and losses (grams per 100 grams of parent rock)
volume factor

Figure 6.14

Composition-volume diagram of samples of Gray Gneiss and c-type mylonite.

Samples used : LST15, CT01

Balanced equation using a volume factor of 0.9 :

100g LST15 + 2.62g Fe_2O_3T + 1.48g MgO + 0.47g K_2O + 0.04g P_2O_5 + 0.27g TiO_2 0.65g LOI

==> 13.72g SiO_2 + 1.12g Al_2O_3 + 0.42g CaO + 0.82g Na_2O + 89.45g CT01

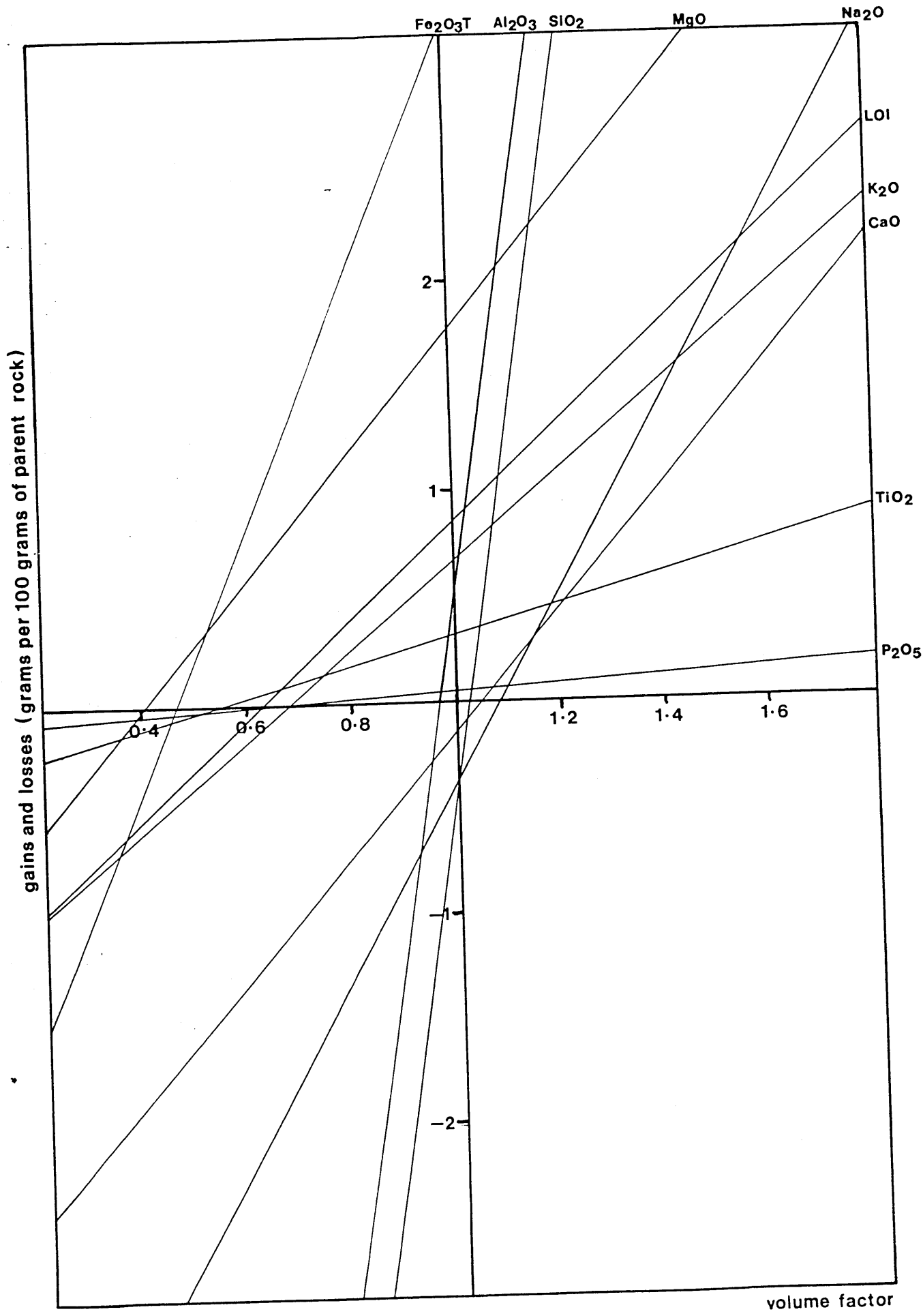

Fe2O3T
Al2O3
SiO2
MgO
Na2O
LOI
K2O
CaO
TiO2
P2O5
2
1
−1
−2
0·4
0·6
0·8
1·2
1·4
1·6
gains and losses (grams per 100 grams of parent rock)
volume factor

Figure 6.15

Composition-volume diagram of samples of Gray Gneiss and c-type mylonite.

Samples used : ARDPT02, BT03

Balanced equation using a volume factor of 0.8 :

100g ARDPT02 + 1.21g Fe_2O_3T + 1.47g MgO + 0.71g CaO + 0.89g K_2O + 0.07g P_2O_5 + 0.04g TiO_2 + 1.16g LOI

==> 19.39g SiO_2 + 0.14g Al_2O_3 + 0.46g Na_2O + 85.57g BT03

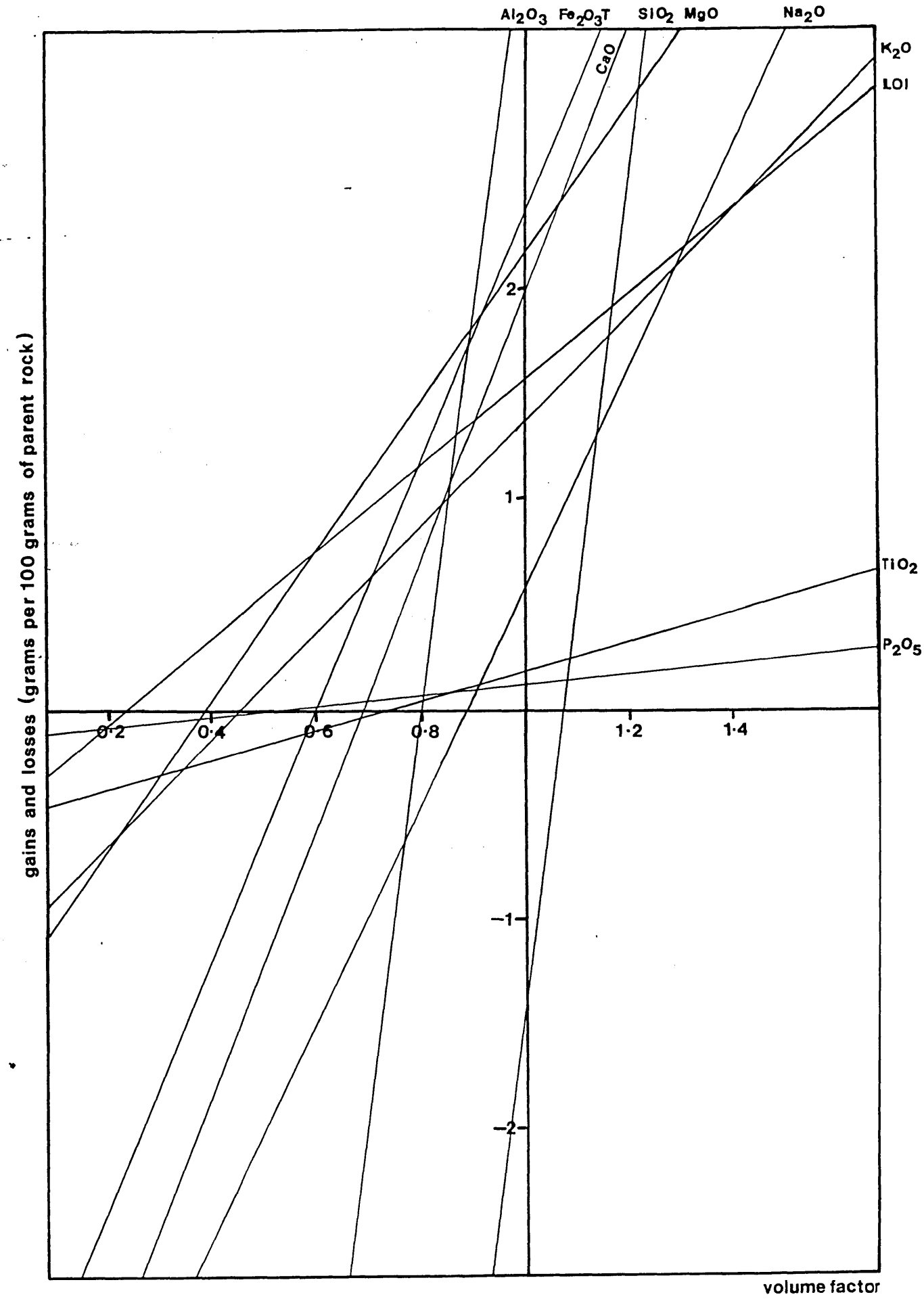

Al2O3
Fe2O3T
SiO2
MgO
Na2O
K2O
LOI
CaO
TiO2
P2O5
2
1
−1
−2
0·2
0·4
0·6
0·8
1·2
1·4
gains and losses (grams per 100 grams of parent rock)
volume factor

Figure 6.16

Variation of Mg/(Mg + Fe) with Si content of amphiboles from Corodale Gneiss and derivatives.

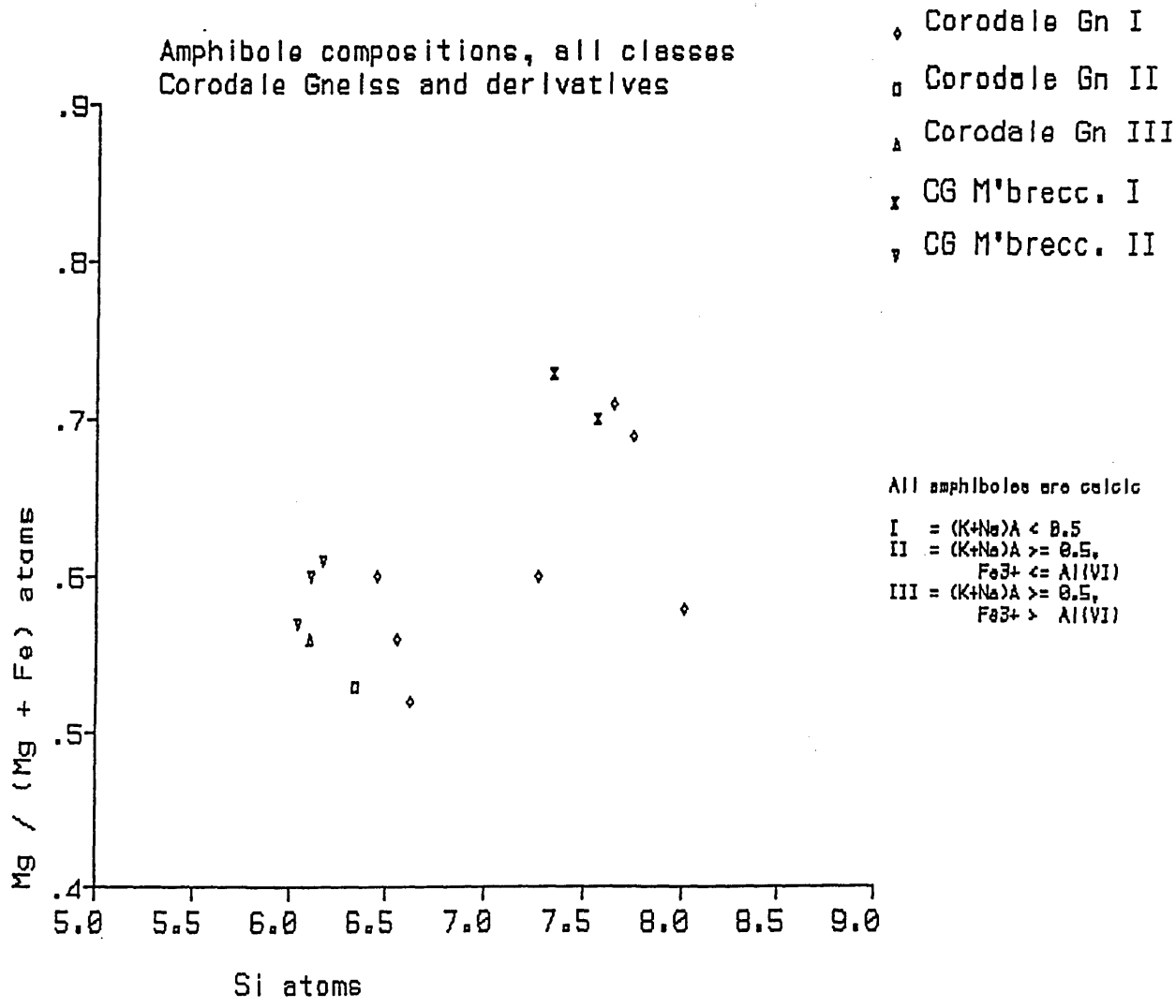

Amphibole compositions, all classes
Corodale Gneiss and derivatives
Corodale Gn I
Corodale Gn II
Corodale Gn III
CG M'brecc. I
CG M'brecc. II
All amphiboles are calcic
I = (K+Na)A < 0.5
II = (K+Na)A >= 0.5, Fe3+ <= Al(VI)
III = (K+Na)A >= 0.5, Fe3+ > Al(VI)
Mg / (Mg + Fe) atoms
.9
.8
.7
.6
.5
.4
5.0
5.5
6.0
6.5
7.0
7.5
8.0
8.5
9.0
Si atoms

Figure 6.17

Variation of Mg/(Mg + Fe) with Si content of amphiboles from Gray Gneiss and derivatives.

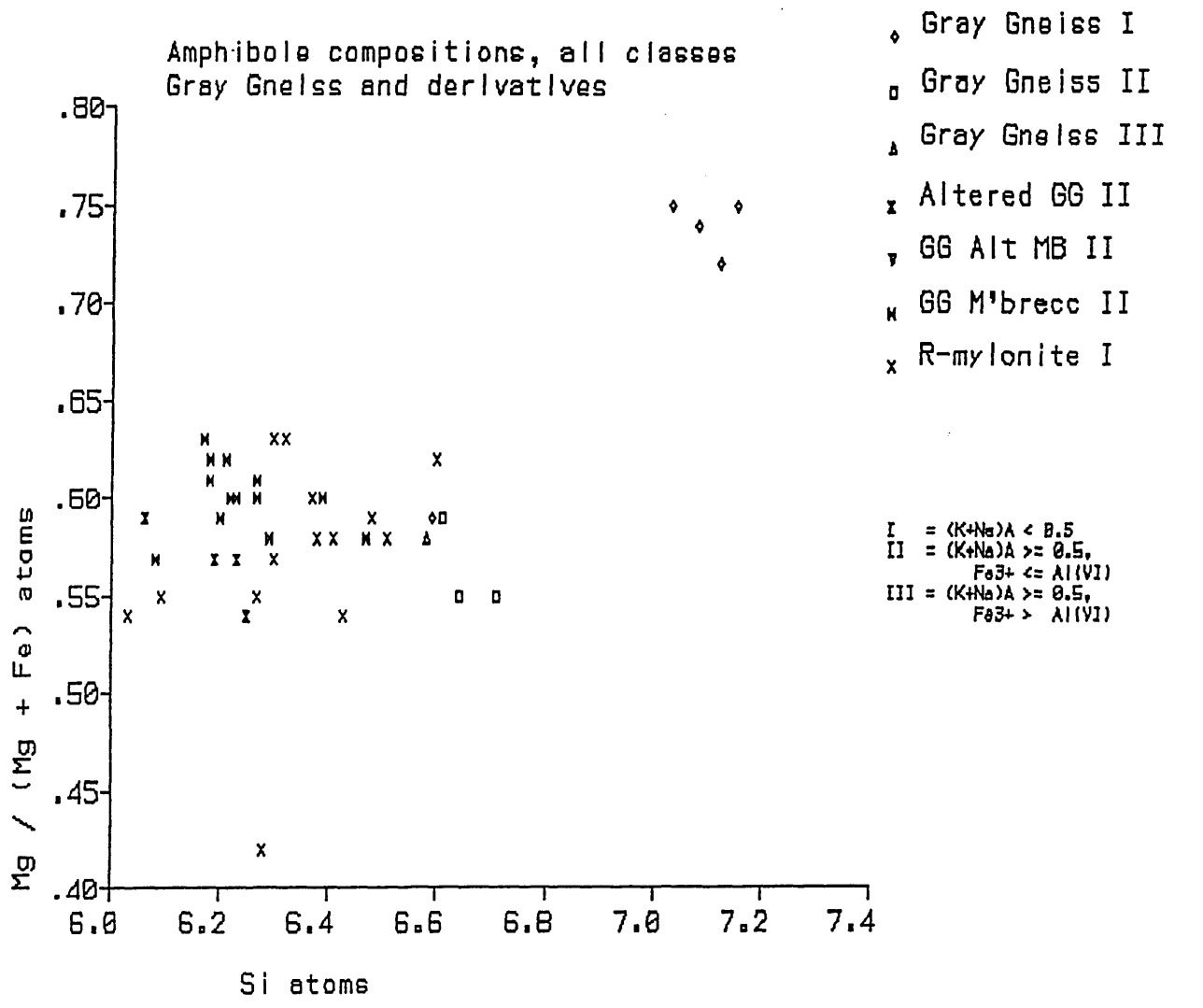

Amphibole compositions, all classes
Gray Gneiss and derivatives
Mg / (Mg + Fe) atoms
Si atoms
.80
.75
.70
.65
.60
.55
.50
.45
.40
6.0
6.2
6.4
6.6
6.8
7.0
7.2
7.4
◊ Gray Gneiss I
□ Gray Gneiss II
Δ Gray Gneiss III
x Altered GG II
▼ GG Alt MB II
M GG M'brecc II
x R-mylonite I
I = (K+Na)A < 0.5
II = (K+Na)A >= 0.5, Fe3+ <= Al(VI)
III = (K+Na)A >= 0.5, Fe3+ > Al(VI)

Table 6.1

Average Analyses for all Major Rock Types

Sampno = Number of samples
Rocktyp = Rock type

GG = Gray Gneiss
C = Corodale Gneiss
CPYR = Corodale Gneiss pyroxenite
MG = Mashed Gneiss
AGG = Altered Gray Gneiss
GGMB = Gray Gneiss derived microbreccias
AMB = Altered Gray Gneiss derived microbreccia
CMB = Corodale Gneiss derived microbreccia
CMYL = C-type mylonite
RMYL = R-type Mylonite

SAMPNO	av of 26	av of 4	av of 1	av of 4	av of 14	av of 22	av of 23	av of 6	av of 19	av of 11	
ROCKTYP	GG	C	CPYR	MG	AGG	GGMB	AMB	CMB	CMYL	RMYL	
SIO2	65.63	53.22	51.92	70.61	62.22	61.60	61.00	57.87	59.54	65.52	SIO2
AL2O3	15.32	17.21	3.65	13.89	16.31	15.12	15.88	17.71	15.44	15.14	AL2O3
FE2O3T	5.29	9.04	7.31	3.47	5.22	6.47	6.34	6.16	6.77	5.15	FE2O3T
MGO	1.75	4.43	14.19	1.57	2.72	3.29	3.09	2.76	3.97	2.33	MGO
MNO	0.08	0.14	0.18	0.04	0.08	0.10	0.09	0.09	0.10	0.07	MNO
CAO	4.16	7.30	19.37	2.55	4.89	5.17	4.71	5.00	4.40	4.70	CAO
NA2O	4.03	4.21	2.36	4.64	4.30	4.19	4.29	5.49	4.38	3.95	NA2O
K2O	1.97	1.48	0.13	1.67	1.94	1.49	2.15	2.14	1.79	1.71	K2O
P2O5	0.20	0.23	0.09	0.13	0.12	0.17	0.19	0.28	0.21	0.09	P2O5
TIO2	0.65	0.79	0.44	0.36	0.48	0.64	0.67	0.67	0.66	0.50	TIO2
LOI	0.67	1.73	0.96	1.50	1.74	1.84	1.77	1.40	2.19	0.80	LOI
TOTAL	99.44	98.02	98.14	98.92	98.29	98.24	98.45	98.14	97.25	99.17	TOTAL
TOT+LOI	100.11	99.75	99.10	100.42	100.03	100.08	100.22	99.54	99.44	99.97	TOTAL
BA	762	811	27	536	596	556	815	1022	564	494	BA
BE	0.80	0.85	0.75	0.70	0.98	0.93	1.05	1.12	1.00	0.95	BE
CO	64.3	40.5	33.6	36.4	45.7	49.5	40.1	39.4	37.4	53.9	CO
CR	26.5	89.2	401.5	40.4	125.1	105.5	88.2	58.0	100.8	60.9	CR
CU	37.0	56.3	230.6	14.6	21.8	53.0	46.1	29.5	32.5	21.3	CU
LA	26.1	22.1	19.5	18.4	24.7	19.2	31.5	28.8	30.1	20.6	LA
NI	5.4	28.4	38.4	-5.1	21.9	32.2	31.9	7.1	47.2	17.8	NI
SR	412	936	67	395	327	441	440	847	501	341	SR
V	70.9	170.0	432.4	18.5	66.5	97.5	92.9	91.6	108.4	58.6	V
ZN	60.6	93.0	54.5	34.5	61.3	74.8	80.6	75.3	77.0	75.9	ZN
ZR	151.7	51.1	136.4	118.3	132.4	112.7	135.9	154.2	139.6	134.6	ZR

Chapter 7

Synthesis

7.1 Introduction

This chapter presents a model of the history of the Outer Hebrides Fault Zone based on the interpretation of the work described in the earlier chapters and the work of other authors. The aim was to integrate as many as possible of the elements present in the Fault Zone and to define the conditions of formation of the various fault rock types and their interrelationships (figure 7.1) for each tectonic phase, to assign probable dates to these phases and to describe the geometries of the main tectonic features. Controls on each phase will be discussed. The chapter begins with the Gray Gneiss already formed and continues through time to account for the last phase of deformation. It attempts to correlate these various phases in the Outer Hebrides with regional events.

The fault zone as a whole is believed to have developed through two major post-Scourian compressional phases of deformation, followed by at least one major extensional phase. An early phase of compressional faulting, leading to the formation of the r-type mylonites and the early pseudotachylytes, was followed by a late compressional phase, giving rise to the microbreccias and the late pseudotachylytes. Finally one or more extensional phases caused faulting and associated hydration and alteration,

during which the c-type mylonites were formed.

Section 7.6 presents a discussion of some aspects of the model, and section 7.7 mentions its limitations. Those rock units described in earlier chapters that do not fit the model are also discussed in section 7.7. A brief comparison with other models is outlined in section 7.8, and a summary is presented in section 7.9.

7.2 Pre-Laxfordian Deformation

Prior to the Laxfordian, the rocks of the Outer Hebrides underwent metamorphism and deformation to granulite facies gneisses in the Scourian, followed by injection of basic magmas to form part of the Scourie dyke swarm of NW Scotland and with the subsequent emplacement of the South Harris Igneous Complex. Neither the origin of the precursors of the gneiss, nor the style of deformation, are discussed here (see section 3.2). They are not of importance to this model, except insofar as inherited Scourian gneissose foliation exerted a control over the development of Laxfordian structures (Fettes and Mendum, 1987).

7.3 Laxfordian Compression

Overview On the basis of field relations, microstructures and mineral assemblages, the r-type mylonites and the brown pseudotachylytes have been assigned to the Laxfordian episode (section 5.8). As their outcrop is restricted to central Lewis and South Uist, the ideas presented here are only applicable to these areas. It is unclear from the field evidence whether a large-scale fault zone existed at this stage. If this is the case, then much of it may subsequently have been obliterated by later reactivation. This would explain why the distribution of r-type mylonite and early pseudotachylyte is so restricted.

Tectonic Regime and Style of Deformation The Laxfordian was represented by a widespread retrogressive metamorphic event to lower amphibolite facies. This was accompanied by variable amounts of folding and transposition of Scourian fabrics (Fettes and Mendum, 1987) and gave way to cooling and uplift, resulting in extensive jointing (sections 3.2 and 3.4). In addition to folding, some deformation was accomodated by localised shearing, with variable strain rates accounting for the formation of both brittle and crystal plastic fault rocks (figure 7.1). The regime was, at least locally, compressive, as inferred from the microstructures present within the r-type mylonites (section 5.8). Maximum compressive stress, from quartz

stretching lineations, was orientated roughly SE in the Malasgair/Shiltenish area (section 4.2), although the presence of pre-existing large scale folds may complicate the situation by having allowed layer-parallel slip.

No evidence has been found for any tectonic events between the Laxfordian and the next compressional phase some 1000 My later.

Temperature and Pressure The stable mineral assemblages within the r-type mylonites (section 5.8) suggest their formation in the lower amphibolite facies. This is supported by extensive recrystallisation of quartz and amphibole, and by infrequent recrystallisation of pseudotachylytes. Fettes and Mendum (1987) have undertaken garnet-biotite geothermometry which indicates temperatures around 540 degrees C ($\pm$ 50 degrees C), characteristic of the lower amphibolite facies. They suggest a depth of around 10 - 15 km. This seems a little high in the crust when compared to other inferred orogenic geotherms (e.g. the Dalradian) but fits in well with the inferred lower limits of pseudotachylyte generation (Maddock, 1986), and geothermal gradients may well have been higher in the Laxfordian.

Movement Direction The r-type mylonites formed in a compressional environment. Evidence for this is from

asymmetric folding of the mylonitic foliation (section 4.2), asymmetry of augen tails and quartz c-axis fabrics (section 5.8). The r-type mylonite bands are predominantly orientated north-east/south-west (figure 4.1), suggesting a local direction of maximum compressive stress roughly orthogonal to this, i.e. south-east/north-west for this area. There appears to have been no extensional relaxation along the direction of former compression, as the only features attributable to uplift are late-stage, east-west trending sub-vertical fractures in the pseudotachylytes and the surrounding Gray Gneiss (section 4.2).

The movement directions obtained from the r-type mylonites cannot be applied outwith this area, as the mylonites formed along folded foliation planes. Similarly, the majority of the pseudotachylyte also formed by failure along foliation surfaces. The presence of these pre-existing foliation planes would allow local preferential failure of the gneiss along them for a wide variety of stress orientations, and thus the SE/NW stress orientation is not regionally applicable.

Chronology of Fault Rock Formation The spatial coincidence of the pseudotachylyte and the r-type mylonites suggest that they formed during the same event. Brittle failure (pseudotachylyte generation) probably continued intermittently throughout the Laxfordian, with

progressive reworking by folding (section 4.2), and is mainly confined to Lewis and the Corodale Gneiss of South Uist (section 4.5). There are no constraints on the relative timing of formation of the crystal plastic fault rocks, although they are not often found to be reworked, suggesting that the majority formed late on in the Laxfordian.

Controls on Fault Rock Formation The Gray Gneiss foliation has exerted a strong influence on the formation of the r-type mylonite bands (figure 4.1) and, to a lesser extent, the pseudotachylytes. This was the predominant control on localisation of shearing, with the pseudotachylyte forming by preferential failure along the gneissose foliation.

Fault Zone Geometry Narrow, inpersistent bands of r-type mylonite (figure 4.1) and isolated pseudotachylyte outcrops running roughly north-south parallel to the gneissose foliation give a discontinuous, linear geometry to the fault zone at this time. It has been suggested that the fault rocks represent a major Laxfordian shear zone (McQuillin and Watson, 1973), stretching along the entire length of the present island chain, and acting as a locus for subsequent deformation. It is possible that, in turn, such a shear zone may have been reactivating earlier (?Scourian) structures. The field evidence neither

supports nor disproves this idea.

7.4 Caledonian Compression

Overview The formation of large quantities of microbreccia is ascribed to the effects of the Caledonian orogenic event. Strain rates were variable, and gave rise to subordinate amounts of ultracataclasite and pseudotachylyte when they were higher or when deformation became more localised.

Tectonic Regime and Style of Deformation The Caledonian orogeny on mainland Scotland was marked by a phase of east-south-east orientated compression. This compressive phase generated a number of NNE trending thrust-sense faults, the most notable being the Moine Thrust (figure 3.5). The proximity of the Outer Hebrides block to the Caledonian orogenic margin resulted in brittle fracturing of the Gray Gneiss and production of a variety of fault rocks (figure 7.1), chiefly large amounts of microbreccia, which became the Outer Hebrides Fault Zone (figure 1.2).

The differing reaction to the same compressional stress between the Moine Thrust (formation of a discrete fault plane) and the Outer Hebrides Fault Zone (formation of a complex assemblage of fault rocks and a wide zone of brecciation) is probably best explained in terms of lithology. Whereas the Moine Thrust disrupted a sedimentary succession, which gave it layers to propagate

along, the Outer Hebrides Fault Zone affected rock which was essentially isotropic on a large scale.

Temperature and Pressure The brittle nature of much of the deformation suggests that it took place at high crustal levels. The sub-horizontal orientation of the fractures within the microbreccias are strongly suggestive of conditions such that the direction of minimum compressive stress was approximately vertical (figure 7.2). This, coupled with the large amount of dilatancy seen across these fractures, implies conditions of low overburden, probably no more than 3 to 5 km deep. This would imply pressures of around 1 - 1.5 kbars and temperatures of around 90 to 150 degrees centigrade (assuming a geothermal gradient of 30 degrees C/km for an orogenic belt).

Movement Direction There was very little displacement along fractures during this deformational episode. Instead, deformation was taken up in the formation of the zone of microbreccia, in which blocks tended to rotate relative to one another, and few discrete fault planes developed. Consequently, unambiguous sense-of-shear indicators are scarce. However, it can be inferred that the overall environment was one of compression,with the maximum compression orientated predominantly east-south-east.

Formation of Fault Rocks The microbreccia formed by propagation of two pervasive sets of undulating fractures, dipping gently in opposing directions, which broke the Gneiss up into a series of rhombohedral blocks. Displacement along most of the fractures was minimal, with small offsets detected by rotation of the intervening blocks. The microbreccia responded to continuing deformation by further rotation of blocks, grain size reduction to give cataclasites and formation of pseudotachylyte along failure surfaces.

The presence of large quantities of microbreccia demonstrate that brittle failure was the dominant mode of deformation, implying that the rocks were at higher crustal levels than in the Laxfordian. Strain rates were variable, giving rise to pseudotachylyte when they were high. Deformation was complex and continued for some time after initial formation of the microbreccias was complete, as cataclasites are frequently observed to be cut and offset by small movements along fractures, and pseudotachylyte continued to be generated. The whole zone behaved as a complicated network of interrelating elements, all continuing to deform and rotate.

Controls on Fault Rock Formation The most important control was the orientation of the gneissose foliation

with respect to the direction of maximum compressive stress. Where the gneissose foliation is sub-parallel to the fault zone (i.e. striking perpendicular to the direction of maximum compressive stress) the degree of brecciation in the microbreccia is less than where it is at a high angle (figure 7.3).

On South Uist, localisation of the fault zone may have been influenced by the boundaries between adjacent lithological units. The microbreccias formed at the boundary between the Gray Gneiss and the Corodale Gneiss, possibly because of the relatively high competence of the Corodale Gneiss unit.

It is also possible that the presence of a Laxfordian shear zone running the length of the islands acted as a control over the development of Caledonian structures. Deformation could have resulted in reactivation of this zone of weakness, which may not have been in quite the right orientation to allow complete reactivation. This would allow outcrop of the r-type mylonites below the base of the 'new' fault system in Lewis, but further south they would be incorporated into the hanging wall, and would now be somewhere under the Minch.

Various authors have considered the possibility of such an inherited control over later deformation in the

Hebrides area (Watson (1977); Smythe et al. (1982); Brewer and Smythe (1986); Jones (1981)), although there is no evidence for its existence.

Fault Zone Geometry The end of the phase of Caledonian compression saw the presence of a wide band of microbreccia (up to 10 km in width as seen at present, but conceivably greater than this, as some may be under the Minch) running down what is now the eastern seaboard of the Outer Hebrides. Brecciation is generally stronger to the east. The band of microbreccia strikes roughly north-north-east and its lower margin appears to dip to the east at around 30 degrees, although it is not known whether this boundary has been modified by later reactivation.

The pseudotachylyte is mainly confined to the western side of the fault zone, and to the Gray Gneiss below the basal fault, suggesting that rapid failure was localised in this area, with generally lower strain rates affecting the east.

7.5 Post-Caledonian Extension

Overview Discrete fault planes developed within the zone of microbrecciation and, as fluids became available,

c-type mylonites formed along them. It is thought that the two events were separated in time, although both were extensional in nature.

Tectonic Regime At some time after the end of Caledonian compression, an extensional regime became dominant. Deformation ceased to be taken up by rotation of the microbreccia blocks and was localised onto a series of fractures, predominantly dipping to the east, although some dip west, and steeper than those formed in the microbreccias. With continued deformation, the fractures developed into discrete fault planes. Nearly all of the faults show grain size reduction to some degree, and cataclasites and ultracataclasites (figure 7.1) developed along some of them. Discrete occurrences of cataclasites also formed, mostly to the western side of the fault zone, and are usually found as small veins injected into dilatant cracks. The major cataclasite bands of South Uist are thought to have begun developing at this stage, although they may have begun to form earlier, during Caledonian compression.

The fault planes acted as conduits when a source of fluids became available, giving easy access into the microbreccias. This allowed the development of c-type mylonites along the fault planes with continuing deformation, and widespread static alteration of the

pre-existing fault rocks (figure 7.1).

The fluids involved in this stage of the deformation enriched the forming c-type mylonites in certain elements, notably Fe and Mg, and depleted them in others, notably Si. The excess Si, together with surplus amounts of Fe and Mg, then passed along the fracture system and into the microbreccias, cementing them by precipitation of quartz, minor amounts of Fe oxide or sulphide and traces of Mg-bearing minerals along fractures (figure 7.4) - for a more quantitative account of the processes involved, see the mass balance calculations (section 6.4). Hydrothermal circulation, precipitation and alteration continued for an unknown length of time after the cessation of deformation.

At no point during the extensional episode is pseudotachylyte generated, suggesting that strain rates were much lower than in the previous regimes. A series of late-stage, vertical, roughly east-west trending faults cut all earlier structures at several localities (notably Malasgair and Shiltenish (figure 4.1), Scalpay (figure 4.2), North Lee (figure 4.4) and Usinish (figure 4.5)). There is no evidence for their absolute ages, but they all show a sinistral displacement of variable magnitude.

Temperature and Pressure It is thought that temperatures and pressures during initial extension were similar to

those during the Caledonian compressional phase, that is, around 100 degrees C and 1.5 kbars, as deformation continued to be in the brittle field and there is no evidence for post-Caledonian burial of this area. However, the mineralogy developed in the c-type mylonites (section 5.7) suggests that temperatures during their formation were equivalent to those of the lower greenschist facies (section 6.6), i.e. around 300 degrees C. Thus, the fluids coming into the rock were hotter than the rock itself, as supported by the precipitation of silica leached from the c-type mylonite bands and redeposited away from them in the presumably cooler microbreccias.

Movement Direction There are two lines of evidence for the deformation being extensional. The first lies in the orientation of the discrete fault planes within the microbreccia. Subsequent fault planes shallow in dip as one moves eastwards across the fault zone (figure 4.6), implying that they formed in an extensional environment, with the main axis of extension running roughly east-south-east.

Secondly, within the c-type mylonites that formed along these fault planes, a variety of extensional structures and microstructures (sections 4.3, 4.4, 4.5 and 5.7) are found. These indicate extension for both the east and the west dipping c-type mylonite bands. However, very little

extensional movement would be required to reset earlier compressional microstructures if the c-type mylonites had formed prior to this, and it is thought that the orientation of the bands themselves is a more reliable indication that they formed in an extensional environment.

Controls on Fault Rock Formation The localisation of the c-type mylonite bands were controlled by the existence of the fault planes within the Gray Gneiss microbreccia. It is uncertain what caused the development of the fault planes where they did, and what governed their orientation, other than that they formed within the weak microbreccias. It is possible that the fractures within the microbreccias exerted some control, with the faults developing initially step-wise along them.

Competence contrasts played a part in exerting control over the formation of the c-type mylonite bands. For example, the c-type mylonites at the neck of the Usinish peninsula exploited the junction between the Corodale Gneiss and the Mashed Gneiss. The effects of competence contrasts are also seen on a smaller scale. The c-type mylonites on Scalpay contain many good examples (see figure 4.2) of the mylonitic foliation curving around the margins of basic pods; indeed, the foliation is often intensified at such boundaries. It is possible this is a feature inherited from the Laxfordian, as the margins of

basic pods and dykes within the Gray Gneiss often show a similar deflection and intensification of gneissose foliation.

Fault Zone Geometry The main feature of this phase is the development of linear, continuous faults within the wide zone of microbrecciation inherited from the Caledonian. The dip of successive faults shallows to the east. In addition, narrow c-type mylonite bands formed along some of these faults, and in places (e.g. North Uist - figures 4.3 and 4.4) they form an anastomosing network along which deformation has been localised.

Possible Ages of Extension In view of widespread post-Caledonian reactivation in adjacent areas (Coward and Enfield. 1987; Enfield and Coward, 1987), it is thought likely that the earliest extension began in the Devonian. This seems the most plausible age for the formation of the discrete fault planes. Formation of the c-type mylonites may have been at this time too, although it is hard to envisage a large enough source of warm fluids to allow such large-scale alteration and changes in bulk chemistry (chapter 6) to have occurred, and a Tertiary age is preferred for this event. The possible age(s) of the extensional phase(s) is discussed in more detail in section 7.6.

7.6 Discussion - Aspects of the Model

Facies Discrepancies

As discussed in section 2.2, the Outer Hebrides Fault Zone was originally thought to represent a thrust as it was thought that thrusting was the only way of getting the granulite facies Corodale Gneiss above the lower amphibolite facies Gray Gneiss.

It is also possible that, due to the difference in bulk composition between the two rock types, both could have been metamorphosed at the same grade, but would have developed different mineral assemblages. This would have allowed the juxtaposition of rocks of apparently different facies without recourse to thrusting.

The mineralogy and geochemistry (chapter 6) supports this hypothesis by showing differences in the bulk chemistry of the two rock types. Furthermore, it shows the Corodale Gneiss to be an extremely dry rock, so it is possible that during the Laxfordian it maintained its pyroxene-bearing assemblage, as it contained insufficient fluid to allow the pyroxenes to retrogress to amphiboles. Additionally, it is well known that at least one portion

of the mainland Lewisian escaped the influences of the Laxfordian and kept its Scourian assemblage and structure - it is possible that the Corodale Gneiss is an Outer Hebridean equivalent.

Figure 7.5 summarises the possible mechanisms for the juxtaposition of granulite facies rocks above those of lower amphibolite facies. The second mechanism is preferred in view of the pod-like outcrop pattern of the Corodale Gneiss observed in the field (figure 1.2). This is not to say that the Corodale Gneiss was never at a deeper crustal level than the Gray Gneiss, only that it is not necessary to have had thrusting of sufficient magnitude to account for a 200 degree C difference in metamorphic grade (roughly equivalent to 7 km vertical displacement, or 16.5 km along a fault plane dipping at 25 degrees).

Relative amounts of compressional and extensional movement

It is difficult to quantify the amount of displacement associated with any of the deformational phases owing to the absence of any stratigraphic markers. The microstructures present in the various fault rocks reveal nothing about magnitudes of displacement. About the Laxfordian phase of compression, it is impossible to infer anything, for the above reasons. Furthermore, if it were

possible to, it would be hard to separate its effects from those of the Caledonian compression.

Several attempts have been made to estimate the overall displacement towards the southern end of the fault zone. Most of these estimates involve the correlation across the fault of an antiformal fold limb within the gneiss near Barra. The figures obtained range from 4.8 km (Sibson, 1977b) to 10 km (Francis and Sibson, 1973), with a strong component of rotation present in addition to dip-slip. Coward (1969) inferred from the thickness and distribution of the ultracataclasite zones on South Uist that east-west shortening must have had a minimum value of 2 to 3 km in this area.

The major problems with these estimates is that presumably they represent finite dip-slip displacement across the fault zone, i.e. account for both of the compressional phases and the extension, and that the correlation of the fold limbs across the fault zone is not good, as can be seen from the discrepancies between the various estimates. Calculations for the amount of extensional dip-slip can be made from the seismic profiles undertaken to the north of Lewis, and gives a figure of around 21 km for the Outer Hebrides Fault Zone in the North Lewis basin, representing a maximum extension of around 130 %. This would give values of 23 to 31 km for

the combined compressional displacement.

Unfortunately, it cannot be reasonably assumed that amounts of up-dip and down-dip displacement were similar for both the north and the south of the area. furthermore, the angle of the fault on the seismic sections is lower than that seen on land, giving a larger than would be expected figure for extension, although a small element of rotation during reactivation could account for this. Along the length of the fault it would be possible to absorb a component of rotation without necessarily producing obvious oblique sense of shear indicators. This might be the case if the directions of compression and extension were not parallel, and there is no reason to assume that they were. Furthermore, the feature termed the Outer Hebrides Fault Zone on the seismic sections is offset considerably in a sinistral sense from the continuation of the feature of the same name on land, due to the inferred presence of an east-west fault off the north coast of Scotland, so that it may not in fact represent the same structure.

In conclusion, the estimates made for both finite dip-slip and extensional dip-slip are unreliable, and it appears impossible to ascribe absolute amounts of movement to any of the deformational phases.

Deformation in the Corodale Gneiss

The Corodale Gneiss appears to have undergone an early phase of pseudotachylyte generation, correlated with the Laxfordian, as it is post-dated by an episode of jointing, correlated with late Laxfordian uplift and cooling. After this, the Corodale Gneiss behaved as a virtually inert pod, allowing deformation to be accomodated by the Gray Gneiss to the west, and the formation of a c-type mylonite band at its eastern boundary with the Mashed Gneiss, best explained in terms of competence contrast. The only signs of internal post-Laxfordian deformation are the presence of two minor fault planes, which die out laterally, inland of Usinish, and some late stage faulting which sinistrally offsets the western margin (figure 4.5).

Extensional phases and their ages

A problem with the extension is whether the c-type mylonites formed during the same episode as the fault planes, or at a later date. If they were part of the same episode, then a source of fluid had to have become available part way through, to allow c-type mylonite formation. If they represent two separate episodes, then it is suggested here that the earlier one was predominantly dry and the later one wet.

It seems probable that post-Caledonian (Devonian) relaxation accounted for at least the formation of the fault planes, and the Minch basins (Enfield and Coward, 1987), although there is no confirmatory evidence for this from the ages of basin infills in the grabens. If this phase is also to account for the c-type mylonite formation, then a source of warm, aqueous Fe and Mg bearing fluids has to be found. A suitable source may have been water interacting with the magma of Devonian calc-alkaline volcanics of the Midland Valley. If the c-type mylonites were formed during a later episode of deformation, then a suitable age may be the Tertiary, owing to availability of Tertiary magmatic fluids. The relative merits of these two ideas are summed up below.

Devonian extension

For Devonian extension is known to have affected basins to the north-east (e.g. the west Orkney Basin).

Some of the sediments in the Minch prisms could be of this age (other possibilities include Torridonian and Permo-Triassic).

Late Caledonian dates have been obtained for some of the c-type mylonites.

Against Possibly there was not enough magmatism in the

immediate area to supply the necessary quantities of fluids, as most of the Devonian magmatism is a considerable distance away.

The volcanism was calc-alkaline, not basic, and therefore not ideal for generation of fluids of the required composition.

The Devonian is not known to have been a major phase of extension in this area, and might not have been sufficient to give the amount of extension seen in the Minch.

Tertiary extension

For

The Tertiary represents a major phase of crustal extension, with rifting and basic magmatism.

The presence of major igneous centres on Skye less than 48 km away could have provided a suitable source of fluids.

Tertiary dykes are found on the Hebrides, indicating that igneous activity occurred at close proximity to the fault zone.

The Madadhs (section 3.2) suggest that basic magma was intruded up a fault plane, implying ready access to magma and associated fluids along the faults.

On Scalpay, Tertiary dykes are seen to be

truncated, giving evidence for post- or syn-Tertiary tectonism.

The basic nature of the Tertiary magmas would have provided Fe and Mg to interreact with the fluids.

Against The large time gap between the Caledonian and the Tertiary, during which tectonism is known to have occurred - why is there no evidence of any reactivation from these episodes (e.g. Permo-Triassic)?

There is a third possibility which could be considered as a date for either phase of extension - the Permo-Triassic. Formation of the Minch graben system has been assigned to this event by some authors (e.g. Fettes and Mendum, 1987) and there are intrusives of known Permo-Triassic age on Barra and South Uist. Thus, the Permo-Triassic could account either for the formation of the extensional faults in the microbreccia, or for provision of fluids for the formation of the c-type mylonites.

The first of these possibilities is discounted as other authors (e.g. Enfield and Coward, 1987) consider that the Minch graben system was initiated in the Devonian, during

late Caledonian relaxation - this is supported by interpretations of seismic sections, which show Devonian sediments at the bases of some of the half grabens (see figure 2.2). The formation of the c-type mylonites in the Permo-Triassic is also not considered very likely, as the intrusives are very restricted. It is highly unlikely that there would have been a sufficiently large volume of fluids associated with them to bring about the widespread retrogression necessary for c-type mylonite formation. In addition, the intrusives are not basic enough to have provided the amounts of Fe and Mg necessary to result in the chemical changes seen in the c-type mylonites.

On balance, it is preferred that the initial formation of the fault planes occurred during the Devonian, and that the c-type mylonites formed during the Tertiary.

7.7 Discussion - Deficiencies of the Model

Problem lithologies - the Mashed Gneiss

It has proven impossible to fit this lithology into the model as so little is known about its history and structural significance. It is tempting to assign its brecciation to the Caledonian compressional phase to tie in with the microbrecciation of the Gray Gneiss, but

jointing would seem to post-date the brecciation in the Mashed Gneiss, and it is hard to assign a date to this if the brecciation is Caledonian. If it were to prove to be Caledonian, the later formation of the c-type mylonites provides a convenient source of silica-rich fluids to give rise to alteration of the rock and cementation of fragments by quartz.

Problem lithologies - the Gouge

This is not really much of a problem, as its outcrop is so confined (section 4.3). It is restricted to one late stage fault on Scalpay, and presumably indicates that fluids were still around at this at this stage in the fault zone evolution. This late stage fault truncates some Tertiary dykes, hence it is thought that the gouge is syn- or post-Tertiary. It is unknown why an incohesive fault rock rather than a c-type mylonite should have formed, unless the fluid reacting with the Gray Gneiss to form gouge was cooler than that giving rise to the c-type mylonites. This suggests that the gouge probably post-dates the the formation of the c-type mylonites, which fits with the fact that the eastwards continuation of the late stage fault disrupts c-type mylonite-bearing faults (figure 4.2).

Radiometric dating of the fault rocks

K-Ar dating of some of the fault rocks has been carried out and the results are presented in Sibson (1977b). Pseudotachylytes give varying dates of 2650 My to 442 My. These could be interpreted as representing Laxfordian and Caledonian ages for the pseudotachylytes, which would tie in with the model. However, it is felt that in general, pseudotachylytes do not remain molten for long enough to allow complete geochemical resetting, so that the dates recorded are predominantly influenced by the age of the host rock. A similar spread of ages was obtained for the ultracataclasites, and these probably reflect variable amounts of degassing, as well as the parent rock content. Those c-type mylonites analysed record dates of between 947 and 394 My, which would put them in the Caledonian, although, as with the other dates obtained, there is no reason to suppose that they are accurate. In summary, radiometric dating is of little help in assigning ages to the relevant episodes of deformation.

Late stage faulting

As already mentioned above, it is thought that the late stage sinistral faulting found throughout many of the

areas studied represents a phase of late Tertiary deformation, post-dating the formation of the c-type mylonites and intrusion of the Tertiary dykes.

7.8 Discussion - Comparison with Other Models

Sibson's model

Briefly, the model presented by Sibson (1977b) is that of a fault zone transecting a two-layer crust. In the upper layer, extending down to c. 15 km depth, the fault is essentially a single planar feature, with movement accomodated by seismic slip. Fault rocks generated are brittle; cataclastite and pseudotachylyte. Below 15 km, movement is by aseismic slip, deformation is crystal plastic and r-type mylonites are produced along a fault plane which becomes progressively wider with depth. The boundary between the two layers (the brittle/crystal plastic transition) defines the approximate lower limit of pseudotachylyte generation. The r-type mylonites of Lewis are thought to represent the exhumed remains of the lower crustal layer, and the fault rocks of the islands further south represent the upper layer. This difference in exposed crustal level is due to tilting and/or differential erosion, and the complete fault zone is

thought to have been Caledonian in age.

There are several problems with this model when applied to the Outer Hebrides Fault Zone. Firstly, it implies that a single phase of compressional deformation (with a slight amount of lag sliding due to relaxation) could account for the formation of the whole fault zone. There is evidence for two compressional phases in the Hebrides, one high temperature/crystal plastic and one cooler/cataclastic, and at least one extensional phase.

It could be argued that, as the rocks due to the two compressional phases are so different in character and outcrop in differing areas, they represent exposure of different levels within a single fault zone. This is not thought to be the case, as on Lewis both phases are seen adjacent to one another. It is not possible to interpret this as representing the brittle/crystal plastic transition as if this were so then the grade of the fault rock products ought to increase towards the hanging wall, whereas in fact the cooler, more brittle fault rocks are nearer the hanging wall. Additionally, even if the fault rocks did all belong to a single deformational episode, with a simple (high grade in the north, lower grade in the south) distribution, then there is no known post-Caledonian tectonic event which would have allowed N/S crustal tilting of sufficient magnitude to allow

exposure of such deep crustal levels in the north.

Fettes and Mendum's model

Fettes and Mendum (1987) propose initiation of the fault zone in the Laxfordian, with formation of the r-type mylonites, pseudotachylytes, cataclasites and microbreccias. The c-type mylonites formed during Caledonian compression, and an episode of late Caledonian extension caused folding of the mylonitic foliation. This was followed by further extension in the Permo-Triassic, which gave rise to the Minch and related basins.

Problems with this model lie mainly in that it is hard to envisage formation of large quantities of microbreccia and cataclasite in the lower amphibolite facies conditions inferred for the r-type mylonite formation. The c-type mylonites could have formed in the late Caledonian as the extensional structures observed in them could easily have resulted by transposition of their fabrics during the late Caledonian extension. However, this does not explain the decrease in the dip of successive c-type mylonite bands and fault planes to the east (figure 4.6), which suggests that they formed in an extensional environment (section 4.6). A further problem with Caledonian generation of the c-type mylonites is the lack of a suitable source of fluids. It has been stated earlier that formation of the

Minch basin was probably late Caledonian rather than Permo-Triassic - if it was Permo-Triassic then it might be expected that there would have been reactivation of the existing structures on land.

7.9 Summary

A brief summary of the conditions of deformation, the fault rocks produced and associated events, is given in table 7.1, and a cartoon version of the history of the fault zone is presented in figure 7.6. An initial phase of compression gave rise to lower amphibolite r-type mylonites and an early phase of pseudotachylytes on Lewis (column 1, table 7.1 and figure 7.6*a*). This phase is attributed to the Laxfordian and represents temperatures of around 540 degrees C and depths of about 15km.

This was followed by a further phase of compression, attributed to the Caledonian orogeny, which occurred at much higher crustal levels (3 to 5 km depth, 90 to 150 degrees C). A wide zone of microbreccia, pervaded by sets of sub-horizontal fractures, formed (figure 7.6*b*). Subsidiary amounts of ultracataclasite and a late phase of pseudotachylyte (column 2, table 7.1) formed where deformation was more intense, or strain rate was higher.

The discrete fault planes and small amounts of

cataclasite formed during a post-Caledonian phase of extension (column 3, table 7.1, figure 7.6*c*), thought to be Devonian in age. After this, the c-type mylonites were generated as deformation continued (figure 7.6*d*) and Fe and Mg bearing fluids entered into the rocks, bringing about alteration of the existing fault rocks (figure 7.1; column 3, table 7.1) and causing veining as silica was removed from the forming c-type mylonites and precipitated in the fractures within the microbreccias (figure 7.4). This stage is tentatively ascribed to the Tertiary. Late stage (?late Tertiary) faulting then occurred, offsetting the earlier features in a sinistral sense.

Figure 7.1

Sequence of development of fault rocks within the Outer Hebrides Fault Zone, showing their relationships and conditions of formation.

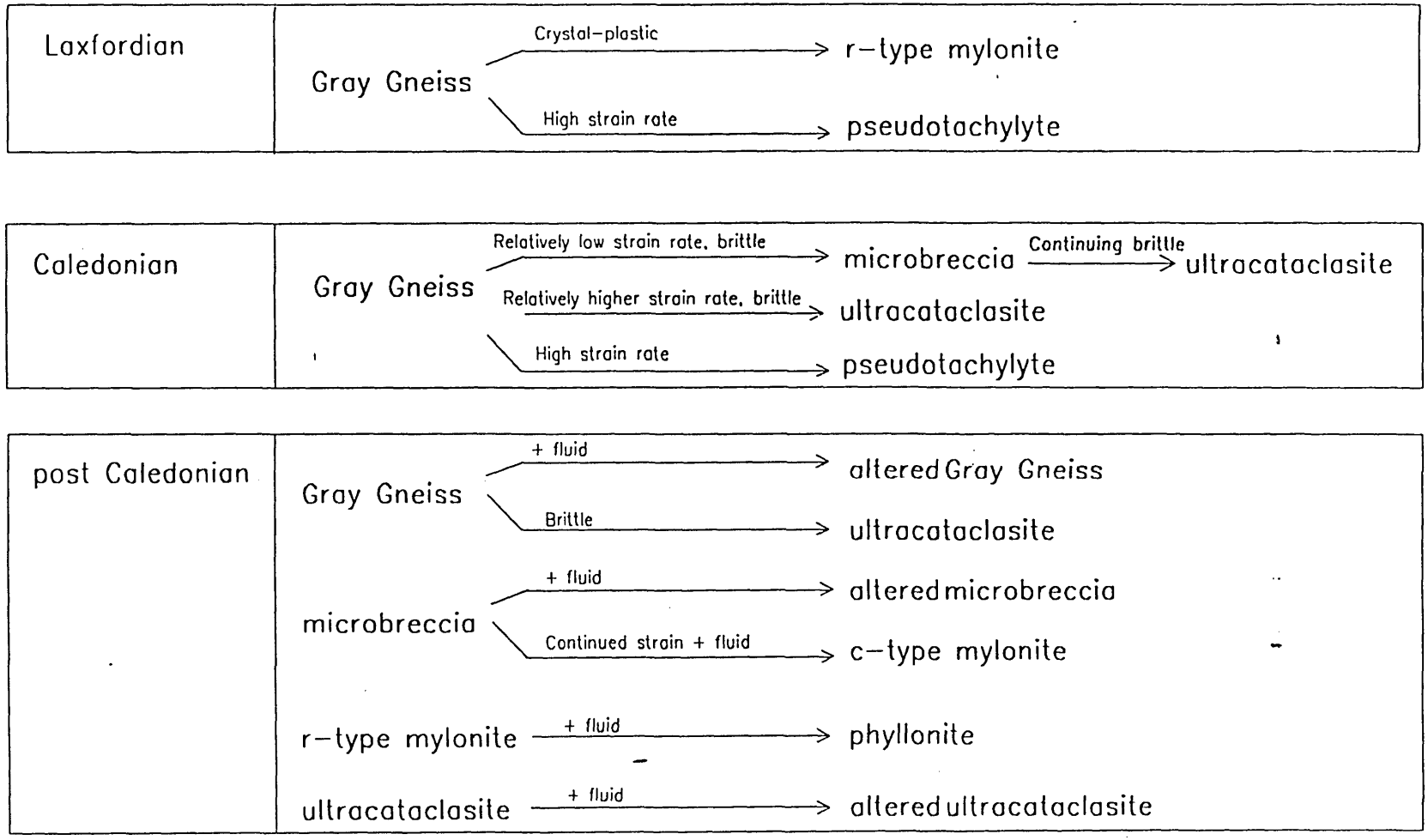

Laxfordian
Gray Gneiss
Crystal–plastic
r–type mylonite
High strain rate
pseudotachylyte
Caledonian
Gray Gneiss
Relatively low strain rate, brittle
microbreccia
Continuing brittle
ultracataclasite
Relatively higher strain rate, brittle
ultracataclasite
High strain rate
pseudotachylyte
post Caledonian
Gray Gneiss
+ fluid
altered Gray Gneiss
Brittle
ultracataclasite
microbreccia
+ fluid
altered microbreccia
Continued strain + fluid
c–type mylonite
r–type mylonite
+ fluid
phyllonite
ultracataclasite
+ fluid
altered ultracataclasite

Figure 7.2

Theoretical relative orientations for maximum dilatancy and fracture formation under compressional and extensional conditions, with respect to the principal stress directions. Dilatant cracks (fracture orientation) form approximately perpendicular to the direction of minimum stress (Brace et al., 1966). The intermediate principal stress direction is assumed to be roughly parallel to the strike of the fault zone, and is perpendicular to the page.

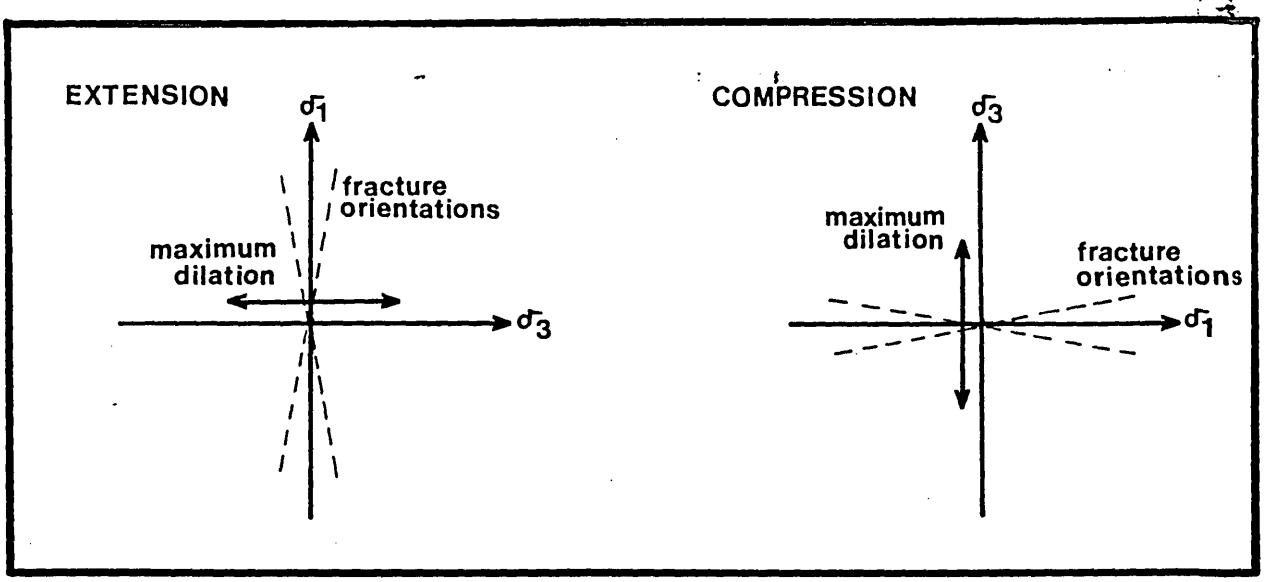

EXTENSION
σ1
fracture orientations
maximum dilation
σ3
COMPRESSION
σ3
maximum dilation
fracture orientations
σ1

Figure 7.3

Relationship between the orientation of gneissose foliation and the degree of brecciation developed within the microbreccia.

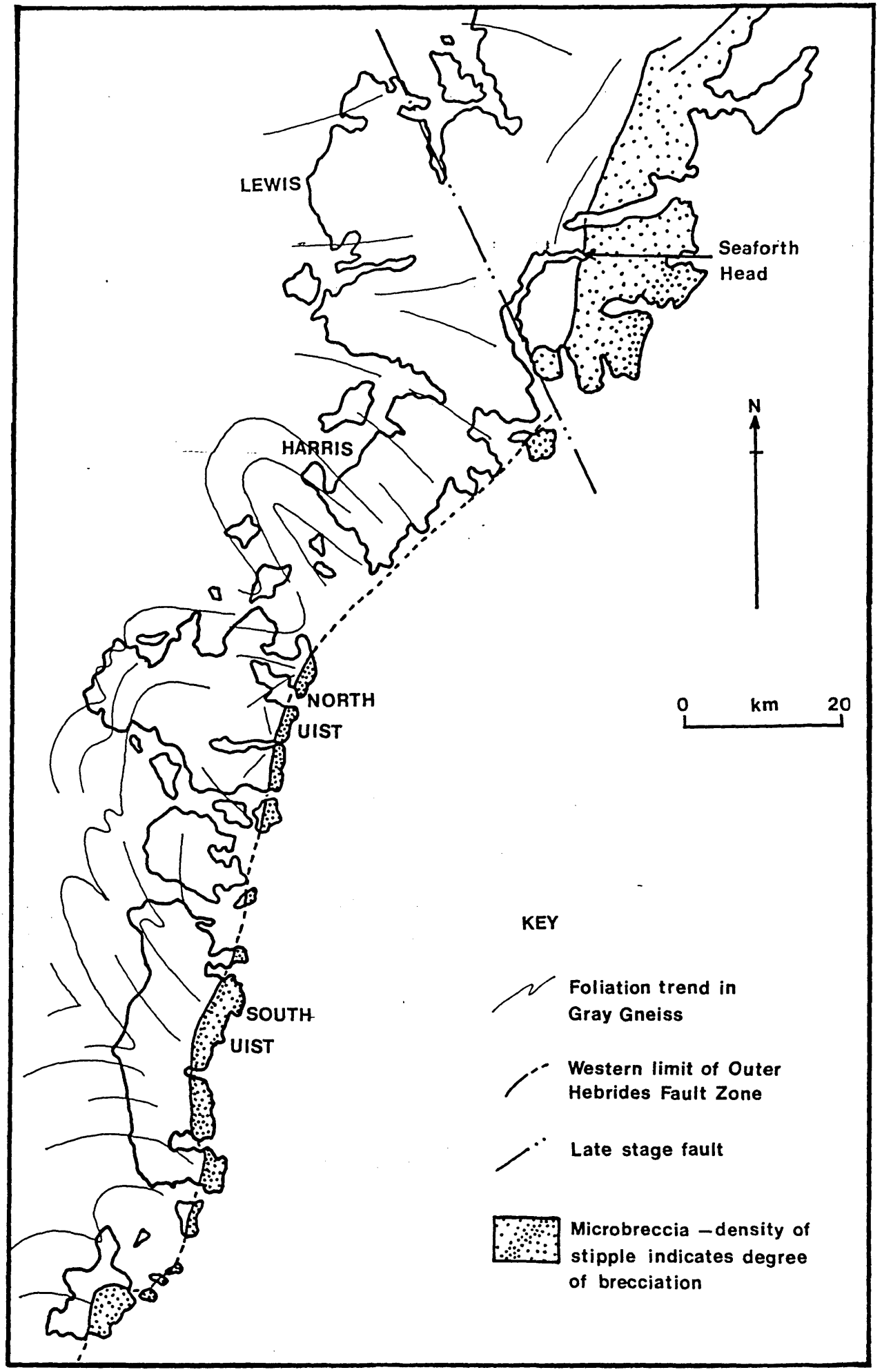
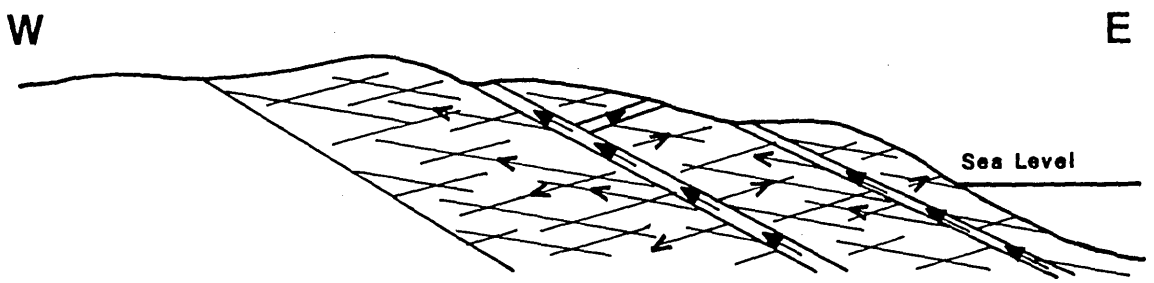

LEWIS
Seaforth Head
HARRIS
N
NORTH UIST
0 km 20
KEY
Foliation trend in Gray Gneiss
Western limit of Outer Hebrides Fault Zone
Late stage fault
Microbreccia —density of stipple indicates degree of brecciation
SOUTH UIST

Figure 7.4

Schematic representation of fluid flow in the Outer Hebrides Fault Zone. Cross-hatching denotes microbreccia, solid parallel lines denote c-type mylonite bands.



← ingress of Fe,Mg bearing fluid along developing c–type mylonite bands

← ingress of fluid into microbreccia fractures, bearing Si dissolved from c–type mylonite bands

Figure 7.5

Possible mechanisms for the outcrop of granulite facies rocks at higher structural levels than amphibolite facies rocks.

a Conventional model, in which thrusting of a layered crust results in granulite facies rocks at a higher structural level than amphibolite facies rocks.

b Alternative model, in which a granulite facies pod exists within amphibolite facies rock as a result of non-retrogression or differing bulk chemistry during metamorphism. Faulting can then produce granulite facies rocks at higher structural levels than amphibolite facies rocks. Note that motion along the fault plane in this model could be up-dip or down-dip.

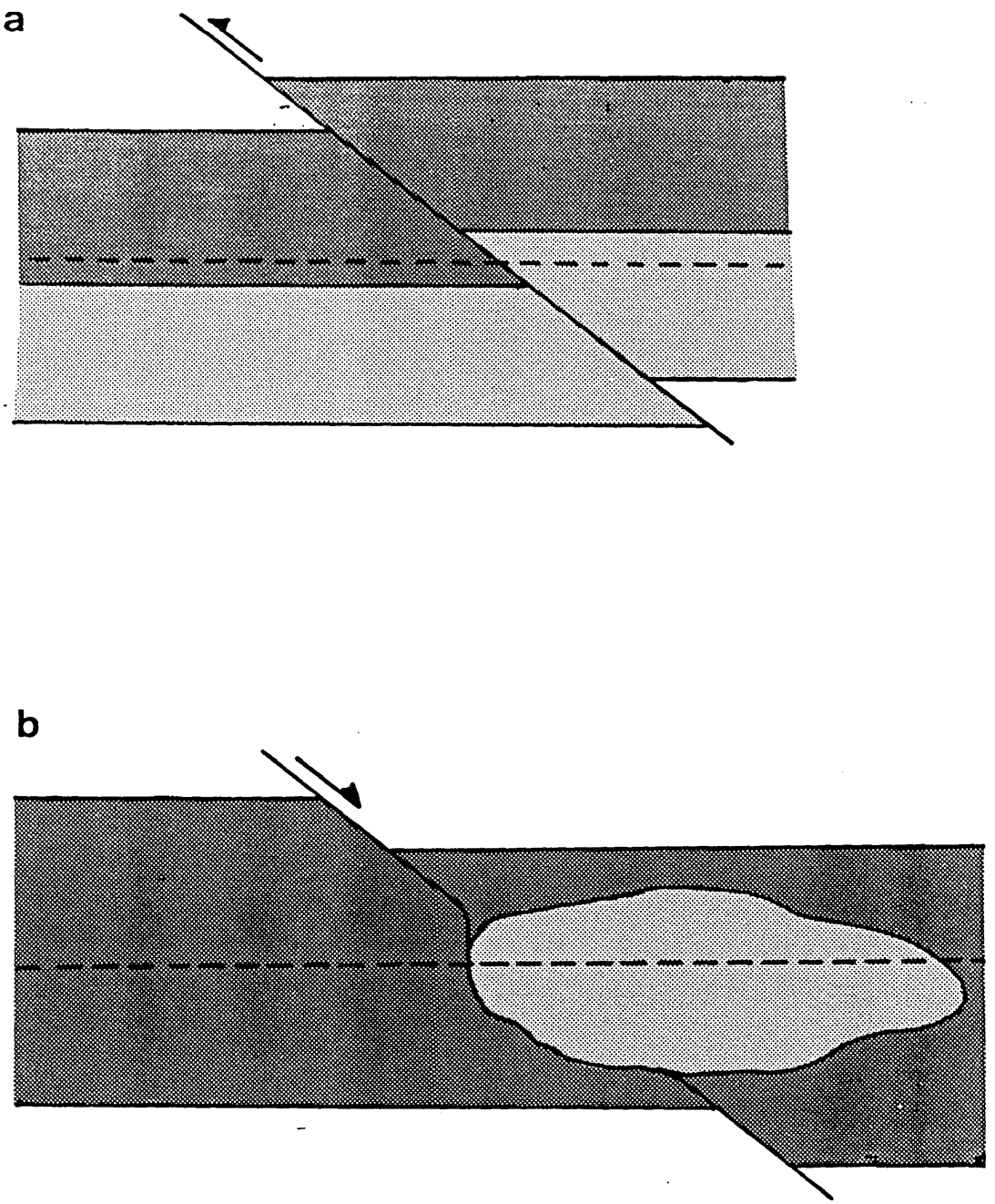

a
b
KEY
Amphibolite facies
Granulite facies
Present–day erosion level

Figure 7.6

Major stages in the evolution of the Outer Hebrides Fault Zone.

a Initial phase of compression, giving rise to r-type mylonites in Lewis, and the early phase of pseudotachylyte. Assigned to the Laxfordian

b Second phase of compression, producing microbreccias with sub-horizontal fractures, some ultracataclasite and the later phase of pseudotachylyte. Assigned to the Caledonian.

c Phase of extension, giving rise to discrete fault planes within the microbreccia, and small amounts of cataclasite. Assigned to the Devonian.

d Phase of extension, with increased availability of fluids. Formation of the c-type mylonite bands, alteration of pre-existing fault rocks, veining. Assigned to the Tertiary.

Full arrows - direction of compression/extension, half arrows - direction of fault movement, cross-hatching - microbreccia, dashes - c-type mylonite bands.

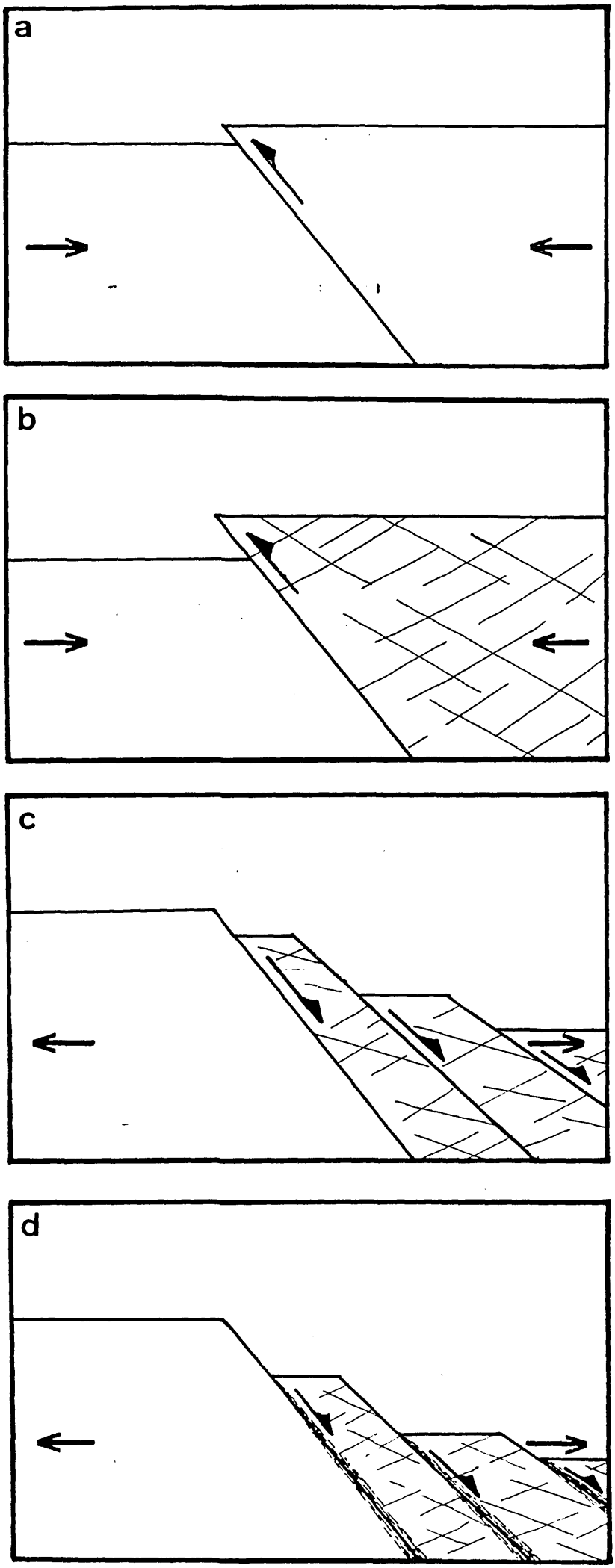

a
b
c
d

Table 7.1

Summary of the deformation history of the Outer Hebrides Fault Zone

Phase	**Laxfordian**	**Caledonian**	**post Caledonian**
Tectonic regime	compression, high P, high T	compression, low P, low T	extension, low P, low T
Fault rocks	r-type mylonites, early pseudotachylyte	microbreccia, ultracataclasite, late pseudotachylyte	c-type mylonites, ultracataclasite
Other events	cooling, jointing		alteration of microbreccias and ultracataclasites, veining, discrete faults

Chapter 8

Conclusions and Further Work

Conclusions

These are split into two sections. Firstly, there are those which apply to the fault zone as a whole, and secondly, those that apply to the formation of the fault rocks.

Fault Zone Conclusions

1. A minimum of three distinct movement phases can be identified within the fault zone. Two of these were compressional, and the third was extensional.

2. Conditions of deformation differed between the movement phases. One of the compressional phases occurred at high metamorphic grades (amphibolite facies), producing r-type mylonites. The other compressional phase was at lower temperatures and pressures, and gave rise to large volumes of microbreccia. The extensional phase is characterised by an introduction of fluids part way through, splitting it into two episodes, one predominantly under dry conditions and the other under wet conditions. The dry phase produced discrete fault planes in the microbreccia, and the introduction of fluids allowed development of c-type mylonites along these fault planes.

3. The movement phases can be arranged chronologically, and can be correlated with regional events. Thus, an early Laxfordian phase of compressionn was followed by a Caledonian phase of compression, which in turn was followed by post-Caledonian extension. The introduction of fluids may be Tertiary in age.

4. It is not necessary to have had thrust-sense faulting to juxtapose granulite-facies Corodale Gneiss and amphibolite-facies Gray Gneiss.

5. The discrete fault planes within the microbreccias must have formed during an extensional regime, as their dip decreases towards the hanging wall of the fault zone.

Fault Rock Conclusions

1. Fluid availability played an important part in the later development of fault rocks, giving rise to c-type mylonites and altered microbreccias.

2. The r-type mylonites formed under dry conditions by crystal plastic deformation. The microbreccias also formed under dry conditions, but resulted from brittle deformation. Pseudotachylyte was generated under both sets of conditions, during episodes of higher strain rates. The

c-type mylonites formed by brittle deformation under wet conditions.

3. It is possible to produce a foliation in fault rocks forming under brittle conditions. This is especially so if deformation is occurring when fluid is present.

4. Formation of r-type mylonites involved virtually no change in bulk composition when compared to the parent rock. C-type mylonite formation involved large bulk chemical changes when compared to parent rock.

5. The fluids involved in c-type mylonite formation were aqueous based and carried dissolved impurites of Fe and Mg. They were warmer than the surrounding rocks.

6. Silica was dissolved from the parent rock by the passage of these fluids as the c-type mylonites formed.

7. Fluids from the forming c-type mylonites passed into the microbreccias, sealing up the microcracks as they cooled and precipitated out their dissolved silica.

8. A minimum of 13 litres of fluid is required to have passed through each kg of parent rock to produce the c-type mylonites.

9. Deformation has not affected the composition of the amphiboles present in the fault rocks.

Suggestions for Further Work

1. Oxygen isotope ratios may help to decide the source of the fluids responsible for c-type mylonite formation. This, in turn, may help to resolve the problem of the age of this episode of faulting.

2. Further fieldwork, particularily in the South Uist/Barra region, may reveal more about the nature of the Corodale Gneiss/ Gray Gneiss boundary. The complex area between Seaforth Head and Stornoway might reveal something more about the early, high grade deformation, and the extent of the control it exerted over later faulting.

3. More detailed studies of the mineralogy of the fault rocks may enable more precise figures to be obtained for temperatures and/or pressures of deformation.

References

Alexander, G.B., Heston, W.M. and Iler, H.K. 1954. The solubility of amorphous silica in water. J. Phys. Chem. 58, 453-455..

Armour, A.R. 1977. A seismic refraction study of the crustal structure of northwest Scotland and the adjacent continental margin. Unpublished PhD thesis, University of Durham.

Bamford, D. 1979. Seismic constraints on the deep geology of the Caledonides of northern Britain. in: A.L. Harris, C.H. Holland and B.E. Leake (eds); The Caledonides of the British Isles - Reviewed. Spec. Publ. Geol. Soc. London 8, 43-96.

Bamford, D., Nunn, K., Prodehl, C. and Jacob, B 1978. LISPB:IV Crustal structure of northern Britain. Geophys. J. R. Astron. Soc. 54, 43-60.

Beach, A. 1976. The inter-relations of fluid transport, deformation, geochemistry and heat flow in early Proterozoic shear zones in the Lewisian complex. Phil. Trans. Roy. Soc. Lond. Ser. A 280, 569-604.

Beach, A. 1980. Retrogressive metamorphic processes in shear zones with special reference to the Lewisian complex. J. Struct. Geol. 2, 257-263.

Beach, A. and Fyfe, W.S. 1972. Fluid transport and shear zones at Scourie, Sutherland: evidence of overthrusting? Contribs. Mineral. and Petrol. 36, 175-180.

Binns, P.E., McQuillin, R. and Kenolty, N. 1974. The Geology of the Sea of the Hebrides. Rep. Inst. Geol. Sci. 73/14.

Blundell, D.J. 1984. Deformation of the Caledonide lithosphere of Northwest Scotland. Tectonophysics 109, 137-145.

Blundell, D.J., Hurich, C.A. and Smithson, S.B. 1985. A model for the MOIST seismic reflection profile, N. Scotland. J. Geol. Soc. Lond. 142, 245-258.

Bott, M.H.P., Armour, A.R., Himsworth, E.M., Murphy, T. and Wylie, G. 1979. An explosion seismology investigation of the continental margin west of the Hebrides, Scotland, at 58 degrees N. Tectonophysics 59, 217-231.

Bowes, D.R. and Hopgood, A.M. 1973. Framework of the Precambrian crystalline complex of Northwestern Scotland. in: Pidgeon, Macintyre, Sheppard and van Breeman (eds); Geochronology and isotope chronology of Scotland: Field Guide and Reference ECOG III.

Bowes, D.R., Barooah, B.C. and Khoury, S.G. 1971. Original nature of Archaean rocks of Northwest Scotland. Spec. Publ. Geol. Soc. Austral. 3, 77-92.

Brewer, J.A. and Smythe, D.K. 1984. MOIST and the continuity of crustal reflector geometry along the Caledonian-Appalachian orogen. J. Geol. Soc. Lond. 141, 105-120.

Brewer, J.A. and Smythe, D.K. 1986. Deep structure of the Foreland to the Caledonian Orogen, N.W. Scotland: results of the BIRPS WINCH profile. Tectonics 5, 171-195.

Brewer, J.A., Matthews, D.H., Warner, M.R., Hall, J., Smythe, D.K. and Whittington, R.J. 1983. BIRPS deep seismic reflection studies of the British Caledonides. Nature 305, 206-210.

Bridgwater, D., Watson, J. and Windley, B.F. 1973. The Archaean craton of the North Atlantic region. Phil. Trans. Roy. Soc. Lond. Ser. A 273, 493-512.

Brodie, K.H. and Rutter, E.H. 1985. On the relationship between deformation and metamorphism, with special reference to the behaviour of basic rocks. in: A.B. Thompson and D.C. Rubie (eds); Metamorphic reactions: Kinetics, textures and deformation. Springer-Verlag, New York. 138-179.

Bullerwell, W. 1965. Section 5, Geophysical Department. Mem. Geol. Surv. Summ. Prog. 1964, 84.

Butler, R.H.W. and Coward, M.P. 1984. Geological constraints, structural evolution, and deep geology of the northwest Scottish Caledonides. Tectonophysics 3, 347-365.

Cheadle, M.J., McGeary, S., Warner, M.R. and Matthews, D.H. 1987. Extensional structures on the Western UK continental shelf: a review of evidence from deep seismic profiling. in: M.P. Coward, J.F.Dewey and P.L. Hancock (eds); Continental extensional tectonics, Geol. Soc. Spec. Publ. 28 445-465.

Chesher, J.A., Smythe, D.K. and Bishop, P. 1983. The geology of the Minches. Inner Sound and Sound of Raasay. Rep. Inst. Geol. Sci. 83/6.

Cliff, R.A., Gray, C.M. and Huhma, H. 1983. A Sm-Nd isotopic study of the South Harris igneous complex. Contribs. Mineral. and Petrol. 82, 91-98.

Coward, M.P. 1969. The structural and metamorphic geology of South Uist, Outer Hebrides. Unpublished PhD thesis, University of London.

Coward, M.P. 1972. The eastern gneisses of South Uist. Scott. J. Geol. 8, 1-12.

Coward, M.P. 1973a. The structure and origin of areas of anomalously low intensity finite deformation in the basement gneiss complex of the Outer Hebrides. Tectonophysics 16, 117-140.

Coward, M.P. 1973b. Heterogeneous deformation in the development of the Laxfordian complex of South Uist, Outer Hebrides. J. Geol. Soc. Lond. 129, 139-160.

Coward, M.P. 1984. Major shear zones in the Precambrian crust; examples from NW Scotland and southern Africa and their significance. in: A. Kroner and S.R. Greiling (eds); Precambrian Tectonics Illustrated. Stuttgart. 207-235.

Coward, M.P. and Park, R.G. 1987. The role of mid-crustal shear zones in the Early Proterozoic evolution of the Lewisian. in: R.G. Park and J. Tarney (eds); Evolution of the Lewisian and comparable Precambrian High Grade Terrains. Geol. Soc. Spec. Publ. 27, 127-138.

Coward, M.P., Francis, P.W., Graham, R.H. and Watson, J.V. 1970. Large-scale Laxfordian structures of the Outer Hebrides in relation to those of the Scottish mainland. Tectonophysics 10, 425-435.

Coward, M.P., Francis, P.W., Graham, R.H., Myers, J.S. and Watson, J. 1969. Remnants of an early metasedimentary assemblage in the Lewisian complex of the Outer Hebrides. Proc. Geol. Assoc. 80, 387-408.

Davies, F.B., Lisle, R.J. and Watson, J. 1975. The tectonic evolution of the Lewisian complex in northern Lewis, Outer Hebrides. Proc. Geol. Assoc. 86, 45-61.

Dearnley, R. 1962. An outline of the Lewisian complex of the Outer Hebrides in relation to that of the Scottish mainland. Q.J.G.S. Lond. 118, 143-176.

Dearnley, R. 1963. The Lewisian complex of South Harris: with some observations on the metamorphosed basic intrusives of the Outer Hebrides, Scotland. Q.J.G.S. Lond. 119, 243-312.

Dearnley, R. and Dunning, F.W. 1968. Metamorphosed and deformed pegmatites and basic dykes in the Lewisian complex of the Outer Hebrides and their geological significance. Q.J.G.S. Lond. 123, 353-378.

Dickinson, B.B. 1974. The metamorphic evolution of the Leverburgh Supracrustal belt, South Harris, with special reference to textural variations. Unpublished PhD thesis, University of London.

Dickinson, B.B. and Watson, J. 1976. Variations in crustal level and geothermal gradient during the evolution of the Lewisian complex of NW Scotland. Precambrian Res. 3, 363-374.

Dougal, J.W. 1928. Observations on the Geology of Lewis (Outer Hebrides). Trans. Edin. Geol. Soc. 12, 12-18.

Enfield, M.A. and Coward, M.P. 1987. The structure of the West Orkney Basin, northern Scotland J. Geol. Soc. Lond. 144, 871-884.

Etheridge, M.A., Wall, V.J. and Vernon, R.H. 1983. The role of the fluid phase during regional metamorphism and deformation. J. Met. Geol. 1, 205-226.

Evans, C.R. 1965. Geochronology of the Lewisian basement near Lochinver, Sutherland. Nature 207, 54-56.

Evans, C.R. and Lambert, R.St.J. 1974. The Lewisian of Lochinver, Sutherland; the type area for the Inverian metamorphism. J. Geol. Soc. Lond. 130, 125-150.

Fettes, D.J. and Mendum, J.R. 1987. The evolution of the Lewisian complex in the Outer Hebrides. in: R.G. Park and J. Tarney (eds); Evolution of the Lewisian and comparable Precambrian High Grade Terrains. Geol. Soc. Spec. Publ. 27, 27-44.

Fettes, D.J., Mendum, J.R., Smith, D.I. and Watson, J.V. press. The Geology of the Outer Hebrides. Mem. Geol. Surv. U.K..

Fournier, R.O. and Rowe, J.J. 1966. Estimation of underground temperature from the silica content of water from hot springs and wet-stream wells. Am. J. Sci. 264, 685-697..

Francis, P.W. 1969. Some aspects of the Lewisian geology of the Isle of Barra and adjacent small islands. Unpublished PhD thesis, University of London.

Francis, P.W. 1972. The pseudotachylyte problem. Comments Earth Sci.: Geophys. 3, 35-53.

Francis, P.W. 1973. Scourian-Laxfordian relationships in the Barra Isles. J. Geol. Soc. Lond. 129, 161-189.

Francis, P.W. and Sibson, R.H. 1973. The Outer Hebrides Thrust. in: R.G. Park and J. Tarney (eds); The early Precambrian of Scotland and related rocks of Greenland 95-104, Geol. Dept., Univ. of Keele.

Francis, P.W., Moorbath, S. and Welke, H.J. 1971. Isotopic age data from Scourian intrusive rocks on the Isle of Barra, Outer Hebrides, north-west Scotland. Geol. Mag. 108, 13-22.

Gibbs, A.D. 1984. Structural evolution of extensional basin margins. J. Geol. Soc. Lond. 141, 609-620.

Graham, R.H. 1969. A structural analysis of the Lewisian rocks in parts of North Uist and the sound of Harris, Outer Hebrides. Unpublished PhD thesis, University of London.

Graham, R.H. 1980. The role of shear belts in the structural evolution of the South Harris igneous complex. J. Struct. Geol. 2, 29-37.

Greenberg, S.A. and Price, E.W. 1957. The solubility of silica in solutions of electrolytes. J. Phys. Chem. 61, 1539-1541..

Hall, J. 1978. 'LUST' - a seismic refraction survey of the Lewisian basement complex in NW Scotland J. Geol. Soc. Lond. 135, 555-563.

Hall, M.G. and Lloyd, G.E. 1981. The SEM examination of geological samples with a semi-conductor back-scattered electron detector. Am. Mineral. 66, 362-368.

Hall, S.H. 1983. The Post-Alpine tectonic evolution of S.E. Spain and the structure of fault gouges. Unpublished PhD thesis, University of London.

Hamilton, P.J., Eversen, N.M., O'Nions, R.K. and Tarney, J. 1979. Sm-Nd systematics of Lewisian gneisses: implications for the origin of granulites. Nature 277, 25-28.

Heddle, M.F. 1888. notes in: "A vertebrate Fauna of the Outer Hebrides" by J.A. Harrier-Brown and T.E. Buckley.

Higgins, M.W. 1971. Cataclastic rocks. Prof. Paper U.S. Geol. Surv. 687.

Holland H.D. and Malinin, S.D. 1979. Solubility and occurrence of non ore minerals in: H.L. Barnes (ed.); The Geochemistry of hydrothermal ores. J. Wiley and sons, 2nd edition, 461-508.

Holland, J.G. and Lambert, R.St.J. 1973. Comparative major element geochemistry of the Lewisian of Scotland. in: R.G. Park and J. Tarney (eds); The early Precambrian of Scotland and related rocks of Greenland. University of Keele.

Hopgood, A.M. 1964. Unpublished PhD thesis, University of St. Andrews.

Hopgood, A.M. 1971. Structure and tectonic history of Lewisian Gneiss, Isle of Barra, Scotland. Kristalinikum 7, 27-60.

Hopgood, A.M. and Bowes, D.R. 1972. Application of Structural Sequence to the Correlation of Precambrian Gneisses, Outer Hebrides, Scotland. Bull. Geol. Soc. Amer. 83, 107-128.

Horsley, R.J. 1978. Geochemistry of meta-igneous rocks from the South Harris complex, Outer Hebrides. Unpublished PhD thesis, University of London.

Humphries, F.J. and Cliff, R.A. 1982. Sm-Nd dating and cooling history of Scourian granulites, Sutherland Nature 295, 515-517.

Hussain, A. and Hipkin, R.G. 1981. Bouguer anomaly map of the British Isles, northern sheet. University of Edinburgh, Edinburgh.

Hutton, V.R.S., Ingham, M.P. and Mhipom, E.W. 1980. An electrical model of the crust and upper mantle in Scotland. Nature 287, 30-33.

Institute of Geological Sciences 1972. Aeromagnetic map of Great Britain Sheet 1, scale 1:625 000. London.

Jehu, T.J. and Craig, R.M. 1923. Geology of the Outer Hebrides, part I, the Barra Isles. Trans. Roy. Soc. Edin. 53, 419-441.

Jehu, T.J. and Craig, R.M. 1925. Geology of the Outer Hebrides, part II, South Uist and Eriskay. Trans. Roy. Soc. Edin. 53, 615-641.

Jehu, T.J. and Craig, R.M. 1926. Geology of the Outer Hebrides, part III, North Uist and Benbecula. Trans. Roy. Soc. Edin. 54, 467-489.

Jehu, T.J. and Craig, R.M. 1927. Geology of the Outer Hebrides, part IV, South Harris. Trans. Roy. Soc. Edin. 55, 457-488.

Jehu, T.J. and Craig, R.M. 1934. Geology of the Outer Hebrides, part V, North Harris and Lewis. Trans. Roy. Soc. Edin. 57, 839-874.

Jones, E.J.W. 1978. Seismic evidence for sedimentary troughs of Mesozoic age on the Hebridean continental margin. Nature 272, 789-792.

Jones, E.J.W. 1981. Seismic refraction shooting on the continental margin west of the Outer Hebrides, northwest Scotland. J. Geophys. Res. 86, 11553-11574.

Jones, E.J.W., White, R.S., Hughes, V.J., Matthews. D.H. and Clayton, B.R. 1984. Crustal structure of the continental shelf off northwest scotland from two-ship seismic experiments. Geophysics 49, 1605-1621.

Kerrich, R. 1986. Fluid infiltration into fault zones: Chemical, isotopic and mechanical effects. Pure and Appl. Geophys. 124 1/2, 225-269.

Kerrich, R. and Hyndman, D. 1986. Thermal and fluid regimes in the Bitterroot lobe - Sapphire block detachment zone, Montana: evidence from 18 O/16 O and geological relations. Bull. Geol. Soc. Amer. 97, 147-155.

Kerrich, R., La Tour, T.E. and Willmore, L. 1984. Fluid participation in deep fault zones: evidence from geological, geochemical and 18 O/16 O relations. J. Geophys. Res. 89 B6, 4331-4343.

Knopf, E.B. 1931. Retrogressive metamorphism and phyllonitization Part 1. Am. J. Sci. 121, 1-27.

Krauskopf, K.B. 1956. Dissolution and precipitation of silica at low temperatures. Geochim. Cosmochim. Acta 10, 1-26..

Kursten, M. 1957. The metamorphic and tectonic history of parts of the Outer Hebrides. Trans. Edin. Geol. Soc. 17, 1-31.

Lambert, R.St.J., Myers, J.S. and Watson, J.V. 1970. An apparent age for a member of the Scourie dyke suite in Lewis, Outer Hebrides. Scott. J. Geol. 6, 214-220.

Lapworth, C. 1885. The highland controversy in British geology: its causes, course and consequence. Nature 32, 558-559.

Leake, B.E. 1978. Nomenclature of Amphiboles. Canadian Mineralogist 16, 501-520.

Lisle, R.J. 1974. The applications of methods of structural analysis to the study of the basement complex in north-west Lewis. Unpublished PhD thesis, University of London.

Lisle, R.J. 1986. Sinistral strike-slip faulting in the Minch deduced from the trend of the Scourie Dyke swarm. Abstract for poster for Strike-slip tectonics and sedimentation conference, TSG/BSRG, Univ. College, Swansea.

Livingstone, A. 1963. Geochemical studies of ultrabasic rocks from the Outer Hebrides. Unpublished PhD thesis, University of Manchester.

Livingstone, A. 1967. A garnet peridotite and a garnet-amphibole pyroxenite from S. Harris, Outer Hebrides, and their bearing on the South Harris eclogite facies status. Min. Mag. 36, 380-388.

Lloyd, G.E. 1985. Review of instrumentation, techniques and applications of SEM in mineralogy. in: J.C. White (ed); Short course in applications of electron microscopy in the earth sciences. Short Course Handbook 11, 151-188.

Lowman, P.D. 1984. Formation of the earliest continental crust: inferences from the Scourian Complex of Northwest Scotland and geophysical models of the lower continental crust. Precambrian Res. 24, 199-205.

MacCulloch, J. 1819. A description of the Western Isles of Scotland, including the Isle of Man. 3 vols. Hurst, Robinson and co, London; Archibald, Constable and co, Edinburgh (XV, 578p;VII, 589p; plates and maps).

Macintyre 1973. Lower Tertiary Geochronology of the North Atlantic Continental Margins. in: Pidgeon, Macintyre, Sheppard and van Breeman (eds); Geochronology and Isotope Chronology of Scotland: Field Guide and Reference ECOG III.

Maddock, R.H. 1986. The petrology and geological significance of some fault generated pseudo-tachylites. Unpublished PhD thesis, University of London.

Matthews, D.H. and Cheadle, M.J. 1986. Deep reflections from the Caledonides and Variscides west of Britain and comparison with the Himalayas. in: M. Barazangi and M.L. Brown (eds); Reflection seismology; a global perspective. Am. Geophys. Union, Geodynamics Series 13, 5-19.

McCaig, A.M. 1984. Fluid-rock interaction in some shear zones from the Pyrenees. J. Met. Geol. 2, 129-141.

McCaig, A.M. 1987. Deformation and fluid-rock interaction in metasomatic dilatant shear bands. in: H.J. Zwart, M. Martens, I. van der Molen, C.W. Passchier, C. Spiers and R.L.M. Vissers (eds); Tectonic and structural processes on a Macro-, Meso-,and Micro-scale. Tectonophysics 135, 121-132.

McGeary, S. and Warner, M.R. 1985. Seismic profiling the continental lithosphere. Nature 317, 795-797.

McQuillin, R. and Binns, P.E. 1973. Geological structure in the Sea of the Hebrides. Nature Phys. Sci. 241, 2-4.

McQuillin, R. and Watson, J. 1973. Large scale basement structures of the Outer Hebrides in the light of geophysical evidence. Nature Phys. Sci. 245, 1-3.

Moorbath, S. 1973. The bearing of Lead Isotope Studies on the Evolution of the Lewisian Basement Complex of Northwest Scotland. in: Pidgeon, Macintyre, Aftalion and van Breeman (eds); Geochronology and Isotope Chronology of Scotland: Field Guide and Reference, ECOG III.

Moorbath, S., Powell, J.L. and Taylor, P.T. 1975. Isotopic evidence for the age and origin of the "gray gneiss" complex of the Southern Outer Hebrides, Scotland. J. Geol. Soc. Lond. 131, 213-222.

Moorbath, S., Welke, H. and Gale, N.H. 1969. The significance of lead isotope studies in ancient, high-grade metamorphic basement complexes, as exemplified by the Lewisian rocks of Northwest Scotland. E.P.S.L. 6, 245-256.

Myers, J.S. 1968. The tectonic and metamorphic history of the Lewisian Migmatite Complex of Western Harris, Outer Hebrides, Scotland. Unpublished PhD thesis, University of London.

Myers, J.S. 1971. The late Laxfordian granite-migmatite complex of Western Harris, Outer Hebrides. Scott. J. Geol. 7, 254-284.

Nature Conservancy Council 1977. Outer Hebrides - localities of Geological and Geomorphological Importance. Geology and Physiography Section.

O'Hara, M.J. 1961. Petrology of the Scourie dyke, Sutherland. Min. Mag. 32, 848-865.

Palmer, K. 1971. Comparative study of two PreCambrian Gneiss areas: the Suportoq region, East Greenland and South Harris, Outer hebrides, and their bearing on PreCambrian crustal evolution. Unpublished PhD thesis, University of Birmingham.

Park, R.G. 1970. Observations on Lewisian chronology Scott. J. Geol. 6, 379-399.

Park, R.G. and Tarney, J. 1987. The Lewisian complex: a typical Precambrian high-grade terrain? in: R.G. Park and J. Tarney (eds); Evolution of the Lewisian and comparable Precambrian High Grade Terrains. Geol. Soc. Spec. Publ. 27, 13-25.

Passchier, C.W. 1982. Pseudotachylyte and the development of ultramylonite bands in the Saint-Barthelemy Massif, French Pyrenees. J. Struct. Geol. 4, 69-79.

Peach, B.N. and Horne, J. 1930. Chapters on the Geology of Scotland. Oxford Univ. Press, London 232pp.

Peddy, C. P. 1984. Displacement of the Moho by the Outer Isles Thrust shown by seismic modelling. Nature 312, 628-630.

Pidgeon, R.T. and Aftalion, M. 1972. The geochronological significance of discordant U-Pb ages of oval-shaped zircons from a Lewisian gneiss from Harris. E.P.S.L. 17, 269-274.

Roberts, D.G., Hunter, P.M. and Laughton, A.S. 1977. Bathymetry of the Northeast Atlantic, Sheet 2 1:2.4 million. Hydrogr. Dept., Taunton.

Rutter, E.H. 1986. On the nomenclature of mode of failure transitions in rocks. Tectonophysics 122, 381-387.

Rutter, E.H. and Brodie, K.H. 1985. The permeation of water into hydrating shear zones. in: A.B. Thompson and D.C. Rubie (eds); Metamorphic reactions;kinetics, textures and deformation. Springer-Verlag, New York, 242-250.

Sheraton, J.W. 1970. The origin of the Lewisian gneisses of Northwest Scotland, with particular reference to the Drumbeg area, Sutherland. E.P.S.L. 8, 301-310.

Sibson, R.H. 1975a. Generation of pseudotachylyte by ancient seismic faulting. Geophys. J. R. Astron. Soc. 43, 775-794.

Sibson, R.H. 1975b. Seismic pumping - a hydrothermal fluid transport mechanism. J. Geol. Soc. Lond. 131, 653-659.

Sibson, R.H. 1977a. Fault rocks and fault mechanisms. J. Geol. Soc. Lond. 133, 191-213.

Sibson, R.H. 1977b. The Outer Hebrides Thrust: its structure, mechanism and deformation environment. Unpublished PhD thesis, University of London.

Sibson, R.H. 1977c. Kinetic shear resistance, fluid pressures and radiation efficiency during seismic faulting. Pure and Appl. Geophys. 115, 387-400.

Siever, R. 1962. Silica solubility, 0 - 200 C and the diagenesis of siliceous sediments. J. Geol. 70, 127-150..

Simpson, C. and Schmidt, S.M. 1983. An evaluation of criteria to deduce the sense of movement in sheared rocks. Bull. Geol. Soc. Amer. 94, 1281-1288.

Skinner, A.C. 1970. Geochemical studies of the Lewisian of NW Scotland and comparable rocks in E. Greenland. Unpublished PhD thesis, University of Birmingham.

Smith, P.J. and Bott, M.H.P. 1975. Structure of the crust beneath the Caledonian foreland and Caledonian belt of the north Scottish Shelf region. Geophys. J. R. Astron. Soc. 40, 187-205.

Smythe, D.K. 1980. The deep structure of the Moine and Outer Isles Thrusts north of Cape Wrath and Lewis. Geophys. J. R. Astron. Soc. 61, 199.

Smythe, D.K. 1982. Results of the Moine and Outer Isles Seismic Traverse (MOIST). Abstract in Newsl. Geol. Soc. Lond. 11, 11.

Smythe, D.K. 1987. Deep seismic reflection profiling of the Lewisian foreland. in: R.G. Park and J. Tarney (eds); Evolution of the Lewisian and comparable Precambrian High Grade Terrains. Geol. Soc. Spec. Publ. 27, 193-203.

Smythe, D.K., Dodinson, A., McQuillin, R., Brewer, J.A., Matthews, D.H., Blundell, D.J. and Kelk, B. 1982. Deep structure of the Scottish Caledonides revealed by the Moist reflection profile. Nature 299, 338-340.

Soldin, S.R. 1977. The tectonic evolution and geochemistry of the Lewisian complex of North Harris. Unpublished PhD thesis, University of London.

Soldin, S.R. 1978. The tectonic evolution and geochemistry of the Lewisian complex of North Harris Unpublished PhD thesis, University of London.

Steel, R.J. and Wilson, A.C. 1975. Sedimentation and tectonism (?Permo-Triassic) on the margin of the North Minch basin, Lewis. J. Geol. Soc. Lond. 131, 183-202.

Sutton, J. 1963. Long-term cycles in the evolution of the continents. Nature 198, 731-735.

Sutton, J. and Watson, J. 1951. The pre-Torridonian metamorphic history of the Loch Torridon and Scourie areas in the northwest Highlands, and its bearing on the chronological classification of the Lewisian. Q.J.G.S. Lond. 106, 241-307.

Tarney, J. 1963. Assynt dykes and their metamorphism. Nature 199, 672-674.

Van Breeman, O., Aftalion, M. and Pidgeon, R.T. 1971. The age of the granitic injection complex of Harris, Outer Hebrides. Scott. J. Geol. 7, 139-152.

Watson, J. 1968. Post-Scourian metadolerites in relation to Laxfordian deformation in Great Bernera, Outer Hebrides. Scott. J. Geol. 4, 53-67.

Watson, J. 1969. The pre-Cambrian gneiss complex of Ness, Lewis, in relation to the effects of Laxfordian regeneration. Scott. J. Geol. 5, 269-285.

Watson, J. 1975. The Lewisian complex. in: A.L. Harris, R.M. Shackleton, J. Watson, W.B. Harland, and S. Moorbath (eds); A correlation of PreCambrian rocks in the British Isles Spec. Rep. Geol. Soc. London 6, 15-29.

Watson, J.V. 1973. Effects of reworking on high-grade gneiss complexes. Phil. Trans. Roy. Soc. Lond. Ser. A 273, 443-455.

Watson, J.V. 1977. The Outer Hebrides: a geological perspective. Proc. Geol. Assoc. 88, 1-14.

Watterson, J. 1978. Proterozoic intraplate deformation in the light of southeast Asian neotectonics. Nature 273, 636-640.

Weaver, B.L. and Tarney, J. 1980. Rare-earth geochemistry of Lewisian granulite-facies gneisses, northwest Scotland: implications for the petrogenesis of the Archaean continental crust. E.P.S.L. 51, 279-296.

Wenk, H.R. 1987. Are pseudo-tachylites products fracture or fusion? Geology 6, 507-511.

Wernicke, B. 1986. Whole-lithosphere normal simple shear: an interpretation of deep reflection profiles in Great Britain. in: M. Barazangi and M.L. Brown (eds); Reflection seismology: the continental crust Am. Geophys. Union. Geodynamics Series 14, 331-339.

White, R.S., Jones, E.J.W., Hughes, V.J. and Matthews, D.H. 1982. Crustal structure from two-ship multichannel seismic profiles on the continental shelf off northwest Scotland. Tectonophysics 90, 167-178.

White, S.H. 1982. Fault rocks of the Moine Thrust Zone: a guide to their nomenclature. Textures and Microstructures 4, 211-221.

White, S.H. and Glasser, J. 1987. The Outer Hebrides Fault Zone: Evidence for normal movements. in: R.G. Park and J. Tarney (eds); Evolution of the Lewisian and comparable Precambrian High Grade Terrains, Geol. Soc. Spec. Publ. 27, 175-183.

White, S.H. and Huggett, J.M. 1984. The use of back scattered electron imaging for the petrographic study of sandstones and shales. J. Sed. Pet. 54, 487-494.

White, S.H., Bretan, P.G. and Rutter, E.H. 1986. Fault zone reactivation; kinematics and mechanisms. in: H.G. Reading, J. Watterson and S.H. White (eds); Major crustal lineaments and their influence on the geological history of the continental lithosphere, Phil. Trans. Roy. Soc. London Series A 317, 81-92.

Whittow, J.B. 1979. Geology and Scenery in Scotland. Penguin Books, Middlesex 362pp.

Wise, D.U., Dunn, D.E., Engelder, J.T., Geiser, P.A., Hatcher, R.D., Kish, S.A., Odom, A.L. and Schamel, S. 1984. Fault related rocks; suggestions for terminology. Geology 12, 391-394.

Witty, G.J. 1975. The Geochemistry of the Roneval anorthosite, South HArris, Scotland. Unpublished PhD thesis, University of London.

Zeck, H.P. 1974. Cataclasites, hemiclasites, holoclasites, blastoclasites and myloblastites; cataclastic rocks. Am. J. Sci. 274, 1064-1073.

Appendix I: Amphibole Analyses

These were carried out on standard polished, carbon coated electron microprobe sections, using energy dispersive spectrometry (EDS). The instrument used was a Jeol 733 Superprobe because of its back-scattered facility and superior imaging as compared to the Cambridge Instruments, Microscan. A set of standards was analysed at the start of each session to check machine calibration. The compositions of amphiboles from a variety of rock types are presented below.

C = Corodale Gneiss
CMB = Corodale Gneiss derived microbreccia
GG = Gray Gneiss
GGMB = Gray Gneiss derived microbreccia
RAGG = Retrogressed/altered Gray Gneiss
RAMB = Retrogressed/altered Gray Gneiss derived microbreccia
RMYL = R-type mylonite

SAMPNO	BT1/2	BT1/3	BT1/3	BT1/4	BT1/4	BT1/5	BT1/6	BT1/7	BT1/8	BNHT5/3	
ROCKTYP	C	C	C	C	C	C	C	C	C	CMB	
SIO2	39.55	58.99	40.97	56.19	40.21	53.14	50.37	41.68	43.86	38.43	SIO2
AL2O3	12.55	19.88	10.87	5.20	10.21	22.92	23.37	12.16	10.83	17.33	AL2O3
MGO	10.55	0.00	9.84	13.58	9.26	2.09	2.31	9.01	9.39	14.82	MGO
MNO	0.34	0.06	0.52	0.21	0.08	0.09	0.01	0.27	0.36	0.12	MNO
CAO	8.63	4.30	10.02	10.73	10.31	0.33	0.41	10.92	11.16	0.12	CAO
NA2O	1.48	7.83	1.58	2.47	1.49	3.67	2.95	1.80	1.15	0.65	NA2O
K2O	0.77	2.43	0.99	0.18	0.96	6.88	7.78	1.18	1.15	9.60	K2O
TIO2	1.28	0.18	1.32	0.00	1.52	0.14	0.13	1.90	1.75	4.27	TIO2
TOTAL	94.97	94.90	92.08	98.67	89.00	93.09	91.37	96.16	96.61	97.85	TOTAL

SAMPNO	BNHT5/6	BNHT5/7	BNHT5/9	LST6/2	LST6/3	LST6/3	LST6/4A	LST6/5	LST6/8	ARDPT01	
ROCKTYP	CMB	CMB	CMB	CMB	CMB	CMB	CMB	CMB	CMB	GG	
SIO2	50.92	59.47	53.91	51.43	40.05	37.16	50.88	40.73	40.23	44.06	SIO2
AL2O3	19.05	13.24	14.73	4.73	15.14	21.30	3.50	13.47	12.51	9.91	AL2O3
MGO	8.23	6.36	10.62	15.77	10.37	6.42	14.49	11.46	11.08	10.61	MGO
MNO	0.15	0.02	0.11	0.26	0.27	1.75	0.42	0.05	0.97	0.36	MNO
CAO	0.46	0.92	0.21	13.20	11.32	5.73	11.95	11.69	11.55	11.86	CAO
NA2O	1.18	2.43	0.79	0.53	1.83	0.14	0.68	1.78	1.53	1.42	NA2O
K2O	6.48	4.52	6.80	0.21	2.67	0.00	0.44	2.72	2.61	1.59	K2O
TIO2	2.84	1.60	3.41	0.50	3.36	0.17	0.21	3.38	3.17	1.53	TIO2
TOTAL	98.10	100.34	99.18	98.58	97.10	97.14	94.98	97.75	95.67	97.19	TOTAL

SAMPNO	ARDPT01	ARDPT01	B6I/11	B6I/13	B6I/9A	EV1/2	EV1/3	EV1/4	EV1/5	EV1/6	
ROCKTYP	GG	GG	GG	GG	GG	GG	GG	GG	GG	GG	
SIO2	44.53	43.55	43.91	44.89	38.53	49.55	49.94	49.75	48.72	48.71	SIO2
AL2O3	9.52	9.43	10.44	10.09	15.72	5.59	6.41	5.99	5.60	6.39	AL2O3
MGO	10.42	10.73	10.51	10.92	12.72	14.95	14.75	15.34	14.68	14.64	MGO
MNO	0.38	0.53	0.44	0.41	0.10	0.35	0.34	0.18	0.18	0.26	MNO
CAO	11.53	11.36	11.49	11.67	0.07	10.55	11.58	11.84	11.42	11.55	CAO
NA2O	1.22	1.48	1.20	1.68	0.35	1.58	1.73	1.94	1.90	1.60	NA2O
K2O	1.46	1.36	1.33	1.34	9.73	0.46	0.46	0.37	0.45	0.48	K2O
TIO2	1.89	1.82	1.42	1.56	5.14	1.10	0.98	0.93	1.11	0.93	TIO2
TOTAL	96.76	95.99	96.64	99.40	97.52	97.56	99.59	99.34	96.88	97.81	TOTAL

SAMPNO	BT6/1	BT6/1	BT6/2	BT6/3	BT6/3	BT6/4	BT6/4	BT6/5	BT6/5	BT6/6	
ROCKTYP	GGMB	GGMB	GGMB	GGMB	GGMB	GGMB	GGMB	GGMB	GGMB	GGMB	
SIO2	38.03	38.04	43.12	44.44	43.43	40.92	44.24	42.74	42.83	42.87	SIO2
AL2O3	13.28	13.02	12.95	11.10	13.43	14.85	13.55	12.95	13.36	13.25	AL2O3
MGO	19.29	18.24	12.20	11.38	11.31	9.28	12.00	11.19	11.77	10.88	MGO
MNO	0.45	0.39	0.16	0.12	0.36	0.18	0.09	0.24	0.26	0.13	MNO
CAO	4.33	4.23	12.19	12.12	12.33	9.72	12.30	11.94	11.81	11.88	CAO
NA2O	0.44	0.32	2.15	1.56	1.60	1.48	2.29	1.19	1.91	1.48	NA2O
K2O	0.00	0.00	2.32	1.98	2.37	2.64	2.43	2.35	2.50	2.25	K2O
TIO2	0.04	0.00	2.07	2.03	2.28	2.04	2.23	2.50	2.37	2.27	TIO2
TOTAL	94.11	93.23	101.52	100.42	102.56	98.16	104.08	99.34	101.15	99.54	TOTAL

SAMPNO	BT6/6	BT6/7	BT6/7	BT6/8	BT6/8	NT1/1	NT1/2	NT1/3	NT1/4	NT4/14B	
ROCKTYP	GGMB	GGMB	GGMB	GGMB	GGMB	RAGG	RAGG	RAGG	RAGG	RAMB	
SIO2	43.57	43.48	43.22	42.42	44.98	41.10	41.12	41.63	41.81	37.74	SIO2
AL2O3	13.77	11.23	13.46	12.75	14.38	12.30	13.69	12.96	13.33	14.34	AL2O3
MGO	11.57	11.73	11.78	11.28	12.45	10.19	10.75	10.46	10.62	15.27	MGO
MNO	0.24	0.33	0.30	0.26	0.33	0.20	0.14	0.13	0.14	0.15	MNO
CAO	12.07	11.98	12.23	11.56	12.50	11.62	11.79	11.53	11.58	0.19	CAO
NA2O	2.04	1.81	2.05	1.79	2.10	1.82	1.82	1.64	1.74	1.74	NA2O
K2O	2.33	2.07	2.25	2.34	2.37	2.37	2.47	2.38	2.38	9.76	K2O
TIO2	2.38	2.41	2.48	2.00	2.45	2.44	2.43	2.13	2.58	0.61	TIO2
TOTAL	102.30	99.57	102.29	98.64	106.16	97.27	99.69	98.03	99.08	95.21	TOTAL

SAMPNO	NT4/23	NT8/1	NT8/3	13A/12	13B/1	13B/2	13B/3	13B/4	13B/5	13B/6	
ROCKTYP	RAMB	RAMB	RAMB	RMYL	RMYL	RMYL	RMYL	RMYL	RMYL	RMYL	
SIO2	53.94	45.07	48.55	41.29	42.52	42.49	38.88	42.09	43.61	44.96	SIO2
AL2O3	2.12	11.54	8.14	11.95	12.27	11.11	10.55	11.68	12.48	10.55	AL2O3
MGO	17.77	11.38	13.19	10.59	10.05	10.28	9.21	9.32	11.38	11.61	MGO
MNO	0.53	0.42	0.45	0.14	0.27	0.29	0.29	0.37	0.32	0.36	MNO
CAO	12.26	11.78	12.00	11.79	11.72	11.68	10.79	11.77	11.71	11.97	CAO
NA2O	0.68	2.29	1.70	1.26	1.69	1.01	1.04	0.94	1.28	0.87	NA2O
K2O	0.30	1.17	0.71	0.99	1.26	1.43	1.25	1.44	1.45	1.30	K2O
TIO2	0.15	1.13	1.45	1.06	1.42	1.33	0.99	1.46	1.33	1.42	TIO2
TOTAL	98.17	101.66	103.08	94.51	98.55	94.84	96.16	95.80	100.27	98.27	TOTAL

SAMPNO	13B/7	13B/8	13B/9	34A/1	34A/2	34A/3	34A/4	
ROCKTYP	RMYL	RMYL	RMYL	RMYL	RMYL	RMYL	RMYL	
SIO2	43.22	43.20	43.17	42.19	40.75	44.83	42.98	SIO2
AL2O3	11.73	12.31	11.81	12.85	12.71	12.76	13.83	AL2O3
MGO	10.20	10.73	10.45	9.35	9.14	11.07	10.07	MGO
MNO	0.30	0.36	0.44	0.46	0.47	0.31	0.47	MNO
CAO	11.61	11.79	11.44	11.79	14.82	12.40	12.18	CAO
NA2O	1.63	1.12	1.12	1.54	1.29	1.48	1.53	NA2O
K2O	1.25	1.42	1.28	1.98	1.73	1.82	1.94	K2O
TIO2	1.14	1.57	1.28	1.67	1.48	1.50	1.58	TIO2
TOTAL	98.18	98.31	96.39	102.31	98.45	102.39	100.39	TOTAL

Appendix II: Whole Rock Analyses

Rock samples were chosen to be representative of the various rock types. Each sample to be analysed was first split and crushed to 0.5 cm by jaw crusher, then ground to pass 200 mesh in a tungsten carbide Tema mill. Care was taken to avoid contamination between specimens. Loss on ignition (LOI) was then determined for each sample, and then a solution was prepared for analysis by an inductively coupled plasma (ICP) vacuum polychromator. A comparison of determination of volatile content between LOI and carbon-hydrogen-nitrogen (CHN) analysis wqs undertaken on selected samples. Error on the ICP results was determined in two ways - for each run of analyses, in-house standard reference materials and duplicate samples were analysed, and a precision run, to quantify machine and preparation error, was undertaken. Techniques and results are presented below.

Determination of Fluid

As already noted in chapter 6, the accurate determination of the fluid content of rocks is problematical. Two methods were utilised in this project, and neither proved entirely satisfactory. Firstly, loss on ignition (LOI) was determined for all samples; results are presented in this appendix. A value for LOI is obtained by heating the previously dried specimen to 950 C overnight, with the aim of driving off volatiles and converting all Fe^{2+} to Fe^{3+} in order that the whole rock Fe_2O_3 may be determined. There is some doubt as to whether this process completely dehydrates all amphiboles, and the presence of volatile elements (such as sulphur, chlorine and CO_2) in addition to H_2O, will also affect the results as they may be driven off and will be included with the measured total.

The second method used to determine fluid content was the CHN analyser, which quantifies the amounts of carbon, hydrogen and nitrogen present in a sample. Results are presented in table 1. Disadvantages of this method include the tiny sample size that must be used (6 milligrams), the fact that the calibration material was an organic substance resulting in calibration for levels far higher than those expected in the Hebridean rocks, and the relatively low temperature (660 degrees centigrade) at which the analysis is carried out. As a result, it is uncertain exactly what is being measured (only some structurally bound water, e.g. that in clay minerals, will come off). The inadequacies of the calibration method lead to a high degree of inaccuracy.

There is, however, a fairly good correlation in trend between the two methods, even though the total amounts

measured are obviously different - see table 1 for a comparison. It is therefore thought that, although the absolute values for fluids in the samples are unlikely to be accurate, the results are useful in reflecting the underlying trends. In the tabulation of whole rock results which concludes this appendix, the fluid values quoted are for LOI.

Determination of Whole Rock Chemistry

Analyses were performed by an ARL 34000 ICP vacuum polychromator. This is a relatively new method, and involves forming a plasma from the specimen in argon. This is done by stripping of electrons and the strength and position of lines on the resultant emission spectrum indicates quantities of each element present. Samples for analysis were prepared by a standard lithium metaborate fusion technique followed by solution in nitric acid. The resultant fluid was introduced into the ICP by a nebulizer at a natural (unpumped) rate of 0.7 ml min^{-1}. The stabilization time used was 20 s, with 3 x 5 s integration periods, the output being the average of these three readings.

The data processing methods were still being developed during the course of this project, and several changes have been made. Most importantly, more recently-run samples used a lithium normalisation routine to correct for short-term machine instabilities. This means that results from these runs are not always directly comparable with those done earlier.

The preparation is faster than that for X-Ray Fluorescence analysis, and the ICP measures the major and selected trace elements from a single solution. Ten major and eleven trace elements were measured: Si, Al, Fe (as Fe3+), Mg, Mn, Ca, Na, K, P, Ti, Ba, Be, Co, Cr, Cu, La, Ni, Sr, V, Zn and Zr.

Great care was taken with this technique to quantify error, both machine and preparation, within runs and between runs. The results of these determinations are presented in this Appendix.

PROCEDURE

Weigh 0.1000 $\pm$ 0.0001 g of dried, powdered sample, ground to pass a 200 mesh sieve, into a clean porcelain crucible and mix intimately with 0.300 g of lithium metaborate using a plastic stirring rod. Transfer the mixture completely, using a narrow spatula and a small brush, to a pre-ignited graphite crucible and fuse at 1000 C in an electric muffle furnace for 30 minutes. Carefully remove the crucible from the furnace and rotate it slowly

so that the molten bead swirls round inside the crucible combining with any smaller beads. Pour the red-hot bead into a 100 ml plastic beaker containing 50 ml of 0.4 HNO_3.

Dissolve the shattered bead by using amagnetic stirrer without any heat for 30 minutes. When the graphite crucible has cooled, examine it carefully to see if any small beads are adhering to the internal surfaces. If any are found, which only rarely happens, dislodge them with a spatula and add them to the solution in the beaker. Transfer this solution, when the bead has completely dissolved, to a clean 100 ml volumetric flask. Rinse the beaker thoroughly with deionised water and add the rinsings to the flask. Dilute to volume and shake well to mix. Filter the solution through a Whatman 12.5 cm No. 41 filter paper into a plastic bottle. Seal the bottle well with a piece of plastic under the cap.

NOTES:

1. The moisture content (H_2O^-) and loss on ignition (LOI) of samples must be determined before fusion of the samples for ICP analysis.

2. % H_2O^- is determined by heating the sample (about 4 gm, accurately weighed into a porcelain crucible) overnight at 110 C.

3. After the % H_2O^- has been determined, 0.2500 $\pm$ 0.0001 g of the dried sample is weighed into a clean porcelain crucible. This will then be used for the ICP preparation.

4. The remainder of the dried powder is then reweighed and the % LOI is determined on this portion. The % LOI is determined by heating the dried sample from room temperature to 950 C in a muffle furnace and keeping at 950 C overnight.

5. Before weighing samples after drying and ignition they must be allowed to cool to room temparature in a dessicator for at least 3 hours.

6. After use the porcelain crucibles are cleaned by washing with tap water and then boiled in 25 % HCl for about 5 minutes. They are then rinsed with deionised water and dried.

7. If the LOI of a sample is greater than 5 %, it must be fused for ICP analysis by inserting the graphite crucible containing the flux-powder mixture into a cold furnace which is then heated to 1000 C. Fusion is at 1000 C for 20 minutes.

8. Samples prepared for ICP analysis are numbered in a

manner consistent with XRF preparation numbers. Each sample is given a four figure analysis number which must lie between 2000 and 7990 and end with a zero. Duplicate preparations are given the same numbers as the original sample, but ending with a 3 instead of a zero; a second duplicate will have the same number but ending with a 6. Replicate analyses of the same sample are given the original number increased by 1; a second replicate will have the the original number increased by 2.

9. In every set of 30 samples at least 4 in-house reference materials must be included. A blank solution and at least five duplicate preparations must also be analysed together with the main batch of samples. (Total number of unknown solutions analysed = 40).

10. For every set of samples the recommended running order and maximum total number of solutions (81) must be adhered to. If there are more than 30 samples to be analysed, another ICP run must be undertaken.

11. A set of 14 samples can be analysed as a "1/2 run" group. The analysis will also include a blank, 3 duplicates and 2 in-house reference materials. (Total number of unknown solutions analysed = 20). Total number of solutions = 45.

12. One in-house reference material must be included in every group of 10 solutions when analysis is undertaken.

Use the following running order for the solutions.

	No. of solutions
Blank	1
Drift	1
Standards	10
Blank	1
Drift	1
Samples	10
Std + 2000 ppm	1
Drift	1
Samples	10
Blank	1
Drift	1
Standards	5
Blank	1
Drift	1
Samples	10
Std + 4000 ppm	1
Drift	1
Samples	10
Blank	1

Drift	1
Standards	10
Blank	1
Drift	1

Standards used are:-

BR	9010	UB-N	9060
GA	9020	NIM-G	9070
GH	9030	DTS-1	9080
NIM-N	9040	AN-G	9090
SY-2	9050	MICA-MG	9100

The underlined standards are run in the middle of the procedure.

Blank is designated 9000.
Drift is designated 9999.

Full run uses 81 solutions.
Half run uses the first 45 solutions.

Table 1

Comparison of Values Obtained for Volatile Content of Selected Rocks as Measured by CHN Analyser and Loss On Ignition

Sample number	$H_2O + CO_2$*	LOI
BNH2/6	0.67	0.29
CNHc	2.24	2.22
CNH02	1.45	1.25
CNH04	2.38	1.74
BV05	1.72	1.54
BV07	3.69	3.67
BV08	2.52	2.41
BV09	1.99	1.86
BV10	3.27	3.09
EV04	1.49	1.06
GS01	0.49	0.29

* as determined using the CHN analyser

Whole rock analyses by ICP

SAMPNO	SH01	BQ03	BQ05	BQ06	BQ07	CR01	CR01R	CR02	CR08	CR08R	
SIO2	65.53	48.94	47.65	48.40	49.70	50.04	49.92	47.07	45.95	45.72	SIO2
AL2O3	15.12	16.36	9.71	16.49	14.37	12.09	12.15	10.15	11.39	11.30	AL2O3
FE2O3T	5.15	12.50	16.85	12.81	12.57	12.48	12.42	14.58	16.18	16.09	FE2O3T
MGO	2.57	6.40	9.97	5.83	7.09	10.19	10.07	12.27	8.67	8.62	MGO
MNO	0.08	0.20	0.31	0.18	0.21	0.19	0.20	0.24	0.16	0.16	MNO
CAO	5.53	9.61	9.24	8.61	11.57	10.40	10.25	11.07	11.82	11.77	CAO
NA2O	4.30	3.39	1.03	3.68	2.26	2.09	2.09	1.28	2.72	2.71	NA2O
K2O	1.17	1.06	1.29	1.42	0.36	1.08	1.07	1.17	0.65	0.67	K2O
P2O5	0.13	0.42	0.17	0.15	0.07	0.06	0.06	0.08	0.08	0.08	P2O5
TIO2	0.37	0.94	1.93	1.28	0.97	0.67	0.68	0.78	2.06	2.04	TIO2
LOI	0.72	1.16	1.48	0.86	0.71	0.76	0.76	0.95	0.65	0.65	LOI
TOTAL	99.95	99.82	98.14	98.85	99.16	99.29	98.91	98.69	99.68	99.16	TOTAL
TOT+LOI	100.67	100.98	99.62	99.71	99.87	100.05	99.67	99.64	100.33	99.81	TOT+LOI
BA	505	431	449	536	70	171	171	172	74	72	BA
BE	0.90	1.22	1.48	1.01	0.59	1.04	0.81	0.83	1.03	0.92	BE
CO	41.4	65.6	73.1	65.7	82.4	73.6	67.1	68.2	77.3	78.0	CO
CR	66.7	88.6	1074.0	23.0	126.5	825.0	824.6	998.3	79.9	84.5	CR
CU	25.9	38.9	7.8	27.9	82.0	37.9	29.2	13.1	58.2	56.6	CU
LA	13.7	39.0	5.8	19.3	-2.1	64.4	52.8	35.6	1.6	-6.8	LA
NI	40.6	25.8	237.0	10.6	74.1	264.1	254.3	396.5	205.6	206.5	NI
SR	371	472	54	417	159	145	145	63	289	288	SR
V	56.1	225.6	249.4	249.8	279.6	205.9	197.0	206.6	449.1	445.8	V
ZN	55.1	182.8	322.9	195.3	68.0	154.8	149.8	186.3	83.8	86.5	ZN
ZR	141.2	113.3	104.5	107.6	50.2	76.9	62.5	68.7	83.9	86.1	ZR

SH01 : R-type mylonite with later cataclasis, some alteration. First crags between B 8060 and Beinn Mheadhonach, Shildenish.
: Grid Reference NB 2982 1947

BQ03 : Basic Gray Gneiss, amphibolitic. Quarry on Gairbh-eilean, between Grimsay and North Uist.
: Grid Reference NF 8476 5885

BQ05 : Basic Gray Gneiss, amphibole and biotite. Quarry on Gairbh-eilean, between Grimsay and North Uist.
: Grid Reference NF 8479 5882

BQ06 : Basic/intermediate Gray Gneiss, amphibolitic. Quarry between Gairbh-eilean and North Uist.
: Grid Reference NF 8480 5881

BQ07 : Basic Gray Gneiss, garnet-bearing. Quarry on Gairbh-eilean, between Grimsay and North Uist.
: Grid Reference NF 8481 5880

CR01 : Basic/intermediate Gray Gneiss; hornblende-biotite-plagioclase-quartz-k feldspar. Stromban, North Uist.
: Grid Reference NF 9006 6829

CR02 : Basic Gray Gneiss, hornblendite pod. Stromban, North Uist.
: Grid Reference NF 9006 6829

CR08 : Basic Gray Gneiss, amphibolitic, en echelon epidote veins. Strumore, North Uist.
: Grid Reference NF 9093 6919

SAMPNO	CR09	GT05	M01	BT01	ET01	ET01R	LST07b	LST08	BNHT01	BNHT04	
SIO2	43.32	45.28	49.52	56.34	49.81	49.81	55.42	51.31	56.39	60.00	SIO2
AL2O3	12.65	12.67	13.69	16.27	14.06	14.01	18.59	19.89	18.27	18.83	AL2O3
FE2O3T	18.53	16.80	14.67	8.02	13.26	13.33	6.89	7.97	6.58	3.34	FE2O3T
MGO	6.50	8.49	6.37	4.43	6.46	6.49	3.19	3.65	2.31	1.56	MGO
MNO	0.15	0.27	0.22	0.12	0.19	0.19	0.12	0.10	0.09	0.06	MNO
CAO	13.04	9.87	10.33	6.64	9.34	9.46	5.75	7.46	4.70	4.10	CAO
NA2O	2.10	2.46	2.37	4.07	2.08	2.06	5.42	5.24	6.34	7.27	NA2O
K2O	0.62	1.56	0.54	1.62	1.36	1.35	1.68	1.26	3.25	2.11	K2O
P2O5	0.10	0.08	0.12	0.17	0.15	0.15	0.32	0.26	0.39	0.21	P2O5
TIO2	2.03	1.30	1.14	0.69	1.05	1.06	0.63	0.80	0.89	0.53	TIO2
LOI	1.26	1.07	0.28	1.65	1.96	1.96	1.52	1.78	0.65	0.60	LOI
TOTAL	99.04	98.78	98.97	98.37	97.77	97.91	98.01	97.94	99.21	98.15	TOTAL[1]
TOT+LOI	100.30	99.85	99.25	100.02	99.73	99.87	99.53	99.72	99.86	98.75	TOT+LOI
BA	65	191	158	417	405	410	1268	1154	1520	1134	BA
BE	0.95	1.20	0.68	1.19	0.67	0.82	0.97	0.58	1.81	0.60	BE
CO	90.7	55.4	73.8	49.8	49.9	52.0	29.2	33.0	55.7	36.6	CO
CR	24.6	250.1	145.7	121.2	178.7	191.4	38.9	18.0	31.8	32.4	CR
CU	438.3	36.0	111.7	20.6	126.7	125.2	55.0	22.9	29.7	39.4	CU
LA	-5.0	19.0	5.1	7.5	33.7	30.3	20.2	27.2	49.2	31.1	LA
NI	147.1	85.4	56.1	54.5	69.0	74.6	-22.7	12.8	-8.7	2.5	NI
SR	759	149	169	520	271	275	1418	1535	926	709	SR
V	564.5	331.3	321.3	146.6	280.6	293.7	97.9	155.1	97.5	34.0	V
ZN	82.1	236.7	134.6	104.5	113.4	112.8	86.0	68.0	92.5	29.7	ZN
ZR	68.3	69.2	69.1	80.0	68.8	73.5	29.9	25.8	264.3	333.8	ZR

CR09 : Gray Gneiss, amphibolitic, slight alteration and epidotisation. Strumore, North Uist.
: Grid Reference NF 9094 6919
GT05 : Basic Gray Gneiss, amphibolitic. Northern end of Bagh Clann Alisdair, East Gerinish Traverse, South Uist.
: Grid Reference NF 8506 4002
M01 : Basic Gray Gneiss, garnet-bearing. 450 m north-east of Seaforth Head, Malasgair, Lewis.
: Grid Reference NB 2988 1655
BT01 : Corodale Gneiss, altered. Eigneig Mhor, Burrival Traverse, North Uist.
: Grid Reference NF 9291 6129
ET01 : Corodale Gneiss, alteration and pseudotachylyte. 550 m north of spot height on Floddaybeg, Eaval Traverse, North Uist.
: Grid Reference NF 9194 5864
LST07b : Corodale gneiss, altered. 350 m west-north-west of shieling on Rubha Rossel, Loch Skipport Traverse, South Uist.
: Grid Reference NF 8544 3667
LST08 : Corodale gneiss, altered. 550 m north-east of summit of Maol Martaig, Loch Skipport Traverse, South Uist.
: Grid Reference NF 8494 3692
BNHT01 : Corodale derived microbreccia, very slight alteration. Eastern end of Sloc Dubh na Hafn, Ben na Hoe Traverse, South Uist
: Grid Reference NF 8163 2724
BNHT04 : Corodale derived microbreccia, some alteration. West end of Sloc Dubh na Hafn, Ben na Hoe Traverse, South Uist.
: Grid Reference NF 8145 2752

SAMPNO	BNHT05	ET04	LST06	LST10	LST10R	BNHT02	BG01	BG02	BT03	BT04	
SIO2	69.86	58.44	52.40	50.10	50.31	48.25	55.72	62.14	56.11	66.30	SIO2
AL2O3	16.04	15.11	19.16	18.85	18.95	10.89	16.14	16.95	18.80	15.25	AL2O3
FE2O3T	2.18	7.40	8.70	8.73	8.74	15.53	7.75	4.87	5.62	4.78	FE2O3T
MGO	0.72	3.84	4.05	4.04	4.03	6.28	4.54	2.65	3.30	2.21	MGO
MNO	0.01	0.10	0.15	0.12	0.12	0.13	0.11	0.05	0.08	0.06	MNO
CAO	2.60	5.98	5.93	6.63	6.61	8.24	7.04	3.06	6.02	1.79	CAO
NA2O	5.04	5.46	4.97	3.83	3.85	4.56	4.35	4.77	4.90	5.38	NA2O
K2O	2.10	1.20	1.81	2.33	2.35	2.19	1.19	2.81	2.42	1.55	K2O
P2O5	0.07	0.18	0.37	0.41	0.41	0.50	0.18	0.17	0.25	0.10	P2O5
TIO2	0.23	0.76	0.84	0.75	0.75	2.96	0.75	0.54	0.68	0.47	TIO2
LOI	0.77	1.95	1.29	3.12	3.12	0.14	2.14	2.00	1.93	1.99	LOI
TOTAL	98.85	98.47	98.38	95.79	96.12	99.53	97.77	98.01	98.18	97.89	TOTAL
TOT+LOI	99.62	100.42	99.67	98.91	99.24	99.67	99.91	100.01	100.11	99.88	TOT+LOI
BA	437	424	1139	1477	1481	1339	383	1076	664	410	BA
BE	0.90	1.27	1.30	0.78	0.75	0.81	1.24	0.73	1.59	0.74	BE
CO	40.4	38.7	33.8	30.9	29.4	64.3	28.8	25.6	37.2	29.7	CO
CR	28.4	153.5	55.5	46.5	44.8	30.7	107.4	90.3	104.5	98.0	CR
CU	8.9	52.5	39.0	7.5	5.4	232.4	27.7	8.0	59.1	6.5	CU
LA	16.4	24.8	21.4	30.1	24.6	49.9	29.4	24.9	23.7	28.3	LA
NI	-3.9	62.5	-14.0	3.9	-1.4	41.1	50.0	20.5	19.2	3.8	NI
SR	437	410	1141	1460	1469	477	886	474	532	260	SR
V	0.6	111.3	161.7	144.4	145.5	437.9	109.9	51.4	83.1	48.1	V
ZN	20.9	86.8	133.1	89.1	88.7	98.5	102.5	55.8	68.6	66.0	ZN
ZR	85.3	143.4	86.7	11.9	10.0	59.1	137.5	138.1	132.3	120.0	ZR

BNHT05 : Corodale derived microbreccia, slight alteration. 400 m north-east of Meall Mor, Ben na Hoe Traverse, South Uist.
: Grid Reference NF 8136 2760

ET04 : Corodale microbreccia, strong alteration. 550 m north of inlet on west side of Floddaybeg, Eaval Traverse, North Uist.
: Grid Reference NF 9185 5857

LST06 : Corodale microbreccia, garnet bearing. Rubha Rossel, Loch Skipport Traverse, South Uist.
: Grid Reference NF 8572 3680

LST10 : Corodale microbreccia. 350 m south-east of east end of Loch Bein, Loch Skipport Traverse, South Uist.
: Grid Reference NF 8483 3696

BNHT02 : Corodale derived ultracataclasite in microbreccia. Sloc Dubh na Hafn, Ben na Hoe Traverse, South Uist.
: Grid Reference NF 8155 2736

BG01 : C-type mylonite, very strong alteration, some microveining. Creag Scalan, Beinn Grotta Traverse, North Uist.
: Grid Reference NF 9637 7061

BG02 : C-type mylonite, strong alteration, some microveining. West of Loch Scalan, Beinn Grotta Traverse, North Uist.
: Grid Reference NF 9616 7091

BT03 : C-type mylonite, much chlorite developed. 300 m west of inlet to north of Eigneig Mhor, Burrival Traverse, North Uist.
: Grid Reference NF 9263 6140

BT04 : C-type mylonite with folds. Northern shore of north-east trending arm of Loch an Tomain, Burrival Traverse, North Uist.
: Grid Reference NF 9207 6158

SAMPNO	BT07	BV07	BV08	BV08R	BV09	BV10	CH02	CNH02	CNH04	CNHc	
SIO2	55.71	47.58	56.18	57.40	64.50	54.97	63.08	69.33	62.78	63.94	SIO2
AL2O3	15.61	6.45	14.26	14.58	15.87	18.04	14.70	14.16	14.97	15.44	AL2O3
FE2O3T	9.30	12.77	8.34	8.63	5.05	8.72	6.59	3.34	5.54	5.16	FE2O3T
MGO	5.05	18.71	4.38	4.56	1.78	4.14	2.39	1.44	2.32	2.55	MGO
MNO	0.14	0.20	0.11	0.11	0.03	0.05	0.08	0.04	0.07	0.07	MNO
CAO	6.56	9.01	5.21	5.39	1.52	1.13	7.56	1.74	4.27	2.61	CAO
NA2O	3.07	0.32	3.66	3.50	4.67	4.92	2.93	4.51	4.58	5.82	NA2O
K2O	1.35	0.79	1.77	1.78	2.48	3.01	1.19	2.78	1.39	0.75	K2O
P2O5	0.15	0.09	0.18	0.18	0.15	0.56	0.16	0.10	0.19	0.13	P2O5
TIO2	0.89	0.33	0.81	0.88	0.49	0.84	0.77	0.33	0.71	0.51	TIO2
LOI	2.16	3.67	2.41	2.41	1.86	3.09	1.70	1.25	1.74	2.22	LOI
TOTAL	97.83	96.24	94.90	97.02	96.53	96.38	99.45	97.76	96.81	96.97	TOTAL
TOT+LOI	99.99	99.91	97.31	99.43	98.39	99.47	101.15	99.01	98.55	99.19	TOT+LOI
BA	284	102	545	554	414	376	419	694	301	133	BA
BE	0.89	0.60	1.19	1.29	0.89	1.21	1.19	0.77	0.99	0.89	BE
CO	40.6	96.8	28.5	43.8	30.4	18.5	43.8	29.0	22.7	40.6	CO
CR	158.7	100.3	89.2	95.7	22.8	75.9	104.4	67.2	114.4	161.8	CR
CU	47.2	8.0	31.1	34.9	18.9	65.6	72.9	25.1	24.3	21.7	CU
LA	5.8	21.5	36.1	44.1	22.4	9.8	23.2	37.5	55.5	29.8	LA
NI	67.3	329.6	58.4	51.5	10.4	41.3	9.2	27.4	43.1	63.1	NI
SR	344	60	432	444	154	46	783	341	532	285	SR
V	166.2	75.2	189.7	194.0	81.9	215.2	112.7	63.0	122.1	92.0	V
ZN	109.7	178.3	115.0	115.6	56.7	90.6	50.3	46.1	70.3	68.5	ZN
ZR	125.0	105.2	131.1	170.5	139.8	102.0	146.9	137.7	227.5	144.1	ZR

BT07 : C-type mylonite, shear bands. 500 m south of summit of Burrival, Burrival Traverse, North Uist.
: Grid Reference NF 9103 6163

BV07 : C-type mylonite with metabasic material. 100 m northeast of Druim h-Uamh, Burrival, North Uist.
: Grid Reference NF 9186 6159

BV08 : C-type mylonite with asymmmetric folds. Northeastern-most point of Loch an Tomain, Burrival, North Uist.
: Grid Reference NF 9220 6150

BV09 : C-type mylonite, dark coloured. Small promontary in bay south of Eigneig Bheag, Burrival, North Uist.
: Grid Reference NF 9205 5981

BV10 : C-type mylonite. Small promontary in bay south of Eigneig Bheag, Burrival, North Uist.
: Grid Reference NF 9205 5981

CH02 : C-type mylonite, extensive alteration and microveining. 500 m south of Dun Mhic Laitheann, Crogary na Hoe, North Uist.
: Grid Reference NF 9777 7299

CNH02 : C-type mylonite with quartz veining. On coast south west of Dun Mhic Laitheann, Crogary na Hoe, North Uist.
: Grid Reference NF 9777 7299

CNH04 : C-type mylonite. From crags above coast, southeast of Crogary na Hoe, North Uist.
: Grid Reference NF 9767 7222

CNHc : C-type mylonite, well foliated. 250 m north east of Loch na Cointich, Crogary na Hoe, North Uist.
: Grid Reference NF 9668 7240

SAMPNO	CT01	ET03	ET03R	ET12b	LST05	Mg03	NT02	ARDPT01	ARDPT02	ARDPT03	
SIO2	62.21	57.33	58.10	60.31	53.30	67.01	52.71	65.80	67.22	68.82	SIO2
AL2O3	15.56	15.42	15.63	15.87	17.81	14.76	17.44	16.03	16.17	15.86	AL2O3
FE2O3T	6.08	6.92	7.00	6.40	7.75	4.90	8.85	4.94	3.58	3.39	FE2O3T
MGO	2.93	3.86	3.92	3.11	3.53	2.57	3.98	1.37	1.34	1.11	MGO
MNO	0.07	0.10	0.10	0.08	0.12	0.06	0.11	0.06	0.04	0.04	MNO
CAO	2.86	2.51	2.57	4.17	6.71	2.91	6.71	4.72	4.42	4.16	CAO
NA2O	4.42	5.66	5.68	4.98	4.29	5.22	4.60	4.75	4.64	4.68	NA2O
K2O	2.08	1.47	1.49	1.45	2.64	1.07	1.80	1.02	1.17	1.15	K2O
P2O5	0.16	0.22	0.24	0.34	0.41	0.11	0.37	0.15	0.14	0.16	P2O5
TIO2	0.69	0.84	0.85	0.72	0.67	0.41	1.03	0.55	0.53	0.46	TIO2
LOI	2.29	3.45	3.45	2.05	2.02	1.58	2.22	0.95	0.48	0.44	LOI
TOTAL	97.06	94.33	95.59	97.44	97.23	99.03	97.60	99.39	99.25	99.83	TOTAL
TOT+LOI	99.35	97.78	99.04	99.49	99.25	100.61	99.82	100.34	99.73	100.27	TOT+LOI
BA	401	472	484	667	913	388	2077	242	357	333	BA
BE	1.01	0.89	0.90	1.07	1.01	0.79	1.34	0.99	0.69	0.61	BE
CO	30.7	48.9	51.1	29.2	38.4	58.4	32.9	61.8	65.3	72.1	CO
CR	177.9	132.3	133.7	91.7	37.9	143.2	36.5	19.4	15.8	14.2	CR
CU	51.9	19.0	20.3	52.1	4.5	8.9	64.1	17.6	1.7	1.0	CU
LA	31.9	44.4	51.7	50.6	29.1	24.2	44.6	12.4	7.0	7.4	LA
NI	48.4	32.9	41.5	28.2	-7.1	47.1	4.2	-13.4	-7.3	-6.8	NI
SR	408	111	115	751	1714	292	1115	382	383	344	SR
V	98.1	111.8	118.0	98.1	115.8	58.9	166.6	31.9	21.2	12.0	V
ZN	70.5	74.9	82.9	68.9	75.9	1.6	92.0	76.0	64.6	67.3	ZN
ZR	139.9	162.6	159.4	159.9	32.4	225.2	145.1	162.6	156.1	154.1	ZR

CT01 : C-type mylonite, shear bands and epidote veining. Leac na Hoe, Crogary na Hoe Traverse, North Uist.
: Grid Reference NF 9793 7246
ET03 : C-type mylonite, shear bands. 500 m north of spot height on Floddaybeg, Eaval Traverse, North Uist.
: Grid Reference NF 9187 5860
ET12b : C-type mylonite. 1000 m east of Eilean nan Gearr, Eaval Traverse, North Uist.
: Grid Reference NF 9030 5846
LST05 : C-type mylonite. West side of Mol a' Tuath, Loch Skipport Traverse, South Uist.
: Grid Reference NF 8572 3547
Mg03 : C-type mylonite. 100 m onsore west of Sgeir Tanish, Marvig, Lochs, Lewis.
: Grid Reference NB 4186 1919
NT02 : C-type mylonite. 100 m north-west of Scor na Caillich, North Lee Traverse, North Uist.
: Grid Reference NF 9442 6590
ARDPT01 : Gray Gneiss, slight alteration. Ardivachar Point, South Uist
: Grid Reference NF 7422 4678
ARDPT02 : Gray Gneiss. Ardivachar Point, South Uist.
: Grid Reference NF 7422 4678
ARDPT03 : Gray Gneiss. Ardivachar Point, South Uist.
: Grid Reference NF 7421 4679

SAMPNO	BG07	BG07R	BNHT06	BNHT07	BQ01	BQ02	CR03	CR04	CR06	CR10	
SIO2	63.31	63.22	64.51	69.03	55.46	66.04	67.01	50.11	61.19	47.21	SIO2
AL2O3	15.48	15.49	16.26	15.98	15.33	15.32	16.72	12.64	16.32	13.58	AL2O3
FE2O3T	6.23	6.22	4.64	1.91	11.17	5.29	3.18	17.40	7.38	17.50	FE2O3T
MGO	2.94	2.94	1.81	0.79	2.11	1.37	1.41	4.88	3.40	5.55	MGO
MNO	0.10	0.10	0.07	0.02	0.18	0.07	0.04	0.26	0.09	0.15	MNO
CAO	6.14	6.12	3.85	2.42	6.67	4.79	4.60	9.45	3.05	9.23	CAO
NA2O	4.48	4.49	5.06	5.45	4.21	4.47	4.44	1.38	4.52	3.43	NA2O
K2O	0.91	0.92	2.39	2.97	0.91	0.95	1.30	1.07	2.15	0.79	K2O
P2O5	0.15	0.15	0.21	0.10	0.96	0.25	0.11	0.22	0.21	0.14	P2O5
TIO2	0.53	0.54	0.50	0.25	1.70	0.69	0.31	1.83	0.77	2.35	TIO2
LOI	0.64	0.64	0.40	0.77	0.38	0.52	0.41	0.38	1.29	0.41	LOI
TOTAL	100.28	100.19	99.30	99.00	98.69	99.23	99.12	99.24	99.08	99.93	TOTAL[1]
TOT+LOI	100.92	100.83	99.70	99.77	99.07	99.75	99.53	99.62	100.37	100.34	TOT+LOI
BA	210	205	836	1115	346	474	407	192	598	104	BA
BE	1.20	1.22	1.13	0.93	0.74	0.72	0.92	1.05	1.17	1.24	BE
CO	79.5	77.4	51.2	42.6	64.4	125.2	55.4	63.0	64.6	86.5	CO
CR	82.1	81.0	21.5	19.0	7.0	16.8	13.1	27.1	188.4	14.2	CR
CU	78.5	81.2	8.6	18.8	37.1	3.4	41.9	123.0	106.9	218.4	CU
LA	8.3	9.3	49.9	8.6	35.2	12.0	18.7	11.3	26.9	10.8	LA
NI	23.8	29.3	15.6	-10.0	9.9	0.5	3.6	10.1	85.4	15.7	NI
SR	551	547	649	687	484	530	434	106	341	369	SR
V	113.9	113.5	48.3	6.7	60.2	36.2	7.4	397.6	140.4	436.2	V
ZN	84.4	87.5	60.6	23.6	158.7	80.2	50.6	141.9	39.7	70.4	ZN
ZR	103.6	101.6	162.7	58.8	82.0	90.9	122.4	127.1	145.9	120.0	ZR

BG07 : Gray Gneiss, slight alteration of feldspar. Opposite side of road to Loch an t-Sagairt, Beinn Grotta Traverse, N. Uist.
: Grid Reference NF 9490 7227
BNHT06 : Gray Gneiss. North side of Sloc Dubh, Ben na Hoe Traverse, South Uist.
: Grid Reference NF 8078 2842
BNHT07 : Gray Gneiss, slight alteration, with pseudotachylyte. North-western end of Sloc Dubh, Ben an Hoe Traverse, South Uist.
: Grid Reference NF 8011 2910
BQ01 : Gray Gneiss, slight alteration. Quarry on Gairbh-eilean, between Grimsay and North Uist.
: Grid Reference NF 8474 5885
BQ02 : Gray Gneiss. Quarry on Gairbh-eilean, between Grimsay and North Uist.
: Grid Reference NF 8474 5885
CR03 : Gray Gneiss; quartz-plagioclase-biotite-k feldspar-hornblende. Stromban, North Uist.
: Grid Reference NF 9006 6829
CR04 : Gray Gneiss; biotite-hornblende-garnet-quartz. Stromban, North Uist.
: Grid Reference NF 9018 6828
CR06 : Gray Gneiss; k feldspar-biotite-quartz-garnet, extensive quartz veining. Strumore, North Uist.
: Grid Reference NF 9091 6914
CR10 : Gray Gneiss with pseudotachylyte veining. Strumore, North Uist.
: Grid Reference NF 9099 6921

SAMPNO	GS01	GT02a	GT07	LP01	LP01R	LST15	NG02	NG06	NT10	RA01	
SIO2	70.54	73.86	66.83	70.84	70.38	70.24	70.89	70.73	71.47	61.56	SIO2
AL2O3	15.22	14.05	15.77	15.18	15.05	15.26	15.43	14.72	14.88	16.55	AL2O3
FE2O3T	2.81	0.25	4.18	3.30	3.29	2.90	2.04	2.54	3.34	6.28	FE2O3T
MGO	0.88	0.09	1.97	0.93	0.92	1.18	0.90	1.01	0.81	1.89	MGO
MNO	0.02	0.00	0.04	0.04	0.04	0.03	0.02	0.05	0.04	0.09	MNO
CAO	3.72	0.26	4.15	4.64	4.61	3.02	2.71	2.92	3.52	5.16	CAO
NA2O	4.43	2.11	4.37	4.40	4.35	4.84	4.46	3.86	4.15	4.68	NA2O
K2O	1.08	8.38	1.42	0.86	0.86	1.42	2.78	3.56	0.68	2.12	K2O
P2O5	0.08	0.00	0.10	0.15	0.13	0.11	0.09	0.08	0.08	0.40	P2O5
TIO2	0.30	0.04	0.47	0.38	0.38	0.36	0.32	0.21	0.33	0.84	TIO2
LOI	0.29	0.41	0.72	0.44	0.44	1.43	0.61	0.89	0.96	0.74	LOI
TOTAL	99.10	99.04	99.30	100.72	100.02	99.36	99.64	99.69	99.30	99.59	TOTAL
TOT+LOI	99.39	99.45	100.02	101.16	100.46	100.79	100.25	100.58	100.26	100.33	TOT+LOI
BA	322	3760	440	254	254	491	733	1560	282	1234	BA
BE	0.68	-0.09	0.56	0.43	0.60	0.92	0.65	0.51	0.61	0.82	BE
CO	24.1	79.3	51.8	67.0	67.1	37.3	57.2	70.3	52.2	73.8	CO
CR	8.0	-1.8	31.9	13.3	10.2	39.0	14.5	21.8	14.6	13.9	CR
CU	5.1	12.3	25.9	17.4	12.1	20.0	7.2	7.5	54.0	49.8	CU
LA	7.3	-0.1	7.8	33.1	37.0	16.4	-5.2	22.9	3.4	44.5	LA
SR	334	467	305	229	230	410	339	412	227	585	SR
V	31.7	42.5	19.7	30.3	27.3	10.4	25.0	30.8	-7.9	78.5	V
ZN	45.3	-0.8	64.4	22.4	29.7	35.2	17.9	30.1	60.8	89.8	ZN
ZR	175.5	-15.3	112.9	193.4	193.8	127.9	119.3	107.1	162.2	258.3	ZR

GS01 : Gray Gneiss. Westernmost point of Gary a-siar, Benbecula.
: Grid Reference NF 7555 5330

GT02a : Gray Gneiss, slight alteration of feldspars. West coast of Caolas Luirsay, East Gerinish Traverse, South Uist.
: Grid Reference NF 8587 4004

GT07 : Gray Gneiss, slight alteration. 350 m east of souterrain near Lon Dubh, East Gerinish Traverse, South Uist.
: Grid Reference NF 8458 3995

LP01 : Gray Gneiss. Junction of A 865 with Lochportain road, 650 m east of the summit of Crogary Beag.
: Grid Reference NF 8852 7319

LST15 : Gray Gneiss, slight alteration. 350 m south-west of shieling nearest Caolas Mor, Loch Skipport Traverse, South Uist.
: Grid Reference NF 8347 3758

NG02 : Gray Gneiss, very slight alteration. 900 m north-east of the summit of Hartabreck, North Glendale Traverse, South Uist.
: Grid Reference NF 8244 1582

NG06 : Gray Gneiss, slight alteration. 75 m NW of junction of North and South Glendale tracks, North Glendale Traverse, S. Uist
: Grid Reference NF 7947 1726

NT10 : Gray Gneiss, garnet/biotite bearing. 300 m NW of triangulation point on North Lee, North Lee Traverse, North Uist.
: Grid Reference NF 9290 6665

RA01 : Gray Gneiss, slight alteration. Geodha Garbh, Rubha Ardvule, South Uist.
: Grid Reference NF 7092 3001

SAMPNO	RA01R	RA02	RA03	RA04	VS01	VS01R	VS02	BG04	BG05	BG05R	
SIO2	62.11	66.60	62.47	74.87	64.18	65.27	65.79	69.33	55.49	54.87	SIO2
AL2O3	16.68	15.28	15.79	12.87	16.29	16.49	15.48	13.91	16.44	16.22	AL2O3
FE2O3T	6.35	5.03	7.14	2.47	4.16	4.21	4.39	4.72	8.47	8.45	FE2O3T
MGO	1.92	1.54	1.99	0.63	1.63	1.66	1.89	2.29	4.26	4.23	MGO
MNO	0.10	0.07	0.10	0.02	0.06	0.06	0.06	0.05	0.13	0.13	MNO
CAO	5.25	0.49	4.84	2.29	3.60	3.69	3.14	1.36	8.04	7.95	CAO
NA2O	4.69	0.08	4.41	3.37	4.11	4.18	4.03	4.11	3.88	3.81	NA2O
K2O	2.15	0.58	1.98	2.84	3.62	3.68	3.14	1.51	1.14	1.12	K2O
P2O5	0.40	0.28	0.34	0.11	0.18	0.19	0.20	0.13	0.20	0.21	P2O5
TIO2	0.85	0.74	0.85	0.41	0.59	0.60	0.63	0.54	0.91	0.91	TIO2
LOI	0.74	0.59	0.61	0.47	0.76	0.76	1.68	2.86	1.83	1.83	LOI
TOTAL	100.48	99.98	99.91	99.88	98.40	100.04	98.75	97.95	98.97	97.90	TOTAL
TOT+LOI	101.22	100.57	100.52	100.35	99.16	100.80	100.43	100.81	100.80	99.73	TOT+LOI
BA	1242	1080	736	1552	1140	1145	1009	171	237	277	BA
BE	0.78	0.77	0.71	0.22	1.42	1.12	1.04	1.02	0.95	1.40	BE
CO	73.5	75.6	39.1	90.0	71.6	74.7	50.2	28.8	47.9	45.1	CO
CR	15.8	9.2	9.4	8.4	30.9	33.6	36.4	37.3	124.6	119.8	CR
CU	49.8	36.2	27.3	9.2	17.2	24.2	15.4	39.0	81.0	74.5	CU
LA	49.9	74.9	69.4	67.6	63.7	65.7	63.8	18.6	8.1	19.0	LA
NI	17.4	7.6	-8.2	1.3	7.9	8.5	8.9	41.4	85.3	76.3	NI
SR	586	473	492	455	374	378	363	74	598	592	SR
V	78.8	55.5	73.5	27.4	53.2	57.7	59.6	76.2	153.7	158.9	V
ZN	81.1	65.8	92.3	23.0	50.3	47.6	61.7	46.1	87.2	81.9	ZN
ZR	261.4	253.1	234.2	221.6	267.1	269.4	239.8	138.0	123.8	131.4	ZR

RA02 : Gray Gneiss, with pseudotachylyte, epidote and k feldspar. 50 m west of triangulation point, Rubha Ardvule, South Uist.
: Grid Reference NF 7086 2993

RA03 : Gray Gneiss, slight alteration. 250 m south-west of Dun Dulan, Rubha Ardvule, South Uist.
: Grid Reference NF 7107 2961

RA04 : Gray Gneiss, slight alteration. 250 m south-west of Dun Dulan, Rubha Ardvule, South Uist.
: Grid Reference NF 7107 2962

VS01 : Gray Gneiss, much k feldspar. Bagh nan Craobhag, Vallay, North Uist.
: Grid Reference NF 7718 7674

VS02 : Gray Gneiss, much k feldspar. Bagh nan Craobhag, Vallay, North Uist.
: Grid Reference NF 7721 7676

BG04 : Gray Gneiss derived altered microbreccia. 200 m west of Loch Scalan, Beinn Grotta Traverse, North Uist.
: Grid Reference NF 9579 7091

BG05 : Gray Gneiss derived microbreccia, slight alteration. Beinn Grotta, Beinn Grotta Traverse, North Uist.
: Grid Reference NF 9547 7097

SAMPNO	BNHT08	BNHT09	BT06	CH06I	CR07	CT02	CT03	CT03R	ET08	ET17	
SIO2	71.53	68.22	56.01	54.32	59.35	63.95	82.81	82.49	57.14	58.57	SIO2
AL2O3	12.97	15.10	18.76	19.16	16.67	14.47	7.92	7.87	15.66	15.72	AL2O3
FE2O3T	4.19	3.30	6.27	7.33	7.57	6.54	2.19	2.20	7.82	6.65	FE2O3T
MGO	1.32	1.21	3.02	3.40	4.10	3.47	0.98	0.98	3.80	2.12	MGO
MNO	0.04	0.05	0.10	0.10	0.06	0.09	0.04	0.04	0.12	0.09	MNO
CAO	2.48	2.45	4.32	4.82	2.96	4.32	1.07	1.05	5.64	4.77	CAO
NA2O	4.35	5.44	4.97	5.49	4.50	4.02	3.16	3.18	4.38	4.62	NA2O
K2O	1.84	1.97	2.67	1.22	2.91	0.65	0.59	0.58	1.53	1.18	K2O
P2O5	0.13	0.13	0.27	0.24	0.21	0.13	0.04	0.05	0.26	0.24	P2O5
TIO2	0.56	0.35	0.82	0.60	0.87	0.53	0.21	0.20	0.83	0.87	TIO2
LOI	0.81	1.91	2.20	3.52	1.26	2.50	1.32	1.32	2.13	4.25	LOI
TOTAL	99.41	98.22	97.21	96.68	99.20	98.17	99.01	98.64	97.18	94.81	TOTAL
TOT+LOI	100.22	100.13	99.41	100.20	100.46	100.67	100.33	99.96	99.31	99.06	TOT+LOI
BA	668	700	1532	284	778	225	188	184	652	354	BA
BE	0.56	0.79	1.10	0.89	1.11	0.95	0.28	0.42	1.05	0.76	BE
CO	86.9	47.5	26.5	27.9	49.5	28.6	53.4	53.9	30.4	54.5	CO
CR	27.0	26.4	50.6	38.3	188.3	59.0	22.9	19.7	126.1	43.6	CR
CU	87.0	8.4	16.8	108.8	106.9	10.2	26.9	22.6	50.5	110.7	CU
LA	15.5	9.2	29.3	12.5	25.9	2.1	2.4	-4.5	35.4	16.9	LA
NI	-2.8	-0.2	46.8	14.3	79.0	28.9	-6.8	-7.5	12.7	19.1	NI
SR	272	370	610	501	468	529	168	167	611	190	SR
V	26.4	7.3	87.5	109.2	160.4	84.1	-8.2	-12.4	131.5	89.5	V
ZN	58.0	64.4	93.2	93.6	76.6	74.7	31.1	22.9	82.0	91.6	ZN
ZR	127.8	129.3	61.0	73.1	131.1	108.8	77.0	73.8	137.1	158.5	ZR

BNHT08 : Gray Gneiss microbreccia, shear fractures. North-western end of Sloc Dubh, Ben na Hoe Traverse, South Uist.
: Grid Reference NF 7991 2907
BNHT09 : Gray Gneiss microbreccia, garnet-bearing. 500 m east of Arinambane, Ben na Hoe Traverse, South Uist.
: Grid Reference NF 7986 2861
BT06 : Gray Gneiss microbreccia. 200 m south of Loch a' Ghlinne-dorcha, Burrival Traverse, North Uist.
: Grid Reference NF 9142 6173
CH06I : Gray Gneiss microbreccia, microveining. 700 m west-north-west of the summit of Crogary na Hoe, North Uist.
: Grid Reference NF 9642 7228
CR07 : Gray Gneiss microbreccia, some sheared ultracataclasite. Strumore, North Uist.
: Grid Reference NF 9093 6918
CT02 : Gray Gneiss microbreccia, very slight alteration. 300 m south-west of Leac na Hoe, Crogary na Hoe Traverse, North Uist.
: Grid Reference NF 9771 7257
CT03 : Gray Gneiss microbreccia, very slight alteration. 200 m N of summit of Crogary na Hoe, Crogary na Hoe Traverse, N. Uist.
: Grid Reference NF 9746 7267
ET08 : Gray Gneiss microbreccia. 600 m north of coast of small island west of Duibh-eilean, Eaval Traverse, North Uist.
: Grid Reference NF 9122 5853
ET17 : Gray Gneiss microbreccia, slight alteration. 450 m north-east of Eilean nan Gearr, Eaval Traverse, North Uist.
: Grid Reference NF 8958 5865

SAMPNO	LST09b	LST12a	LST12b	LST12c	LST14	M03c	NG01a	NG01aR	NT06	NT07	
SIO2	52.56	52.83	52.73	51.16	47.84	70.64	69.59	69.92	64.69	63.63	SIO2
AL2O3	18.03	15.57	15.14	10.67	13.57	15.37	14.12	14.14	15.93	15.62	AL2O3
FE2O3T	8.46	9.52	9.94	11.47	13.88	1.94	4.28	4.31	4.31	5.80	FE2O3T
MGO	3.78	5.10	5.48	10.49	6.36	0.82	1.75	1.76	1.84	3.01	MGO
MNO	0.12	0.14	0.16	0.21	0.22	0.02	0.08	0.08	0.07	0.08	MNO
CAO	8.45	9.89	9.84	11.64	10.53	2.59	4.15	4.21	3.19	3.71	CAO
NA2O	5.07	3.93	3.62	2.17	3.28	4.28	4.42	4.44	4.36	3.66	NA2O
K2O	0.55	0.68	0.82	0.70	1.10	3.08	0.99	0.99	3.21	1.45	K2O
P2O5	0.50	0.28	0.16	0.06	0.14	0.07	0.04	0.04	0.17	0.14	P2O5
TIO2	1.00	0.69	0.73	0.67	1.36	0.28	0.35	0.37	0.51	0.49	TIO2
LOI	2.57	1.26	1.36	1.44	1.34	0.59	0.61	0.61	1.21	2.20	LOI
TOTAL	98.52	98.64	98.62	99.23	98.29	99.09	99.78	100.26	98.28	97.59	TOTAL
TOT+LOI	101.09	99.90	99.98	100.67	99.63	99.68	100.39	100.87	99.49	99.79	TOT+LOI
BA	817	150	177	137	313	1029	201	213	2141	419	BA
BE	1.03	1.47	1.54	1.06	0.71	0.60	1.19	1.54	0.79	1.16	BE
CO	48.1	44.9	62.2	62.7	64.6	52.0	66.5	66.9	39.3	57.9	CO
CR	63.8	113.4	50.4	815.6	185.8	20.4	54.1	56.1	16.4	180.4	CR
CU	54.6	116.5	61.3	29.0	100.2	8.2	14.1	12.4	21.4	61.0	CU
LA	49.2	28.1	28.2	13.8	5.5	22.8	5.7	6.5	60.8	14.3	LA
NI	5.4	57.7	50.9	152.9	55.9	-6.1	26.8	19.4	-10.4	49.0	NI
SR	1767	431	392	197	193	380	350	351	567	330	SR
V	150.5	156.3	181.3	223.7	285.8	-6.3	70.4	75.8	26.4	74.9	V
ZN	117.0	72.9	75.8	112.3	143.4	34.3	53.8	42.6	74.5	76.1	ZN
ZR	116.9	112.4	85.5	49.0	100.2	118.5	43.1	50.2	195.7	97.2	ZR

LST09b : Gray Gneiss microbreccia, altered ultracataclasite. 500 m north-east of Maol Martaig, Loch Skipport Traverse, South Uist
: Grid Reference NF 8489 3695

LST12a : Basic Gray Gneiss microbreccia. 500 m north of summit of Maol Martaig, Loch Skipport Traverse, South Uist.
: Grid Reference NF 8475 3697

LST12b : Basic Gray Gneiss microbreccia, altered. 500 m north of summit of Maol Martaig, Loch Skipport Traverse, South Uist.
: Grid Reference NF 8475 3697

LST12c : Basic Gray Gneiss microbreccia, 500 m north of summit of Maol Martaig, Loch Skipport Traverse, South Uist.
: Grid Reference NF 8475 3697

LST14 : Gray Gneiss microbreccia, strong alteration of mafics. 550 m W of W end of Loch Bein, Loch Skipport Traverse, South Uist
: Grid Reference NF 8357 3752

M03c : Altered Gray Gneiss microbreccia, strong alteration. 150 m north-west of cairn on Mullach Breac Malasgair, Lewis.
: Grid Reference NB 2996 1675

NG01a : Gray Gneiss microbreccia, slight alteration. 350 m north-west of Eilean Dubh, North Glendale Traverse, South Uist.
: Grid Reference NF 8262 1558

NT06 : Gray Gneiss microbreccia. Crag above top tributary junction with Allt Gleann-tuis, North Lee Traverse, North Uist.
: Grid Reference NF 9354 6634

NT07 : Gray Gneiss microbreccia. 150 m north-east of triangulation point on North Lee, North Lee Traverse, North Uist.
: Grid Reference NF 9523 6649

SAMPNO	NT09	SH03a	LST01	LST02	LST03	LST04	BNH2/6	BNHT03	BNHT03R	BQ04	
SIO2	64.92	68.01	64.68	68.10	74.74	74.92	55.76	51.92	51.70	75.45	SIO2
AL2O3	16.31	15.68	14.33	16.32	12.65	12.29	16.75	3.65	3.67	13.66	AL2O3
FE2O3T	4.54	2.87	5.87	3.51	1.98	2.54	8.19	7.31	7.28	0.64	FE2O3T
MGO	2.19	1.29	2.46	1.56	0.87	1.39	4.23	14.19	14.16	0.09	MGO
MNO	0.05	0.03	0.08	0.04	0.03	0.03	0.11	0.18	0.18	0.01	MNO
CAO	3.61	4.27	5.49	2.06	2.39	0.27	6.91	19.37	19.26	0.80	CAO
NA2O	3.70	4.74	3.51	5.28	4.78	4.99	4.33	2.36	2.22	3.61	NA2O
K2O	1.98	1.22	1.24	2.72	1.03	1.66	1.87	0.13	0.13	5.46	K2O
P2O5	0.10	0.09	0.20	0.11	0.04	0.15	0.34	0.09	0.09	0.01	P2O5
TIO2	0.43	0.47	0.59	0.36	0.15	0.32	0.82	0.44	0.43	0.06	TIO2
LOI	2.33	0.93	1.99	1.51	1.11	1.36	0.29	0.96	0.96	0.47	LOI
TOTAL	97.83	98.67	98.45	100.06	98.66	98.56	99.32	99.10	99.13	99.79	TOTAL
TOT+LOI	100.16	99.60	100.44	101.57	99.77	99.92	99.61	100.06	100.09	100.26	TOT+LOI
BA	689	358	535	701	345	562	1095	27	27	1543	BA
BE	0.87	0.84	0.91	0.90	0.60	0.40	1.03	0.75	0.68	0.35	BE
CO	53.3	54.7	35.7	42.5	34.6	32.8	49.4	33.6	27.5	100.5	CO
CR	49.0	27.2	52.7	55.5	32.5	20.8	113.4	401.5	397.5	4.6	CR
CU	50.0	4.4	14.3	31.7	11.5	0.9	85.1	230.6	235.1	2.8	CU
LA	8.6	10.3	33.2	22.3	14.2	4.0	36.5	19.5	5.1	3.4	LA
NI	8.4	-0.7	-10.5	4.0	-3.0	-11.0	55.1	38.4	17.0	-1.9	NI
SR	287	410	838	389	263	89	935	67	67	294	SR
V	36.3	28.3	70.6	17.6	-12.5	-1.8	191.5	432.4	431.6	6.0	V
ZN	56.0	30.2	59.6	39.8	17.3	21.4	91.4	54.5	37.4	-14.0	ZN
ZR	151.1	145.4	143.0	121.1	62.8	146.1	129.9	136.4	124.3	64.2	ZR

NT09 : Gray Gneiss microbreccia. 600 m south-west of Creag a' Chriobhain, North Lee Traverse, North Uist.
: Grid Reference NF 9302 6665
SH03a : Gray Gneiss microbreccia, microveining. 700 m west of Cnoc Loch an Iaruinn, Shildenish, Lewis.
: Grid Reference NB 2972 1976
LST01 : Mashed Gneiss, ultracataclasite, strong alteration. Lighthouse on Usinish peninsula, Loch Skipport Traverse, South Uist.
: Grid Reference NF 8726 3511
LST02 : Mashed Gneiss microbreccia. Creag Dhughaill, Usinish peninsula, Loch Skipport Traverse, South Uist.
: Grid Reference NF 8715 3527
LST03 : Mashed Gneiss microbreccia, strong alteration. 450 m north-west of Beinn a' Tuath, Loch Skipport Traverse, South Uist.
: Grid Reference NF 8647 3566
LST04 : Mashed Gneiss, cataclasite. Mol a' Tuath, Usinish, Loch Skipport Traverse, South Uist.
: Grid Reference NF 8581 3538
BNH2/6 : Dark-coloured ultracataclasite. Ben na Hoe, South Uist.
: Grid Reference NF 8133 2923
BNHT03 : Corodale pyroxenite. Sloc Dubh na Hafn, Ben na Hoe Traverse, South Uist.
: Grid Reference NF 8149 2744
BQ04 : Alkali feldspar, epidote and quartz vein. Quarry on Gairbh-eilean, between Grimsay and North Uist.
: Grid Reference NF 8477 5884

SAMPNO	BV05	CH04b	ET15	ET15R	ET16	EV04	GT02b	GT02bR	LST07a	LST07aR	
SIO2	65.32	65.63	52.94	53.57	63.23	51.85	47.52	48.08	51.00	50.82	SIO2
AL2O3	15.36	13.26	16.36	16.64	14.96	14.88	13.18	13.26	14.06	14.01	AL2O3
FE2O3T	4.68	6.91	7.17	7.26	6.03	12.41	14.36	14.54	10.85	10.86	FE2O3T
MGO	2.06	1.12	6.90	7.02	2.99	4.79	6.53	6.62	8.04	8.05	MGO
MNO	0.05	0.07	0.11	0.11	0.09	0.19	0.21	0.21	0.16	0.16	MNO
CAO	3.50	8.08	8.03	8.11	4.62	7.84	10.90	11.12	8.68	8.69	CAO
NA2O	4.34	2.06	4.04	4.08	4.32	3.45	1.75	1.77	2.64	2.63	NA2O
K2O	1.87	0.79	0.33	0.33	1.79	1.48	1.25	1.26	0.33	0.32	K2O
P2O5	0.14	0.07	0.10	0.10	0.11	0.38	0.15	0.14	0.18	0.19	P2O5
TIO2	0.51	0.31	0.77	0.77	0.61	1.35	1.61	1.62	1.36	1.36	TIO2
LOI	1.54	1.58	1.96	1.96	1.69	1.06	1.16	1.16	1.96	1.96	LOI
TOTAL	97.82	98.30	96.73	97.98	98.75	98.62	97.46	98.62	97.30	97.09	TOTAL
TOT+LOI	99.36	99.88	98.69	99.94	100.44	99.68	98.62	99.78	99.26	99.05	TOT+LOI
BA	478	333	155	153	516	483	324	325	181	180	BA
BE	1.05	0.73	0.29	0.36	0.94	1.28	0.65	0.73	0.60	0.63	BE
CO	34.2	39.3	56.4	55.4	43.8	52.7	64.8	66.2	62.2	63.1	CO
CR	70.4	56.8	278.6	283.1	113.9	94.5	189.9	192.1	348.0	346.7	CR
CU	49.0	16.6	57.5	60.3	61.3	155.0	68.2	71.3	74.8	72.6	CU
LA	24.1	-0.5	-1.7	-3.3	42.2	39.2	-2.0	2.4	6.4	7.2	LA
NI	45.3	-8.5	209.6	208.4	64.5	56.1	52.0	58.9	177.5	182.3	NI
SR	408	1240	490	501	341	417	342	343	295	296	SR
V	93.5	149.6	76.5	77.4	83.0	307.9	339.9	346.7	182.1	181.9	V
ZN	55.9	33.2	72.5	83.1	64.9	109.9	144.3	147.8	109.0	103.5	ZN
ZR	152.1	84.0	47.0	43.7	121.9	139.5	102.3	106.7	66.3	68.5	ZR

BV05 : Ultracataclasite. Summit of Burrival, North Uist.
: Grid Reference NF 9025 6217
CH04b : Strongly altered ultracataclasite, extensive microveining and alteration. Leac na Hoe, Crogary na Hoe, North Uist.
: Grid Reference NF 9767 7222
ET15 : Dolerite. 375 m south of summit of Beinn na h-Aire, Eaval Traverse, North Uist.
: Grid Reference NF 9000 5849
ET16 : Ultracataclasite. 1.95 km south of summit of Eaval, Eaval Traverse, North Uist.
: Grid Reference NF 8989 5859
EV04 : Ultracataclasite, very dark. 350 m south of Eaval, North Uist.
: Grid Reference NF 8985 6015
GT02b : Basic gneiss, hornblende-epidote, some microveining. West coast of Caolas Luirsay, East Gerinish Traverse, South Uist.
: Grid Reference NF 8587 4004
LST07a : Dolerite, slightly altered. 350 m west-north-west of shieling on Rubha Rossel, Loch Skipport Traverse, South Uist.
: Grid Reference NF 8544 3667

SAMPNO	M02	NG01m	SH03b	SH04a	GT03a	BT02	BT05	BT08	BT08R	ET09	
SIO2	50.93	51.54	55.23	68.30	48.21	61.82	70.55	63.02	62.85	66.91	SIO2
AL2O3	13.56	13.75	14.81	15.46	13.91	16.01	14.54	17.33	17.31	14.73	AL2O3
FE2O3T	15.83	13.26	9.59	3.51	14.86	6.19	3.09	4.88	4.84	3.76	FE2O3T
MGO	5.32	5.97	5.02	1.36	5.98	2.33	1.22	2.28	2.26	1.66	MGO
MNO	0.25	0.27	0.14	0.04	0.24	0.07	0.03	0.05	0.05	0.06	MNO
CAO	9.51	8.35	7.84	3.91	10.44	2.75	1.68	2.34	2.32	2.81	CAO
NA2O	1.97	3.23	3.61	4.44	2.56	4.91	4.56	4.27	4.26	4.74	NA2O
K2O	0.35	1.27	1.50	2.01	0.58	2.26	2.34	2.55	2.54	2.94	K2O
P2O5	0.14	0.10	0.12	0.12	0.18	0.21	0.06	0.26	0.27	0.14	P2O5
TIO2	1.35	1.00	0.81	0.44	1.80	0.63	0.29	0.50	0.50	0.48	TIO2
LOI	-0.04	0.81	1.14	0.69	0.58	3.67	1.48	2.21	2.21	1.70	LOI
TOTAL	99.21	98.73	98.67	99.59	98.76	97.18	98.36	97.48	97.20	98.23	TOTAL
TOT+LOI	99.17	99.54	99.81	100.28	99.34	100.85	99.84	99.69	99.41	99.93	TOT+LOI
BA	81	154	237	758	167	329	733	564	563	1581	BA
BE	0.66	2.70	1.11	0.84	0.81	1.06	0.71	1.43	1.40	1.21	BE
CO	70.2	56.4	46.4	51.8	64.2	30.7	43.7	38.9	41.2	43.3	CO
CR	79.7	188.3	144.6	28.8	160.3	48.8	22.4	45.3	40.9	52.7	CR
CU	289.9	9.5	72.7	25.2	253.7	27.1	12.1	16.5	12.7	20.1	CU
LA	-1.2	18.1	11.0	10.6	5.9	20.8	24.1	6.8	-3.4	49.3	LA
NI	29.8	59.9	75.6	13.5	46.0	5.8	-10.1	5.5	10.6	-1.7	NI
SR	88	237	307	416	209	71	327	300	299	418	SR
V	317.1	275.8	207.4	32.5	343.7	62.8	6.7	59.1	56.6	51.4	V
ZN	113.6	168.4	94.4	40.9	114.9	82.2	65.5	77.5	70.2	42.5	ZN
ZR	85.7	66.7	89.6	117.8	113.0	184.8	93.0	37.8	43.0	41.3	ZR

M02 : Cataclased basic Gray Gneiss. 150 m west of cairn on Mullach Breac Malasgair, Malasgair, Lewis.
: Grid Reference NB 2995 1664

NG01m : Basic Gray Gneiss microbreccia, slight alteration. 350 m north-west of Eilean Dubh, North Glendale Traverse, South Uist.
: Grid Reference NF 8262 1558

SH03b : Cataclasite with ultramylonite. 700 m west of Cnoc Loch an Iaruinn, Shildenish, Lewis.
: Grid Reference NB 2972 1976

SH04a : R-type mylonite, extensive later brecciation. 325 m east of Beinn Mheadhonach, Shildenish, Lewis.
: Grid Reference NB 2975 1978

GT03a : Basic gneiss microbreccia, garnet bearing. Inlet at southern end of Caolas Luirsay, East Gerinish Traverse, South Uist.
: Grid Reference NF 8585 4002

BT02 : Altered Gray Gneiss, heavily altered. Eigneig Mhor, Burrival Traverse, North Uist.
: Grid Reference NF 9278 6125

BT05 : Altered Gray Gneiss, strong alteration. 500 m north-east of cave on Druim na h-Uamh, Burrival, North Uist.
: Grid Reference NF 9176 6174

BT08 : Gray Gneiss, altered. 450 m south-south-west of the summit of Burrival, Burrival Traverse, North Uist.
: Grid Reference NF 9074 6184

ET09 : Altered Gray Gneiss, coarse grained. 500 m north of east end of island of Haunary, Eaval Traverse, North Uist.
: Grid Reference NF 9097 5851

SAMPNO	ET09R	ET18	GT03d	GT04	GT06	GT06R	LST11	LST13I	LST13II	LST13IIR	
SIO2	66.94	47.13	55.92	64.42	70.69	70.24	49.73	66.51	55.36	55.22	SIO2
AL2O3	14.78	28.01	16.86	15.12	14.85	14.80	9.73	16.69	18.95	18.95	AL2O3
FE2O3T	3.74	2.64	7.90	5.58	2.81	2.79	12.09	3.17	7.20	7.14	FE2O3T
MGO	1.66	1.14	4.60	2.56	0.93	0.93	11.68	1.16	2.71	2.68	MGO
MNO	0.06	0.05	0.10	0.07	0.02	0.02	0.24	0.05	0.11	0.11	MNO
CAO	2.77	14.06	6.36	2.13	2.93	2.90	12.86	4.28	6.22	6.14	CAO
NA2O	4.64	4.27	3.58	4.80	3.67	3.66	1.64	4.89	6.30	6.29	NA2O
K2O	2.92	0.82	2.09	1.53	2.10	2.09	0.49	1.37	1.16	1.17	K2O
P2O5	0.14	0.05	0.16	0.09	0.06	0.05	0.06	0.03	0.19	0.18	P2O5
TIO2	0.48	0.16	0.70	0.67	0.36	0.36	0.71	0.21	0.48	0.48	TIO2
LOI	1.91	2.35	1.31	2.31	1.55	1.55	0.98	1.58	1.58	1.58	LOI
TOTAL	98.11	98.33	98.27	96.97	98.42	97.84	99.23	98.35	98.69	98.37	TOTAL
TOT+LOI	100.02	100.68	99.58	99.28	99.97	99.39	100.21	99.93	100.27	99.95	TOT+LOI
BA	1573	125	566	488	879	875	108	236	265	265	BA
BE	1.07	0.29	1.31	0.41	0.69	0.66	0.48	1.41	1.87	1.79	BE
CO	40.2	27.3	50.0	45.6	69.3	69.4	72.5	27.3	31.6	30.1	CO
CR	52.0	26.5	99.0	145.2	9.4	6.5	1038.1	21.5	53.1	53.2	CR
CU	15.0	25.3	10.6	21.2	12.8	10.5	24.3	6.1	45.1	44.6	CU
LA	10.6	5.2	20.9	87.8	11.3	10.1	-2.6	31.8	32.1	38.2	LA
NI	-4.8	17.6	-7.1	23.4	-11.1	-10.9	159.2	16.9	43.8	33.6	NI
SR	414	247	369	299	332	330	146	384	569	566	SR
V	41.6	-1.6	142.9	69.0	-0.6	1.6	245.1	5.0	88.5	78.5	V
ZN	38.8	23.0	75.5	59.5	25.7	32.1	140.5	18.5	66.8	66.8	ZN
ZR	34.3	46.5	120.6	196.1	107.7	108.6	49.9	359.0	117.4	126.3	ZR

ET18 : Altered basic Gray Gneiss, strong alteration. 200 m east of the shieling of Eaval, Eaval Traverse, North Uist.
: Grid Reference NF 8896 5909
GT03d : Altered Gray Gneiss, moderate alteration. Inlet at southern end of Caolas Luirsay, East Gerinish Traverse, South Uist.
: Grid Reference NF 8585 4002
GT04 : Altered Gray Gneiss, moderate alteration. Northern side of Bagh Clann Alisdair, East Gerinish Traverse, South Uist.
: Grid Reference NF 8537 3995
GT06 : Altered Gray Gneiss, strong alteration. 700 m north-west of Rubha fo Deas, East Gerinish Traverse, South Uist.
: Grid Reference NF 8492 3987
LST11 : Altered basic Gray Gneiss. 400 m south-east of east end of Loch Bein, Loch Skipport Traverse, South Uist.
: Grid Reference NF 8481 3694
LST13I : Altered Gray Gneiss, very coarse grained. 200 m east of east end of Loch Bein, Loch Skipport Traverse, South Uist.
: Grid Reference NF 8465 3699
LST13II : Altered Gray Gneiss, very coarse grained. 200 m east of east end of Loch Bein, Loch Skipport Traverse, South Uist.
: Grid Reference NF 8465 3699

SAMPNO	NG03	NG05	NG05R	NT01	NT01R	BG03	BG03R	BG06	CR05	CR11	
SIO2	70.71	66.77	66.34	61.47	61.73	58.20	57.78	49.37	61.96	61.49	SIO2
AL2O3	14.20	15.26	15.25	16.06	16.10	18.20	18.08	16.01	16.24	15.49	AL2O3
FE2O3T	2.97	4.60	4.60	6.27	6.30	5.32	5.28	10.18	7.03	7.19	FE2O3T
MGO	0.74	2.20	2.20	2.97	2.99	3.15	3.13	8.01	3.21	3.47	MGO
MNO	0.03	0.06	0.06	0.09	0.08	0.08	0.08	0.16	0.07	0.07	MNO
CAO	1.90	4.24	4.23	3.88	3.87	5.48	5.44	10.57	1.98	3.07	CAO
NA2O	3.69	4.17	4.15	4.65	4.68	4.93	4.93	2.48	4.29	4.20	NA2O
K2O	4.08	1.86	1.87	1.59	1.61	2.38	2.38	0.67	2.75	1.33	K2O
P2O5	0.12	0.16	0.16	0.16	0.16	0.20	0.21	0.06	0.18	0.18	P2O5
TIO2	0.38	0.46	0.47	0.71	0.69	0.57	0.57	0.61	0.71	0.73	TIO2
LOI	0.73	0.99	0.99	1.99	1.99	1.82	1.82	2.49	1.87	2.44	LOI
TOTAL	98.82	99.79	99.34	97.85	98.21	98.52	97.86	98.13	98.42	97.22	TOTAL
TOT+LOI	99.55	100.78	100.33	99.84	100.20	100.34	99.68	100.62	100.29	99.66	TOT+LOI
BA	1149	587	587	728	722	660	654	190	1637	499	BA
BE	1.09	1.15	0.77	0.68	0.69	1.17	1.10	0.21	0.99	1.18	BE
CO	65.5	57.2	57.8	36.8	36.4	28.3	28.1	59.8	40.6	36.8	CO
CR	14.0	58.9	57.9	116.1	117.7	106.6	108.3	212.3	159.2	176.1	CR
CU	6.5	39.9	38.5	38.1	35.5	33.2	33.9	70.8	77.0	83.6	CU
LA	8.9	34.7	35.3	14.4	14.6	16.6	16.6	1.3	27.1	29.9	LA
NI	-2.3	36.2	27.3	30.6	30.2	34.8	33.7	169.3	80.5	64.7	NI
SR	291	353	360	476	474	473	474	281	266	236	SR
V	28.9	72.0	71.4	102.3	98.9	89.9	86.3	209.8	121.5	129.2	V
ZN	38.8	56.3	48.8	86.6	90.8	42.4	44.1	67.6	134.7	96.3	ZN
ZR	218.9	126.7	125.2	154.1	159.3	82.8	81.0	42.6	122.3	144.4	ZR

NG03 : Altered Gray Gneiss. On track 300 m west of hill between Hartavagh and Marulaig Bay, North Glendale Traverse, South Uist
: Grid Reference NF 8232 1591

NG05 : Altered Gray Gneiss, moderate alteration. On track 500 m east of Glac Ruairidh, North Glendale Traverse, South Uist.
: Grid Reference NF 8067 1703

NT01 : Altered Gray Gneiss, strong alteration, microveining. Midway between Scor na Caillich and Partachal, North Lee Traverse.
: Grid Reference NF 9449 6592

BG03 : Gray Gneiss derived microbreccia, moderate alteration, microveining. 175 m W of cave, Beinn Grotta Traverse, North Uist.
: Grid Reference NF 9593 7097

BG06 : Gray Gneiss derived altered microbreccia. Midway between loch Hacklett and Loch Gille-ghoid, Beinn Grotta Traverse.
: Grid Reference NF 9547 7125

CR05 : Altered Gray Gneiss microbreccia, moderate alteration. Stromban, North Uist.
: Grid Reference NF 9092 6907

CR11 : Gray Gneiss microbreccia, strong alteration. Strumore, North Uist.
: Grid Reference NF 9101 6911

SAMPNO	CR11R	CT06	CT07	CT07R	ET02	ET05	ET06	ET07	ET10	ET11	
SIO2	62.25	63.91	75.50	75.45	65.68	57.72	58.27	59.26	48.99	53.00	SIO2
AL2O3	15.54	15.59	13.07	13.04	15.67	15.55	14.70	19.28	14.86	18.07	AL2O3
FE2O3T	7.22	5.27	2.15	2.16	4.50	8.11	8.30	4.18	12.24	7.66	FE2O3T
MGO	3.49	2.37	0.74	0.73	1.97	4.32	5.11	1.60	5.53	4.16	MGO
MNO	0.07	0.08	0.02	0.03	0.06	0.12	0.12	0.06	0.19	0.11	MNO
CAO	3.07	2.80	1.78	1.78	2.25	6.58	4.88	3.63	8.79	5.54	CAO
NA2O	4.23	4.28	5.32	5.34	4.73	3.66	4.11	6.15	3.86	5.18	NA2O
K2O	1.33	2.42	1.05	1.07	2.63	1.35	1.41	3.42	1.28	3.02	K2O
P2O5	0.17	0.11	0.06	0.05	0.16	0.09	0.21	0.21	0.23	0.45	P2O5
TIO2	0.73	0.58	0.23	0.23	0.53	0.57	0.77	0.56	1.37	1.12	TIO2
LOI	2.44	2.13	0.90	0.90	1.98	1.77	3.09	2.39	2.28	2.49	LOI
TOTAL	98.10	97.41	99.92	99.88	98.19	98.07	97.88	98.36	97.34	98.31	TOTAL
TOT+LOI	100.54	99.54	100.82	100.78	100.17	99.84	100.97	100.75	99.62	100.80	TOT+LOI
BA	502	1297	340	335	700	465	546	1343	662	896	BA
BE	1.27	0.62	0.67	0.76	1.03	0.94	0.92	1.25	0.85	1.45	BE
CO	39.1	42.2	43.0	42.3	30.0	41.7	33.6	22.1	42.5	24.4	CO
CR	183.3	118.0	23.6	17.2	34.4	58.9	233.8	25.2	41.5	53.2	CR
CU	86.6	42.7	37.0	26.5	16.2	51.8	19.1	64.7	134.7	23.6	CU
LA	31.0	14.6	25.8	24.8	47.8	15.6	32.8	28.4	14.6	78.7	LA
NI	59.6	35.7	-1.5	-4.9	19.4	21.8	49.2	-7.2	12.5	3.9	NI
SR	238	389	232	232	401	354	318	531	748	697	SR
V	130.1	68.8	-6.5	-8.0	44.1	108.8	111.3	28.7	270.5	128.3	V
ZN	88.7	74.0	90.2	90.5	70.0	94.0	105.3	40.1	138.6	113.4	ZN
ZR	121.9	112.1	94.3	109.9	155.3	197.7	145.9	76.9	86.9	270.3	ZR

CT06 : Altered Gray Gneiss microbreccia, strong alteration. 400 m south of Bagh Chaise, Crogary Na Hoe Traverse, North Uist.
: Grid Reference NF 9685 7293
CT07 : Altered Gray Gneiss microbreccia, moderate alteration. 250 m south of Strom, Crogary na Hoe Traverse, North Uist.
: Grid Reference NF 9646 7296
ET02 : Altered Gray Gneiss microbreccia, microveining. 475 m north of spot height on Floddaybeg, Eaval Traverse, North Uist.
: Grid Reference NF 9191 5859
ET05 : Altered Gray Gneiss microbreccia, strong alteration. 450 m N of promontory on west side of Floddaybeg, Eaval, North Uist
: Grid Reference NF 9169 5860
ET06 : Altered Gray Gneiss microbreccia, very strong alteration. 150 m north of loc. ET05, Eaval Traverse, North Uist.
: Grid Reference NF 9146 5867
ET07 : Altered Gray Gneiss microbreccia, strong alteration. 550 m north of coast of Duibh-eilean, Eaval Traverse, North Uist.
: Grid Reference NF 9136 5855
ET10 : Altered Gray Gneiss microbreccia, strong alteration. 400 m north of west end of Haunaray, Eaval Traverse, North Uist.
: Grid Reference NF 9076 5842
ET11 : Altered Gray Gneiss microbreccia, strong alteration. 500 m south-east of Beinn na h-Aire, Eaval Traverse, North Uist.
: Grid Reference NF 9037 5850

SAMPNO	ET14b	ET14bR	ET14c	M03a	NG04	NG04R	NT03	NT04	NT05	NT08	
SIO2	64.91	65.22	63.87	67.74	59.17	59.09	62.27	60.70	55.23	66.81	SIO2
AL2O3	16.65	16.76	15.99	15.07	15.74	15.75	14.99	18.22	16.39	17.19	AL2O3
FE2O3T	4.02	4.04	4.81	4.16	6.88	6.81	6.76	3.88	8.98	2.93	FE2O3T
MGO	1.51	1.53	2.50	1.76	2.76	2.74	3.27	0.99	4.37	1.55	MGO
MNO	0.06	0.06	0.07	0.05	0.15	0.15	0.09	0.05	0.12	0.03	MNO
CAO	4.18	4.21	4.53	3.86	8.21	8.10	3.82	1.55	5.61	3.43	CAO
NA2O	4.56	4.60	4.98	4.29	3.96	4.02	3.67	3.64	4.08	5.56	NA2O
K2O	1.70	1.72	1.36	2.30	0.87	0.87	1.99	8.73	1.82	1.18	K2O
P2O5	0.12	0.11	0.17	0.15	0.54	0.55	0.14	0.21	0.26	0.13	P2O5
TIO2	0.44	0.44	0.56	0.46	0.72	0.71	0.64	0.71	1.06	0.36	TIO2
LOI	1.61	1.61	1.65	0.66	1.49	1.49	2.11	1.33	2.15	1.46	LOI
TOTAL	98.15	98.69	98.83	99.84	98.99	98.78	97.64	98.68	97.92	99.17	TOTAL
TOT+LOI	99.76	100.30	100.48	100.50	100.48	100.27	99.75	100.01	100.07	100.63	TOT+LOI
BA	671	677	535	621	263	260	666	4062	838	461	BA
BE	1.02	1.00	1.29	0.96	3.00	2.48	0.74	0.53	1.14	0.80	BE
CO	35.6	32.8	29.2	51.0	59.5	60.1	32.4	31.4	32.6	33.5	CO
CR	39.0	38.8	72.6	42.0	49.1	52.4	191.7	13.7	121.7	23.8	CR
CU	15.8	11.7	33.0	35.1	15.6	16.6	73.1	30.5	62.4	45.8	CU
LA	29.9	34.4	55.1	31.0	93.8	90.6	27.3	48.0	37.4	6.3	LA
NI	-9.9	-5.1	33.7	13.4	33.1	21.2	69.4	-21.2	13.7	-14.9	NI
SR	425	429	519	357	923	933	500	246	755	578	SR
V	23.4	25.1	63.3	34.5	112.0	110.5	110.8	-0.6	119.6	12.1	V
ZN	38.3	29.5	40.7	57.7	126.9	126.5	102.0	26.7	116.1	45.2	ZN
ZR	133.4	126.3	126.0	153.1	211.2	206.6	149.3	119.0	163.6	149.3	ZR

ET14b : Altered Gray Gneiss microbreccia, strong alteration. 450 m south of Beinn na h-Aire, Eaval Traverse, North Uist.
: Grid Reference NF 9019 5840
ET14c : Altered Gray Gneiss microbreccia, strong alteration and altered pseudotachylyte. Same locality as ET14b.
: Grid Reference NF 9019 5840
M03a : Altered Gray Gneiss microbreccia, strong alteration. 150 m north-west of cairn on Mullach Breac Malasgair, Lewis.
: Grid Reference NB 2996 1675
NG04 : Gray Gneiss microbreccia, with microveining. On burn 400 m west of Marulaig Bay, North Glendale Traverse, South Uist.
: Grid Reference NF 8198 1625
NT03 : Gray gneiss microbreccia, strong alteration. 400 m north-west of Scor na Caillich, North Lee Traverse, North Uist.
: Grid Reference NF 9417 6600
NT04 : Gray Gneiss microbreccia, strong alteration. 650 m north-west of Scor na Caillich, North Lee Traverse, North Uist.
: Grid Reference NF 9398 6612
NT05 : Gray Gneiss microbreccia, strong alteration. Midway between North Lee and Scor na Caillich, North Lee Traverse, N. Uist.
: Grid Reference NF 9390 6621
NT08 : Gray Gneiss microbreccia, strong alteration. 200 m north of triangulation point on North Lee, North Uist.
: Grid Reference NF 9318 6660

SAMPNO	SH04b	SH08	SH09c	SH09cR	M05a	M05b	M05c	M06	M06R	M07a	
SIO2	52.94	68.79	67.56	67.44	66.73	65.65	62.57	70.66	70.36	62.05	SIO2
AL2O3	13.45	13.92	14.96	14.94	15.10	15.52	15.55	15.45	15.46	14.54	AL2O3
FE2O3T	13.39	4.01	4.17	4.17	4.92	4.79	6.15	2.75	2.71	7.87	FE2O3T
MGO	5.04	1.74	2.27	2.27	2.11	2.11	2.68	1.02	0.99	3.57	MGO
MNO	0.20	0.04	0.04	0.04	0.07	0.07	0.09	0.03	0.03	0.12	MNO
CAO	9.09	3.48	3.29	3.30	4.48	4.62	5.35	3.80	3.73	5.81	CAO
NA2O	2.59	3.49	4.62	4.61	3.99	4.13	3.98	4.37	4.36	3.61	NA2O
K2O	1.16	2.83	1.77	1.76	1.35	1.34	1.29	1.32	1.34	1.26	K2O
P2O5	0.17	0.11	0.14	0.15	0.11	0.12	0.12	0.12	0.11	0.07	P2O5
TIO2	1.42	0.36	0.42	0.42	0.55	0.46	0.54	0.40	0.40	0.60	TIO2
LOI	0.84	1.07	0.67	0.67	0.79	0.77	0.94	0.55	0.55	0.83	LOI
TOTAL	99.45	98.77	99.24	99.10	99.41	98.81	98.32	99.92	99.49	99.50	TOTAL
TOT+LOI	100.29	99.84	99.91	99.77	100.20	99.58	99.26	100.47	100.04	100.33	TOT+LOI
BA	215	973	202	204	358	307	278	385	383	199	BA
BE	1.10	0.94	0.97	0.97	0.77	0.87	0.75	0.96	0.59	1.20	BE
CO	60.0	62.4	50.3	50.7	59.7	55.0	54.6	65.4	62.0	48.3	CO
CR	102.9	80.0	48.6	50.4	55.9	49.0	67.9	17.2	11.8	136.1	CR
CU	83.6	3.2	8.5	7.8	29.7	27.9	21.9	28.1	21.9	40.0	CU
LA	9.1	30.4	23.6	31.3	17.1	20.4	11.1	42.0	32.4	16.6	LA
NI	39.4	36.1	57.9	65.5	31.6	11.2	21.3	5.3	-3.1	43.1	NI
SR	243	300	352	353	268	287	255	306	301	291	SR
V	303.5	28.9	25.8	31.1	41.6	31.0	56.2	6.3	0.6	126.8	V
ZN	141.3	42.8	50.0	47.2	76.4	73.0	91.5	62.8	56.1	124.8	ZN
ZR	130.2	117.0	142.2	138.1	184.6	174.0	141.2	204.5	205.0	66.0	ZR

SH04b : Gray Gneiss microbreccia, strong alteration, pseudotachylyte. 325 m east of Beinn Mheadhonach, Shildenish, Lewis.
: Grid Reference NB 2975 1978

SH08 : Gray Gneiss microbreccia, strong alteration, pseudotachylyte. 450 m north-east of Loch Mor an Iaruinn, Shildenish, Lewis
: Grid Reference NB 3038 1973

SH09c : Gray Gneiss microbreccia, moderate alteration. New quarry by B 8060 south of Loch Mor an Iaruinn, Shildenish, Lewis.
: Grid Reference NB 2998 1927

M05a : R-type mylonite. North end of Loch na Craoibhe, Malasgair, Pairc district, Lewis.
: Grid Reference NB 2972 1877

M05b : R-type mylonite. North end of Loch na Craoibhe, Malasgair, Pairc district, Lewis.
: Grid Reference NB 2972 1877

M05c : R-type mylonite. North end of Loch na Craoibhe, Malasgair, Pairc district, Lewis.
: Grid Reference NB 2972 1877

M06 : R-type mylonite, slight alteration. Eastern inlet at north end of Loch na Craoibhe, Malasgair, Pairc district, Lewis.
: Grid Reference NB 2975 1886

M07a : R-type mylonite. South end of burn connecting Loch na Craoibhe to Loch Dubh, Malasgair, Pairc district, Lewis.
: Grid Reference NB 2984 1884

SAMPNO	M07c	M09a	M09b	SH07	SH09a	SH09b	
SIO2	71.29	60.01	61.18	70.12	72.41	58.03	SIO2
AL2O3	15.14	15.50	14.46	15.68	14.57	15.11	AL2O3
FE2O3T	2.50	6.96	7.39	2.73	1.82	8.80	FE2O3T
MGO	1.04	3.69	3.41	1.03	0.52	4.39	MGO
MNO	0.03	0.11	0.11	0.04	0.01	0.13	MNO
CAO	3.37	5.69	5.62	3.35	2.35	7.19	CAO
NA2O	4.19	3.95	3.48	4.27	4.13	3.41	NA2O
K2O	2.21	1.69	1.30	2.47	3.03	1.51	K2O
P2O5	0.08	0.07	0.07	0.11	0.06	0.11	P2O5
TIO2	0.30	0.69	0.69	0.36	0.25	0.75	TIO2
LOI	0.58	0.99	1.40	0.49	0.48	0.91	LOI
TOTAL	100.15	98.36	97.71	100.16	99.15	99.43	TOTAL
TOT+LOI	100.73	99.35	99.11	100.65	99.63	100.34	TOT+LOI
BA	1058	374	286	978	978	231	BA
BE	0.93	1.14	1.08	1.03	0.60	1.15	BE
CO	65.0	45.4	52.4	50.6	52.8	43.3	CO
CR	14.1	80.7	60.4	10.5	9.3	168.6	CR
CU	10.1	11.8	27.6	19.8	5.0	12.6	CU
LA	21.5	18.5	21.8	12.8	15.9	28.9	LA
NI	-3.1	38.5	16.5	-0.4	-11.5	43.2	NI
SR	389	375	341	453	431	359	SR
V	13.0	105.1	108.0	12.2	-8.2	153.0	V
ZN	44.0	92.7	88.5	42.1	39.4	100.1	ZN
ZR	95.8	119.9	138.7	137.8	56.7	160.9	ZR

M07c : R-type mylonite, acid. South end of burn connecting Loch na Craoibhe to Loch Dubh, Malasgair, Pairc district, Lewis.
: Grid Reference NB 2984 1884

M09a : R-type mylonite. Northern end of east side of Loch na Craoibhe, Malasgair, Pairc district, Lewis.
: Grid Reference NB 3022 1829

M09b : R-type mylonite, moderate alteration. Northern end of east side of Loch na Craoibhe, Malasgair, Pairc district, Lewis.
: Grid Reference NB 3022 1829

SH07 : R-type mylonite. 400 m east of end of track leaving B 8060 east of Cnoc Loch an Iaruinn, Shildenish, Lewis.
: Grid Reference NB 3069 1982

SH09a : R-type mylonite. New quarry beside B 8060 south of Loch Mor an Iaruinn, Shildenish, Lewis.
: Grid Reference NB 2998 1927

SH09b : R-type mylonite grading to ultramylonite. New quarry beside B 8060 south of Loch Mor an Iaruinn, Shildenish, Lewis.
: Grid Reference NB 2998 1927

Precision run data

SAMPNO	LST12b36	LST12b20	LST12b3	LST12b43	LST12b46	LST12b34	LST12b23	LST12b2	LST12b25	LST12b33	
SIO2	51.97	51.91	51.82	51.90	52.29	52.56	51.98	52.90	52.80	52.54	SIO2
AL2O3	14.92	14.93	14.91	14.95	15.04	15.10	14.94	15.17	15.17	15.11	AL2O3
FE2O3T	9.87	9.82	9.82	9.83	9.92	9.96	9.86	10.08	10.04	9.97	FE2O3T
MGO	5.56	5.50	5.50	5.51	5.55	5.60	5.53	5.65	5.64	5.58	MGO
MNO	0.15	0.16	0.16	0.15	0.16	0.16	0.16	0.16	0.16	0.16	MNO
CAO	9.83	9.73	9.74	9.75	9.85	9.88	9.78	10.05	10.00	9.90	CAO
NA2O	3.54	3.54	3.56	3.55	3.57	3.59	3.54	3.64	3.62	3.59	NA2O
K2O	0.78	0.79	0.77	0.77	0.80	0.79	0.78	0.82	0.80	0.78	K2O
P2O5	0.15	0.15	0.16	0.15	0.16	0.16	0.15	0.14	0.15	0.16	P2O5
TIO2	0.73	0.73	0.73	0.73	0.74	0.74	0.73	0.75	0.75	0.74	TIO2
LOI	1.36	1.36	1.36	1.36	1.36	1.36	1.36	1.36	1.36	1.36	LOI
TOTAL	97.50	97.26	97.17	97.29	98.08	98.54	97.45	99.36	99.13	98.53	TOTAL
TOT+LOI	98.86	98.62	98.53	98.65	99.44	99.90	98.81	100.72	100.49	99.89	TOT+LOI
BA	167	166	167	166	169	169	169	169	171	169	BA
BE	1.55	1.48	1.52	1.44	1.47	1.58	1.58	1.67	1.65	1.58	BE
CO	63.5	60.9	62.5	62.9	63.0	65.4	65.6	66.4	62.8	65.6	CO
CR	75.2	70.5	72.1	68.7	73.2	75.6	74.2	80.5	76.7	74.2	CR
CU	56.6	54.6	57.0	50.7	56.3	60.2	54.6	61.5	60.0	54.6	CU
LA	7.6	1.1	1.8	1.3	2.5	14.0	7.4	8.9	11.2	7.4	LA
NI	40.2	31.6	30.9	27.8	31.4	36.0	31.6	40.0	22.9	31.6	NI
SR	383	383	384	386	386	387	389	391	390	389	SR
V	175.5	169.0	170.3	169.2	171.8	175.1	173.5	178.0	177.0	173.5	V
ZN	89.0	90.7	79.9	75.8	94.3	89.4	85.5	94.7	85.0	85.5	ZN
ZR	93.7	101.3	92.0	82.8	103.3	96.7	104.3	103.0	102.6	104.3	ZR

SAMPNO	ET12b1	ET12b2	ET12b3	ET12b4	ET12b5	ET12b6	ET12b7	ET12b8	ET12b9	ET12b10	
SIO2	60.27	60.66	60.72	60.28	60.60	60.94	61.62	60.87	60.91	60.09	SIO2
AL2O3	15.91	15.99	16.02	15.89	15.99	16.08	16.23	16.07	16.04	15.88	AL2O3
FE2O3T	6.28	6.36	6.34	6.30	6.34	6.36	6.44	6.36	6.36	6.28	FE2O3T
MGO	3.12	3.15	3.15	3.11	3.14	3.14	3.19	3.14	3.16	3.11	MGO
MNO	0.08	0.09	0.08	0.09	0.08	0.09	0.09	0.09	0.08	0.09	MNO
CAO	4.15	4.21	4.20	4.16	4.18	4.20	4.25	4.20	4.21	4.15	CAO
NA2O	5.03	5.12	5.10	5.07	5.09	5.12	5.17	5.12	5.12	5.07	NA2O
K2O	1.44	1.45	1.46	1.45	1.45	1.47	1.49	1.47	1.47	1.45	K2O
P2O5	0.34	0.35	0.33	0.33	0.35	0.35	0.34	0.35	0.35	0.34	P2O5
TIO2	0.72	0.73	0.72	0.72	0.73	0.73	0.75	0.73	0.73	0.72	TIO2
LOI	2.05	2.05	2.05	2.05	2.05	2.05	2.05	2.05	2.05	2.05	LOI
TOTAL	97.34	98.11	98.12	97.40	97.95	98.48	99.57	98.40	98.43	97.18	TOTAL
TOT+LOI	99.39	100.16	100.17	99.45	100.00	100.53	101.62	100.45	100.48	99.23	TOT+LOI
BA	659	666	666	661	665	668	675	669	669	662	BA
BE	0.97	1.10	1.00	1.08	1.01	1.12	1.29	1.15	1.13	1.09	BE
CO	28.7	30.7	29.5	28.2	28.3	27.7	31.0	28.3	25.3	25.0	CO
CR	98.4	14.3	100.1	98.0	98.8	99.9	103.3	96.7	96.7	95.2	CR
CU	43.8	49.7	47.4	48.1	45.3	48.4	53.9	52.8	51.9	41.9	CU
LA	39.7	44.0	39.6	41.4	38.3	40.8	49.4	41.7	43.1	34.7	LA
NI	12.1	9.2	9.5	19.7	16.6	16.1	28.1	7.3	15.8	19.7	NI
SR	757	763	762	759	764	765	776	770	770	762	SR
V	85.2	87.5	87.3	86.6	85.5	85.6	89.0	86.5	88.2	84.7	V
ZN	70.0	71.1	63.7	70.0	69.4	63.2	68.0	66.9	68.1	63.7	ZN
ZR	163.0	166.2	164.7	161.5	162.6	166.1	168.7	163.6	165.9	160.5	ZR

Appendix III: Fe^{2+} Determinations

Selected samples of representative rock types were analysed for their Fe2+ content to determine the oxidation state of iron.

REAGENTS REQUIRED:

Metavanadate reagent, approximately 0.05 N
Ferrous ammonium sulphate, approximately 0.055 N
Acid mixture, 40% sulphuric acid and 40% phosphoric acid
Indicator solution, 0.04% barium diphenylamine sulphonate
Boric acid solution, 5%
Standard potassium dichromate solution, 0.05000 N

PROCEDURE:

1. Into a series of 125 ml plastic bottles, pipette 10.00 ml of the metavanadate reagent. The pipette must be very clean and must be allowed to drain completely. Use a safety pipette filler.

2. Weigh 0.2000 ± 0.0002 g of each sample into a small aluminium dish and wash into a plastic bottle through a plastic funnel. Keep two bottles to serve as blanks.

3. To each bottle, placed inside a fume cupboard, add 8 ± 1 ml of "A.R." concentrated 40% HF. Swirl to form a slurry and stand inside the fume cupboard, with the cap on, for two days. Some samples may need a longer period of standing of up to seven days.

4. To each bottle, add 60 ml of the boric acid solution. Stand overnight to facilitate the dissolution of any precipitate.

5. Still working inside the fume cupboard,transfer the comtents of the bottles to a series of clean 600 ml beakers and rinse out the plastic bottles with a further 120 ml of the boric acid solution. Add the rinsings to the beakers.

6. Pipette 10.00 ml of the ferrous ammonium sulphate solution into each beaker just before the titration is commenced. Stir the solution with a plastic stirring rod to ensure it is completely clear.

7. Pipette 2 ml of the indicator solution into the beaker.

8. Titrate slowly with the standard potassium dichromate solution using a 10 ml or 5 ml microburette.

9. When the violet colour of the indicator, which is

produced by the addition of the titrant, only just disappears, add 5 ml of the acid mixture to the solution using a safety pipette. Stir well and continue the titration slowly until the grey-green colour just turns to violet, the final end-point.

CALCULATION:

% FeO = (ml $K_2Cr_2O_7$ (sample) - ml $K_2Cr_2O_7$ (blank)/ sample wt (g))
x N $K_2Cr_2O_7$ x 7.185
= (ml $K_2Cr_2O_7$ (sample) - ml $K_2Cr_2O_7$ (blank)) x 1.7963
for a sample weight of 0.2000 g and using 0.05000 N
$K_2Cr_2O_7$.

Correction Factors
1. For samples which stand in HF for two days, multiply the answer by 1.004.
2. For samples which stand in HF for seven days, multiply the answer by 1.006.

NOTES:

1. All operations involving hydrofluoric acid, HF, MUST be carried out inside a fume cupboard. Goggles, rubber or plastic gloves and a laboratory coat MUST be worn and the gloves MUST be well washed afterwards.

2. All samples should be less than 200 mesh. The following minerals dissolve only with difficulty unless ground extremely fine (i.e. less than 400 mesh); tourmaline, staurolite, pyrite, ilmenite, magnetite, garnet, siderite, chromite.

3. For samples with less than 6 % FeO, a sample weight of 0.5000 g may be taken. for samples with more than 15 % FeO, a sample weight of 0.1000 g must be taken.

4. Samples containing sulphide minerals and/or organic carbon will give unreasonably high values for ferrous iron.

5. The plastic bottles used must be rinsed thoroughly with water (5 times) after use.

6. The basic reactions involved are:-
$2\ NaVO_3 + 2\ FeSO_4 + 4\ H_2SO_4 \rightarrow 2\ VOSO_4 + Fe_2(SO_4)_3 + Na_2SO_4 + 4\ H_2O$.
$6\ FeSO_4 + K_2Cr_2O_7 + 7\ H_2SO_4 \rightarrow K_2SO_4 + Cr_2(SO_4)_3 + 3\ Fe_2(SO_4)_3 + 7\ H_2O$.

Fe^{2+} Determination Results, including duplicate samples

Sample number	Rock type	Fe^{2+}	Fe_2O_3T	FeO/Fe_2O_3
CR08	amphibolite	10.67	16.18	2.47
M01	"	11.05	14.67	4.62
LST07b	Corodale Gneiss	3.77	6.89	1.40
BNHT01	Cor. m'breccia	3.18	6.58	1.07
"	"	3.25	6.58	1.09
LST06	"	4.98	8.70	1.58
BNHT02	"	7.66	15.53	1.07
"	"	7.54	15.53	1.05
BV07	C-type mylonite	10.34	12.77	8.14
BV08	"	5.25	8.34	2.10
BV09	"	2.27	5.05	0.91
"	"	2.29	5.05	0.91
BV10	"	3.32	8.72	0.66
CH02	"	3.20	6.59	1.06
CNH02	"	2.05	3.34	1.93
CNH04	"	2.84	5.54	1.19
CNHc	"	3.61	5.16	3.17
ET03	"	4.50	6.92	2.36
LST05	"	4.31	7.75	1.46
ARDPT02	Gray Gneiss	2.55	3.58	3.77
"	"	2.64	3.58	4.08
BNHT07	"	0.92	1.91	1.05
CR03	"	2.54	3.18	7.26
CR06	"	7.90	7.38	-5.79
"	"	7.84	7.38	-5.88
GS01	"	1.81	2.81	2.56
"	"	1.94	2.81	2.97
GT07	"	3.15	4.18	4.70
LST15	"	1.31	2.90	0.91
BT06	Gr.Gn. m'breccia	2.98	6.27	1.01
CT02	"	3.46	6.54	1.29
CT03	"	1.35	2.19	1.99
ET17	"	4.00	6.65	1.89
"	"	4.09	6.65	1.94
LST09b	"	4.15	8.46	1.05
"	"	4.04	8.46	1.02
LST14	"	9.25	13.88	2.57
NT06	"	2.52	4.31	1.68
BNH2/6	Cataclasite	4.29	8.19	1.25
BNHT03	"	3.66	7.31	1.13
BV05	"	3.86	4.68	9.90
EV04	"	7.52	12.41	1.90
"	"	7.61	12.41	1.93
BT08	Altered Gr. Gn.	3.29	4.88	2.70
GT04	"	3.80	5.58	2.93
"	"	3.87	5.58	3.03
NT01	"	3.78	6.27	1.83
CR11	"	7.24	7.19	-8.52
CT07	"	1.18	2.15	1.42

ET06	Altered m'breccia	5.03	8.30	1.86
ET14b	"	3.93	4.02	-11.60
NT08	"	1.72	2.93	1.73
"	"	1.74	2.93	1.75
M05b	R-type mylonite	3.42	4.79	3.49
M07a	"	4.94	7.87	2.10
"	"	4.96	7.87	2.10
M09b	"	4.87	7.39	2.49
"	"	4.89	7.39	2.50
SH09b	"	6.14	8.80	3.12

Fe^{2+} determinations for standard compositions, and comparison with accepted values.

Sample number	Fe^{2+} (wt. %)	Accepted value (wt.%)	% Error
DTS-1	7.47	7.17	+ 4.2
W-2	8.33		- 0.1
"	8.31	8.34	- 0.4
DR-N	5.72	5.40	+ 5.9
BR	6.58	6.57	+ 0.2
NIM-N	7.25	7.30	- 0.7
SY-2	3.66	3.62	+ 1.1
2001	10.35	10.26	+ 0.9
91	1.46	1.42	+ 2.8

Appendix IV: Density Determinations

Density determinations were carried out using a standard density bottle technique. Initial determinations used powdered quartz to check the accuracy of the method. Results are presneted below.

Before commencing this determination, 2 litres of a 1 % Decon solution (the addition of the Decon aids wetting of the rock powder) was made and allowed to stand for 24 hours before use. It was allowed to reach the temperature of the room in which the weight determinations were carried out.

PROCEDURE:

1. Fill the 25 cm^3 density bottle with the Decon solution from the wash bottle. Stand for 7 minutes to allow bubbles to escape Place the stopper in the neck and insert with a twisting motion. Check no air has been trapped under the stopper. Carefully dry the bottle with a tissue. Weigh to 4 decimal places (W_1).

2. Weigh 2.0000 $\pm$ 0.0002 g of rock powder into an aluminium boat (W_2).

3. Empty the density bottle and introduce the rock powder into the bottle using a plastic funnel. Wash any powder on the funnel into the density bottle with the Decon solution until the density bottle is half full. Swirl thoroughly to ensure complete wetting of all the rock powder. Stand for 7 minutes.

4. Carefully fill the bottle with the Decon solution and stand for a further 7 minutes. Place the stopper in position as before. Ensure there are no air bubbles in the bottle. Dry carefully. Weigh to four decimal places (W_3).

5. Empty the contents of the bottle into the waste beaker and wash three times with Decon solution. Clean the outside of the bottle too by immersion and swirling in a beaker of Decon solution (when the bottle is emptied, rock powder waste tends to dribble down its sides).

6. Density = $W_2/(W_2 + W_1 - W_3)$

NOTES:

1. The rock powder should not be too fine (>100 microns) or problems will be encountered with settling rates.

2. If the funnel is damp, the powder may clog it up. If this occurs, a fine copper wire can be used to help things along. Adding some Decon solution may also help. Ensure the wire is cleaned off into the bottle afterwards.

3. Check the weight of the density bottle and Decon solution (W_1) after every three samples.

4. Determine the density of the silica standard provided after every three samples (preferably try to get this out of phase with the W_1 weighings).

5. Accuracy of the determination is about $\pm$ 0.02 g cm^{-3}, assuming the density of the Decon solution is 1.00 g cm^{-3}.

6. Duplicate density determinations should be performed on all samples.

7. All operations should be performed with a consistently uniform technique.

Density Determination Results

Sample number	Rock Type	Density Values	Mean
ARDPT02	Gray Gneiss	2.673	
		2.675	2.674
BNHT07	" "	2.630	
		2.603	
		2.621	2.618
CR03	" "	2.718	
		2.699	2.709
CR06	" "	2.780	
		2.764	2.772
LP01	" "	2.711	
		2.692	
		2.709	2.704
LST15	" "	2.705	
		2.727	2.716
VS01	intermediate Gray Gneiss	2.719	
		2.691	2.705
CR01	basic amphibolite	2.985	
		3.005	2.995
M03c	altered microbreccia	2.679	
		2.661	2.670
SH01	cataclased r-type mylonite	2.784	
		2.805	2.794
SH09a	r-type mylonite	2.661	
		2.647	2.654
M05b	" "	2.751	
		2.764	2.758
M07a	" "	2.805	
		2.788	2.797
SH07	" "	2.686	
		2.674	2.680
BT02	altered Gray Gneiss	2.700	
		2.698	2.699
NT01	" " "	2.772	
		2.776	2.774
BT03	c-type mylonite	2.850	
		2.848	2.849
CT01	" "	2.735	
		2.748	2.742
ET03	" "	2.709	
		2.710	2.709
LST05	" "	2.881	
		2.894	
		2.897	2.891

Error for the Density Determinations as determined by repeated analysis of a quartz standard.

Density values

2.614
2.639
2.622
2.633
2.652
2.642
2.654
2.624
2.620
2.641
2.644
2.627
2.664
2.653
2.631
2.661

Mean = 2.639

Standard Deviation = 0.015